Decoherence in one-dimensional electron systems

Clemens Neuenhahn

München 2008

Decoherence in one-dimensional electron systems

Clemens Neuenhahn

Diplomarbeit
am Arnold Sommerfeld Center for Theoretical Physics
der Ludwig–Maximilians–Universität
München

vorgelegt von
Clemens Neuenhahn
aus München

München, den 31. Oktober

Erstgutachter: Dr. Florian Marquardt

Zweitgutachter: Dr. Klaus Hornberger

Inhaltsverzeichnis

Chapter 1

Introduction

Dephasing processes suppress quantum mechanical interference phenomena and are responsible for the transition from the microscopic quantum coherent world into the macroscopic world, which is characterized by the absence of interference effects. Whereas the physics of decoherence has been studied in great detail for single particle systems, only recently a couple of experiments have drawn attention to physical systems, in which many-body effects play an important role. For instance, the coherence of interacting one-dimensional electrons is of great interest. In order to test the electrons' coherence in experiment, e.g., one can send them through an interferometer structure, as a Mach-Zehnder interferometer. The electronic Mach-Zehnder interferometer is one of the simplest systems where the interplay of quantum mechanical coherence and many-body effects can be studied, both in theory and experiment. This electronic analogue to the ubiquitous optical Mach-Zehnder interferometer, was first realized in the group of Moty Heiblum at the Weizmann institute in 2003 [20]. The main idea was to employ integer quantum-hall edge channels playing the role of the interferometer arms. In these quasi one-dimensional channels the electron movement is purely chiral, i.e., all the spin-polarized electrons move in a single direction. The interferometer arms enclose a magnetic flux Φ. Due to the Aharonov-Bohm effect the phase of electrons passing the interferometer through one or the other arm differs. As a result of the interfering paths, the electronic current through the interferometer displays an interference pattern, which can be controlled by changing the flux Φ. Today, there are several groups [27, 28, 42, 39] investigating the electronic Mach-Zehnder interferometer in experimental setups closely related to that pioneering one in [20].

In these experiments, the interference contrast, i.e., the difference between maximum constructive and maximum destructive interference, as a function of voltage and temperature has been analyzed. The interference contrast can be considered as a direct measure for the coherence of the propagating electrons. After the first realization of the Mach-Zehnder interferometer, it became clear that a simple single-particle picture description of the propagating electrons is not sufficient to explain all

the interesting physics emerging in this system. Today, only a fraction of the observed features have been explained by now. For instance, increasing the applied bias voltage between the interferometer arms, even for equal arm lengths, the interference contrast gets suppressed. This effect can not be obtained from a single-particle calculation and it is assumed that a loss of phase coherence the electrons suffer during their propagation is responsible for this effect.

On the theoretical side, dephasing in such a setup has been discussed both for dephasing by external fluctuations [34, 33, 13, 31, 36, 40, 18] (such as phonons, defect fluctuators or Nyquist noise from external gates, or "dephasing terminal" reservoirs), as well as by the intrinsic electron-electron interaction [44, 45, 40, 18, 6, 26]. More recently [39, 27], it was reported that the interference contrast changes periodically with maxima and zero minima increasing the applied bias voltage. This "lobe structure" is one of the most prominent features of the Mach-Zehnder interferometer and motivated the further theoretical investigation of this system, for instance in [40, 18, 45, 6, 26].

1.1   Decoherence in one-dimensional electron systems

In this work, we investigate the coherence properties of interacting electrons in one dimension. We restrict the considerations to spinless, chiral fermion systems, such as edge states in the integer quantum Hall effect, employed for the realization of the Mach-Zehnder interferometer.

One dimensional systems differ crucially from electron system in higher dimensions. The reason for this is the breakdown of the Fermi liquid picture. While in dimensions higher than one, the low-energy excitations can be considered as well defined (Landau) quasi-particles, in one dimension the Fermi liquid theory does not hold. In 1950 Tomonaga proposed an exactly solvable model [46], which was extended by Luttinger in 1963 [29], describing the low-energy properties of one-dimensional electron systems. The main achievement was the recognition that the low-energy excitations in such systems can be considered as (nearly)well defined bosons. These bosonic excitations are closely related to the creation of modulations in the electron density, i.e., the excitation of electron-hole pairs. Furthermore, it turned out that even taking into account electron-electron interactions, the model remains solvable. Today, the bosonization of one-dimensional electron systems has become a standard tool in condensed matter physics [21, 4, 2, 14]. In fact, the chiral interacting electron system is the simplest possible realization of a Luttinger liquid.

Usually, within bosonization one considers point-like interparticle interactions, i.e., in momentum space the interaction potential reduces to a constant. It turns out that in this case the only effect of the interaction shows up as a renormalization of the bare Fermi velocity, such that the chiral Luttinger liquid reduces to an ordinary Fermi liquid. However, taking into account a finite interaction range between the electrons, even the chiral interacting electron system gives rise to some very non-trivial features. Therefore, in this work we assume the interaction between the electrons to be of finite range.

Only recently, taking into account the full interaction potential, in a pioneering work, Chalker, Gefen and Veillette [6] studied the interesting properties of chiral electron systems. There, the influence of the electron-electron interaction on the interference contrast in a Mach-Zehnder interferometer setup is investigated. It is the first atttempt to consider the electrons within one and the same channel as the source of dephasing. The authors modeled the interacting Mach-Zehnder interferometer as consisting of two one-dimensional chiral interacting fermion systems (the arms of the interferometer). The two channels are tunnel-coupled weakly at two locations, representing the quantum point contacts (i.e. the beam splitters) of the experimental setup. In a next step the interferometer current is evaluated in lowest order in tunneling. The result is a formula for the current that only involves the single-particle Green's functions of the interacting channels in the absence of tunneling. These Green's functions are obtained using the tools of bosonization. The main outcome of their study is that at low voltages and temperatures the interference contrast becomes perfect, while the suppression of contrast at increasing voltages and temperatures depends on the details of the interaction potential. However, even taking into account the full electron-electron interaction, no explanation for the lobe structure mentioned above was found. The proposal in [6] serves as a starting point for the analysis presented here.

Starting with the bosonization of the system, the main restriction is that the tunneling between the interferometer arms can be treated only perturbatively. As in the experiment the lobe structure gets more and more pronounced increasing the tunnel coupling between the interferometer arms, an extension of the theoretical description to higher orders in the coupling seems to be fruitful. For example, taking into account higher orders in tunneling, the influence of shot-noise on the coherence of the propagating electrons should become observable. Mainly, this is motivated by the observation in [40, 39]. The authors investigate the influence of so-called non-Gaussian shot noise [1] on the interferometer visibility. There, an external electron channel is coupled to one of the interferometer arms, while the number of electrons in this "detector channel" is assumed to be very small (1-3 electrons). As a result, the detector channel acts as a non-Gaussian noise source. In this model, the interference contrast displays oscillations as a function of the applied bias voltage showing a striking similarity to the reported lobe-structure in [39, 27].

1.2 This work

Analyzing decoherence in one-dimensional electron systems, the main difficulty arises from the fact that in one-dimension the many-body character of the strongly interacting electrons can not be neglected. Thus, investigating the decoherence in such systems, means dealing with renormalization effects resulting from the indistinguishability of the electrons, the influence of the Pauli principle, etc.. We investigate the decoherence of electrons resulting both from the electron-electron interaction and from the coupling to an arbitrary harmonic oscillator bath (consisting for example of two-dimensional phonons).

For this, we employ the Mach-Zehnder interferometer (MZI) to "test" the electrons' coherence. In Chapter 2 we introduce the MZI and derive an expression for the current assuming weakly tunnel-coupled interferometer arms. As it turns out that the interference contrast and therefore the coherence for weakly coupled interferometer arms only depends on the Fourier transform of the single-particle Green's function $G^>(x, \epsilon)$, we consider it as a direct measure for the coherence and devote the main part of this work to its analysis. The Green's function $G^>(\epsilon, x)$ can be interpreted as the amplitude for an electron with energy ϵ to propagate the distance x without losing its phase coherence.

In Chapter 3, assuming a finite range of the electron-electron interaction, we derive the exact solution for the single-particle Green's functions with help of the bosonization method. Whereas the formal calculation of the Green's function is a straightforward task, taking into account an interaction potential of finite range, in the end, it can be evaluated only numerically. The chapter is concluded by a discussion of the Green's function and of the interference contrast. As a main result, only due to the finite interaction range, two distinct energy regimes show up. While the decoherence of low-energy electrons is suppressed strongly, the coherence of electrons flying high above the Fermi sea is destroyed to the full extent. Although bosonization provides us with the exact result for the Green's function, the physical interpretation of the results remains difficult.

Thus, in order to understand the physical mechanism of decoherence in these two energy regimes, there is some need for an alternative point of view. That is why, in Chapter 4, we propose a simple semiclassical model for deriving the Green's function. It asssumes the electron to move ballistically experiencing a fluctuating background potential stemming from the intrinisc density fluctuations in the Fermi sea. Thereby, we neglect any "backaction" of the single electron onto the bath. The only effect of the interaction is that the electron accumulates an additional random phase. In the end, one has to average over these random phases leading to a suppression of the coherence, i.e., of the Green's function $G^>(\epsilon, x)$. It is one of our main results that, compared to the full bosonization solution, this simple semiclassical approach becomes exact considering electrons propagating with large energies. We reported in [41] that at zero temperature in this limit the coherence displays a universal power law $|G^>(\epsilon, x)| \sim 1/x^1$, where most remarkably the exponent turns out to be independent from the coupling strength of the electron-electron interaction.

In Chapter 5, we try to extend the semiclassical approach in order to re-derive the Green's function for electrons of arbitrary energy. While the semiclassical ansatz for the Green's function does not fully reproduce the bosonization solution, nevertheless it might be an interesting starting point for further investigations. It could provide an alternative interpretation of the Green's function and the most general mechanism of decoherence in chiral one-dimensional electron systems.

We conclude the analysis of the single-particle Green's function of interacting electrons employing in Chapter 6 Keldysh perturbation theory up to second order in the inter-electron coupling. Mainly, this perturbative approach is meant to study the decoherence of low-energy electrons. In particular, it clarifies the suppression of decoherence suffered by electrons in close vicinity to the Fermi edge, during their propagation. We formulate the perturbation theory in Keldysh time, as this allows for an ex-

tension to non-equilibrium situations as well. Furthermore, treating the electron-electron interactions perturbatively, in principle one is not restricted to weakly tunnel-coupled interferometers. As already mentioned, to explain many interesting features of the Mach-Zehnder interferometer considering the current only in the lowest order in tunneling is not sufficient. Thus, the Keldysh perturbation theory presented here might be a starting point for going beyond this limitation.

Alternatively, one can remain in the framework of bosonization, taking into account the next non-vanishing order in the tunnel coupling ($\mathcal{O}(t_A^4)$) contributing to the current trough the interferometer. It turns out that in the next highest order, the current depends on two-particle Green's functions. Unfortunately, the resulting expressions for the current involve complicated convolutions of two-particle Green's functions and at this point it is not clear, whether their numerical evaluation is possible at all.

Chapter 7 has to be considered as a first step following these lines. There, we focus on the analysis of two-particle Green's functions of particular interest describing the energy and momentum relaxation of one-dimensional electrons due to electron-electron interaction. The purpose of this Chapter is twofold. On the one hand, relaxation processes in interacting one-dimensional systems out of equilibrium are of greatest interest. For instance, it is an amazing fact [3] that in these systems, electrons, injected with some energy do not transfer its energy to the full extent to the Fermi sea, i.e., they do not "thermalize". The numerical evalutation of the corresponding Green's functions is in agreement with this prediction. On the other hand, in Chapter 7 it is tested, whether the precise numerical evaluation of two-particle Green's functions can be done with some reasonable effort. So far, the main outcome of this investigation is that in fact the numerical evvaluation of these functions is possible, however there is some need for a further optimization of the numerics.

We conclude this work by investigating the influence of an external harmonic oscillator bath on the coherence properties of chiral one-dimensional electrons in Chapter 8. In this case, the single-particle Green's function can still be derived exactly in the framework of bosonization. However, in order to obtain $G^>$, the bath degrees of freedom have to be traced out with help of the imaginary-time functional field integral method. The coupling to a quantum bath is already investigated to a large extent. Following the famous proposal by Castro-Neto et al., here we present a formally exact solution. As a main result, expanding the resulting Green's function $G^>(\epsilon, x)$ up to first order in the coupling between bath and the one-dimensional electron system, we calculate a decay rate for the coherence, which is shown to be in agreement with a simple Fermi's golden rule calculation. While this decay rate was derived earlier in [31, 36, 32, 11], we re-derive their results starting from an exact expression for the Green's function, thereby taking into account possible renormalization effects, etc.. It is shown that the presence of the filled Fermi sea, influences the decoherence of electrons coupled to a quantum bath crucially. The reason is that the Pauli principle does not allow for scattering processes, where the corresponding final state of the scattered electron lies below the Fermi edge. This phenomenon is known as Pauli blocking and suppresses the decoherence of low-energy electrons.

Chapter 2

Mach-Zehnder interferometer

An electronic Mach-Zehnder interferometer is described as two parallel one-dimensional channels in which electrons propagate into the same direction (see Fig. 2.1a). At two tunnel contacts (quantum point contacts (QPC's) in the experimental realization), these channels are coupled by tunneling amplitudes t_A and t_B. Below, we will assume these tunneling probabilities to be small perturbations, coupling lead 1 (left channel) and lead 2 (right channel). Furthermore, a magnetic flux is enclosed by the interferometer, which leads to an Aharonov-Bohm phase ϕ. In the experiment the current I through the interferometer, i.e., the current between the two leads measured at some output port is the quantity of interest (see Fig. 2.1). It contains two types of contributions: one flux-independent constant term and one interference term that depends on$\cos(\phi)$. The contrast of the interference fringes observed in $I(\phi) = I_0 + I_{\mathrm{coh}}(\phi)$ can be quantified via the so-called visibility:

$$v_I = \frac{I_{\max} - I_{\min}}{I_{\max} + I_{\min}}, \tag{2.1}$$

where $I_{\max}$ ($I_{\min}$) is the maximum (minimum) current as a function of flux. This definition is chosen in order for the visibility to be equal to one for perfect interference contrast. The visibility can be used as a direct measure for the coherence of the system.

In this chapter, we derive an expression for the steady state current I in lowest order in tunneling between the interferometer arms (Section 2.1). Then, in Subsection 2.1.1 we define the single-particle Green's functions (GFs) $G^>(x,t)$ describing the coherent propagation of electrons through the interferometer arms in the absence of tunneling. It turns out that the current can be expressed only in terms of these GFs. At this point, there is no need for specifying the GFs in more detail. Making use of the bosonization technique, in Chapter 3 the Green's function will be calculated, thereby taking into account the intrinsic electron-electron interaction. Consequently, the Hamiltonian H_1 responsible for the time evolution of the electrons in the quantum-hall edge channels is introduced there, as well.

In contrast to [6], we decide to present the final expressions for the current in terms of the Fourier transform of the GF, $G^>(\epsilon, x)$. The Green's function in energy and real space $G^>(\epsilon, x)$ gives the amplitude for an electron with energy ϵ to propagate the distance x without loosing its phase coherence. As a result, the current through the interferometer is brought to a transparent form emphasizing the physical origin of each contribution (Subsection 2.1.2). Finally, the visibility can be written in a compact form (Section 2.2).

The main outcome of this first chapter is that the visibility and therefore the coherence of the electron system in lowest order in tunneling only depends on the single-particle Green's function $G^>(\epsilon, x)$. Thus, in the following we sometimes refer to $G^>(\epsilon, x)$ itself as the "coherence" of the electron system.

2.1   Current

The observable of interest in the present setup is the current through the interferometer (cf. Fig. 2.1a) due to a finite bias voltage between the two leads, i.e. $\mu_1 - \mu_2 \neq 0$, where μ_j is the chemical potential of the j-th channel. Dealing with the electron-electron interaction exactly using the bosonization technique has one main disadvantage: one has to treat the tunneling between the channels in perturbation theory. In the following, the quantum point contacts A and B be at positions $x_j^A = 0$ and $x_j^B = x_j$, respectively (where $j = 1, 2$ is the channel index). We introduce the fermionic single-particle operators $\hat{\psi}_j(x)$ ($\hat{\psi}_j^\dagger(x)$), annihilating (creating) an electron at x in channel j. They fulfill the fermionic anti-commutation relations (here the anticommutator is denoted by $\{.., ..\}$)

$$\left\{ \hat{\psi}_i(x), \hat{\psi}_j^{\,\dagger}(x') \right\} = \delta_{ij}\delta(x - x') \qquad \left\{ \hat{\psi}_i(x), \hat{\psi}_j(x') \right\} = \left\{ \hat{\psi}_i(x), \hat{\psi}_j(x') \right\} = 0. \qquad (2.2)$$

With these definitions, the tunneling Hamiltonian is given by

$$\hat{H}^T := t_A \hat{\psi}_1^\dagger(0)\hat{\psi}_2(0) + t_B \hat{\psi}_1^\dagger(x_1)\hat{\psi}_2(x_2) + h.c. \quad . \qquad (2.3)$$

The current into channel 1 is defined as ($q_e < 0$ is the electron charge):

$$\hat{I} = q_e \frac{d}{dt}\hat{N}_1, \qquad (2.4)$$

where as usual the $\hat{N}_j$ is the number operator: $\hat{N}_j \equiv \int dx\, \hat{\psi}_j^\dagger(x)\hat{\psi}_j(x)$. The current can be evaluated making use of the Heisenberg equation of motion (for the remainder of this work we set $\hbar \equiv 1$)

$$\hat{I} \quad = \quad -iq_e \left[\hat{N}_1, \hat{H}_1 + \hat{H}^T \right], \qquad (2.5)$$

where $\hat{H}_1$ (cf. with Eq. (3.11)) denotes the interacting electron Hamiltonian in the absence of tunneling which will explicitly be defined in Chapter 3. The Hamiltonian $\hat{H}_1$ determines the electrons' dynamics
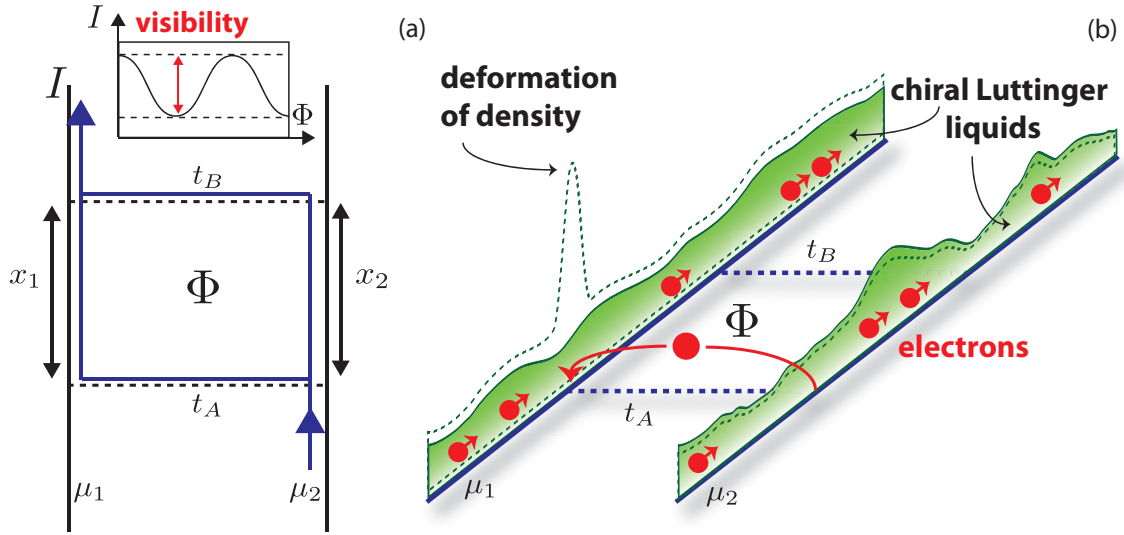
Figure 2.1: (a) Scheme of the interferometer setup. The two channels 1 and 2 of length $x_{1,2}$ and the corresponding chemical potentials $\mu_{1,2}$ are indicated. The electrons can tunnel at QPCs A and B, with tunnel amplitudes t_A and t_B. Tuning the magnetic flux Φ through the interferometer, an interference pattern $I(\phi)$ is observed. The solid blue lines denote the interferring paths (here $\mu_2 > \mu_2$) through the interferometer.

(b) Pictorial plot of the physical situation, we investigate in this work. In the absence of tunneling, the electrons in the quantum-hall edge channels form chiral Luttinger liquids. The bosonization of one-dimensional electron systems (cf. Chapter 3) emphasizes that the bosonic low-energy excitations in these systems are closely related to excitations of density fluctuations (depicted as solid dark green lines). These are of collective nature. In contrast, the tunnel Hamiltonian $\hat{H}^T$ in Eq. (2.3) describes the hopping of single electrons between opposite channels. Once a single electron is created in the opposite interferometer arm, it creates a sharp peak in the electron density (dashed dark green lines). With increasing propagation distance, it suffers a loss of phase coherence due to intrinsic interactions.

inside each interferometer arm. It will be shown that the Hamiltonian $\hat{H}_1$ and the number operators commute. Therefore, applying only the relations Eq. (2.2) we obtain (for the lengthy, but simple calculation see Appendix A.1) :

$$
\begin{aligned}
\hat{I} &= -iq_e \left[\hat{N}_1, \hat{H}^T \right] \\
&= -iq_e \int dx \left[\hat{\psi}_1^\dagger(x)\hat{\psi}_1(x), t_A \hat{\psi}_1^\dagger(0)\hat{\psi}_2(0) + t_B \hat{\psi}_1^\dagger(x_1)\hat{\psi}_2(x_2) + h.c \right] \\
&= -q_e i \left[t_A \hat{\psi}_1^\dagger(0)\hat{\psi}_2(0) + t_B \psi_1^\dagger(x_1)\hat{\psi}_2(x_2) \right] + \text{h.c.} \quad .
\end{aligned}
\tag{2.6}
$$

Now, we change to the interaction picture with respect to $\hat{H}_1$, setting $\hat{A}_{H_1}(t) \equiv e^{i\hat{H}_1 t}\hat{A}e^{-i\hat{H}_1 t}$. We are interested in the steady-state current through the interferometer $I(t) = \langle \hat{I}(t) \rangle$. The thermal average is defined as $\langle \ldots \rangle \equiv \langle e^{-\beta \hat{H}_1} \rangle^{-1} \langle e^{-\beta \hat{H}_1} \ldots \rangle$, where the inverse temperature $\beta = 1/T$ is introduced setting for the remainder of this work $k_B \equiv 1$.

To derive the steady state expectation value of the current operator in Eq. (2.6), we expand $I(t)$ in orders of the tunnel amplitude $t_{A,B}$ employing the identity

$$
e^{i\hat{H}_1 t}e^{-i\hat{H}_1 t - i\int_0^t dt' \, \hat{H}^T} = \hat{T}e^{-i\int_0^t dt' \, \hat{H}_{H_1}^T}.
\tag{2.7}
$$

Here, $\hat{T}$ is the time-ordering symbol, ordering operators with the largest time to the left. Analogously, the anti-time ordering symbol is denoted with $\tilde{T}$ (ordering the largest times to the right)[1]. Restricting to the first non-trivial order in the tunnel amplitude $\mathcal{O}(t_A^2)$, one derives

$$
\begin{aligned}
I &= \left\langle \hat{I} \right\rangle \\
&= \left\langle \left\{ \hat{T}e^{-i\int_{-\infty}^t dt' \, \hat{H}_{H_1}^T} \right\}^\dagger \hat{I}_{H_1}(t) \left\{ \hat{T}e^{-i\int_{-\infty}^t dt' \, \hat{H}_{H_1}^T} \right\} \right\rangle \\
&= \left\langle \left\{ 1 + i\tilde{T}\int_{-\infty}^t dt' \, \hat{H}_{H_1}^T(t') \right\} \hat{I}_{H_1}(t) \left\{ 1 - i\hat{T}\int_{-\infty}^t dt' \, \hat{H}_{H_1}^T(t') \right\} \right\rangle \\
&= \left\langle \hat{I}_{H_1} \right\rangle - i \left\langle \int_\infty^t dt' \, \left[\hat{I}_{H_1}(t), \hat{H}_{H_1}(t') \right] \right\rangle .
\end{aligned}
\tag{2.8}
$$

The first term in Eq. (2.8) vanishes as in the absence of tunneling between the interferometer arms no current can flow at all. Once the system has settled into a steady state (after switching on the tunneling at $t = -\infty$), the average current does not depend on the particular time it is measured. Therefore, we can simply set $t = 0$. The average current I in lowest order in tunneling yields

$$
I = \frac{1}{i} \int_{-\infty}^0 dt \, \left\langle \left[\hat{I}_{H_1}(0), \, \hat{H}_{H_1}^T(t) \right] \right\rangle .
\tag{2.9}
$$

---

[1]Note that for arbitrary operators $\hat{A}(t)$: $(\hat{T}\hat{A}(t_1)\hat{A}(t_2))^\dagger = \tilde{T}\hat{A}^\dagger(t_1)\hat{A}^\dagger(t_2)$

One may note that the current I is obtained as a Kubo-type expression, in linear response with respect to the tunneling Hamiltonian $\hat{H}^T_{H_1}$, at arbitrary bias voltages.

Before we proceed further expressing the interferometer current I in terms of the single-particle Green's functions, we introduce the GFs, which will be employed in the remainder of this work.

2.1.1 Definition of single-particle Green's functions

In the following more general definitions and relations we omit the channel label j. As usual, we define the single particle propagators as [2]:

$$
\begin{aligned}
G^>(x,t) &\equiv -i \left\langle \hat{\psi}(x,t)\hat{\psi}^\dagger(0,0) \right\rangle \\
G^<(x,t) &\equiv i \left\langle \hat{\psi}^\dagger(0,0)\hat{\psi}(x,t) \right\rangle.
\end{aligned}
\tag{2.10}
$$

For later purposes, we also introduce the Fourier transformed Green's function with respect to time

$$
G^>(\epsilon,x) \equiv \int dt\, e^{i\epsilon t} G^{>(<)}(x,t),
\tag{2.11}
$$

as well as the retarded Green's function $G^R(x,t)$, its Fourier transform and the spectral density $\mathcal{A}(\epsilon,k)$

$$
\begin{aligned}
G^R(x,t) &\equiv -i\Theta(t) \left\langle \left\{ \hat{\psi}(x,t), \hat{\psi}^\dagger(0,0) \right\} \right\rangle \\
G^R(\epsilon,k) &= \int dt \int dx\, e^{i\epsilon t - ikx} G^R(x,t) \\
\mathcal{A}(\epsilon,k) &\equiv -\frac{1}{\pi} \mathrm{Im} G^R(\epsilon,k).
\end{aligned}
\tag{2.12}
$$

In the remainder of this work, $G^>(x,t)$ $(G^<(x,t))$ will be referred to as the electron (hole) propagator. It can be interpreted as the amplitude that an electron (hole) propagates the distance x in the one-dimensional interacting electron system without suffering a loss of its phase coherence. To put it differently, one creates an electron at $(x = 0, t = 0)$ and asks for the amplitude for re-extracting an electron at (x,t) whose phase is correlated to that of the injected one. Of course, the same interpretation holds considering holes as well, the only difference being that in diagramatic language holes are moving backwards in time. Equivalently, $G^{>(<)}(\epsilon,x)$ gives the amplitude for an electron (hole) of energy ϵ to propagate after its injection the distance x coherently.

Finally, the spectral density $\mathcal{A}(\epsilon,k)$ is interpreted as a probability function [30]. It is the probability that an electron has momentum k and energy ϵ and therefore fulfills the important sum rule:

---

[2]With $\hat{\psi}(x,t)$, we denote the single particle operators in the interaction picture with respect to the Hamiltonian $\hat{H}_1$ omitting an extra label.

$\int d\omega\, \mathcal{A}(\omega, k) = 1$. The spectral density[3] and the propagators $G^{>(<)}$ are related via the fluctuation-dissipation theorem [4] (with $G^{>}(\epsilon, k) \equiv \int dx\, e^{-ikx} G^{>}(\epsilon, x)$)

$$
\begin{aligned}
iG^{>}(\epsilon, k) &= 2\pi[1 - f(\epsilon)]\mathcal{A}(\epsilon, k) \\
-iG^{<}(\epsilon, k) &= 2\pi f(\epsilon)\mathcal{A}(\epsilon, k),
\end{aligned}
\tag{2.13}
$$

where we introduced the Fermi-Dirac distribution function $f(\epsilon) = [\exp(\beta(\epsilon - \mu)) + 1]^{-1}$. Finally, we can define the tunnel density of states as

$$
\nu(\epsilon) \equiv \int \frac{dk}{2\pi}\, \mathcal{A}(\epsilon, k).
\tag{2.14}
$$

2.1.2   Calculation of the current

The calculation of the current in linear response to the tunnel-operator $\hat{H}_{H_1}^{T}$ is straightforward, but a bit cumbersome. Therefore, the calculation is postponed to Appendix A.2 and only the final results are presented here. The crucial point is that the current consists of two contributions. One of these is independent of the flux Φ through the interferometer, which is why we refer to it as the "classical current". The second contribution is an interference term, dependent on the flux. It is sensitive to the coherence of the electrons flying through the interferometer. This contribution is suppressed as a result of decoherence electrons suffer during their flight. In the following $G_j^{>}$ denotes the bulk Green's function in interferometer arm j. As we consider only the case of weakly tunnel-coupled interferometer arms, both arms are assumed to be in equilibrium.

Flux independent part   The flux-independent part of the current is found using Eqs. (2.3), (2.6) and (2.8)

$$
I_0 = q_e(|t_A|^2 + |t_B|^2) \int_{-\infty}^{\infty} dt\, \left[G_1^{>}(0, -t)G_2^{<}(0, t) - G_1^{<}(0, -t)G_2^{>}(0, t) \right],
\tag{2.15}
$$

which we rewrite by going to the frequency domain

$$
I_0 = q_e \left(|t_A|^2 + |t_B|^2 \right) \int \frac{d\omega}{2\pi}\, \left[G_1^{>}(0, \omega)G_2^{<}(0, \omega) - G_1^{<}(0, \omega)G_2^{>}(0, \omega) \right].
\tag{2.16}
$$

---

[3]For a non-interacting system the spectral density is a δ-function, $\mathcal{A}(\epsilon, k) = \delta(\epsilon - \epsilon_0(k))$ (where $\epsilon_0(k)$ is the dispersion relation of a free electron). In a Fermi liquid the spectral density turns into a Lorentzian of finite width, reflecting the finite lifetime of the quasi-particle excitations. In contrast, in one dimension the spectral density displays characteristic power-laws with exponents depending on the coupling strength of the electron-electron interaction.

To clarify the physical meaning of Eq. (2.16), we employ the fluctuation-dissipation theorem in Eq. (2.13):

$$G^>(x=0,\omega) = \int \frac{dk}{2\pi} G_j^>(k,\omega) = -i2\pi \left[1 - f_j(\omega)\right] \cdot \nu_j(\omega) \tag{2.17}$$

$$G^<(x=0,\omega) = i2\pi f_j(\omega) \cdot \nu_j(\omega). \tag{2.18}$$

Thus, we can reformulate the expression as a function of the tunneling density of states $\nu(\omega)$,

$$I_0 = 4\pi^2 q_e \left(|t_A|^2 + |t_B|^2\right) \int \frac{d\omega}{2\pi} \nu_1(\omega)\nu_2(\omega) \left[\underbrace{f_2(\omega)[1 - f_1(\omega)]}_{2\rightarrow 1} - \underbrace{f_1(\omega)[1 - f_2(\omega)]}_{1\rightarrow 2}\right]$$

which finally yields the most intuitive form describing the sum of tunneling currents at two point-like locations:

$$I_0 = 4\pi^2 q_e \left(|t_A|^2 + |t_B|^2\right) \int \frac{d\omega}{2\pi} \nu_1(\omega)\nu_2(\omega) \left[f_2(\omega) - f_1(\omega)\right] \tag{2.19}$$

In particular, these expressions show that the flux-independent part of the current only depends on the tunneling density of states. It is independent of the length of the interferometer arms. This is to be expected, as that part of the current is insensitive to the electrons' coherence, and therefore the decay of coherence as a function of propagation distance will not enter here.

Interference part The Mach-Zehnder setup is intended to investigate the coherence of the electron system and therefore the most interesting quantity is the interference part of the current, which we define to be the flux-dependent contribution. Using Eqs. (2.3), (2.6) and (2.9) it yields:

$$I_{\mathrm{coh}}(\phi) = q_e \int \frac{d\omega}{2\pi} \left[(t_A t_B^*)e^{-i\phi} \cdot G_1^>(\omega, x_1)G_2^<(\omega, -x_2)\right.$$
$$\left. -(t_A^* t_B)e^{i\phi} \cdot G_1^<(\omega, -x_1)G_2^>(\omega, x_2) + \mathrm{c.c.}\right]. \tag{2.20}$$

At $T = 0$, in a situation where the particle current flows from channel 2 to 1, only the first term (and its complex conjugate) contributes. It might be helpful to see how the structure of this term $G_1^> G_2^<$ can be understood in an intuitive, if slightly imprecise, way, that also relates to our subsequent semiclassical discussion. When the full beam in channel 2 impinges onto the first beam-splitter A, we obtain a superposition between two many-particle states: With an amplitude near unity, nothing happens (no tunneling takes place), and we denote this state as $|0\rangle$. There is a small chance (of amplitude t_A) for a particle to tunnel through A into channel 1, leaving behind a hole in channel 2. As time passes, the second part acquires an amplitude (relative to the first) that is given by the product of propagation amplitudes for the electron (ψ_1) and the hole (ψ_2^*), resulting in:

$$|0\rangle + t_A \psi_1 \psi_2^* |1_p, 2_h\rangle . \tag{2.21}$$
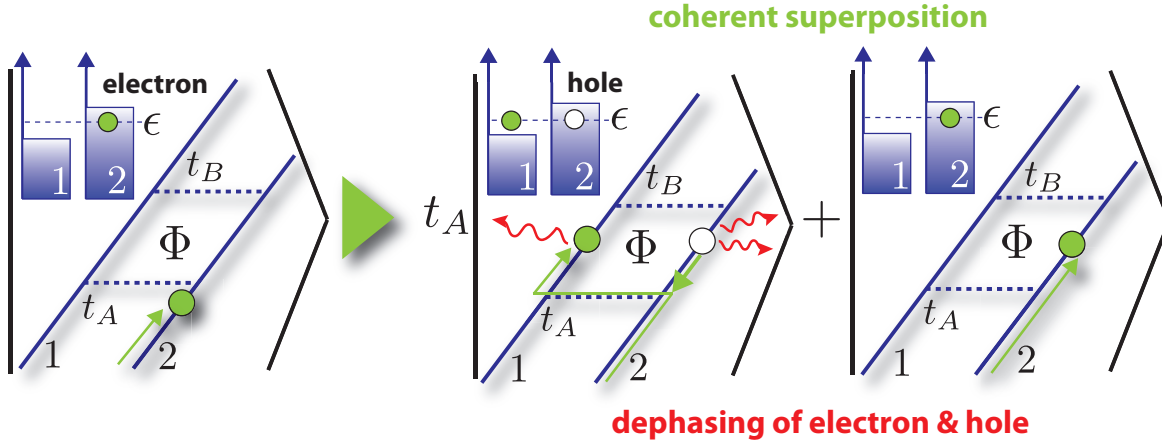
Figure 2.2: Illustration of an electron impinging onto the first beam-splitter A of the Mach-Zehnder interferometer in the situation that electrons flow from 2 to 1 for weakly coupled interferometer arms. One obtains a superposition of the electron flying through channel 1 or channel 2. The crucial point is that phase coherence between the two many-body states is destroyed if the electron and/or the hole is dephased, e.g., due to electron-electron interaction. As only the relative phase between the states is important we let the noise act only on the left ket. In the upper left corner of the pictorial kets the Fermi distributions of the two channels are illustrated.

Including the action of the second beam splitter B, and the Aharonov-Bohm phase, the total probability to detect an extra electron in the output port (channel 1) is therefore

$$\left| t_B e^{i\phi} + t_A \psi_1 \psi_2^* \right|^2, \tag{2.22}$$

which gives rise to the interference term

$$t_A t_B^* e^{-i\phi} \psi_1 \psi_2^* + c.c.. \tag{2.23}$$

Averaging the amplitudes over phase fluctuations induced by the interaction, we arrive at the propagators, replacing $\langle \psi_1 \rangle$ by the particle propagator $G_1^>$, and $\langle \psi_2^* \rangle$ by the hole propagator $G_2^<$. The full analysis keeps track of energy conservation. Thus, in the many-body picture, the observation of an interference term in the current is seen to depend both on the passage of an electron through channel 2 ($G_2^>$) as well as on the coherent propagation of the corresponding hole, of the same energy ω, in channel 1 ($G_1^<$). This issue has been discussed before, both for the Mach-Zehnder interferometer and for weak localization [11, 36, 32, 31]. For instance, in Chapter 8, investigating the influence of an external quantum bath on the coherence of one-dimensional electrons, we will derive a dephasing rate for the Green's function which is a sum of hole and electron scattering rate.

2.2 Visibility

In the Mach-Zehnder setup, the so called visibility is used as a measure of the coherence of the system. There are different definitions (experimentally, often the differential visibility is employed). However, we will define the visibility in terms of the total current, as

$$v_I(V,T) \equiv \frac{\max_\phi I_{coh}(\phi)}{I_0} = \frac{I_{\max} - I_{\min}}{I_{\max} + I_{\min}} . \tag{2.24}$$

The bias voltage is defined as $\mu_1 - \mu_2 = q_e V$ and we set $V > 0$. After a short calculation (see Appendix A.3) the visibility can be written in a compact form:

$$
\begin{aligned}
v_I =\ & \frac{2|t_a t_b^*|}{|t_a|^2 + |t_b|^2} \left(4\pi^2 \int_{-\infty}^{\infty} d\omega\ \nu(\omega) \cdot \nu(\omega - |q_e|\, V)(f(\omega - |q_e|) - f(\omega)) \right)^{-1} \times \\
& \left| \int_{-\infty}^{\infty} d\omega\ G^>(\omega, x_1) \cdot G^<(\omega - |q_e|\, V, -x_2) - G^<(\omega, x_1) \cdot G^>(\omega - |q_e|\, V, -x_2) \right| . \tag{2.25}
\end{aligned}
$$

We will also focus on zero temperature, as this seems to be the most interesting case. For $T = 0$ the visibility yields

$$v_I = \frac{2|t_a t_b^*|}{|t_a|^2 + |t_b|^2} \cdot \frac{\left| \int_0^{|q_e V|} d\omega\ G^>(\omega, x_1) \cdot G^<(\omega - |q_e|\, V, -x_2) \right|}{4\pi^2 \int_0^{|q_e V|} d\omega\ \nu(\omega) \cdot \nu(\omega - |q_e|\, V)} \quad (V \geq 0). \tag{2.26}$$

Note that the channel indices of the Green's functions are omitted, as in this formula the GFs are defined with respect to a fixed density and all the explicit dependence on the bias voltage is shifted to the GF arguments.

2.3 Summary

The main outcome of this introductory chapter is that a compact expression for the current and thereby for the visibiliy in lowest order in tunneling was derived. In lowest order in tunneling, the visibility v_I and therefore the coherence of the one-dimensional electron system only depends on the Green's functions $G^{>/<}(\epsilon, x)$. Therefore, investigating the coherence of one-dimensional electron systems is particularly reduced to the analysis of the Green's function. Consequently, in the upcoming Chapter 3, with help of bosonization we calculate the GF of a one-dimensional interacting electron system and evaluate numerically the current through the interferometer as well as the corresponding visibility.

Chapter 3

Single-particle Green's function

In the previous chapter, restricting the considerations to only weakly tunnel-coupled interferometer arms, the steady state current I and the visbility v_I were derived. The main result was that in this limit, the visibility and therefore the coherence of the electron system only depends on the single-particle Green's functions (GFs) $G^>(\epsilon, x)$ and $G^<(\epsilon, x)$. In the present chapter, we employ bosonization of the chiral one-dimensional electron system in order to calculate the GFs, thereby taking into account the full electron-electron interaction. For this, we follow closely the bosonization procedure in [21, 4, 14, 2, 6] .

Bosonization allows for the calculation of Green's functions even more complicated as the single-particle GFs considered in this chapter. For example, in Chapter 7 four-point correlation functions are derived, employing the bosonization technique. Although, the bosonization provides us with the correct solution for $G^>$, the physical interpretation of the result remains fairly difficult. This is one of the disadvantages of the bosonization formalism. In this work, we are mainly concerned with interpreting the results stemming from bosonization in most physical terms. To put it differently, bosonization serves as reference point for any further analysis. For example, in Chapter 4 we employ a physically motivated semiclassical ansatz for $G^>$ and compare the outcome to the bosonization solution.

It turns out that taking into account the full interaction potential, i.e., going beyond the usually assumed point-like electron interaction, as a main result two distinct energy regimes show up. While electrons flying high above the Fermi sea are dephased to the full extent, the decoherence of electrons in the close vicinity to the Fermi edge is largely suppressed. In general, for low-energy electrons the only significant effect of the electron-electron interaction is a certain velocity renormalization, compared to the non-interacting case. This is why, the chiral Luttinger liquid usually is considered as an effective Fermi liquid. However, allowing for a finite interaction range, in the high-energy limit the spectral properties of chiral systems are completly non-trivial.

While the GF $G^>(x,t)$ was studied in great detail, for instance in [6], besides the analysis in [43] (where the authors consider an artificial interaction potential with a sharp momentum cutoff), up to now, no particular attention was paid to its Fourier transform $G^>(\epsilon, x)$.

In Section 3.1 the bosonization method is introduced in two step: First of all, the bosonized Hamiltonian for the chiral one-dimensional electron system in terms of bosonic operators is derived (Subsection 3.1.1). In a second step, the fermionic field $\hat\psi$ is expressed only in terms of these bosonic modes (Subsection 3.1.2). After deriving the solution for the Green's function $G^>$ in Section 3.2, we discuss the GFs $G^>(x,t)$ and $G^>(\epsilon, x)$ (Subsections 3.2.2 and 3.2.3). Finally, we evaluate the visibility of the Mach-Zehnder interferometer in Eq. (2.26) for some interaction potential (Section 3.3).

3.1   Bosonization

In this section we bosonize the chiral one-dimensional electron system taking into account electron-electron interaction of finite range. Instead of introducing the bosonization with mathematical rigour (cf. [21]), the intention of this short introduction is to emphasize the reason why, in one dimension, one can find an expression for the fermionic field $\hat\psi$ in terms of bosonic operators. The bosonization procedure involves two steps. After introducing bosonic operators, so-called "plasmons", the Hamiltonian for the interacting electron system is re-expressed in terms of these bosonic fields. In a second step, one derives an operator identity connecting the fermionic field $\hat\psi$ and the plasmonic modes.

3.1.1   Bosonized Hamiltonian

We start from the Hamiltonian containing two-particle interactions for spin-polarized electrons moving in both directions

$$
\begin{aligned}
\hat{H}'_1 &= \hat{H}'_0 + \hat{H}'_{\text{int}} \\
&= -\int dx\, \hat\psi^\dagger(x)\left(\frac{1}{2m}\partial_x^2\right)\psi(x) + \hat{H}'_{\text{int}} \\
\hat{H}'_{\text{int}} &= \frac{1}{2}\int dx \int dx'\, \hat\psi^\dagger(x)\hat\psi^\dagger(x')U(x-x')\hat\psi(x')\hat\psi(x),
\end{aligned}
\tag{3.1}
$$

where $U(x)$ denotes the real interaction potential. The fermionic fields are defined as

$$
\hat\psi(x) = \frac{1}{\sqrt{L}}\sum_k e^{ikx}\hat{c}_k,
\tag{3.2}
$$

where $\hat{c}_k^\dagger$ applied to the vacuum state creates an electron with momentum k. Here, we assume a finite interaction range, i.e. the Fourier transform of U, $U_q = \int dx\, e^{-iqx}U(x)$, is cut off for $q \gg q_c$ with

$q_c \ll k_F$. Linearizing the electronic dispersion relation about the Fermi momentum $|k_F|$

$$\hat{H}_0 \quad = \quad \sum_k \left\{ v_F \left(k : \hat{c}^\dagger_{k,R} \hat{c}_{k,R} : -k : \hat{c}^\dagger_{k,L} \hat{c}_{k,L} : \right) - v_F k_F (\delta \hat{N}_R + \delta \hat{N}_L) \right\}, \qquad (3.3)$$

where v_F denotes the Fermi velocity (in the Mach-Zehnder interferometer the edge channel velocity), we introduce the so called Luttinger model. For this, the electrons are separated into two species, i.e., into right- and left moving electrons, $\hat{c}_{k,R}$ and $\hat{c}_{k,L}$ respectively and their linear spectrum is extended down to $-\infty$ [14]. The Fermi sea where all the states below the chemical potential are filled is replaced by a 'Dirac sea' where the infinite number of states with negative energy are assumed to be filled (cf. Fig. 3.1a). Nevertheless, the low-energy properties of $\hat{H}_0$ and $\hat{H}'_0$ are similar, as the interaction potential U_q is cut off for $q \gg q_c$ (where $q_c \ll k_F$) and the deep lying electrons do not contribute to the low-energetic excitations of the system. Formally, the Dirac sea is filled by an infinite number of electrons, which is why we normal order the Hamiltonian $\hat{H}_0$ with respect to the filled, non-interacting Dirac sea (denoted as $|\text{vac}\rangle$). As usual, we label normal ordered operators with $: \cdots :$, where equivalently we could write $: A := \hat{A} - \left\langle \text{vac}|\hat{A}|\text{vac} \right\rangle$. For example, in Eq.(3.3) $\delta \hat{N}_R \equiv \sum_k : \hat{c}^\dagger_{k,R} \hat{c}_{k,R} :$ is the normal ordered number operator. As we are only interested in a chiral electron system, the following considerations are restricted to right-moving electrons. The chiral, interacting part of the Hamiltonian in the momentum representation yields

$$\hat{H}_\text{int} \quad = \quad \frac{1}{2L} \sum_{q,k,k'} U_q : \hat{c}^\dagger_{k,R} \hat{c}^\dagger_{k',R} \hat{c}_{k'-q,R} \hat{c}_{k+q,R} : . \qquad (3.4)$$

In the next step we re-express Eq. (3.4) in terms of density fluctuations.

Density operators   The normal ordered density operator $\hat{\rho}_R(x)$ is introduced for the chiral system consisting of right-moving electrons as

$$\begin{aligned} \hat{\rho}_R(x) \quad &\equiv \quad : \hat{\psi}^\dagger_R(x) \hat{\psi}_R(x) : \\ \hat{\rho}_{q,R} \quad &= \quad \sum_k \hat{c}^\dagger_{k,R} \hat{c}_{k+q,R} \approx \sum_{k>0} \hat{c}^\dagger_{k,R} \hat{c}_{k+q,R}, \quad q \neq 0. \end{aligned} \qquad (3.5)$$

In the second line we safely neglect the low-lying electrons (with formal momentum $k < 0$) as due to the momentum cutoff $q_c \ll k_F$ in the interaction potential U_q they do not contribute to the low-energy properties of the system. We can now re-express the interacting part of the Hamiltonian $\hat{H}_\text{int}$
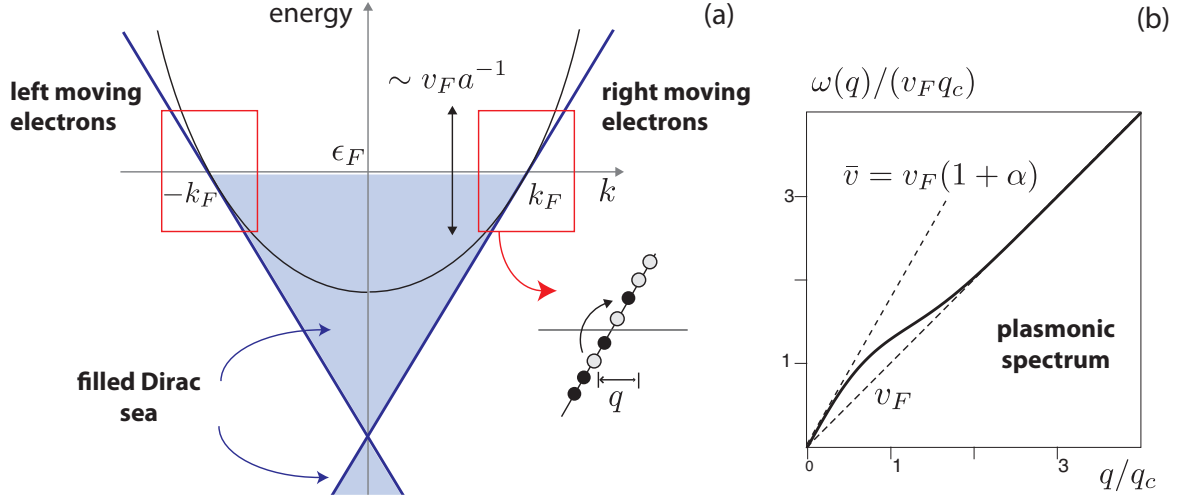
Figure 3.1: (a) Pictorial plot of the dispersion relation of non-interacting one-dimensional electrons (solid gray line). As mentioned in Subsection 3.1.1, the Luttinger theory assumes a spectrum linearized about the Fermi momentum k_F (solid blue lines), which is extended down to $-\infty$. Thereby, the right and left moving electrons are separated into two species. The filled Fermi sea is substituted by the filled "Dirac sea". Due to the linearization procedure, the theory is only valid at low energies, where only electrons in the close vicinity to the Fermi edge are involved in excitations (the finite bandwith, related to the cutoff parameter a (see main text) is indicated by red boxes). Inset: Applying the density operator $\hat{\rho}_q^\dagger$ to the vacuum state creates a superpostion of electron-hole pairs. Basically, these are the relevant low-energy excitations. (b) Dispersion relation of the bosonic modes $\hat{b}_q$ for an interaction potential $U_q = 2\pi\alpha v_F e^{-(q/q_c)^2}$ with $2\pi\alpha = 5$. For $q \ll q_c$, the velocity of the plasmons is renormalized to $\bar{v} = v_F(1+\alpha)$, while due to the finite interaction range in the limit $q \gg q_c$ the bare velocity v_F is reproduced, i.e., there are two distinct energy regimes.

Eq. (3.4) in terms of the density operators $\hat{\rho}_{q,R}$:

$$
\begin{aligned}
\hat{H}_{\mathrm{int}} &= \frac{1}{2} \sum_{q,k,k'} U_q : \hat{c}_{k,R}^\dagger \hat{c}_{k',R}^\dagger \hat{c}_{k'-q,R} \hat{c}_{k+q,R} : \\
&= \frac{1}{L} \sum_{q>0} U_q \hat{\rho}_{q,R}^\dagger \hat{\rho}_{q,R} + \underbrace{\frac{1}{2L} U(q=0) : \left[\sum_k \hat{c}_k^\dagger \hat{c}_k \right]^2 :}_{\text{Hartree term}} - \underbrace{\frac{U(x=0)}{2} \sum_k : \hat{c}_k^\dagger \hat{c}_k :}_{\text{Fock term}} . \quad (3.6)
\end{aligned}
$$

The emerging of the Hartree-Fock terms in Eq. (3.6) has to be noted in particular. The Fock correction naturally cancels out contributions stemming from the unphysical interaction of the electrons with itself, as the Pauli principle does not allow for two particles to be exactly at the same position in space. For small changes in the particle number we can linearize the Hartree-Fock term in $\delta \hat{N}_R$. As a consequence, we can simply incorporate the Hartree-Fock contribution into a re-definition of the chemical potential. The main point is that it is obviously possible to reformulate the interacting part of the Hamiltonian only in terms of the density operators $\hat{\rho}_{q,R}$.

Bosonic operators $\{\hat{b}_q, \hat{b}_q^\dagger\}$ The crucial step behind the bosonization of the Hamiltonian Eq. (3.3) is that it is possible to find operators $\{\hat{b}_q, \hat{b}_q^\dagger\}$ which diagonalize the Hamiltonian and fulfill the bosonic commutation relations. It can be shown [21, 14, 4] that for the Tomonaga-Luttinger model (where the linearized dispersion relation is is extended down to $-\infty$) the operators

$$
(q>0) \quad \hat{b}_q = \left(\frac{2\pi}{Lq} \right)^{1/2} \hat{\rho}_{q,R} \qquad \hat{b}_q^\dagger = \left(\frac{2\pi}{Lq} \right)^{1/2} \hat{\rho}_{-q,R} \quad (3.7)
$$

represent well defined bosonic excitations, i.e., they fulfill

$$
[\hat{b}_q, \hat{b}_{q'}^\dagger] = \delta_{q,q'}. \quad (3.8)
$$

In the remainder of this work we will refer to these modes as 'plasmons', i.e., modulations in the electron density. Furthermore, it turns out [21, 4, 14] that the free part of $\hat{H}_0$ can be written in terms of those operators:

$$
\hat{H}_0 \quad \sim \quad \sum_{q>0} v_F q \hat{b}_q^\dagger \hat{b}_q. \quad (3.9)
$$

Formula Eq. (3.9) lies at the root of the bosonization method; however, we still have to fix the constant in Eq. (3.9). As the bosonic operators $\{\hat{b}_q, \hat{b}_q^\dagger\}$ only describe the low-energetic excitations of the chiral interacting electron system, we have to add the energy related to a change in the electron number.

Adding n electrons to the filled Fermi sea increases the energy by

$$\frac{2\pi v_F}{L} \sum_{j=\bar{N}_R}^{\bar{N}_R+n} j \;\; = \;\; \frac{\pi v_F}{L} \left\{ \left(n + \bar{N}_R\right)\left(n + \bar{N}_R + 1\right) - \bar{N}_R\left(\bar{N}_R + 1\right) \right\}. \tag{3.10}$$

where $\bar{N}_R$ is the mean electron number in the channel. Therefore, up to a constant we have to add the contribution $\frac{\pi v_F}{L}(\hat{N}_R + \bar{N}_R)(\hat{N}_R + \bar{N}_R + 1)$.

Bosonized Hamiltonian   Finally, we can sum up the different terms. Linearizing the part depending on the normal ordered electron number $\delta\hat{N}_R$, i.e., keeping only terms linear in $\delta\hat{N}_R$ yields the bosonized Hamiltonian (omitting a further constant)

$$\hat{H}_1 \;\; = \;\; \sum_{q>0} \omega_q \hat{b}_q^\dagger \hat{b}_q + \mu\delta\hat{N}_R, \tag{3.11}$$

where $\mu = u + 2\pi v_F \bar{\rho}_R$ (with $\bar{\rho}_R = \bar{N}_R/L$) and u is a constant which fixes the chemical potential of the channel. For example, u contains the energy shift due to the Hartree-Fock contribution in Eq. (3.6) and to any external applied gate voltage (here we set $u = 0$). The plasmonic dispersion relation (see Fig. 3.1b) is given by

$$\omega_q \;\; = \;\; v_F q \left(1 + \frac{U_q}{2\pi v_F}\right). \tag{3.12}$$

For the following discussions, we introduce the dimensionless coupling constant $\alpha = \frac{U(q\to 0)}{2\pi v_F}$, where $\alpha \in]-1, \infty[$. The renormalized plasmon velocity at small wavenumbers is $\bar{v} = v_F(1 + \alpha)$. Negative values of the coupling constant are related to attractive interactions, positive values to repulsion (at small wavenumbers). For $\alpha \to -1$ the plasmon velocity tends to zero, $\bar{v} \to 0$. For $\alpha < -1$ the system is unstable, i.e. formally $\omega(q) < 0$ for $q > 0$. To conclude, we sucessfully mapped the Hamiltonian (quartic in fermionic fields) in Eq. 4.39 to a representation diagonal (and quadratic) in bosonic operators (Eq. (3.11)). However, this is not the whole story. As we are interested in electronic properties of the system, such as the single particle Green's function $G^>(x, t)$, we still have to establish a connection between the bosonic operators $\{\hat{b}_q, \hat{b}_q^\dagger\}$ and the fermionic fields $\{\hat{\psi}, \hat{\psi}^\dagger\}$.

3.1.2   Bosonization of the Fermionic field

There are various ways to introduce the bosonization of fermionic operators, ranging from mathematical rigorous derivations of the underlying operator identity [21, 14] to more intuitive and rather simple approaches, for instance presented in [14, 2]. Here, we want to point out the physical reason why in one dimension a representation of a fermionic field in terms of bosons can be found. The bosonic representation is constructed "from scratch", closely following the derivation in [2]. What

are the physical properties a fermionic operator $\hat{\psi}^\dagger(x)$ must fulfill? First of all, it has to create a particle at x thereby deforming the particle density and it has to increase the particle number by one unit. Secondly, it has to fulfill the fermionic exchange statistics, i.e. $\{\hat{\psi}^\dagger(x_1), \hat{\psi}^\dagger(x_2)\} = 0$. The construction scheme starts from a bosonic field $\hat{B}^\dagger(x)$ creating a unit charge excitation at x and the corresponding density operator $\delta\hat{\rho}(x) \equiv \hat{B}^\dagger(x)\hat{B}(x) - \bar{\rho}$. Note that we introduced $\delta\hat{\rho}$ as the density operator describing the deviations from the mean particle density $\bar{\rho}$. The operator $\delta\hat{\rho}$ is closely related to the operators $\hat{\rho}_R$ we introduced in the previous subsection, however it also contains the homogeneous change in the density by a variation of the total particle number: $\delta\hat{\rho} = \hat{\rho} + \delta\hat{N}/L$. The main point is that in one dimension, with help of a Jordan-Wigner transformation, one can re-express the fermionic field in terms of the bosons $\hat{B}$:

$$\hat{\psi}^\dagger(x) = \exp\left(i\pi m \int_{-\infty}^{x} dx' \; [\delta\hat{\rho}(x') + \bar{\rho}]\right) \hat{B}^\dagger(x), \tag{3.13}$$

where m is an arbitrary odd integer. The physical meaning of the exponent in Eq. (3.13), the so-called Wigner string, is rather simple. Namely, it counts the number of particles to the left of the particle created at x. This ensures the fermionic exchange statistics, as (we set $x_1 > x_2$ and let $\bar{N}$ denote the number of particles in the vacuum state $|\text{vac}\rangle$)

$$\begin{aligned}
\hat{\psi}^\dagger(x_1)\hat{\psi}^\dagger(x_2)\,|\text{vac}\rangle &= e^{i\pi \int_{-\infty}^{x_1} dx' \, \hat{\rho}(x')} \hat{B}^\dagger(x_1) e^{i\pi \int_{-\infty}^{x_2} dx' \, \hat{\rho}(x')} \hat{B}^\dagger(x_2)\,|\text{vac}\rangle \\
&= e^{i2\pi\bar{N} + i\pi} \hat{B}^\dagger(x_1)\hat{B}^\dagger(x_2)\,|\text{vac}\rangle,
\end{aligned}$$

but

$$\begin{aligned}
\hat{\psi}^\dagger(x_2)\hat{\psi}^\dagger(x_1)\,|\text{vac}\rangle &= e^{i\pi \int_{-\infty}^{x_2} dx' \, \hat{\rho}(x')} \hat{B}^\dagger(x_2) e^{i\pi \int_{-\infty}^{x_1} dx' \, \hat{\rho}(x')} \hat{B}^\dagger(x_1)\,|\text{vac}\rangle \\
&= e^{i2\pi\bar{N}} \hat{B}^\dagger(x_2)\hat{B}^\dagger(x_1)\,|\text{vac}\rangle.
\end{aligned}$$

Therefore, it follows that the representation in Eq. (3.13) produces an additional minus sign interchanging two fermionic creation or annihilation operators. Yet this is exactly what was demanded. Now, we can define a bosonic field

$$\hat{\phi}(x) \equiv -\pi \int_{-\infty}^{x} dx' \, \delta\hat{\rho}(x'), \tag{3.14}$$

yielding: $\delta\hat{\rho}(x) = -\nabla\hat{\phi}(x)/\pi$. In a next step, we switch to the usual phase-density representation of the bosonic field $\hat{B}(x)$

$$\begin{aligned}
\hat{B}(x) &\equiv (\bar{\rho} + \delta\hat{\rho}(x))^{1/2} \, e^{i\hat{\theta}(x)} \\
\hat{B}^\dagger(x) &\equiv (\bar{\rho} + \delta\hat{\rho}(x))^{1/2} \, e^{-i\hat{\theta}(x)}, \tag{3.15}
\end{aligned}$$

where the hermitian field $\hat{\theta}(x)$ takes care of the phase of the bosonic excitation created by $\hat{B}^\dagger$. In order to fulfill the bosonic commutation relations $[\hat{B}(x), \hat{B}^\dagger(x')] = \delta(x - x')$ one can show that the density $\delta\hat{\rho}(x)$ and $\hat{\theta}(x)$ are required to form a canonically conjugated pair. Thus, the important relation follows:

$$[\delta\hat{\rho}(x), \hat{\theta}(x')] = [\hat{\theta}(x'), \frac{1}{\pi}\nabla\hat{\phi}(x)] = i\delta(x - x'). \tag{3.16}$$

The meaning of the identity Eq. (3.16) is obvious, thinking of the analogous situation in single particle quantum mechanics. There, the position operator $\hat{x}$ and the momentum operator $\hat{p}$ form such a conjugated pair and the application of $\exp(-i\hat{p}x)$ shifts the whole wave functionby x. This is why $\hat{p}$ is denoted as the generator of translation. Remaining in this picture, Eq. (3.16) identifies $\hat{\theta}(x)$ with the generator of a 'charge shift', i.e. the application of $\exp(i\hat{\theta}(x))$ to the vacuum state increases the charge by one unit. Note that in Eq. (3.13) some ambiguity arises as the relation is valid for any odd integer m. The most general representation of $\hat{\psi}$ is given by a superposition of all possible terms. To derive the final result (to get , e.g., the correct normalization, etc.) one can invoke the fermionic anti-commutation relation $\left\{\hat{\psi}(x), \hat{\psi}^\dagger(x')\right\}$, yielding

$$\hat{\psi}^\dagger(x) = \left(\bar{\rho} - \frac{1}{\pi}\nabla\hat{\phi}\right)^{1/2} \sum_{m \text{ odd}} \left\{\exp\left(i\pi m \int_{-\infty}^{x} dx' \, [\delta\hat{\rho}(x') + \bar{\rho}]\right) e^{-i\hat{\theta}(x)}\right\}. \tag{3.17}$$

$$= \left(\bar{\rho} - \frac{1}{\pi}\nabla\hat{\phi}\right)^{1/2} \sum_{m \text{ odd}} \left\{e^{im\pi(\bar{\rho}x - \hat{\phi}(x)/\pi)} e^{-i\hat{\theta}(x)}\right\}. \tag{3.18}$$

In a one-dimensional system consisting of right- and left moving electrons, the average density is given by: $\bar{\rho} = k_F/\pi$. Thus it follows that the representation in Eq. (3.17) contains terms proportional to $e^{\pm ik_F x}$, but also higher momenta. However, as we are interested only in the low-energy properties of the system it suffices to restrict to the contributions with $e^{\pm ik_F x}$ [2, 14]. This approximation sometimes serves as a starting point of the bosonization and is equivalent with assuming that only the part of the single-particle operator acting close to the Fermi edge determines the low-energy properties [14]. Then, separating the right- and left moving electron one can write

$$\hat{\psi}(x) = \frac{1}{\sqrt{L}} \sum_k e^{ikx} \hat{c}_k$$

$$\approx \frac{1}{\sqrt{L}} \sum_{k \sim k_F} e^{ikx} \hat{c}_k + \frac{1}{\sqrt{L}} \sum_{k \sim -k_F} e^{ikx} \hat{c}_k$$

$$= \hat{\psi}_R + \hat{\psi}_L. \tag{3.19}$$

Turning back to Eq. (3.17) in the lowest order of $\nabla\hat{\phi}$ leads us to:

$$\hat{\psi}(x) \approx \sqrt{\bar{\rho}} e^{ik_F x} e^{i(\hat{\theta}(x) - \hat{\phi}(x))} + \sqrt{\bar{\rho}} e^{-ik_F x} e^{i(\hat{\theta}(x) + \hat{\phi}(x))}. \tag{3.20}$$

Klein factors   Before the final expression for the single particle operators in terms of bosonic fields can be given, there is still one problem left. Namely, the expression for the fermionic field does not fulfill all of the demanded criteria, as it does not increase the fermion number of the system by one unit. For this task one introduces so-called Klein factors $\hat{F}_R$, which annihilates a fermion in a spatially homogeneous way and obeys the following commutation relations (where the label $j = R, L$ the chirality of the electron created):

$$\{F_i, F_j^\dagger\} = \delta_{ij}; \ \{F_i, F_j\} = \{F_i^\dagger, F_j^\dagger\} = 0. \tag{3.21}$$

In addition the Klein factors are assumed to commute with the bosonic excitations $\hat{b}$. This yields the final expression for the chiral fermionic fields $\hat{\psi}_{R,L}(x)$

$$
\begin{aligned}
\hat{\psi}(x) &\approx \hat{F}_R \sqrt{\bar{\rho}} e^{ik_F x} e^{i(\hat{\theta}(x) - \hat{\phi}(x))} + \hat{F}_L \sqrt{\bar{\rho}} e^{-ik_F x} e^{i(\hat{\theta}(x) + \hat{\phi}(x))} \\
&\equiv \hat{\psi}_R + \hat{\psi}_L.
\end{aligned}
\tag{3.22}
$$

In the following we focus our attention on the right-moving electrons:

$$\hat{\psi}_R(x) = \hat{F}_R \sqrt{\bar{\rho}} e^{ik_F x} e^{i(\hat{\theta}(x) - \hat{\phi}(x))}. \tag{3.23}$$

The only step left is, to find the expression for the bosonic fields $\hat{\phi}$ and $\hat{\theta}$ in terms of the bosonic operators $\{\hat{b}_q, \hat{b}_q^\dagger\}$, whose dynamics are governed by the bosonized Hamiltonian in Eq. (3.11).

Finite bandwith and chiral field $\hat{\psi}_{\mathbf{R}}(\mathbf{x})$ The Hamiltonian in Eq. (3.9) describes the low-energy properties of a one-dimensional electron system under the assumption of a linearized dispersion relation. In the framework of the Luttinger model one extends the linear dispersion relation down to $-\infty$. As a consequence, the commutation relations (Eq. (3.8)) for the fields $\hat{b}_q, \hat{b}_q^\dagger$ are fulfilled exactly. In turn, one has to introduce a finite bandwith, i.e., a cutoff parameter a with the dimension of a length ($[a] = m$) regularizing the involved momentum integrals (cf. Fig. 3.1a). Formally, the cutoff parameter sets the length scale of the system. However, in the end one recovers the Luttinger model by taking the limit $a \to 0$. Under the assumption of a finite interaction range (i.e., $U_q \to 0$ for $q \gg q_c$) this is possible, as in the final expressions we can replace the original cutoff a by q_c^{-1} (we will see this when calculating the single particle Green's function $G^>(x, t)$). Therefore, in the remainder of this work the length scale is set by q_c^{-1}. To stay in the low-energy regime where the linearisation of the dispersion relation is valid, the involved momenta are demanded to be much smaller than k_F. Therefore, for the cutoff parameter and q_c it follows: $a, q_c^{-1} \gg k_F^{-1}$.

The canonical conjugated fields $\hat{\phi}$ and $\hat{\theta}$ What is the explicit form of the bosonic fields $\hat{\phi}$ and $\hat{\theta}$ if we consider only right-moving particles? At this point, one has to establish the connection between the operators $\{\hat{b}_q, \hat{b}_q^\dagger\}$, whose dynamics are governed by the Hamiltonian $\hat{H}_0$ in Eq. (3.9) and the fields $\hat{\phi}$ and $\hat{\theta}$. This can be done, comparing each of those fields to the density operators $\hat{\rho}_q$, i.e., considering Eqs. (3.7) and (3.14). By definition, $\hat{\phi}$ is given by $-\frac{1}{\pi}\nabla\hat{\phi}(x) \equiv \hat{\rho}_R(x) + \delta\hat{N}_R/L$. Thus we have

$$\hat{\phi}(x) \quad = \quad -\frac{\pi x}{L}\delta\hat{N}_R + i\pi\sum_{q>0}\frac{1}{\sqrt{2\pi Lq}}e^{-aq/2}\left\{\hat{b}_q e^{iqx} - \text{h.c.}\right\}. \tag{3.24}$$

Furthermore, from the commutation relation between $\hat{\theta}$ and $\hat{\rho}_R$, $\left[\hat{\rho}_R(x), \hat{\theta}(x')\right] = i\delta(x-x')$, for chiral systems, it follows that

$$\hat{\theta}(x) \quad = \quad -\hat{\phi}(x). \tag{3.25}$$

In the limit of infinitely large chiral electron systems $L \to \infty$ we can drop the first term in Eq. (3.24). According to Eq. (3.22) we can combine the fields $\hat{\phi}$ and $\hat{\theta}$ into one chiral bosonic field $\hat{\Phi}(x)$, such that the single-particle operator $\hat{\psi}_R(x)$ can be written as

$$\hat{\psi}_R(x) \quad = \quad \frac{\hat{F}_R}{\sqrt{2\pi a}}e^{ik_F x}e^{-i\hat{\Phi}(x)}$$

$$\hat{\Phi}(x) \quad = \quad i\sum_{q>0}\sqrt{\frac{2\pi}{Lq}}e^{-aq/2}\left\{\hat{b}_q e^{iqx} - \text{h.c.}\right\}. \tag{3.26}$$

Note that here we substituted the mean density $\bar{\rho}_R$ by $(2\pi a)^{-1}$, as $\bar{\rho}_R = \int_{-\infty}^0 (dk)\,e^{ak} = (2\pi a)^{-1}$.

3.2   Single particle Green's function

In Chapter 2 it was derived that the effect of the intrinsic electron-electron interactions on the coherence properties of a Mach-Zehnder interferometer in the weak-tunneling limit is contained in the single-particle Green's function. In this section, with help of the bosonization method, the Green's function is evaluated explicitly.

3.2.1   Green's function from bosonization

The single-particle Green's function $G^>(x,t)$ defined in Eq. (2.10), can be evaluated explicitly using the bosonized single particle operators $\hat{\psi}$ defined in Eq. (3.26). The calculation is done quickly using the fact, that the Hamiltonian in terms of the bosonic operators is quadratic, i.e. the field $\hat{\Phi}[\hat{b}, \hat{b}^\dagger]$ can be treated like a Gaussian (quantum) variable. In terms of the bosonized representation the Green's

function for right moving electrons yields (where we omit the label noting the chirality)

$$
\begin{aligned}
G^>(x,t) &= -i\left\langle \hat{\psi}_R(x,t)\hat{\psi}_R^\dagger(0,0)\right\rangle \\
&= \frac{-i}{2\pi a}e^{ik_F x}\left\langle \hat{F}_R(t)\hat{F}_R^\dagger\right\rangle\left\langle e^{-i\hat{\Phi}(x,t)}e^{i\hat{\Phi}(0,0)}\right\rangle.
\end{aligned}
\tag{3.27}
$$

The time dependence of the Klein factors can be obtained from the Heisenberg equation $\frac{d}{dt}\hat{F}_R = -i[\hat{F}_R,\hat{H}_0]$. While the Klein factors commute with the bosonic operators $\hat{b}_q$, the commutator with the number operators yields: $[\hat{F}_R,\delta\hat{N}_R]=\hat{F}_R$. Therefore, from Eq. (3.11) it follows: $\hat{F}_R(t)=e^{-i\mu t}\hat{F}_R$. For a chiral electron system we have $\mu = 2\pi v_F\bar{\rho}_R$ and $\bar{\rho}_R = k_F/2\pi$. Thus, the Green's function can be simplified to

$$
\begin{aligned}
G^>(x,t) &= \frac{-i}{2\pi a}e^{-i\mu(t-x/v_F)}\left\langle e^{-i\hat{\Phi}(x,t)}e^{i\hat{\Phi}(0,0)}\right\rangle \\
&= \frac{-i}{2\pi a}e^{-i\mu(t-x/v_F)}\exp\left[\left\langle \hat{\Phi}(x,t)\hat{\Phi}(0,0)\right\rangle - \left\langle \hat{\Phi}(0,0)^2\right\rangle\right],
\end{aligned}
\tag{3.28}
$$

where in the last line we make use of the fact that the bosonic field $\hat{\Phi}$ is a linear function of the operators $\{\hat{b}_q,\hat{b}_q^\dagger\}$. As the Hamiltonian is quadratic in those operators, the well known formula for averages over Gaussian random variables $\hat{\varphi}: \left\langle e^{-i\hat{\varphi}}\right\rangle = \exp\left(-\frac{1}{2}\left\langle \hat{\varphi}^2\right\rangle\right)$ can be applied. In a very last step, we only have to calculate the exponent in Eq. (3.28). For this, we start from the definition of the chiral field $\hat{\Phi}$ in Eq. (3.26):

$$
\begin{aligned}
\left\langle \hat{\Phi}(x,t)\hat{\Phi}(0,0)\right\rangle &= -\frac{2\pi}{L}\sum_{q,q'>0}\frac{1}{\sqrt{qq'}}e^{-a(q+q')}\{ \\
&\quad \left\langle \left(\hat{b}_q(t)e^{iqx}-\hat{b}_q^\dagger(t)e^{-iqx}\right)\left(\hat{b}_{q'}-\hat{b}_{q'}^\dagger\right)\right\rangle\} \\
&= \frac{2\pi}{L}\sum_{q,q'>0}\frac{1}{\sqrt{qq'}}e^{-a(q+q')}\{ \\
&\quad e^{i(qx-\omega_q t)}\left\langle \hat{b}_q\hat{b}_q^\dagger\right\rangle\delta_{q,q'} + e^{-i(qx-\omega_q t)}\left\langle \hat{b}_q^\dagger\hat{b}_q\right\rangle\delta_{q,q'}\},
\end{aligned}
$$

where we plugged in the time dependence of the bosonic operators $\hat{b}_q(t) = e^{-i\omega_q t}\hat{b}_q$. Finally the exponent in Eq. (3.28) yields (introducing the Bose-Einstein distribution function $\bar{n}(\omega) \equiv [\exp(\beta\omega)-1]^{-1}$)

$$
\begin{aligned}
\left\langle \hat{\Phi}_j(x,t)\hat{\Phi}_j(0,0)\right\rangle - \left\langle \hat{\Phi}_j(0,0)^2\right\rangle &= \int_0^\infty \frac{dq}{q}e^{-aq}\left\{\left[e^{i(qx-\omega_q t)}-1\right](\bar{n}(\omega_q)+1)\right. \\
&\quad \left.\left[e^{-i(qx-\omega_q t)}-1\right]\bar{n}(\omega_q)\right\}.
\end{aligned}
\tag{3.29}
$$

In the end we have to send $a \to 0$. Therefore we replace the cutoff parameter a by the interaction range q_c^{-1}. This can be achieved by factoring off the non-interacting Green's function $g_j^>(x,t)$.

Following, the same lines we can easily derive the corresponding expressions for the hole Green's function $G^< \equiv i\langle\hat{\psi}_R^\dagger(0,0)\hat{\psi}_R(x,t)\rangle$. The result is

$$G^{>/<}(x,t) = e^{-i\mu(x/v_F-t)}g^{>/<}(x,t)\exp[S_R(x,t)\pm iS_I(x,t)], \qquad (3.30)$$

where the non-interacting Green's function for right moving electrons is given by (for instance, see [21])

$$g^{>/<}(x,t) = \frac{1}{2\beta v_F}\cdot\frac{1}{\sinh[\frac{\pi}{\beta v_f}(x-v_Ft\pm i0^+)]}. \qquad (3.31)$$

One may note the following identities for $\mu = 0$: $G^{>/<}(x,t) = -[G^{>/<}(-x,-t)]^*$ and $[G^{>/<}(x,t)]^* = G^{</>}(x,t)$. All the effects of the interaction are now included in the exponent where we have to subtract the non-interacting contribution, as we factored off the non-interacting Green's function

$$S_R = \int_0^\infty \frac{dq}{q}\{\underbrace{\coth[\frac{\beta\omega_q}{2}]\,[\cos[qx-\omega_qt]-1]}_{\tilde{S}_R(\omega_q)}-\tilde{S}_R(\omega_q\to qv_F)\} \qquad (3.32)$$

$$S_I = \int_0^\infty \frac{dq}{q}\{\underbrace{\sin[qx-\omega_qt]}_{\tilde{S}_I(\omega_q)}-\tilde{S}_I(\omega_q\to qv_F)\}. \qquad (3.33)$$

One may note that in Eqs. (3.32) and (3.33) the non-interacting parts $\tilde{S}_{R,I}$ regularize the integrand, as in the limit $q/q_c \to \infty$ the interacting dispersion relation turns into the non-interacting one: $\omega_q \to v_Fq$.

3.2.2   Discussion of the Green's function in space and time

In this section, we discuss the Green's function as a function of space and time. A more detailed discussion can be found in [6]. The modulus of the Green's function $G^>(x,t)$ is shown in Fig. 3.2, at zero temperature (to which we restrict our discussion).In the following, all numerical evaluations are performed using a generic smooth interaction potential $U_q = U_0e^{-(|q|/q_c)^s}$. We note that all the qualitative results are valid for potentials which are finite at zero momentum ($U_0 \neq 0$) and which are cut off beyond some momentum scale. Those assumptions are not restrictive and, for example, are fulfilled for a Coulomb potential with screening in a quasi one-dimensional channel of finite width. In Fig. 3.2, we observe as the main feature that the Green's function splits into two parts during its propagation. One of them propagates with the bare Fermi velocity v_F and represents the unperturbed Green's function, i.e. the high energy part. For increasing time its weight decreases, i.e., the amplitude of the bare electron to arrive at x without being scattered decreases. The other peak represents the low energy part, stemming from energies below $\epsilon - \mu \sim v_Fq_c$. It moves with the renormalized velocity $\bar{v}$.

We can obtain this structure of $G^>(x,t)$ from a crude approximation. Namely for $T = 0$, in a first
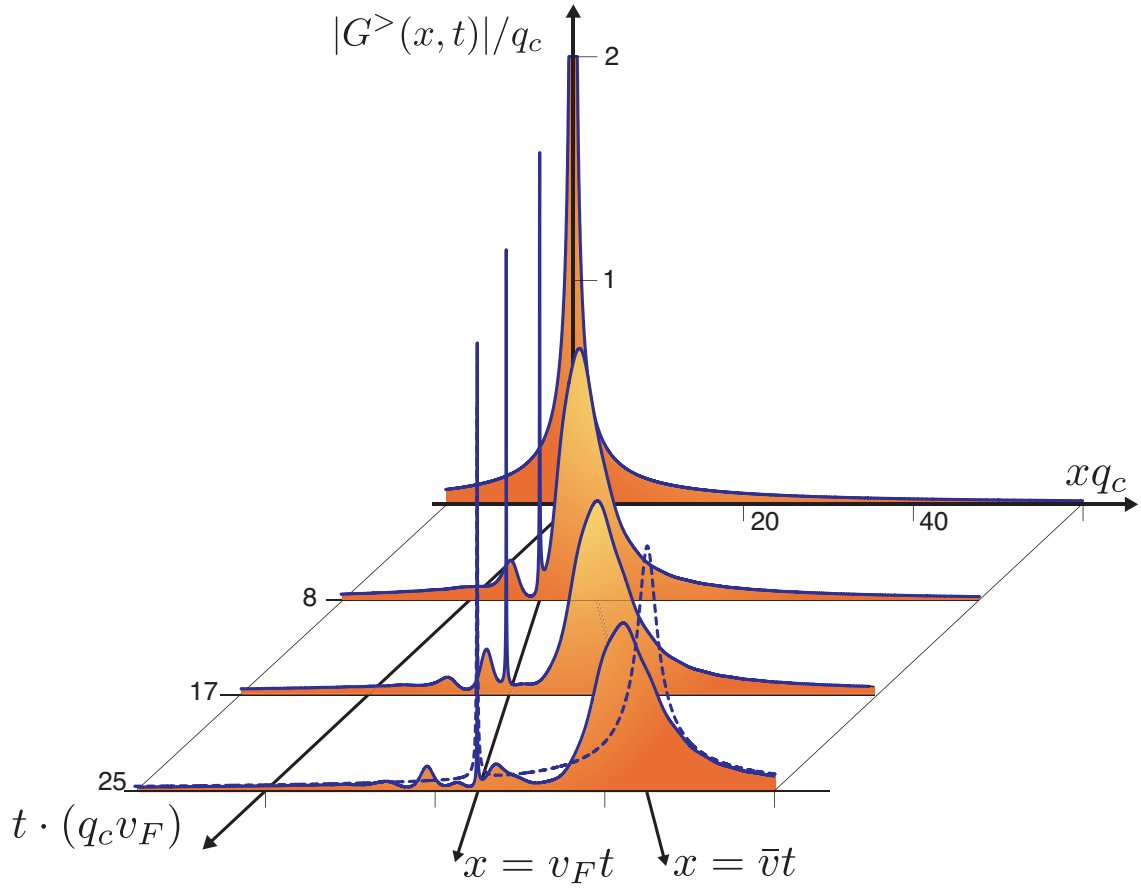
Figure 3.2: Numerical evaluation of $|G^>(x,t)|$ at zero temperature $T = 0$ resulting from bosonization, as a function of x and t (solid blue lines). The weight of the sharp peak at $x = v_F t$ decreases for increasing propagation times t. The dashed blue line shows an approximation of the Green's function (see Eq. (3.35)), which yields good qualitative agreement with the full solution. The plot is done for $U_q = U_0 e^{-(q/q_c)^2}$ with $\frac{U_0}{v_F} = 2\pi\alpha = 5$.

approximation we can cut the momentum integral due to the fact that for $q \gg q_c$ the integrand vanishes, i.e.,

$$S[x,t] \equiv S_R + iS_I \approx \int_0^\infty \frac{dq}{q} e^{-q/q_c} \left[\exp[iq(x - \bar{v}t)] - 1\right] - \int_0^\infty \frac{dq}{q} e^{-q/q_c} \left[\exp[iq(x - v_F t)] - 1\right].$$

The integrals are known and yield

$$S[x,t] \approx \ln\left[\frac{x - v_F t + iq_c^{-1}}{x - \bar{v}t + iq_c^{-1}}\right]. \tag{3.34}$$

The structure of the Green's function is thus given by

$$G_{T=0}^>(x,t) \approx \frac{1}{2\pi} \frac{1}{x - v_F t + i0^+} \cdot \left[\frac{x - v_F t + iq_c^{-1}}{x - \bar{v}t + iq_c^{-1}}\right], \tag{3.35}$$

displaying both the sharp peak at $x = v_F t$ and the broadened peak at $x = \bar{v}t$, whose width is set by q_c^{-1}. In Fig. 3.2 one can observe a fairly good agreement between the full result and this first approximation.

3.2.3   Green's function vs. position and energy

As shown above in Eq. (2.20) and (2.26), the current through the interferometer is determined by the propagators $G^{>/<}(\epsilon, x)$. Therefore, in the following our main focus will be on this function, which can be thought of as the amplitude for an electron of energy ϵ to propagate unperturbed over a distance x. The function is shown in Fig. 3.3, where we plot the numerical evaluation of the exact result obtained using the bosonization technique. This is done for two values of coupling strength α and for different interaction potentials. There are some main features which can be observed in Fig. 3.3:

- At $x = 0$, where $|G^>(x = 0, \epsilon)| = 2\pi\nu(\epsilon)$ equals the tunneling density of states, there is a finite dip at low energies. This is a static interaction effect. For repulsive interactions it represents the suppression of the tunneling density by a factor $v_F/\bar{v}$, due to the interaction-induced increase of the velocity $\bar{v}$. At high energies ($\epsilon \gg v_F q_c$), the non-interacting density of states is recovered.

- At any fixed energy ϵ, the Green's function decays with increasing propagation length x. The shape of the decay (as a function of x) becomes independent of energy for high energies. In contrast, the decay is suppressed for energies below $\epsilon \sim v_F q_c$, and there is no decay in the limit $\epsilon \to 0$. The decay of the GF is equivalent to dephasing (since in our model there are no interbranch interactions and correspondingly no vertex corrections). As a consequence, the absence of decay at zero energy will lead to perfect visibility at $T = 0, V \to 0$.

- At larger x, there are oscillations in the Green's function. These result from the double-peak structure in the time-domain, with peaks at $x = vt$ and $x = \bar{v}t$. These lead to a beating term
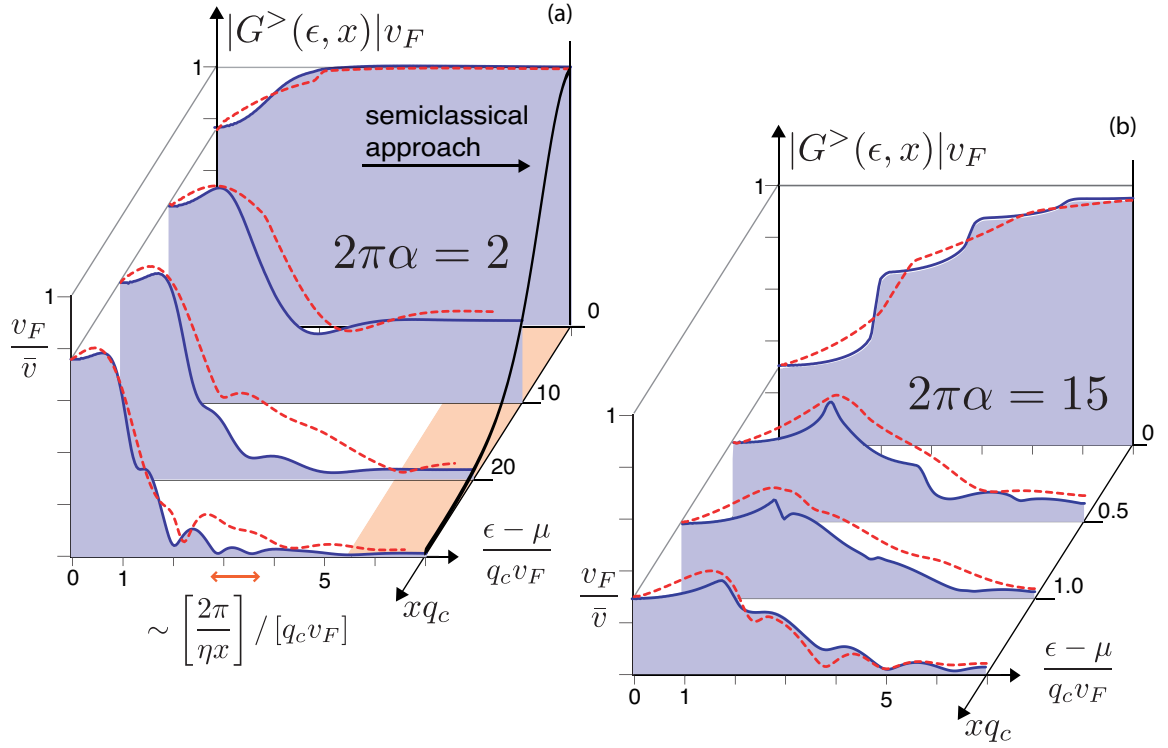
Figure 3.3: a) The electron Green's function $|G^>(x, \epsilon)|$ for various lengths x as a function of energy ϵ, evaluated using bosonization, for $U(q) = U_0 e^{-(q/q_c)^2}$ [solid blue lines] and for $U(q) = U_0 e^{-|q/q_c|}$ [dashed red lines]. At high energies, the result coming from the semiclassical approach for the Gaussian potential [solid black line] is shown. The red area indicates the regime of validity for the semiclassical (high-energy) approximation we introcude in Chapter 4. The interaction strengths are: $2\pi\alpha = 2$ (a) and $2\pi\alpha = 15$ (b). In the high-energy limit, the semiclassical solution is valid for arbitrary coupling strength. However, the energies for which the description is valid become larger for increasing coupling strength. In (b) this limit is beyond the presented energy interval. Therefore, the semiclassical solution is not shown here.

$\exp[i\omega x(v^{-1} - \bar{v}^{-1})]$ in $|G^>(x, \omega)|$. Therefore, the period of oscillations in the energy domain is determined by the difference between the bare and the renormalized velocity (see Fig.3.3), viz.:

$$\delta\epsilon \approx \frac{2\pi}{x\eta}; \text{ with } \eta = \frac{1}{v} - \frac{1}{\bar{v}}. \tag{3.36}$$

For small energies the decoherence is largely suppressed. This relies on the well known fact that in this regime chiral one-dimensional electrons can be considered as Landau quasiparticles described by the usual Fermi liquid theory. For this, we refer to reader to the analysis in [43], where the spectral density of a chiral "Luttinger liquid" is considered.

3.2.4   Large coupling constants

In this subsection we want to discuss briefly the shape of the Green's function in terms of the coupling strength. We emphasize that once the shape of the interaction potential is given, the only dimensionless parameter left is the coupling constant $\alpha = U_0/(2\pi v_F)$. All the other parameters may be absorbed into a rescaling of the result.

In Fig. 3.4 we show $|G^>(\epsilon, x)|$ as a function of energy for various coupling strengths (different curves), both at $x = 0$ and at some finite propagation distance $x \neq 0$. For small coupling $\alpha > 0$, we just observe the suppression of the tunneling density of states discussed above. Upon increasing the coupling strength, a series of rounded steps emerges, suppressing the tunneling density even further. The same features can be seen in the shape of the GF at finite x, though there they are superimposed by the decay (describing decoherence) and the oscillations as a function of energy (discussed in the preceding section). To identifiy the oscillations in energy which we observe even for small coupling strength in Fig. 3.4c we divide the GF for $x \neq 0$ showed in Fig. 3.4b by the tunnel density of states. As expected, these oscillations are robust against a change in the coupling strength. We have not found any simple analytical model to discuss the structures observed here. However, note that in Fig.3.3b one observes that the step structure is more pronounced for the Gaussian potential compared to the results for the exponential shape. That shows the strong influence of the shape of the interaction potential on the step structure. We note that previous discussion in the (ϵ, k)-space (as opposed to (ϵ, x)) had found non-analytic structures for the case of a box-shape potential U_q [43].

3.3   Visibility and Current

As mentioned in Chapter 2, the results for the GF $G^>(\epsilon, x)$ we worked out in the foregoing section can be applied directly to the evaluation of the current and the visibility (Fig. 3.5). Fig. 3.5a shows the current through the interferometer as a function of voltage for different arm lengths. Here, we restrict the considerations to the symmetric case, i.e. $x_1 = x_2$. For $x = 0$ the coherent part of the current
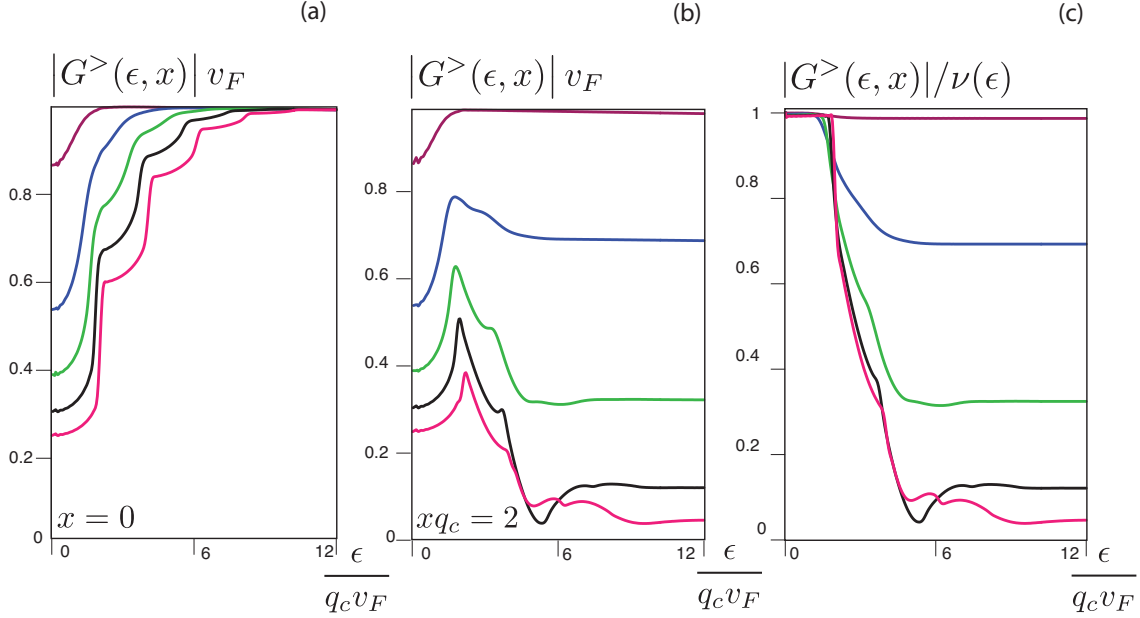
Figure 3.4: Green's function at zero temperature $T = 0$ as a function of energy ϵ for various coupling strengths α, at $x = 0$ (a) and $xq_c = 2$ (b).
c) $|G^>(\epsilon, x)|$ for $xq_c = 2$, divided by the tunnel density of states $2\pi\nu(\epsilon) = |G^>(\epsilon, x = 0)|$. This might be interpreted as the electron's coherence as a function of propagation energy and distance.
Here the potential is $U_q = 2\pi\alpha v_F e^{-(q/q_c)^2}$, where the various values of α are (from top to bottom): $\alpha = 0.16, 0.9, 1.6, 2.3, 3$.

obviously is identical with the flux-independent part, which implies a perfect visibility (at $T = V = 0$). The suppression of the current at small voltages is due to the velocity renormalization which lowers the tunnel density (for repulsive interactions). However, as the change in the tunnel density influences the classical and the coherent part in the same way, it does not show up in the visibility at all, i.e. $v_I(V, x = 0) \equiv 1$ (see Fig. 3.5b). In the limit of high voltages V and $T = 0$ the visibility is determined by the factor $|G^>(\epsilon \to \infty, x)|^2$. This follows from the fact that for higher voltages the contribution of the high-energy electrons becomes dominant. As the Green's function saturates for large energies (cf. Subsection 3.2.3), it also implies that the visibility at high voltages becomes voltage-independent. For $x \neq 0$ the dephasing reduces the coherent (flux-dependent) part of the current which leads to a decrease of the visibility. At small voltages $|q_e V| \ll q_c v_F$ the visibility decays only very slowly with increasing interferometer length (see the discussion of the Green's function in subsection 3.2.3). In the limit $V \to 0$ the visibility is approaching unity $v_I \to 1$, which is consistent with the fact that in equilibrium and at zero temperature there is no dephasing. In contrast to the Green's function itself, which shows oscillations as a function of ϵ, the visibility does not show pronounced oscillations as a
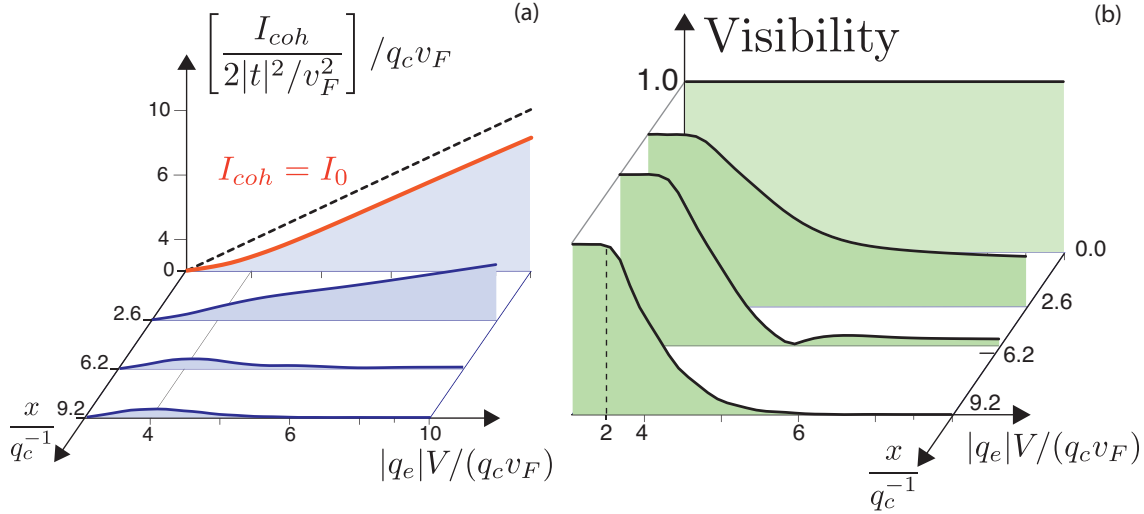
Figure 3.5: a) The amplitude of the coherent (flux-dependent) part of the current I_{coh} through the interferometer for different arm lengths x. The curve for $x \equiv 0$ is equal to the flux-independent current $I_{\text{coh}}(x \equiv 0, V) = I_0(V)$ (red line), which implies that the interference contrast is perfect at zero armlength.
b) The visibility v_I as a function of bias voltage V for various arm-lengths $x_1 = x_2 = x$. The red line denotes the semiclassical calculation we introduce in Chapter 4. The small deviations from the bosonization result vanish completly for larger V. The plot is done for $U_q = U_0 e^{-(q/q_c)^2}$ with $\frac{U_0}{v_F} = 2\pi\alpha = 3$.

function of V.

3.4   Summary

In this Chapter 3 we introduced the bosonization of the one-dimensional electron system providing us with the single-particle Green's function $G^>(\epsilon, x)$, which in the previous Chapter was shown to determine the coherence properties of the system. Assuming a finite range of the electron-electron interaction, it was evaluated numerically. The main result is that, only due to the finite interaction range, two distinct energy regimes energe. While the decoherence of low-energy electrons is suppressed strongly (as for these the Fermi liquid theory applies), the coherence of electrons flying high above the Fermi sea is destroyed to the full extent. Finally, the visibility was evaluated. In agreement with the analysis of Chalker et al. [6], even taking into acount the full interaction potential the reported "lobe structure" is not observed.

Chapter 4

Universal dephasing and semiclassical approach

At low energies and temperatures, chiral interacting fermions form a Fermi liquid and are fully coherent at $T = 0$ and $\epsilon = \epsilon_F$. The deviations when slightly increasing the energies in general depend on the details of the interaction potential [43]. In this Chapter however, we will study the coherence of interacting chiral fermions at high energies, i.e., $\epsilon \gg v_F q_c$. In [41], we reported on the central result that (at $T = 0$) there is a universal power-law $(1/x)$ decay of the single particle Green's function $G^>(\epsilon, x)$ with propagation distance, where in the leading order the exponent turns out to be independent of the interaction strength α.

This is derived within a semiclassical ansatz for $G^>(\epsilon, x)$, which becomes exact in the high-energy limit. It is based on the observation that at high energies the electrons propagate at the unperturbed speed v_F. For example, this can be obtained from the corresponding limiting behaviour of the plasmonic dispersion relation, $\lim_{q \to \infty} \omega_q = v_F q$. In addition, the Keldysh perturbation theory in Chapter 6 shows that the influence of exchange processes leading to a renormalization of the electron velocity is restricted to electrons in close vicinity to the Fermi edge. The main idea is to consider the electron propagating ballistically through the channel in the presence of the plasmonic bath formed by all the other electrons. Neglecting the backaction of the moving electron onto the bath, the electron is assumed to experience only a fluctuating potential landscape (which has its origin in the plasmonic bath) at its classical position $x = v_F t$ (Fig. 4.1). This is why the method is called "semiclassical". To model the effective, bosonic bath acting on the single electron, we make use of the plasmonic dispersion relation which was derived with help of the full bosonization of the system (cf. Eq. (3.12)). Due to the intrinsic fluctuations of the plasmonic quantum bath, the electron moving ballistically with v_F accumulates a random phase (even at $T = 0$, as a result of the zero point fluctuations). In the end one has to average over all possibe bath configurations (this is exactly what is done in an

experiment, measuring a large number of electrons). As a result of the averaging, the coherence is suppressed, which is equivalent to the decay of $G^>(\epsilon, x)$.

From a theoretical point of view, the correctness of this simple model in the high-energy limit has important implications. Especially the fact that the decoherence of a high-energy chiral electron is only related to a dephasing process, i.e., during its propagation the electron is not scattered out of its initial state, enables a deeper understanding of such systems, e.g., of its non-equilibrium properties (cf. Chapter 7).

The Chapter is structured as follows. First, we introduce the semiclassical approach as a physicallly motivated ansatz resulting in an expression for $G^>(\epsilon, x)$ that is in a next step shown to be exact in the high-energy limit (Section 4.1). This is done by comparison with the full bosonization solution given in Chapter 3. While starting from bosonization the Fourier transform of $G^>(x, t)$ can only be obtained numerically, the advantage of the semiclassical approach is that it provides us with an analytical expression for $G^>(\epsilon, x)$. It turns out that it is only the fluctuation spectrum of the plasmonic bath, experienced in the electron frame of reference, which determines the properties of the Green's function. In Section 4.2 it is shown that the low-frequency spectrum in this co-moving frame is of the ohmic type, i.e., the spectrum increases linearly with frequency. Most importantly, the slope of the low-frequency spectrum turns out to be independent of the coupling strength α. At $T = 0$, in the leading order this fact is shown to translate into a universal power-law decay of $G^>(\epsilon, x) \sim 1/x$ (Section 4.3). We will also discuss deviations from the leading behaviour and the situation at finite temperatures. Finally, we will motivate the semiclassical ansatz with some more rigour referring to the "equations of motion" approach used in [11, 36, 32, 31] to describe the decoherence of non-interacting electrons subjected to a quantum bath (Section 4.4).

4.1 Dephasing of high-energy electrons

We propose a very simple description of dephasing in chiral one-dimensional electron systems for electrons flying high above the Fermi sea. The main advantage is that the formalism emphasizes the physical origin of dephasing in those systems. The method is inspired by the equations of motion approach [36, 32, 31], which will be discussed in more detail in Section 4.4 and by the physical picture the bosonization of the problem suggests. The equations of motion approach was proposed in order to study the decoherence of electrons subjected to some external noise potential in presence of a filled Fermi sea. The main idea is that the electrons moving ballistically with v_F experience some fluctuating potential due to the coupling to the external bath, thereby collecting a random phase (Fig.4.1). In the end, averaging over all possible bath configurations the coherence of the electrons effectively gets suppressed. The backaction of the flying electron onto the bath is included taking into account the quantum nature of the bath. It turns out that this has important consequences for the coherence properties of the electron, as it introduces the influence of the Fermi edge. Namely,
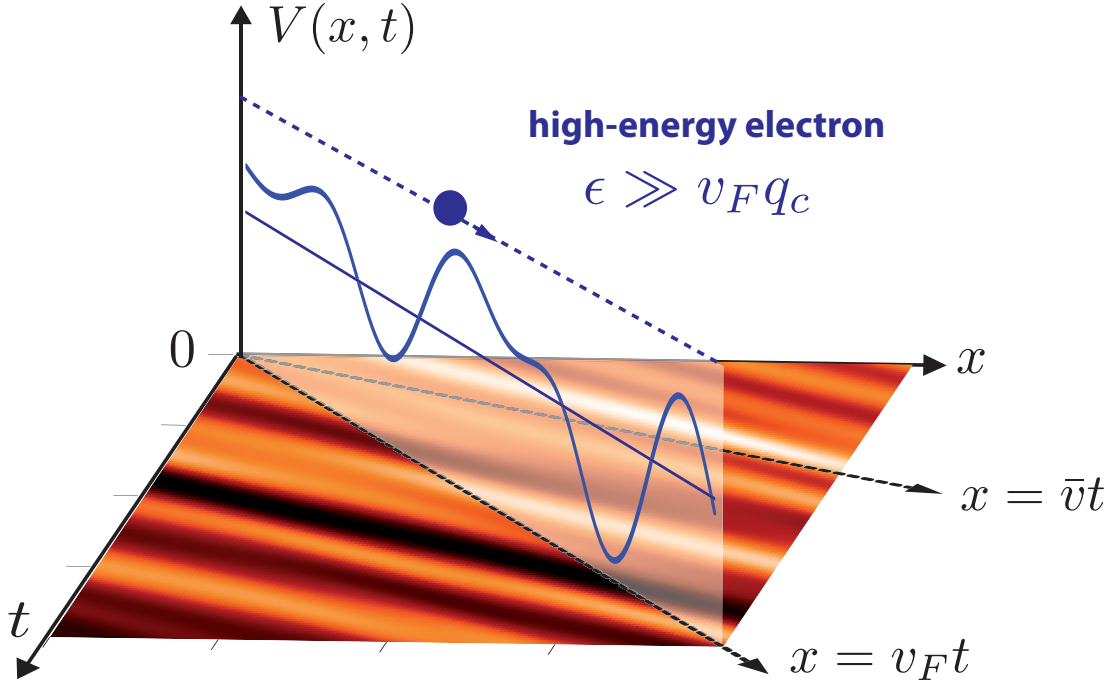
Figure 4.1: A single electron propagating at high energies feels a fluctuating quantum potential $\hat{V}(t)$, due to the interaction with the density fluctuations in the sea of other electrons. We show a density plot of the potential, which is produced by the electronic density fluctuations (plasmons) in the channel. The plasmons are moving with a renormalized velocity $\bar{v}$ (see main text) while the high-energy electron moves with the bare Fermi velocity v_F. It picks up a random phase, which leads to dephasing. This is the picture underlying the semiclassical approach we apply in this Section.

the Pauli principle precludes any inelastic scattering processes which would transfer the electron to an occupied state below the Fermi edge. This effect is known as Pauli blocking.

The equations of motion approach was applied, e.g., studying the influence of a quantum noise potential (i.e., the noise source itself is treated quantum mechanically) on the weak localization of electrons [11] and on the visibility of a Mach-Zehnder interferometer [36, 32, 31].

However, here we are interested in the influence of the electron-electron interactions on the coherence properties of the injected electron. The main question is, whether one can replace the complicated interparticle interactions by considering all the other electrons to form an effective "external" quantum bath. The density fluctuations in this effective electron bath, the plasmons, would give rise to a random quantum potential dephasing the inserted electron. Indeed, it turns out that if the energy of the injected electron is large enough, i.e., $\epsilon \gg q_c v_F$, this approach exactly reproduces the Green's

function $G^>(\epsilon, x)$ calculated with help of bosonization.

The plasmonic bath is assumed to be governed by the full dispersion relation ω_q, derived in the framework of bosonization (cf. Eq. (3.12)). At first sight this idea suggesting to start from a ballistically moving single electrons seems to contradict the main message of the bosonization technique: in one dimension, instead of single electrons one has to think of collective, bosonic modes. Nevertheless, it is crucially inspired by the bosonization method. Namely, in the semiclassical approach as well as in the bosonization of the system, all the information concerning the electron-electron interaction is exclusively stored into the plasmonic dispersion relation ω_q. As we will see in the upcoming section, in the semiclassical description of the system the dispersion relation determines the fluctuation spectrum of the plasmonic bath.

In this chapter we restrict the considerations to high-energy electrons ($\epsilon \gg v_F q_c$) as those move with the bare Fermi velocity v_F, while in Chapter 5 we investigate a more general anatz and try to extend the approach to arbitrary energies. The semiclassical approximation we propose here, first has the status of an intuitive physical ansatz, resulting in an expression for the single particle Green's function $G^>(\epsilon, x)$. This is compared to the full bosonization solution, thereby verifying the ansatz in the high-energy limit. To start, we consider an electron moving with v_F and being coupled to the potential stemming from the interactions with the plasmonic modes $\{\hat{b}_q\}$. The potential acting on such a single high-energy electron is obtained by convoluting the density fluctuations $\hat{\rho}$ with the interaction potential $U(x)$ (which is identical to the one used in the bosonization of the problem):

$$\hat{V}(t) = \int dx' \, U(x' - v_F t) \hat{\rho}(x', t). \tag{4.1}$$

The definition implies, that the effective potential fluctuations $\hat{V}(t)$ experienced by the single electron are just the fluctuations of the bath evaluated at the classical electron position $x = v_F t$ at time t. This is why we call this model "semiclassical". In the many-body language the particles are represented by the particle fields $\hat{\psi}$ whose time-evolution reflects this additional potential by collecting an extra phase. If we were dealing with a classical fluctuating potential $V(t)$, the electron would simply pick up a random phase $\varphi(t) = -\int_0^t dt' \, V(t')$, i.e. $\hat{\psi}(t) \to \hat{\psi}(t)e^{i\varphi(t)}$. Therefore, in that case the non-interacting Green's function $g^>(x, \epsilon)$ would have to be multiplied by a factor $e^{-F(t)} = \langle e^{i\varphi(t)} \rangle$ (where one has to take the average with respect to the bath degrees of freedom) to obtain the full Green's function. Then the ansatz reads (for $\epsilon \gg q_c v_F$)

$$G^>(\epsilon, x) \;\; = \;\; g^>(\epsilon, x) \cdot e^{-F(x)}, \tag{4.2}$$

where in the exponent we replaced t by x/v_F. In the following, the factor $e^{-F(x)}$ is denoted as the 'coherence' of the electron. However, if the quantum nature of the bath becomes important one has take care of the non-commutativity of the operator $\hat{V}(t)$ at different times. This can be done by

introducing a time-ordering symbol:

$$
\begin{aligned}
e^{-F(x)} &\equiv \left\langle \hat{T} \exp\left[-i \int_0^t dt' \hat{V}(t')\right]\right\rangle \\
&= \exp\left[-\frac{1}{2}\int_0^t dt_1 \int_0^t dt_2 \left\langle \hat{T}\hat{V}(t_1)\hat{V}(t_2)\right\rangle\right].
\end{aligned}
\tag{4.3}
$$

Again, the time $t = x/v_F$ in Eq. (4.3) is determined by the propagation length. In the last line we made use of the well known identity $\left\langle e^{-i\hat{\varphi}}\right\rangle = \exp\left(-\frac{1}{2}\left\langle\hat{\varphi}^2\right\rangle\right)$ for Gaussian random variables $\hat{\varphi}$. One may note that this is actually identical to the decay of the coherence of a single level whose energy fluctuates. In various contexts, this is known as the "independent boson model" [30], or the case of "pure dephasing" in a (longitudinally coupled) spin-boson model [48]. The same kind of approach to dephasing of ballistically propagating electrons has been introduced previously, both for a situation with a general quantum bath [34, 31, 32, 36], as well as for two coupled Luttinger liquids [24].

Furthermore we note that the decay is independent of energy ϵ. This is because the propagation speed is energy-independent, and the distance to the Fermi edge becomes unimportant at high energies as well. Qualitatively, we have seen this feature before in our discussion of the full bosonization solution (see Section 3.2.3 and Fig.3.3).

In the following we calculate the time-ordered bath correlation function $\langle\hat{T}\hat{V}(t_1)\hat{V}(t_2)\rangle$, which solely determines the coherence properties of the high-energy electron.

4.1.1 Calculation of the correlation function

In this subsection, we rewrite the exponent of Eq. (4.3) in terms of the spectrum of the plasmonic excitations in frequency space. The decay of the electron coherence, described by $F(t)$, is completely determined by the fluctuation spectrum $\langle\hat{V}\hat{V}\rangle_\omega \equiv \int dt\, e^{i\omega t}\langle\hat{V}(t)\hat{V}(0)\rangle$ of the potential seen by the electron in the moving frame. To proceed further, we express the time-ordered correlator $\langle\hat{T}\hat{V}(t_1)\hat{V}(t_2)\rangle$ as a sum of commutator and anti-commutator part:

$$
\left\langle\hat{T}\hat{V}(t_1)\hat{V}(t_2)\right\rangle = \frac{1}{2}\left[\left\langle\left\{\hat{V}(t_1),\hat{V}(t_2)\right\}\right\rangle + \mathrm{sgn}(t_1-t_2)\left\langle\left[\hat{V}(t_1),\hat{V}(t_2)\right]\right\rangle\right].
\tag{4.4}
$$

As a general property the commutator part of the correlation function is purely imaginary reflecting its origin in the quantum nature of the potential $\hat{V}$ (a classical noise correlator is purely real). The commutator part represents the linear response of the bath potential to a change in the electron density. Therefore, even if we assume that the fluctuations of the bath are only the intrinsic ones (at $T = 0$ the zero point fluctuations), due to the quantum nature of the bath some kind of response automatically is included in the correlation function in Eq. (4.4). The real part of $F(t)$ and therefore the decay of the Green's function depends only on the symmetrized part of the correlator. Formally, this part is similar to the correlator of classical noise, though it also contains the zero-point fluctuations

of the plasmon field:

$$\begin{aligned}
\mathrm{Re}F &= \frac{1}{4}\int_0^t dt_1 \int_0^t dt_2 \left\langle \left\{ \hat{V}(t_1), \hat{V}(t_2) \right\} \right\rangle \\
&= \frac{1}{4}\int \frac{d\omega}{2\pi} \left| \int_0^t dt_1\, e^{-i\omega t_1} \right|^2 \left\langle \left\{ \hat{V}, \hat{V} \right\} \right\rangle_\omega \\
&= \int_{-\infty}^{+\infty} \frac{d\omega}{2\pi} \frac{\sin^2(\omega x/2v_F)}{\omega^2} \left\langle \left\{ \hat{V}, \hat{V} \right\} \right\rangle_\omega,
\end{aligned} \tag{4.5}$$

where in the last line we replace the propagation time by $\frac{x}{v_F} = t$. In addition, a phase $-\mathrm{Im}F$ shows up in the exponent. As already mentioned, it is related to the commutator of $\hat{V}$ for different times and thus represents a purely quantum mechanical contribution. In terms of the Fourier transform of the spectrum we get

$$\begin{aligned}
i\mathrm{Im}F &= \frac{1}{4}\int_0^t dt_1 \int_0^t dt_2\, \mathrm{sgn}(t_1 - t_2) \left\langle \left[\hat{V}(t_1), \hat{V}(t_2) \right] \right\rangle \\
&= \frac{1}{4}\int \frac{d\omega}{2\pi} \left\{ \int_0^t dt_1 \int_0^t dt_2\, \mathrm{sgn}(t_1 - t_2) e^{-i\omega(t_1 - t_2)} \right\} \left\langle \left[\hat{V}, \hat{V} \right] \right\rangle_\omega \\
&= \frac{i}{2}\int \frac{d\omega}{2\pi} \mathrm{Im}\left\{ \int_0^t dt_1 \int_0^{t_1} dt_2\, e^{-i\omega(t_1 - t_2)} \right\} \left\langle \left[\hat{V}, \hat{V} \right] \right\rangle_\omega \\
&= -\frac{i}{2}\int_{-\infty}^{\infty} \frac{d\omega}{2\pi} \left[\frac{t}{\omega} - \frac{\sin(\omega t)}{\omega^2} \right] \left\langle \left[\hat{V}, \hat{V} \right] \right\rangle_\omega.
\end{aligned} \tag{4.6}$$

In a next step we have to calculate the potential correlators experienced in the electron frame of reference (the co-moving frame) determing the exponent $F(x,t)$. Those are directly obtained from the definition of the potential $\hat{V}$ Eq. (4.1). We use that the convolution Eq. (4.1) can be written as: $\hat{V}(t) = \int (dq)\, e^{iqv_F t} U_q \hat{\rho}_q(t)$. It follows

$$\begin{aligned}
\left\langle \hat{V}\hat{V} \right\rangle_\omega &= \int dt\, e^{i\omega t} \int \frac{dq}{2\pi} e^{iqv_F t} |U_q|^2 \left\langle \hat{\rho}_q(t)\hat{\rho}_{-q} \right\rangle \\
&= \int \frac{dq}{2\pi} |U_q|^2 \left\langle \hat{\rho}\hat{\rho} \right\rangle_{q,\omega+v_F q}.
\end{aligned} \tag{4.7}$$

The argument $\omega + v_F q$ indicates that we are dealing with the Galileo-transformed spectrum of the density fluctuations. As a result of the Galileo transformation, the effective spectrum of the density fluctuations gets tilted compared to the original dispersion relation (see Fig. 4.2). The density-density correlator $\left\langle \hat{\rho}\hat{\rho} \right\rangle_{q\omega}$ of the plasmons is obtained via the fluctuation-dissipation theorem (FDT). In equilibrium it connects the commutator part of the correlator (dissipation) with the symmetrized

part (fluctuations). There are two equivalent versions we will use extensively:

$$\langle\{\hat{\rho},\hat{\rho}\}\rangle_\omega \;\; = \;\; \coth(\frac{\beta\omega}{2})\,\langle[\hat{\rho},\hat{\rho}]\rangle_\omega\,. \tag{4.8}$$

$$\langle\hat{\rho}\hat{\rho}\rangle_\omega \;\; = \;\; \frac{1}{2}(1+\coth(\frac{\beta\omega}{2}))\,\langle[\hat{\rho},\hat{\rho}]\rangle_\omega\,, \tag{4.9}$$

where $\beta = 1/T$ and T denotes the temperature in the laboratory frame. The last statement seems to be somehow redundant, as we already introduced the inverse temperature β. Nevertheless, we show below that while the fluctuation-dissipation theorem holds for the potential fluctuations $\langle\hat{\rho}\hat{\rho}\rangle_{q\omega}$ measured in the laboratory frame, for the potential fluctuations $\langle\hat{V}\hat{V}\rangle_\omega$ experienced in the co-moving frame one has to define an effective temperature $T_{\rm eff}$ such that the fluctuation-dissipation theorem remains valid connecting the various potential correlators. Postponing this important discussion to 4.3.3, in the following derivations we only make use of the FDT in relation to the density correlators itself. For the plasmonic spectrum in the laboratory frame $\langle\hat{\rho}\hat{\rho}\rangle_\omega$ the fluctuation-dissipation theorem yields:

$$
\begin{aligned}
\langle\hat{\rho}\hat{\rho}\rangle_{q\omega} \;\; = \;\; & \frac{1}{2}(1+\coth(\frac{\beta\omega}{2}))\,\langle[\hat{\rho},\hat{\rho}]\rangle_{q\omega} \\
= \;\; & [\bar{n}(\omega)+1]\int dt\,e^{i\omega t}\int dx\,e^{-iqx}\{ \\
& \frac{1}{L^2}\sum_k(\frac{L|k|}{2\pi})e^{ikx}(\Theta_k\left\langle\left[\hat{b}_k(t),\hat{b}_k^\dagger\right]\right\rangle+\Theta_{-k}\left\langle\left[\hat{b}_{|k|}^\dagger(t),\hat{b}_{|k|}\right]\right\rangle)\} \\
= \;\; & [\bar{n}(\omega)+1]\int dk\,\delta(q-k)|k|\left\{\Theta_k\delta(\omega-\omega_k)-\Theta_{-k}\delta(\omega+\omega_{|k|})\right\} \\
= \;\; & [\bar{n}(\omega)+1]|q|\left\{\Theta_q\delta(\omega-\omega_q)-\Theta_{-q}\delta(\omega+\omega_{|q|})\right\}\,. \tag{4.10}
\end{aligned}
$$

We made use of the identity $\hat{\rho}_q = \sqrt{\frac{L|q|}{2\pi}}\hat{b}_q$ (for $q > 0$) (see Eq. (3.7)), noticed the time evolution of the bosonic operators $\hat{b}_q(t) = e^{-i\omega_q t}\hat{b}_q$ and finally used the fact that the bosonic commutation relation holds for the plasmonic operators, i.e. $[\hat{b}_q,\hat{b}_{q'}^\dagger] = \delta_{qq'}$ per construction. The Bose distribution function is denoted as $\bar{n}(\omega)$.

After these preliminary calculations, now we focus on the potential correlation functions experienced by the electrons in the co-moving frame as those are directly responsible for the decoherence properties of the system. The potential correlation functions become

$$\left\langle\left[\hat{V},\hat{V}\right]\right\rangle_\omega \;\; = \;\; \int\frac{dq}{2\pi}|U_q|^2\,\langle[\hat{\rho},\hat{\rho}]\rangle_{q,\omega+qv_F} \tag{4.11}$$

$$\left\langle\left\{\hat{V},\hat{V}\right\}\right\rangle_\omega \;\; = \;\; \int\frac{dq}{2\pi}|U_q|^2\coth(\frac{\beta(\omega+qv_F)}{2})\,\langle[\hat{\rho},\hat{\rho}]\rangle_{q,\omega+v_Fq}\,, \tag{4.12}$$

where we avoid a direct usage of the FDT to connect $\langle\{\hat{V},\hat{V}\}\rangle_\omega$ and $\langle[\hat{V},\hat{V}]\rangle_\omega$. Being interested in

the most general representation of the decoherence, we allow even for attractive interactions, i.e., $\alpha < 0$. The symmetrized and the commutator part of the correlator give (here for $\omega > 0$):

$$
\begin{aligned}
\left\langle \left\{ \hat{V}, \hat{V} \right\} \right\rangle_\omega &= \int_0^\infty \frac{dq}{2\pi} |U_q|^2 q \coth\left(\frac{\beta\omega_q}{2}\right) \delta\left(\omega - \frac{|U_q|q}{2\pi}\right), \\
\left\langle \left[\hat{V}, \hat{V} \right] \right\rangle_\omega &= \operatorname{sgn}(\alpha) \int_0^\infty \frac{dq}{2\pi} |U_q|^2 q \delta\left(\omega - \frac{|U_q|q}{2\pi}\right).
\end{aligned}
\tag{4.13}
$$

Having evaluated the potential correlation functions in the co-moving frame, we can substitute these in the defining equations for the exponent $F(x)$ (Eqs. (4.5) and (4.6)):

$$
\operatorname{Re}F(x) = \int_0^\infty \frac{dq}{q} \coth\left(\frac{\beta\omega(q)}{2}\right) \left[1 - \cos\left(\frac{U_q q}{2\pi}t\right)\right]
\tag{4.14}
$$

$$
\operatorname{Im}F(x) = \int_0^\infty \frac{dq}{q} \sin\left(\frac{U_q q}{2\pi}t\right) - \int_0^\infty dq \left[\frac{U_q}{2\pi}\right] t.
\tag{4.15}
$$

Discussion   In order to compare the ansatz $G^>(\epsilon, x) = g^>(\epsilon, x) \cdot e^{-F(x)}$ with the bosonization solution, we have to evaluate the Fourier transform of $G^>(x, t)$ in Eq. (3.30) numerically in the limit of large energies $\epsilon \gg v_F q_c$. In Fig. 4.2 we compare both the phase and the modulus of the bosonization solution and the semiclassical ansatz, respectively. Obviously, these are identical confirming the semiclassical ansatz (cf. Fig. 3.3)

$$
G^>(\epsilon, x) = g^>(\epsilon, x) \cdot e^{-F(x)} \quad \epsilon \gg v_F q_c.
\tag{4.16}
$$

Furthermore, a comparison of the semiclassical exponent $e^{-F(x)}$, i.e., Eqs. (4.14) and (4.15), with $G^>(x, t)$ in Eq. (3.30) shows that, up to an additional energy renormalization $-\int_0^\infty dq \frac{U_q}{2\pi}$, the ansatz reproduces the Green's function $G^>(x, t)$ along the classical trajectory $x = v_F t$:

$$
G^>(x, t) = g^>(x, t) \cdot e^{-F(x)} \quad x = v_F t,
\tag{4.17}
$$

where we omit the constant energy shift or equivalently incorporate it into a redefinition of the chemical potential. This is exactly what we have done in the derivation of the Green's function with help of the bosonization method. There, the density-density interaction $\frac{1}{2} \int dx' \int dx \, \hat{\rho}(x') U(x - x') \hat{\rho}(x)$ (the first term in the second line of Eq. (3.6)) still contains the unphysical interaction of an electron with itself. However, in principle the Fock term (the third term in Eq. (3.6)), which was incorporated into a redefinition of the chemical potential, cancels against this contribution. For a single electron the shift in energy due to this self-interaction yields: $\frac{1}{2} \int dx \int dx' \, \delta(x) U(x - x') \delta(x - x') = (2\pi)^{-1} \int_0^\infty dq \, U_q$. But this is exactly the energy, which is substracted in Eq. (4.15). In contrast to the Green's function resulting from bosonization (where we hide the Fock term by a redefinition of μ) within the semiclassical approach the Fock term shows up explicitly.

Equation (4.17) proofs that the decoherence of electrons moving along $x = v_F t$ can be understood in terms of a semiclassical approach. This is in agreement with the foregoing analysis of $G^>(x, t)$ in Section 3.2.2. Beside a broad peak moving with $\bar{v}$, one observes a sharp peak in time, moving along the trajectory $x = v_F t$. There, we argued that it is this sharp peak, which is responsible for the contributions to $G^>(\epsilon, x)$ at large energies (cf. Fig. 3.2 and Fig. 3.3). Equations (4.16) and (4.17)
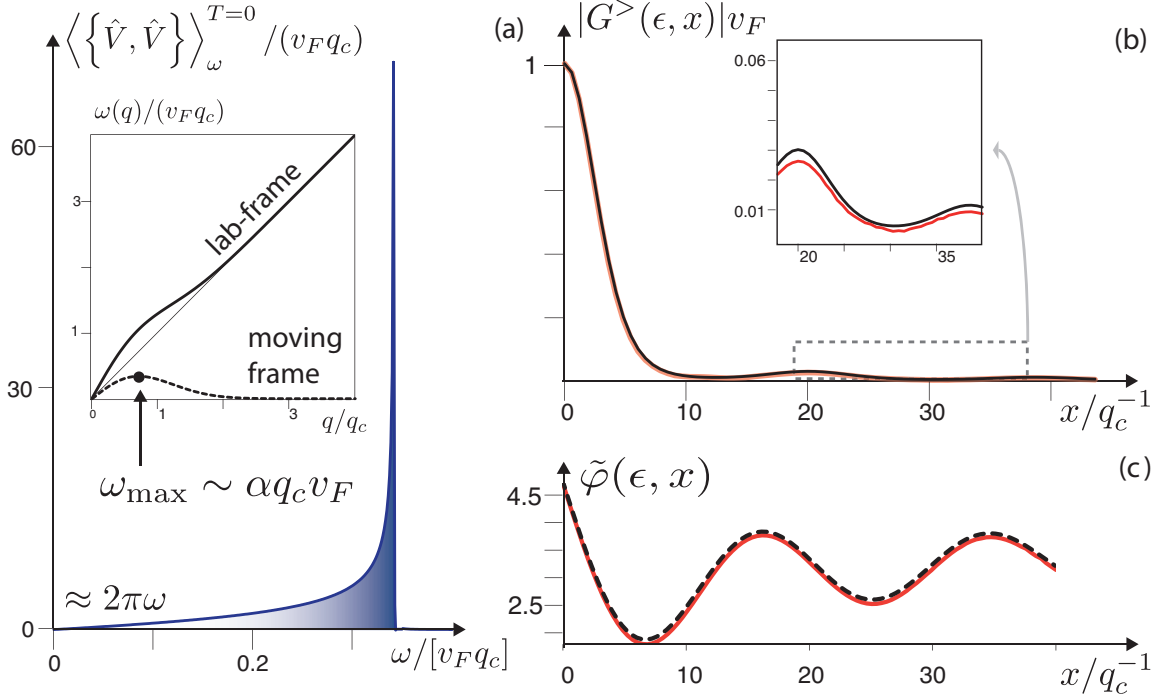
Figure 4.2: a) Plot of the effective spectrum $\langle\{\hat{V}, \hat{V}\}\rangle_\omega^{T=0}$ of the plasmonic bath experienced by the electron in its co-moving frame of reference. The spectrum is linear in ω for small frequencies and diverges like $\frac{1}{\sqrt{\omega_{\max} - \omega}}$ when approaching $\omega_{\max}$. The inset shows the dispersion relation of the plasmonic bath in the laboratory frame of reference as well as in the electron frame of reference, where it is getting tilted [dashed curve].
b) $G^>(\epsilon, x)$ as a function of x for large energies $\epsilon \gg q_c v_F$. The solid orange line denotes the numerical evaluation of the bosonization result, while the solid black line shows the semiclassical result. For a better comparison of the results, the inset shows a blow-up of the oscillations. The small deviations are due to finite numerical precision. (c) Phase $\tilde{\varphi}(\epsilon, x)$ of $G^>(\epsilon, x) = |G^>(\epsilon, x)| \exp(i\epsilon x/v_F + i\tilde{\varphi}(x))$ both from the semiclassical ansatz (dashed, black line) and from the bosonization solution (orange line). Obviously, those are identical. All plots are given for $U_q = U_0 e^{-(q/q_c)^2}$ with $\frac{U_0}{v_F} = 2\pi\alpha = 5$ and $T = 0$.

display one of our main results. First of all the identity in Eq. (4.2) provides us with an analytical expression for the Fourier transformed Green's function $G^>(\epsilon, x)$ at large energies, which enables

the detailed study of the decoherence in this regime. Secondly, the agreement of bosonization and the very simple and intuitive semiclassical approach gives us much more insight into the physics of decoherence in chiral electron systems. It proves that the dephasing of hig-energy electrons relies only on the influence of the fluctuating plasmonic potential $\hat{V}$ created by all the other electrons, but there are no scattering processes involved at all.

The semiclassical approach enables the detailed analysis of the decoherence due to electron-electron interactions, only in terms of the plasmonic spectrum $\langle \hat{V}\hat{V} \rangle_\omega$. In Section 4.3 it becomes clear that exciting physics can be brought to light along these lines.

4.2   Plasmonic spectrum

Having established the connection between the semiclassical approach and the full bosonization solution, we now turn to the properties of the potential spectrum experienced by the injected electron in the co-moving frame. Considering the Green's function within the semiclassical approach, the coherence $G^>(\epsilon, x)$ solely depend on the potential spectrum $\langle \hat{V}\hat{V} \rangle_\omega$, which the electron experiences in the co-moving frame of reference (cf. Eqs. (4.14) and (4.15)).

Therefore, this section is concerned with a detailed study of this spectrum. First, we focus on the zero temperature case $T = 0$ (see Fig. 4.2) and restrict the considerations to analytical interaction potentials of the form $U_q = 2\pi\alpha v_F e^{-|q/q_c|^s}$. In Subsection 4.3.2 we extend the analysis allowing for non-analytic potentials as $U_q = 2\pi\alpha v_F |q/q_c|^{-n}$. Starting from Eqs. (4.7),(4.10), the calculation of the spectrum $\langle \hat{V}\hat{V} \rangle_\omega^{T=0}$ gives (we substitute for $T = 0$: $\frac{1}{2}(1 + \coth(\frac{\beta\omega}{2})) = \Theta(\omega)$)

$$
\begin{aligned}
\left\langle \hat{V}\hat{V} \right\rangle_\omega^{T=0} &= \int \frac{dq}{2\pi} |U_q|^2 \Theta(\omega + qv_F)|q| \left(\Theta_q \delta(\omega + qv_F - \omega_q) - \Theta_{-q}\delta(\omega + qv_F + \omega_{|q|}) \right) \\
&= \int \frac{dq}{2\pi} |U_q|^2 |q| \left(\Theta(\omega_q)\Theta_q \delta(\omega - \frac{U_q|q|}{2\pi}) - \Theta_{-q}\Theta(-\omega_{|q|})\delta(\omega + \frac{U_q|q|}{2\pi}) \right) \\
&= \int_0^\infty \frac{dq}{2\pi} |U_q|^2 |q|\delta(\omega - \frac{U_q|q|}{2\pi}),
\end{aligned}
\tag{4.18}
$$

where we set $\Theta(-\omega_{|q|}) = 0$, as the dispersion relation of the plasmonic excitations has to be positive definite, i.e. $\omega_q \geq 0$. This restricts the range of the coupling constant α to: $\alpha \in (-1, \infty)$. The following analysis of the spectrum shows that there are two distinct features which are of crucial importance for the coherence properties of the system.

4.2.1   Square root singularity in the spectrum

At high frequencies, we obtain a singularity $\langle \{\hat{V}, \hat{V}\} \rangle_{\omega>0}^{T=0} \propto 1/\sqrt{\omega_{\max} - \omega}$ at the cutoff frequency $\omega_{\max} = \max(\omega(q) - v_F q)$ (see Fig.4.2), which is the maximum frequency in the Galilei-transformed plasmon dispersion relation. This can be obtained by expanding the integrand in Eq. (4.13) around

$\omega \approx \omega_{\max} + \delta\omega$. For this we introduce $h \equiv \frac{|U_q|q}{2\pi}$ and $q_{\max}$, such that $\omega_{\max} = h(q_{\max})$. Furthermore we set: $\partial_q^2 h\big|_{q_{\max}} \equiv h''(q_{\max}) \equiv \xi$.

Then the spectrum in the close vicinity to $\omega_{\max}$ yields

$$
\begin{aligned}
\left\langle \left\{ \hat{V}, \hat{V} \right\} \right\rangle_{\omega>0}^{T=0} &\approx \int_0^\infty \frac{dq}{2\pi} |U_q|^2 q \delta\left(\omega_{\max} + \delta\omega - h(q_{\max}) - \frac{1}{2} h''(q_{\max})(q - q_{\max})^2 \right) \\
&= \int_0^\infty \frac{dq}{2\pi} |U_q|^2 q \delta\left(\delta\omega - \frac{1}{2} h''(q_{\max})(q - q_{\max})^2 \right) \\
&= \int_0^\infty \frac{dq}{2\pi} |U_q|^2 q \sum_{i=1,2} \frac{\delta(q - q_i^*)}{|\xi(q_i^* - q_{\max})|},
\end{aligned}
\tag{4.19}
$$

where we set $q_i^* = q_{\max} \pm \sqrt{\frac{2\delta\omega}{\xi}}$. After some further steps we get (for $\omega < \omega_{\max}$)

$$
\begin{aligned}
\left\langle \left\{ \hat{V}, \hat{V} \right\} \right\rangle_{\omega>0}^{T=0} &\approx \frac{4\pi}{q_{\max}\sqrt{2|\xi|}} \cdot \frac{\omega_{\max}^2}{\sqrt{\omega_{\max} - \omega}} \\
&\quad + \frac{(|U_q|^2 q)'\big|_{q_{\max}}}{2\pi} \cdot \left\{ \frac{\sqrt{\frac{2\delta\omega}{\xi}} - \sqrt{\frac{2\delta\omega}{\xi}}}{\sqrt{2\delta\omega\xi}} \right\} \\
&= \frac{4\pi}{q_{\max}\sqrt{2|\xi|}} \cdot \frac{\omega_{\max}^2}{\sqrt{\omega_{\max} - \omega}}
\end{aligned}
\tag{4.20}
$$

Such a maximum frequency arises due to the momentum cutoff in the dispersion relation (which results from the finite range of the interactions). By transforming the potential to the moving frame, it gets tilted (cf. Fig. 4.2). As the velocity of the plasmons in the limit of large momenta is identical to the velocity of the moving frame, the effective dispersion relation shows a maximum. The singularity in the spectrum arises due to the fact that $\omega(q) \approx \omega_{\max} + \omega''(q - q^*)^2/2$ in the vicinity of q^*, where $\omega(q^*) = \omega_{\max}$. Note that an interaction potential U_q with a non-monotonous decay in q may give rise to several such singularities, corresponding to local maxima of $\omega(q) - v_F q$. As a direct consequence, the electron experiences a fluctuating potential with a dominant frequency $\omega_{\max}$, with $\omega_{\max} \sim |\alpha| v_F q_c$. The exact value of $\omega_{\max}$ depends on the particular form of the interaction potential.

4.2.2   Ohmic noise spectrum

At low frequencies $\omega \ll v_F q_c$ and $T = 0$ the spectrum increases linearly in ω, corresponding to "Ohmic" noise, which is ubiquitous in various other physical contexts [48].

Smooth interaction potentials   For interaction potentials that are smooth in real space (i.e., where all the moments of $|U_q|$ are finite), we find that the leading low-frequency behaviour is determined solely by the contribution to Eq. (4.7) stemming from small q. Considering the limit $\omega \to 0$ of

Eq. (4.13) one gets

$$\boxed{\lim_{\omega \to 0} \left\langle \left\{ \hat{V}, \hat{V} \right\} \right\rangle_{\omega}^{T=0} = 2\pi |\omega|}.$$

(4.21)

Most remarkably, the dimensionless prefactor (the slope) of the noise spectrum turns out to be completely independent of the coupling strength α, which drops out of the calculation. This is in contrast to the typically studied non-chiral Luttinger liquids, where an Ohmic spectrum has been found with an interaction-dependent prefactor [24]. As a direct consequence, the electron's Green's function shows a universal power-law decay at long distances, as we will discuss in more detail in the next section.

4.3   Universal dephasing

In this section we show the surprising result that in one-dimensional chiral electron systems, the coherence of an injected electron due to the electron-electron interactions in the leading order decays as $1/x$. The universal behaviour, i.e., the exponent does not depend on the coupling strength α relies on an interplay between the Galileo transformation and the plasmonic dispersion relation. Within the semiclassical approach the decoherence the elecron suffers has its origin in a fluctuating background potential (which has its origin in the fluctuations of the electron density) it experiences in its frame of reference. Therefore, one has apply a Galileo transformation on the noise spectrum in the lab-frame to derive the effective potential fluctuations. In the previous section we showed that as a result the noise spectrum is of the ohmic type, with a linear slope independent on the interaction strength (cf. Eq. (4.21)), i.e. $\langle \{\hat{V}, \hat{V}\}\rangle_{\omega \approx 0} = 2\pi|\omega|$. In the following, we will show that it is this fact, which translates into the universal power-law decay. Before we proceed, we offer a simple explanation for this amazing fact. For this, consider the plasmonic excitations moving with $\bar{v} = v_F(1 + \alpha)$ from the electrons point of view. The electron feels the plasmonic density waves passing it with the relative velocity $\bar{v} - v_F$. Now, decreasing the coupling α lowers the strength of the potential fluctuations thereby suppressing the low-frequency spectrum. However, this is compensated as at the same time the relative velocity is decreased as well, increasing the low-frequency contributions to the noise spectrum.

Inserting the spectrum Eq. (4.21) into the long-distance limit of $F(x)$ Eq. (4.5) yields

$$
\begin{aligned}
\text{Re}F(x) &= 2 \lim_{x \to \infty} \int_0^{+\infty} \frac{d\omega}{2\pi} \frac{\sin^2(\omega x/2v_F)}{\omega^2} \left\langle \left\{ \hat{V}, \hat{V} \right\} \right\rangle_{\omega}^{T=0} \\
&\approx \frac{x^2}{2v_F^2} \int_0^{\frac{v_F}{x}} d\omega\, \omega + \int_{\frac{v_F}{x}}^{\omega_c} \frac{d\omega}{\omega} + 2 \int_{\omega_c}^{\omega_{\max}} \frac{d\omega}{2\pi} \frac{\sin^2(\omega x/2v_F)}{\omega^2} \left\langle \left\{ \hat{V}, \hat{V} \right\} \right\rangle_{\omega}^{T=0} \\
&\approx \text{const.} + \ln\left(\frac{\omega_c x}{v_F} \right) + 2 \int_{\omega_c}^{\omega_{\max}} \frac{d\omega}{2\pi} \frac{\sin^2(\omega x/2v_F)}{\omega^2} \left\langle \left\{ \hat{V}, \hat{V} \right\} \right\rangle_{\omega}^{T=0},
\end{aligned}
$$

(4.22)
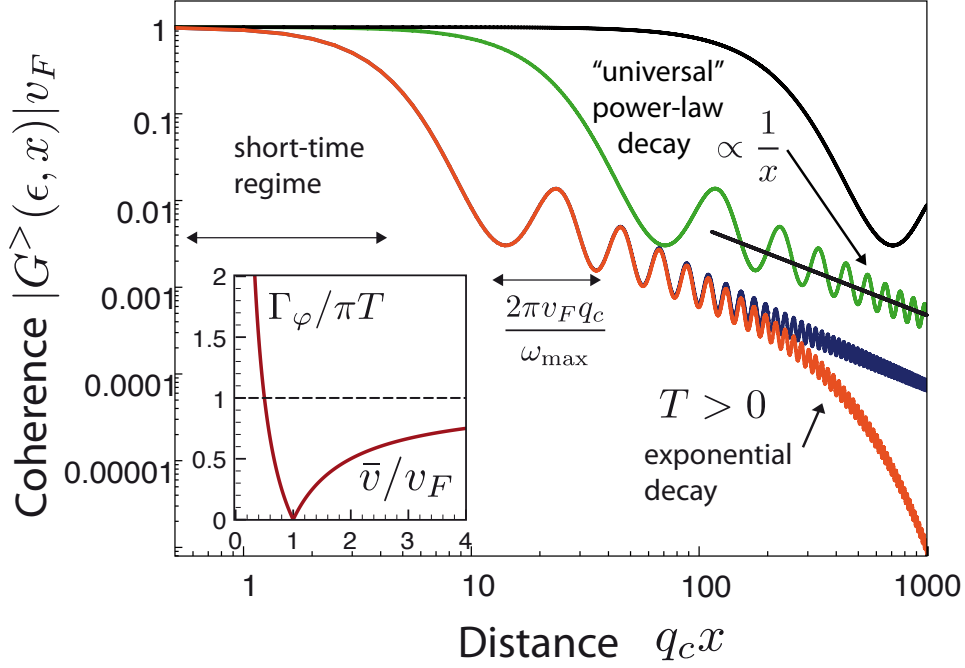
Figure 4.3: Coherence of an electron propagating at high energies in an interacting chiral system, as a function of propagation distance for various values of interaction strength α: $2\pi\alpha = 0.1$ (solid black line), $2\pi\alpha = 1.0$ (solid green line) and $2\pi\alpha = 5.0$ (solid red and blue lines). The potential is taken as $U_q = U_0 e^{-|q/q_c|}$ and temperature is zero except for the red line where $T/q_c v_F = 0.005$. The non-interacting case would give $v_F |G^>(\epsilon, x)| \equiv 1$. The long-distance decay is universally given by $\propto 1/x$, independent of interaction strength. Note that for decreasing coupling strength the asymptotic power-law decay sets in for increasingly larger propagation distances. At finite temperatures, this power-law decay turns into an exponential decay for large x with a decay rate Γ_φ depending on interaction strength (inset).

where the choice of $\omega_c \ll \omega_{\max}$ is arbitrary (but related to the constant), and $|G^>(\epsilon \to \infty, x)| = e^{-\mathrm{Re}[F(x)]}$. As a consequence of the logarithmic contribution to the exponent, the leading asymptotic behaviour of the Green's function is a power-law decay with an interaction-independent exponent 1:

$$\boxed{\left|G^>(\epsilon, x)\right| \propto \frac{1}{x}}. \tag{4.23}$$

More precisely, we claim: $\lim_{x \to \infty} \ln |G^>(\epsilon, x)| / \ln x = -1$. In writing down Eq. (4.22), we have neglected the contributions of large momenta in Eq. (4.7). These will lead to a subleading correction to the power-law, which we discuss in Subsection 4.3.2. The third term in Eq. (4.22) is responsible for oscillations in the coherence $|G^>(\epsilon, x)|$, on top of the decay (cf. Subsection 4.3.1). Fig. 4.3 shows the decay of $G^>(\epsilon \to \infty, x)$ for different coupling constants α. In order to understand how this generic result for the asymptotic decay is compatible with the non-interacting limit ($\alpha = 0$, where $|G^>(\epsilon, x)| \equiv 1$), we have to discuss the range of validity of the asymptotic behaviour. As the linear slope in the effective spectrum $\langle \{\hat{V}, \hat{V}\} \rangle_\omega$ applies only at $\omega \ll \omega_{\max}$, we must certainly require $\omega_{\max} x / v_F \gg 1$. Since $\omega_{\max}$ vanishes linearly with α, the limiting regime is reached at ever larger values of x when the interaction strength is reduced. This shift of the range of validity of the universal power-law decay is shown in Fig. 4.3.

4.3.1   Oscillatory modulation

The oscillatory modulation in $G^>(\epsilon, x)$ is due to the square root singularity at $\omega \to \omega_{\max}$ in the spectrum $\langle \{\hat{V}, \hat{V}\} \rangle_\omega$. Its amplitude depends on the interaction strength $|\alpha|$ but vanishes at long distances. The third term in the long-time limit of the exponent $\mathrm{Re} F(x)$ in Eq. (4.22) is responsible for the oscillations in $G^>(\epsilon \to \infty, x)$. The main contribution to this term stems from the square-root

singularity at $\omega = |\omega_{\max}|$. In the limit $\lim_{x \to \infty}$ this oscillatory part gives (with $\delta\omega > 0$)

$$2 \int_{|\omega_{\max}| - \delta\omega}^{|\omega_{\max}|} \frac{d\omega}{2\pi} \frac{\sin^2(\omega x/(2v_F))}{\omega^2} \cdot \left\langle \left\{ \hat{V}, \hat{V} \right\} \right\rangle_{\omega \approx |\omega_{\max}|}$$

$$\approx \quad \text{const.} - \text{Re} \left\{ \int_{|\omega_{\max}| - \delta\omega}^{|\omega_{\max}|} \frac{d\omega}{2\pi} \frac{e^{i\frac{\omega}{v}x}}{\omega^2} \cdot \left\langle \left\{ \hat{V}, \hat{V} \right\} \right\rangle_{\omega \approx |\omega_{\max}|} \right\}$$

$$\approx \quad \text{const.} - \frac{2}{q_{\max}\sqrt{2|\xi|}} \text{Re} \left\{ \int_{|\omega_{\max}| - \delta\omega}^{|\omega_{\max}|} d\omega \frac{e^{i\frac{\omega}{v_F}x}}{\sqrt{|\omega_{\max}| - \omega}} \right\}$$

$$= \quad \text{const.} - \frac{2}{q_{\max}\sqrt{2|\xi|}} Re \left[\int_0^{\delta\frac{x}{v_F}} d\nu \frac{e^{-i\nu}}{\sqrt{\nu}} \cdot \frac{e^{i|\omega_{\max}|\frac{x}{v_F}}}{\sqrt{t}} \right]$$

$$= \quad \text{const.} - \frac{1}{q_{\max}} \sqrt{\frac{2\pi}{|\xi|}} \frac{\sin\left(|\omega_{\max}|\frac{x}{v_F} + \frac{\pi}{4}\right)}{\sqrt{x/v_F}}$$

$$= \quad \text{const.} - C \cdot \frac{\sin(|\omega_{\max}|x/v_F + \pi/4)}{\sqrt{2\pi|\alpha|q_c x}},$$

where $C \equiv \frac{2\pi}{q_{max}} \sqrt{\frac{|\alpha|q_c v_F}{|\xi|}}$ denotes a numerical prefactor, depending only on the form of the interaction potential, but not on the interaction strength α. Here, we derive this prefactor only for analytical potentials of the type $U_q = 2\pi\alpha v_F \exp(-(q/q_c)^s)$. For this, we have to calculate the constant $\xi = \frac{1}{2\pi}\partial_q^2(qU_q)\big|_{q_{\max}}$ which was introduced in Eq. (4.19). With $q_{\max} = q_c/s^{1/s}$ it follows

$$\xi \quad = \quad \frac{1}{2\pi}\partial_q^2(q|U_q|)\bigg|_{q_{\max}}$$

$$= \quad \frac{1}{2\pi}\left(2|U|' + q|U|''\right)\big|_{q_{\max}}$$

$$= \quad \frac{\omega_{\max}}{q_c^2}\underbrace{\left\{ \frac{s^2}{s^{2-2/s}} - \frac{s(s-1)}{s^{1-2/s}} - \frac{2s}{s^{1-2/s}} \right\}}_{\tilde{\xi}_s}. \tag{4.24}$$

Thus the constant $C = 2\pi e^{\frac{1}{2s}} s^{3/(2s)} |\tilde{\xi}_s|^{-\frac{1}{2}}$.

4.3.2 Subleading contributions to decay

The previous calculation showed that in the leading order the decoherence shows a power-law behaviour. This was derived considering the low-frequency spectrum of

$$\left\langle \left\{ \hat{V}, \hat{V} \right\} \right\rangle_\omega^{T=0} \quad = \quad \int_0^\infty \frac{dq}{2\pi} |U_q|^2 q \delta(\omega - \frac{|U_q|q}{2\pi}).$$

In the derivation of Eq. (4.21) we neglected contributions resulting from large q. Those are strongly suppressed, as the integrand is proportional to U_q^2 decaying for $q \gg q_c$. Here, we calculate these contributions.

For this we introduce q_s as the solution of $[\omega - q|U_q|/(2\pi)] = 0$ in the limit $q \to \infty$. It follows

$$\frac{\omega}{v_F q_c |\alpha|} = \frac{q}{q_c} e^{-(q/q_c)^s}$$

$$\ln\left(\frac{\omega}{v_F q_c |\alpha|}\right) = \ln\frac{q}{q_c} - \left(\frac{q}{q_c}\right)^s$$

$$\ln\left(\frac{v_F q_c |\alpha|}{\omega}\right) \approx \left(\frac{q}{q_c}\right)^s. \tag{4.25}$$

Thus, q_s is given by: $q_s = q_c \ln(\frac{v_F q_c |\alpha|}{\omega})^{1/s}$. Inserting q_s in Eq. (4.12) yields for $T = 0$

$$\left\langle\left\{\hat{V},\hat{V}\right\}\right\rangle_{\omega>0}^{\text{sub}} = \int_0^\infty dq\, |U_q| \underbrace{\frac{|U_q|q}{2\pi}}_{=\omega} \frac{\delta(q - q_s)}{\left|\partial_q\left(\frac{|U_q|q}{2\pi}\right)\right|_{q=q_s}}$$

$$= \frac{2\pi\omega|U_{q_s}|}{\left\|U_q|\left(1 + q\partial_q|U_q|\right)\right|_{q=q_s}}$$

$$\approx \frac{2\pi\omega}{s\ln\left(\frac{q_c v_F}{\omega}|\alpha|\right)}. \tag{4.26}$$

As a result for smooth potentials like $U_q = U_0 e^{-(|q|/q_c)^s}$ the correction to the zero temperature decay is $\langle\{\hat{V},\hat{V}\}\rangle_\omega^{\text{sub}} = 2\pi\omega/(s\ln(|\alpha|\,v_F q_c/\omega))$. In real space this expression translates into a correction $\frac{1}{s}\ln(\ln(|\alpha|q_c x))$ to the decay function F. This can be seen calculating the contribution to the exponent in Eq. (4.22) which results from Eq. (4.26). Setting $\omega^* = q_c v_F |\alpha|$ the subleading contribution gives

$$\int_{v_F/x}^{\omega_c} \frac{d\omega}{2\pi} \frac{1}{\omega^2} \frac{2\pi\omega}{s\ln\left(\frac{q_c v_F |\alpha|}{\omega}\right)} = -\frac{1}{s}\int_{v_F/x}^{\omega_c} d\omega\, \frac{1}{\omega\ln\left(\frac{\omega}{\omega^*}\right)}$$

$$= -\frac{1}{s}\int_{v_F/(x\omega^*)}^{\omega_c/\omega^*} d\omega\, \frac{1}{\omega\ln\omega}. \tag{4.27}$$

This expression can be simplified further as in Eq. (4.22) we have some freedom in the choice of ω_c such that we can set: $\omega_c/\omega_{\text{max}} < 1$. Performing the substitution $\omega = e^{-y}$, yields

$$-\frac{1}{s}\int_{\ln(x\omega^*/v_F)}^{\ln(\omega^*/\omega_c)} dy\, \frac{1}{y} = \frac{1}{s}\ln\ln\frac{x\omega^*}{v_F} - \text{const}$$

$$= \frac{1}{s}\ln\left(\ln\left(xq_c|\alpha|\right)\right). \tag{4.28}$$

To conclude the zero temperature analysis, we sum up the different contributions yielding the long

time limit of the decoherence in chiral one-dimensional electron systems at $T = 0$ and for high-energy electrons (under the assumption of an analytic interaction potential $U_q = 2\pi v_F \alpha e^{-|q/q_c|^s}$):

$$|G^>(\epsilon, x)| \quad \propto \quad 1/x^{1+\frac{1}{s}\ln(\ln(xq_c|\alpha|))/\ln(x)} \exp\left\{ C \cdot \frac{\sin(\omega_{\max}x/v_F + \pi/4)}{\sqrt{2\pi|\alpha|q_c x}} \right\} \quad \epsilon \gg v_F q_c. \quad (4.29)$$

In Fig. 4.4, the modulus of the Green's function in the long-time limit is compared to the approximation in Eq. (4.29). Obviously, those match rather well.

Non-analytic potentials Even assuming non-analytic interaction potentials like ($n > 1$): $U_q = u|q/q_c|^{-n}$, the low-frequency spectrum still is of the ohmic type. However, due to the subleading contributions to the spectrum, here the prefactor depends on the particular form of the potential:

$$\begin{aligned}
\lim_{\omega \to 0} \left\langle \left\{ \hat{V}, \hat{V} \right\} \right\rangle_\omega^{\text{sub}} &= \int_0^\infty (dq)\, U_q^2 q \delta(|\omega| - \frac{|U_q|q}{2\pi}) \\
&= u q_c^n \int_0^\infty dq\, q^{1-2n} \frac{\delta(q - \bar{q})}{|(1-n)q^{-n}|_{\bar{q}}} \\
&= \frac{u}{|1-n|} \bar{q}^{1-n} q_c^n = \frac{2\pi|\omega|}{|1-n|}.
\end{aligned} \quad (4.30)$$

4.3.3   Finite temperature

At finite temperature $T \neq 0$, the long-time limit is given by an exponential decay $|G^>(x, \epsilon)| \propto \exp[-\Gamma_\varphi x/v_F]$, with a decay rate

$$\Gamma_\varphi = \pi T \left| 1 - \frac{v_F}{\bar{v}} \right| = \pi T |1 + \alpha^{-1}|^{-1}. \quad (4.31)$$

This follows from the long-time limit of Eq. (4.5) together with Eq. (4.12) using the identity $\lim_{a \to \infty} \frac{\sin^2(ax)}{ax^2} = \pi\delta(x)$:

$$\begin{aligned}
\lim_{x \to \infty} \text{Re} F(x) &= 2 \int_0^\infty dq\, \frac{\sin^2(q|U_q|x/(4\pi v_F))}{q} \coth(\frac{\omega_q}{2T}) \\
&= 2 \int_0^\infty \frac{dq}{q} \frac{1}{\pi} \frac{\sin^2(q|U_q|x/(4\pi v_F))}{x(|U_q|/(4\pi v_F))^2} \cdot x\pi(|U_q|/(4\pi v_F))^2 \coth(\frac{\omega_q}{2T}) \\
&= x\pi \lim_{q \to 0} \frac{2T}{qv_F(1+\alpha)} \cdot (2\pi|\alpha|v_F/(4\pi v_F)) \\
&= \frac{\pi T}{|1+\alpha^{-1}|} \frac{x}{v_F} = \Gamma_\varphi \frac{x}{v_F}.
\end{aligned} \quad (4.32)$$

Thus, we obtain the aforementioned decay rate Γ_φ.

In Fig. 4.3 the decay rate is shown as a function of the coupling α. For small α, this rate vanishes as $\Gamma_\varphi = \pi T|\alpha|$, i.e., it is non-analytic in $U_0 \propto \alpha$. Such dephasing rates proportional to T have also been found in non-chiral Luttinger liquids [25, 24, 15]. At large repulsive coupling, $U_0 \to +\infty$, we have the universal result $\Gamma_\varphi \to \pi T$. For attractive interaction, Γ_φ diverges upon approaching the instability at $\alpha \to -1$, where $\bar{v} \to 0$ and where the resulting low-frequency modes are thermally strongly excited. We note that this behaviour is somewhat surprising when compared to other problems of dephasing. When considering pure dephasing of a two-level system by an Ohmic bath, a power-law decay $t^{-\gamma}$ at $T = 0$, with an exponent γ set by the coupling, automatically implies an exponential decay at a rate $\Gamma_\varphi = \pi\gamma T$ at finite temperatures. This follows from the fluctuation-dissipation theorem which turns the $T = 0$ Ohmic spectrum into a white-noise spectrum with a weight proportional to T. However, in the present case, we have to take into account the Galileo transformation, which turns the laboratory-frame temperature T into an effective temperature T_{eff} in the frame moving along with the particle at speed v_F. In order to establish the FDT for the effective potential fluctuations in the electron frame of reference we therefore have to define the effective temperature T_{eff} by demanding for $\omega \downarrow 0$

$$
\begin{aligned}
\left\langle \left\{ \hat{V}, \hat{V} \right\} \right\rangle_\omega^\alpha &= \int_0^\infty \frac{dq}{2\pi} |U_q|^2 q \coth(\frac{\omega_q}{2T})\delta(\omega - \frac{|U_q|q}{2\pi}) \\
&\equiv \coth(\frac{\omega}{2T_{\text{eff}}}) \left\langle \left[\hat{V}, \hat{V} \right] \right\rangle_\omega^{|\alpha|}.
\end{aligned}
\tag{4.33}
$$

In this limit we get: $\langle\{\hat{V}, \hat{V}\}\rangle_\omega = 2\pi\omega \cdot \coth[\omega \left|1 + \alpha^{-1}\right|/(2T)]$. Together with the result for $\langle[\hat{V}, \hat{V}]\rangle_{\omega>0}^{|\alpha|}$ at small frequencies: $\langle[\hat{V}, \hat{V}]\rangle_{\omega>0}^{|\alpha|} = 2\pi\omega$, this yields the effective temperature

$$
T_{\text{eff}} \equiv \frac{T}{|1 + \alpha^{-1}|}.
\tag{4.34}
$$

In the moving frame the frequencies are reduced by qv_F and therefore the effective temperature is also smaller. Only for large repulsive interactions ($\bar{v} \gg v_F$), the transformation does not matter. Therefore, in this limit $T_{\text{eff}} = T$ and the universal, coupling-independent power-law for $T = 0$ turns into a universal decay rate at finite temperatures. Fig. 4.4b shows the modulus of $G^>(\epsilon, x)$ for different values of α at finite temperature.

4.3.4   Experimental observation of the power-law decay

To answer the question, whether a direct experimental observation in principle is possible, various aspects has to be taken into account:

- The arms of the interferometer must be long enough, such that the limit of long distances is reached: $x \gg v_F/\omega_{\text{max}}$.

- The applied bias voltage has to be large enough in order to ensure that the energy of the
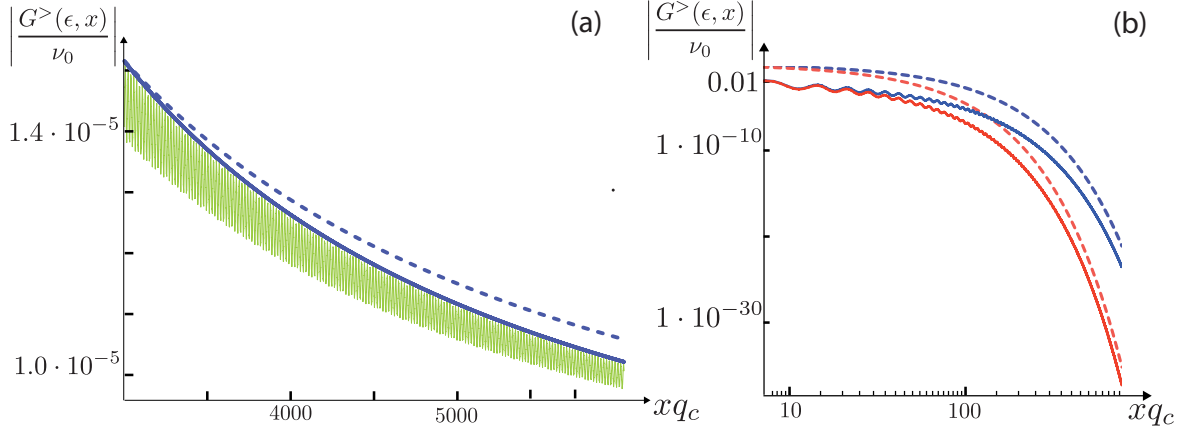
Figure 4.4: (a) Plot of $\lim_{\epsilon \to \infty} |G^>(\epsilon, x)|$ for large x (solid green line, heavily oscillating) and $T = 0$. Here $U_q = 2\pi v_F \alpha \exp(-(q/q_c)^2)$ with $\alpha = 1.0$. The dashed blue line shows $1/x$, while the solid blue line includes the subleading corrections Eq. (4.28) to the universal power-law stemming from large q in Eq. (4.12). (b) Plot of $\lim_{\epsilon \to \infty} |G^>(\epsilon, x)|$ at $T/(q_c v_F) = 0.01$ for $\alpha = 1/4$ (solid blue line) and $\alpha = -1/4$ (solid red line). This is compared to $\exp(-\Gamma_\varphi(\alpha)\frac{x}{v_F})$ (dashed lines).

propagating electrons reaches the high-energy limit: $\epsilon \gg q_c v_F$.

- The temperature must be small enough such that the power-law for intermediate propagation distances can be observed and only for $x \to \infty$ the exponential decay mentioned above comes into play.

- In the long-distance limit, the visibility v_I of the interference contrast has to be large enough in order to ensure the direct observation of the power-law decay.

The following rough estimates are based on the assumption of a screened Coulomb potential:

$$U(x) = \frac{q_e^2}{4\pi\epsilon_0\epsilon_r} \cdot \frac{e^{-q_c\sqrt{x^2+b^2}}}{\sqrt{x^2 + b^2}}, \tag{4.35}$$

where $b \sim 10^{-7}m$ denotes the finite width of the quantum-hall edge channel and q_c is the inverse of the mean screening length. As typically the interferometer sizes [27, 28, 42, 20] are of the order $\sim 10^{-6}m$ and several metallic gates (as the top-bridge used in [39, 20]) screen the electron-electron interactions, for q_c we assume: $q_c^{-1} \sim 10^{-7}m$. The coupling constant α can be estimated starting from the Fourier transformed of Eq. (4.35) in the limit $q \to 0$:

$$\lim_{q \to 0} U_q = \frac{q_e^2}{4\pi\epsilon_0\epsilon_r} \int dx \, \frac{e^{-q_c\sqrt{x^2+b^2}}}{\sqrt{x^2 + b^2}}. \tag{4.36}$$

As the integral is dimensionless, it follows

$$\lim_{q \to 0} U_q = \frac{q_e^2}{4\pi\epsilon_0\epsilon_r} \cdot \mathcal{U}(\sim \ln\left[\frac{1}{q_c a}\right]) \quad \mathcal{U} = \mathcal{O}(1),$$

and we can determine the dimensionless coupling constant $\alpha = \frac{U_0}{2\pi\hbar v_F}$

$$\alpha = \underbrace{\frac{1}{8\pi^2\epsilon_r}}_{\mathcal{O}(10^3)} \cdot \frac{q_e^2}{\epsilon_0} \cdot \frac{1}{\hbar v_F} \cdot \mathcal{C} \tag{4.37}$$

for $\epsilon_r[\text{GaAs}] \sim 10$. In [6] the edge state velocity v_F is quoted as $v_F \sim (10^4 - 10^5)\frac{m}{s}$. With $\frac{q_e^2}{\epsilon_0} \sim 10^{-38}/10^{-11}Jm$ and $\frac{1}{\hbar v_F} \sim 10^{34} \cdot 10^{-4}J^{-1}m^{-1}$ for $v_F = 10^4\frac{m}{s}$, we have

$$\alpha \sim 10^{-3} \cdot 10^{-27} \cdot 10^{30} \sim \mathcal{O}(1). \tag{4.38}$$

The frequency $\omega_{\max} \sim \frac{1}{2\pi\hbar}U_0 q_c = \alpha v_F q_c$ determing the period of the oscillations on top of the decay, is: $\omega_{\max} \sim 10^{11}s^{-1}$. The long-distance limit, in which the power-law decay should emerge is given for $x \gg v_F/\omega_{\max} \sim 10^{-1}\mu m$, which compares to the typical length of the interferometer channels (in [39] the arm length is of the order $\sim 10^1\mu m$). The semiclassical method is only valid in the high-energy regime, i.e., $\hbar v_F q_c \gg 1$. In order to reach that limit we have to apply bias voltages $V \gg \hbar q_c v_F/q_e \sim 10^2\mu V$. Again, this is in the range of the experiments: In [39] the typical bias voltages are of the order $\sim \mu V$. The interferometers usually are cooled down to $T \sim 10^{-3}K$ [39], therefore the inverse decay rate of the coherence is obtained from Eq. (4.32): $\Gamma_\varphi^{-1} = (k_B T/\hbar v_F)^{-1} \sim 10^2\mu m$. As a result there should be some intermediate regime $10^{-1}\mu m \ll x \ll 10^2\mu m$ where the universal power-law decay in principle could be observed (cf. Fig. 4.3 where this intermediate regime for $\alpha = 1$ and $T \neq 0$ obviously shows up). However, as the visibility decays drastically once the long-distance limit is reached, a direct observation might be a difficult experimental task. This can be obtained from Fig. 4.3 where one can observe that in regime of validity the magnitude of the Green's function has already fallen to $|G^>(\epsilon, x)|/|\nu_0(\epsilon)| \sim 10^{-2}$. Therefore, one can estimate the corresponding visibility to be of the order $v_I \sim 10^{-4}$ [cf. Eq. (2.26)].

4.4 Equations of motion approach

To conclude this chapter, we give a more rigorous motivation for the semiclassical ansatz in Eq. (4.3), which served as the starting point of the whole analysis. It is motivated by the equations of motion method proposed in [36, 32, 31] for describing the coherence properties of non-interacting electrons influenced by some external bath. Beside the transparency of the method, the main advantage is that it can deal with many-body effects as Pauli blocking. The equations of motion approach is based on

the Heisenberg equation for the single particle operators $\hat{\psi}(x,t)$. Linearizing the electronic dispersion relation, the normal ordered Hamiltonian in total reads

$$
\begin{aligned}
\hat{H} &= \hat{H}_{\text{el}} + \hat{H}_{\text{bath}} + \hat{H}_{\text{int}} \\
&= -iv_F \int dx\, \hat{\psi}^\dagger(x)\partial_x\hat{\psi}(x) + \hat{H}_{\text{bath}} + \int dx\, \left\{\hat{\psi}^\dagger(x)\hat{\psi}(x)\right\}\hat{V}(x).
\end{aligned}
\tag{4.39}
$$

The time evolution of the single particle operators $\hat{\psi}(x)$ can be obtained from the Heisenberg equation $\frac{d}{dt}\hat{\psi} = -i\left[\hat{\psi},\hat{H}\right]$:

$$
\begin{aligned}
\partial_t\hat{\psi} &= -v_F \int dx'\, \left[\hat{\psi}(x),\hat{\psi}^\dagger(x')\partial_{x'}\hat{\psi}(x')\right] - i\int dx'\, \left[\hat{\psi}(x),\hat{\rho}(x')\right]\hat{V}(x') + \hat{H}_{\text{bath}} \\
&= -v_F \int dx'\, \left\{\hat{\psi}(x),\hat{\psi}^\dagger(x')\right\}\partial_{x'}\hat{\psi}(x') - i\int dx'\, \left\{\hat{\psi}(x),\hat{\psi}^\dagger(x')\right\}\hat{\psi}(x')\hat{V}(x') + \hat{H}_{\text{bath}}.
\end{aligned}
$$

In order to proceed further we make use of the canonical anti-commutation relation for fermionic operators $\left\{\hat{\psi}(x),\hat{\psi}^\dagger(x')\right\} = \delta(x-x')$. Then it follows

$$
\begin{aligned}
\partial_t\hat{\psi}(x) &= -v_F \int dx'\, \delta(x-x')\partial_{x'}\hat{\psi}(x') - i\int dx'\, \delta(x-x')\hat{\psi}(x')\hat{V}(x') + \hat{H}_{\text{bath}} \\
&= -v_F\partial_x\hat{\psi}(x) - i\hat{\psi}(x)\hat{V}(x) + \hat{H}_{\text{bath}},
\end{aligned}
\tag{4.40}
$$

so that finally we are left with an ordinary transport equation determing the dynamics of the single particle operators $\hat{\psi}$:

$$
i\left[\partial_t + v_F\partial_x\right]\hat{\psi}(x,t) = \hat{V}(x)\hat{\psi}(x,t).
\tag{4.41}
$$

Equation (4.41) is the reason why this approach is called "semiclassical", as it suggests thinking of a particle represented by the fermionic field $\hat{\psi}$ collecting some fluctuating phase along its classical trajectory $x = v_F t$. If we were dealing with a classical fluctuating potential $V(t)$, the electron would simply pick up a random phase: $\hat{\psi}(x,t) \sim \exp\left[-i\int_{t_0}^t dt'\, V(x-v_F(t-t'),t')\right]$. However, if the quantum nature of the bath becomes important one has take care of the non-commutativity of the operator $\hat{V}(t)$ at different times. This is done by introducing a time-ordering symbol $\hat{T}$, such that the formal solution of Eq. (4.41) gives

$$
\hat{\psi}(x,t) = \hat{T}\exp\left[-i\int_{t_0}^t dt'\, \hat{V}(x-v_F(t-t'),t')\right]\hat{\psi}(x-v_F(t-t_0),t_0).
\tag{4.42}
$$

We emphasize that here we are dealing with a quantum potential $\hat{V}$, which in general contains the response of the bath to the particle's motion as well (for more details we refer the reader to [31, 36, 32]). The backaction allows for an energy transfer between the electron and the bath; however, here Pauli

blocking comes into play. Namely, it suppresses all transitions that would take the electron into an occupied state. In the end, the Green's function $G^>(x,t) = -i \left\langle \hat{\psi}(x,t)\hat{\psi}^\dagger(0,0) \right\rangle$ for a translational invariant system is found as

$$G^>(x,t) \quad = \quad g^>(x,t) \left\langle \hat{T}e^{-i\int_0^t dt' \, \hat{V}(x-v_F(t-t'),t')} \right\rangle, \tag{4.43}$$

where the average on the right side of Eq. (4.43) refers to the bath degrees of freedom. But this is obviously the expression for the Green's function we used as a physically motivated ansatz in Eq. (4.3), where we restricted the considerations to $G^>(x = v_F t)$. In contrast to the more general equations of motion approach, despite the quantum nature of the plasmonic bath we neglected any backaction effects, i.e., the bath was assumed to evolve autonomously. On the basis of Eq. (4.42) in the upcoming Chapter we will consider the semiclassical ansatz for arbitrary points in the space-time plane, thereby extending the approach to electrons with arbitrary energies.

4.5   Summary

We proposed a simple semiclassical ansatz for the Green's function $G^>(\epsilon, x)$. It is one of our main results that, compared to the full bosonization solution, this simple semiclassical approach becomes exact considering electrons propagating with large energies $\epsilon \gg q_c v_F$. At zero temperature in this limit the coherence displays a universal power-law $|G^>(\epsilon, x)| \sim 1/x^1$, where most remarkably the exponent turns out to be independent from the coupling strength of the electron-electron interaction.

Chapter 5

Semiclassical approach and functional bosonization

Bosonization is a powerful tool for calculating Green's functions of strongly-interacting electron systems. Besides providing us with the single particle Green's function $G^>(x,t)$, we already discussed in Chapter 3 it enables, at least the numerical evaluation of more complicated correlators as the two-particle Green's functions we discuss in Chapter 7. However, the main disadvantage of the bosonization method is that it does not allow for a simple interpretation of its results. This relies on the fact that in physical applications as the Mach-Zehnder interferometer, we are interested in the particle current, i.e. in the physical properties of single electrons. Thus, two very different points of view collide. On the one hand, the bosonization of the one-dimensional systems identifies collective, bosonic modes $\{\hat{b}_q\}$ (the density fluctuations) as the relevant degrees of freedom. All the information about the electron-electron interaction is stored in the plasmonic dispersion relation ω_q. On the other hand, being interested in the electronic properties of a device like the Mach-Zehnder interferometer we have to calculate the appropriate Green's function. For example, considering the propagator function $G^> = -i\langle \hat{\psi}(x,t)\hat{\psi}^\dagger(0,0)\rangle$, we insert a single electron into the strongly interacting system and ask for its phase coherence after some propagation time. The main question is, what happens with the single particle in the moment it tunnels into the liquid? Is it possible to 'trace' the electron after the tunnel event or is it, in some sense, directly absorbed into the liquid?

The semiclassical approach we introduced in the previous Chapter 4 clarifies the nature of chiral one-dimensional electrons in the high-energy limit. Despite of the strong interactions, it suggests to think of single electrons flying through the channel experiencing all the other electrons only in form of a fluctuating potential background (cf. Fig. 4.1). The purpose of this Chapter is to extend the semiclassical approach for describing electrons of arbitrary energies. There are some good reasons to be sceptically about this plan. Especially, it seems to be a well known fact that for small energies the

chiral, interacting electron system is equivalent to an ordinary Fermi liquid (cf. Sections 3.2.2 and 3.2.3). This implies a certain velocity renormalization at low energies, which a description via the semiclassical approach can not take into account.

However, there is one main motivation for analyzing the semiclassical method in more detail. Namely, there is an alternative method for describing interacting one-dimensional electron systems, the so-called "functional bosonization" [12, 23, 10, 16]. This method, based on the functional field integral technique, makes use of an ordinary Hubbard-Stratonovich transformation (HST). The transformation converts the Hamiltonian, containing contributions quartic in fermionic operators, into a new Hamiltonian, which is quadratic in the fermionic fields. In turn, an additional bosonic field ϕ is introduced, which couples to the fermionic degrees of freedom: $S_{el} = \int d\tau \int dx \, \bar{\psi}(\partial_\tau - iv_F\partial_x + i\phi)\psi$ (here $\tau = it$). In one-dimension, the coupling to this bosonic field can be incorporated into a redefinition of the fermionic field ψ via a simple gauge transformation $\psi' = \psi e^{i\theta(x,\tau)}$, where $(\partial_\tau - iv\partial_x)\theta = -\phi$. The gauge transformation entails a non-trivial Jacobian, which influences the dynamics of the bosonic HST-field. The crucial point is that, in the end, the action of the bosonic field turns out to be quadratic, under the assumption of linearising the free electronic dispersion relation, reflecting the famous results of Dzyaloshinski and Larkin [8]. One ends up with a theory which is quadratic in the decoupled fermionic and bosonic degrees of freedom. Thus, the formal calculation of any correlation function can be done as easy as in the standard approach. The resulting imaginary time-ordered Green's function $G_\tau \equiv -\langle\psi\bar{\psi}\rangle$ is a product of the free Green's function and a factor depending only on the bosonic field ϕ, averaged with respect to the bosonic part of the action: $G_\tau(x,\tau) = -g_\tau(x,\tau)\langle e^{-i\theta(x,\tau)}e^{i\theta(0,0)}\rangle_\phi$ (g_τ denotes the non-interacting imaginary time-ordered Green's functions). The Keldysh-time version of the functional bosonziation was applied studying, e.g., the zero bias anomaly in the tunnel density of states for Luttinger liquids out of equilibrium [7]. From a conceptual point of view, the functional bosonization may provide a deeper insight into the physics of one-dimensional electron systems. Namely, it suggests that everything (there is no restriction to high energies) can be understood thinking in terms of free electrons accumulating some phase traversing its classical trajectory. But this is rather close to the interpretation of the semiclassical approach, we introduced in Chapter 4. After an analytical continuation, the functional bosonization reproduces the well known bosonization result for $G^>$. Extracting, the real physics behind this, first of all mathematical identity is a rather difficult task. The comparison of the semiclassical model and the functional bosonization (formulated in Keldysh time) should be helpful for clarifying this question.

In Section 5.1 we start from the formal expression for the fermionic fields $\hat{\psi}(x,t)$ subjected to quantum noise derived in Section 4.4 within the equations of motion approach [31, 32, 36]. In a next step we plug in these fields $\hat{\psi}(x,t)$ into the definition of $G^>(x,t) = -i\langle\hat{\psi}(x,t)\hat{\psi}^\dagger(0,0)\rangle$, thereby introducing the semiclassical ansatz. This ansatz is meant to reproduce the bosonization solution for any (x,t). We argued in Section 4.1 that this is equivalent with extending the approach to arbitrary energies. As in the previous chapter, the non-interacting Green's function $g^>(x,t)$ is multiplied with a factor

$\exp(-F(x,t))$ responsible for the a suppresion of the Green's function. In contrast to the usual equations of motion approach dealing with quantum baths, here the main assumption is that we can neglect any backaction effects. In close analogy to the previous chapter, everything reduces to a calculation of the bath spectrum. In Section 5.2 we concentrate on the plasmonic bath representing all the electrons from the Fermi sea, whose dynamics are goverened by the dispersion relation ω_q (cf. Eq. (3.12)). The semiclassical ansatz essentially is the solution of the Heisenberg equation of motion for the fermionic fields $\hat{\psi}(x,t)$. Therefore, finally we have to fix the appropriate initial condition. This turns out to be a very subtle point, which is discussed in Section 5.3.

The main result is that the semiclassical ansatz reproduces the Green's function only under the assumption of a rather unphysical initial condition. From this point of view it does not reproduce the bosonization solution completely. Nevertheless, in Section 5.3 it is shown that it might be helpful for a better understanding of the bosonization solution.

5.1 Coupling to an external quantum bath without backaction

In this Section we propose an intuitive, semiclassical ansatz in order to derive the full single particle Green's function $G^>(x,t)$ of a chiral, one-dimensional interacting electron system. While in Chapter 4 we employed a semiclassical approach valid only in the high-energy limit, here we drop this restriction. As an ansatz for this analysis, we start with the general expression for the fermionic fields $\hat{\psi}(x,t)$ derived in Section 4.4 describing the time-evolution of an electron subjected to a quantum noise potential $\hat{V}(x,t)$:

$$\hat{\psi}(x,t) \;\; = \;\; \hat{T}\exp\left[-i\int_0^t dt'\,\hat{V}(\delta x + v_F t', t')\right]\cdot\hat{\psi}(\delta x + v_F t_i, t_i), \tag{5.1}$$

where we set $\delta x \equiv x - v_F t$. The physical interpretation of Eq. 5.1 is rather simple. A single electron moving ballistically with v_F, represented by the fermionic field $\hat{\psi}(x,t)$, in the presence of a random quantum potential collects an additional phase $-\int_0^t dt'\,\hat{V}(\delta x + v_F t', t')$. The time ordering symbol $\hat{T}$ takes into account that the potentials $\hat{V}(x,t)$ for different times in general do not commute. As in the previous Chapter, we identify this external bath potential with the potential stemming from the plasmonic excitations present in the one-dimensional electron system. This ansatz tries to map the interaction effects on an injected electron resulting from very complicated interparticle interactions, on a situation where this electron moves ballistically experiencing only the effect of an external background potential.

Within the equations of motion approach due to the quantum nature of the bath potential $\hat{V}(x,t)$, in general one has to take into account the backaction of the electron onto the bath. However, in the previous Chapter neglecting any backaction effects, we were successful in deriving the correct
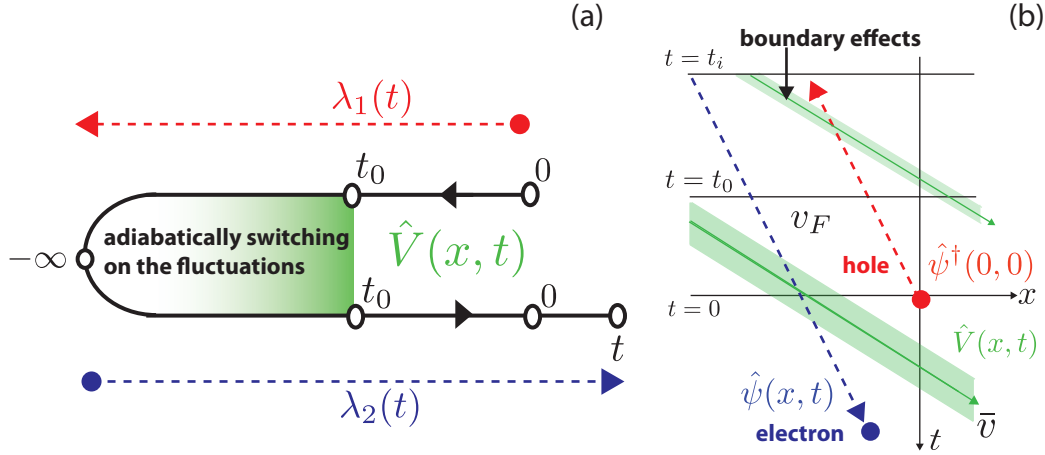
Figure 5.1: (a) Scheme of the Keldysh contour introduced in the main text. (b) Pictorial plot of the boundary effects emerging in the general semiclassical approach. In Chapter 4 we restricted the consideration to the classical trajectory $x = v_F t$. There, the electron and the hole during its time-evolution from t_i to $t = 0$ collect exactly the same phase (with inverted signs), regardless of the specific realization of the bath potential. Calculating the Green's function at $x = v_F t$ this additional phase drops out. Extending the description to arbitrary (x, t) this is not the case anylonger. As we have to fix some initial time t_i boundary effects arise. To tackle this problem we assume the fluctuations to be fade out adiabatically (see main text), supressing these boundary effects

Green's function from the semiclassical approach in the high-energy limit. Therefore, extending the theoretical description to arbitrary energies, we follow the same lines. However, we note that neglecting the backaction is equivalent with demanding that the electron is not scattered inelastically during its propagation. To proceed further, we consider the Green's function $-i\langle\hat{\psi}(x,t)\hat{\psi}^\dagger(0,0)\rangle$, but insert the ansatz for the fermionic fields $\hat{\psi}$ in Eq. (5.1):

$$
\begin{aligned}
-i\left\langle\hat{\psi}(x,t)\hat{\psi}^\dagger(0,0)\right\rangle &= -i\lim_{t_i\to-\infty}\left\langle\hat{\psi}(\delta x+v_F t_i,t_i)\hat{\psi}^\dagger(v_F t_i,t_i)\right\rangle_{\text{el}}\times\\
&\quad\left\langle\left(\hat{T}e^{-i\int_{-\infty}^t dt'\,\hat{V}(\delta x+v_F t',t')}\right)\left(\hat{T}e^{-i\int_{-\infty}^0 dt'\,\hat{V}(v_F t',t')}\right)^\dagger\right\rangle_{\text{Bath}}\\
&\equiv -i\lim_{t_i\to-\infty}\left\langle\hat{\psi}(\delta x+v_F t_i,t_i)\hat{\psi}^\dagger(v_F t_i,t_i)\right\rangle_{\text{el}}e^{-F(x,t)}. \qquad (5.2)
\end{aligned}
$$

As in Chapter 4 we denote the factor $e^{-F(x,t)}$ as the coherence (but here it depends on x and t). In the following, we assume a translational invariant, fluctuating environment, while the coupling to the ballistically moving electron is switched on adiabatically, such that at t_0 the full coupling is achieved. This procedure is the standard way to preclude boundary effects as shown in Fig. 5.1.

We emphasize that it is not the coupling strength α itself, which is increased but the influence of the fluctuations on the propagating electrons. In the end we send γ to zero: $\gamma \to 0$ and show the result to become independent of t_0. This reflects the fact that the exponential suppression of the fluctuations suffices to erase any information about the specific initial conditions. The subtle point is that due to the adiabatic switching on of the fluctuations, some extra terms, dependent on t_0, emerge. However, for electrons subjected to potential fluctuations resulting from plasmons, it turns out that those are suppressed due to the 'ohmic' low-frequency spectrum of the plasmonic bath. We discuss these additional terms in subsection 5.2.3.

The expression in the brackets can be re-expressed by introducing an appropriate Keldysh time-contour (cf. Fig. (5.1)). In Eq. (5.3) we define the abbreviations representing the potentials acting on the forward ($\hat{V}_1$) or the backward branch ($\hat{V}_2$):

$$\hat{V}_i(t') \quad \equiv \quad \begin{cases} i = 1: & \hat{V}(v_F t', t')\lambda_1(t') \\ i = 2: & \hat{V}(\delta x + v_F t', t')\lambda_2(t') \end{cases} . \tag{5.3}$$

The weight functions λ_i control the strength of the fluctuations which is adiabatically switched on:

$$\lambda_i(t') \quad \equiv \quad \begin{cases} i = 1: & \Theta(t_0 - t')e^{\gamma(t_0 - t')} + \Theta(t' - t_0)\Theta(-t') \\ i = 2: & \Theta(t_0 - t') \cdot e^{\gamma(t' - t_0)} + \Theta(t' - t_0)\Theta(t - t') \end{cases} , \tag{5.4}$$

where in the end we send the rate γ to $\gamma \to 0^+$. In addition we define t_0 such that: $t_0 \ll t$. Now, we can write the coherence $e^{-F(x,t)}$ in a compact form (here $\hat{T}_K$ denotes the Keldysh time ordering symbol, ordering the operator with the smallest Keldysh time to the right.) [1]

$$e^{-F(x,t)} \quad = \quad \left\langle \hat{T}_K e^{-i \oint_K \hat{V}} \right\rangle . \tag{5.5}$$

At this point the fact that we are dealing with a bath of harmonic oscillators has an important consequence. Namely, we can make use of the identity for Gaussian random variables, which holds true even for Keldysh time-ordered exponentials:

$$\left\langle \hat{T}_K e^{-i \oint_K \hat{V}} \right\rangle \quad \equiv \quad \exp\left[-\frac{1}{2} \oint_K dt_1 \oint_K dt_2 \left\langle \hat{T}_K \hat{V}(t_1)\hat{V}(t_2) \right\rangle \right] . \tag{5.6}$$

5.1.1 Structure of the exponent

In a first step, one has to calculate the structure of the integrand with some care. The Keldysh time ordering symbol moves the operators with the smallest Keldysh time to the right. Per definition, the Keldysh times on the forward branch are always considered to be smaller than the backward

---

[1] A Keldysh time is considered to be larger than another if it is reached later traversing the Keldysh contour. In particular, times on the forward branch in this sense are always considered to be smaller than times on the backward branch.

branch times. For the explicit calculation of a Keldysh contour integral, first of all one performs the substitution $\oint_K dt' \to \int_\infty^{-\infty} dt_1 + \int_{-\infty}^\infty dt_2$. In the following one introduces additional indices labelling the potentials $\hat{V}(x,t)$ on the backward and on the forward branch. Making use of the definitions in Eq. (5.3) and Eq. (5.4) $F(x,t)$ yields ($\tilde{T}$ denotes the anti-time ordering symbol):

$$
\begin{aligned}
F(x,t) &= \frac{1}{2}\left[\int_1 dt_1 \int_1 dt_2 \left\langle T\hat{V}_1(t_1)\hat{V}_1(t_2)\right\rangle + \int_2 dt_1 \int_2 dt_2 \left\langle \tilde{T}\hat{V}_2(t_1)\hat{V}_2(t_2)\right\rangle\right] \\
&\quad - \frac{1}{2}\left[\int_1 dt_1 \int_2 dt_2 \left\langle \hat{V}_2(t_2)\hat{V}_1(t_1)\right\rangle + \int_2 dt_1 \int_1 dt_2 \left\langle \hat{V}_2(t_1)\hat{V}_1(t_2)\right\rangle\right].
\end{aligned}
\tag{5.7}
$$

For reasons of brevity, here we denote the integral over the forward and the backward branch with $\int_1$ and $\int_2$, respectively. As we are dealing with a quantum potential $\hat{V}_i$ the correlation function is sensitive to the internal ordering of the involved operators. In general, one can express a correlation function $\langle \hat{V}_i \hat{V}_j \rangle$ by a sum of a commutator and an anti-commutator part: $\langle \hat{V}_i \hat{V}_j \rangle = \frac{1}{2}\langle [\hat{V}_i, \hat{V}_j] \rangle + \frac{1}{2}\langle \{\hat{V}_i, \hat{V}_j\} \rangle$. For the (anti)time-ordered correlation function emerging in Eq. (5.7) this translates into:

$$
\begin{aligned}
\left\langle T\hat{V}(t_1)\hat{V}(t_2)\right\rangle &= \frac{1}{2}\left\langle\left\{\hat{V}(t_1), \hat{V}(t_2)\right\}\right\rangle - \text{sgn}(t_1 - t_2)\frac{1}{2}\left\langle\left[\hat{V}(t_1), \hat{V}(t_2)\right]\right\rangle \\
\left\langle \tilde{T}\hat{V}(t_1)\hat{V}(t_2)\right\rangle &= \frac{1}{2}\left\langle\left\{\hat{V}(t_1), \hat{V}(t_2)\right\}\right\rangle + \text{sgn}(t_1 - t_2)\frac{1}{2}\left\langle\left[\hat{V}(t_1), \hat{V}(t_2)\right]\right\rangle
\end{aligned}
\tag{5.8}
$$

Plugging in the expression Eq. (5.8) into the defining equation for the exponent $F(x,t)$ leads to the intermediate result

$$
\begin{aligned}
F(x,t) &= \frac{1}{4}\sum_{j=1,2}\int_j dt_1 \int_j dt_2 \left(\left\{\begin{array}{l} j=1 : \text{sgn}(t_2 - t_1) \\ j=2 : \text{sgn}(t_1 - t_2) \end{array}\right\}\left\langle\left[\hat{V}_j(t_1), \hat{V}_j(t_2)\right]\right\rangle \right. \\
&\quad \left. + \left\langle\left\{\hat{V}_j(t_1), \hat{V}_j(t_2)\right\}\right\rangle\right) - \int_1 dt_1 \int_2 dt_2 \left\langle\hat{V}_2(t_2)\hat{V}_1(t_1)\right\rangle.
\end{aligned}
\tag{5.9}
$$

5.1.2   Calculation of the exponent

The explicit calculation of the exponent now is a straight forward, but rather cumbersome task. Especially, the non-trivial structure of the Keldysh contour requires an accurate book-keeping of the three parts contributing to $F = \sum_{i=1}^3 F_i$: The commutator part F_1 (first term in Eq. (5.9)), the anti-commutator part F_2 (second term), and the correlator part F_3 (third term). The main goal is to express everything in terms of the Fourier transformed correlators, which are directly related to the spectrum of the potential fluctuations. Assuming translational invariance of the fluctuations in time and space, those can be defined as: $\langle \hat{V}\hat{V}\rangle_\omega = \int dt\, e^{i\omega t}\langle \hat{V}(t)\hat{V}(0)\rangle$. In the following, we already present the results of the involved integrals. For completeness the explicit calculations are shown in C.

Commutator part of $\mathbf{F}(\mathbf{x}, \mathbf{t})$ The calculation of the commutator part in Eq. (5.9), $F_1(x, t)$, only involves correlators with time arguments lying on the same contour. In the following, we denote the corresponding Fourier transformed correlators as $\langle [\hat{V}, \hat{V}] \rangle_\omega^{(0)}$. It yields (where we take the limit $\gamma \to 0^+$ in the last step)

$$
\begin{aligned}
F_1 + \delta F_1 &= \frac{1}{4} \int (d\omega) \left\langle \left[\hat{V}, \hat{V} \right] \right\rangle_\omega^{(0)} \sum_{j=1,2} \int_j dt_1 \int_j dt_2 \times \\
&\quad \left\{ \begin{array}{l} j = 1 : \mathrm{sgn}(t_2 - t_1) \\ j = 2 : \mathrm{sgn}(t_1 - t_2) \end{array} \right\} e^{-i\omega(t_1 - t_2)} \lambda_j(t_1) \lambda_j(t_2) \\
&= \frac{i}{2} \int (d\omega) \left\langle \left[\hat{V}, \hat{V} \right] \right\rangle_\omega^{(0)} \times \\
&\quad \mathrm{Im} \left(\int_0^t dt_2 e^{-i\omega t_1} \left\{ \int_{-\infty}^{t_0} dt_1 \, e^{\gamma(t_1 - t_0) + i\omega t_1} + \int_{t_0}^0 dt_1 \, e^{i\omega t_1} \right\} \right. \\
&\quad \left. + \int_0^t dt_1 \int_0^{t_1} dt_2 e^{-i\omega(t_1 - t_2)} \right) \\
&= - \frac{i}{2} \int (d\omega) \left\langle \left[\hat{V}, \hat{V} \right] \right\rangle_\omega^{(0)} \left(\frac{t}{\omega} - \frac{\pi}{\omega} \delta(\omega) \mathrm{Re} \left[e^{i\omega(t_0 - t)} - e^{i\omega t_0} \right] \right). \qquad (5.10)
\end{aligned}
$$

Finally, we can identify a trivial phase shift in the Green's function resulting from this contribution (this phase is related to the energy shift resulting from the Fock diagram we discussed already in Section 4.1)

$$
F_1 = - \frac{i}{2} t \int \frac{(d\omega)}{\omega} \left\langle \left[\hat{V}, \hat{V} \right] \right\rangle_\omega^{(0)}. \qquad (5.11)
$$

The extra term Eq. (5.10) vanishes for a spectrum which fulfills (especially for ohmic spectra): $\langle \hat{V} \hat{V} \rangle_\omega \sim \mathcal{O}(\omega^0)$.

Anti-commutator part of $\mathbf{F}(\mathbf{x}, \mathbf{t})$ In close analogy to the previous calculation, the anti-commutator part F_2 yields (we denote the Fourier transformed correlator of the anti-commutator with time arguments lying on the same branch by $\langle \{\hat{V}, \hat{V}\} \rangle_\omega^0$):

$$
\begin{aligned}
F_2 &= \frac{1}{4} \int (d\omega) \left\langle \left\{ \hat{V}, \hat{V} \right\} \right\rangle_\omega^{(0)} \sum_{j=1,2} \left(\int_j dt_1 \int_j dt_2 \, e^{-i\omega(t_1 - t_2)} \lambda_j(t_1) \lambda_j(t_2) \right) \\
&= \frac{1}{4} \int (d\omega) \left\langle \left\{ \hat{V}, \hat{V} \right\} \right\rangle_\omega^{(0)} \left(\left| \int_{-\infty}^\infty dt_1 \lambda_1(t_1) e^{-i\omega t_1} \right|^2 + \left| \int_{-\infty}^\infty dt_1 \lambda_2(t_1) e^{-i\omega t_1} \right|^2 \right). \qquad (5.12)
\end{aligned}
$$

In the limit of $\gamma \to 0^+$, the integration yields

$$F_2 + \delta F_2 \;\; = \;\; \frac{1}{2} \int (d\omega) \, \frac{\left\langle \left\{ \hat{V}, \hat{V} \right\} \right\rangle_\omega^{(0)}}{\omega^2} + \lim_{\omega \to 0} \left(\left[\frac{t - 2t_0}{4} + \mathcal{O}(\omega) \right] \left\langle \left\{ \hat{V}, \hat{V} \right\} \right\rangle_\omega^{(0)} \right). \tag{5.13}$$

Here, δF_2 denotes the t_0-dependent extra contribution stemming from the switching-on procedure. We will discuss this additional term in subsection 5.2.3.

Correlator part of $\mathbf{F(x,t)}$ Finally, the correlator part F_3 can be evaluated easily. However, here we have to introduce the Fourier transform of the correlator which involves potentials on two different branches:

$$\left\langle \hat{V}\hat{V} \right\rangle_\omega^{(1)} \equiv \int dt \, e^{-i\omega t} \lambda_1^{-1} \lambda_2^{-1} \left\langle \hat{V}_2(t)\hat{V}_1(0) \right\rangle. \tag{5.14}$$

Then the contribution gives:

$$
\begin{aligned}
F_3 \;\; + \delta F_3 = - & \int (d\omega) \left\langle \hat{V}\hat{V} \right\rangle_\omega^{(1)} \int_{-\infty}^{\infty} dt_1 \int_{-\infty}^{\infty} dt_2 e^{-i\omega(t_2 - t_1)} \lambda_2(t_2)\lambda_1(t_1) \\
= & \;\; -\int (d\omega) \left\langle \hat{V}\hat{V} \right\rangle_\omega^{(1)} \left[\frac{e^{-i\omega t}}{\omega^2} \right] - \lim_{\omega \to 0} \left(\left[\frac{t - 2t_0}{2} + \mathcal{O}(\omega) \right] \left\langle \hat{V}\hat{V} \right\rangle_\omega^{(0)} \right).
\end{aligned}
\tag{5.15}
$$

Summing up the three different parts of $F = \sum_{i=1}^{3} F_i$, the exponent finally yields:

$$
\begin{aligned}
F \;\; + \delta F = & \int \frac{(d\omega)}{\omega^2} \left(\frac{1}{2} \left\langle \left\{ \hat{V}, \hat{V} \right\} \right\rangle_\omega^{(0)} - \left\langle \hat{V}\hat{V} \right\rangle_\omega^{(1)} e^{-i\omega t} \right) - \frac{i}{2} \int (d\omega) \left[\frac{\left\langle \left[\hat{V}, \hat{V} \right] \right\rangle_\omega^{(0)}}{\omega} \right] t \\
& + \frac{[t - 2t_0]}{2} \lim_{\omega \to 0} \left\{ \frac{1}{2} \left\langle \left\{ \hat{V}, \hat{V} \right\} \right\rangle_\omega^{(0)} - \left\langle \hat{V}\hat{V} \right\rangle_\omega^{(1)} \right\}.
\end{aligned}
\tag{5.16}
$$

However, resulting from the switching on procedure during the calculation some t_0-dependent contributions emerged: $\delta F = \delta F_1 + \delta F_2$. It depends crucially on the low-frequency spectrum of the bath of interest, whether those can be neglected or not. For our purpose it turns out that these do not contribute to our description, even at finite temperatures, $T \neq 0$. A discussion of δF for an arbitrary ohmic bath is given in 5.2.3.

In the next step we will plug in the spectrum resulting from the plasmons, whose dispersion relation was calculated within the full bosonization of the one-dimensional electron system.

5.2 Bath of plasmons

Equation Eq. (5.16) is a general result. It describes the coherence factor $e^{-F(x,t)}$ for electrons subjected to some quantum bath, neglecting any backaction effects. To proceed further in this section we identify the quantum bath with the plasmonic bath consisting of the electrons of the Fermi sea. We end up with an expression for the coherence factor e^{-F} and compare the semiclassical ansatz in Eq. (5.2) to the bosonization result for the Green's function $G^>(x,t)$.

5.2.1 Correlator of the density fluctuations

In Chapter 4 we already calculated the fluctuations of the potential stemming from a plasmonic bath (cf. Eq. (4.13))). For this we made use of the bosonic dispersion relation $\omega_q = v_F q[1 + \frac{U_q}{2\pi v_F}]$. Here, we extend the description to paths, which are not identical to the classical trajectory of the electron which is inserted. In the preceding calculation therefore an additional correlator showed up, $\langle \hat{V}\hat{V} \rangle_\omega^{(1)}$, which contains the extra information about the spacious correlations of the fluctuations:

$$
\begin{aligned}
\left\langle \hat{V}\hat{V} \right\rangle_\omega^{(1)} &= \int dt\, e^{i\omega t} \left\langle \hat{V}(\delta x + v_F t, t)\hat{V}(0,0) \right\rangle \\
&= \int dt\, e^{i\omega t} \int (d\omega') \int (dq)\, e^{iq(v_F t + \delta x) - i\omega' t} |U_q|^2 \langle \hat{\rho}\hat{\rho} \rangle_{q\omega'} \\
&= \int (dq)\, |U_q|^2 e^{iq\delta x} \langle \hat{\rho}\hat{\rho} \rangle_{q,\omega + qv_F} .
\end{aligned}
\tag{5.17}
$$

Plugging in the expression for the density correlator derived in Eq. (4.10)

$$
\langle \hat{\rho}\hat{\rho} \rangle_{q,\omega} = |q| \left\{ \Theta_q[\bar{n}(\omega_q) + 1]\delta(\omega - \omega_q) + \Theta_{-q}\bar{n}(\omega_q)\delta(\omega + \omega_q) \right\},
\tag{5.18}
$$

where $\bar{n}(\omega)$ denotes the Bose-Einstein distribution function for the plasmonic bosons, the calculation of the Green's function is a straightforward task.

5.2.2 Calculation of the single particle Green's function

Now, we explicitly calculate the single particle Green's function in the frame-work of the semiclassical ansatz, which then is compared to the full bosonization solution. In the following we will calculate every term of Eq. (5.16) separately. Finally, we show that the additional terms δF, which occured in the derivation of the semiclassical exponent $F(x,t)$ vanish for the special type of spectrum resulting from the plasmonic fluctuations.

Calculation of F_1 The part F_1 leads only to some energy renormalization, corresponding to the Fock contribution, which in the derivation of the Green's function via the bosonization was incorpo-

rated into a redefinition of the chemical potential:

$$
\begin{aligned}
F_1 &= -\frac{i}{2}t \int \frac{(d\omega)}{\omega} \left\langle \left[\hat{V},\hat{V}\right]\right\rangle_\omega^{(0)} \\
&= -\frac{i}{2}t \int \frac{(d\omega)}{\omega} \int (dq) U_q^2 |q| \left(\Theta_q \delta(\omega + qv_F - \omega_{|q|}) - \Theta_{-q}\delta(\omega + qv_F + \omega_{|q|})\right) \\
&= -it \int_0^\infty (dq)\, U_q = -i \left[\frac{1}{2}\int_{-\infty}^\infty (dq) U_q\right] t \\
&= -i \left[\frac{U(x=0)}{2}\right] t.
\end{aligned}
\tag{5.19}
$$

Calculation of F_2 Plugging in the expression for $\langle\{\hat{V},\hat{V}\}\rangle_\omega^{(0)}$, which was derived in Eq. (5.13) yields

$$
\begin{aligned}
F_2 &= \frac{1}{2}\int (d\omega)\, \frac{\left\langle\left\{\hat{V},\hat{V}\right\}\right\rangle_\omega^{(0)}}{\omega^2} \\
&= \frac{1}{2}\int \frac{(d\omega)}{\omega^2} \int (dq)\, U_q^2 \coth\left(\frac{\beta(\omega + v_F q)}{2}\right) \langle[\hat{\rho},\hat{\rho}]\rangle_{q,\omega+qv_F} \\
&= \frac{1}{2}\int \frac{(d\omega)}{\omega^2} \int (dq)\, U_q^2 \coth\left(\frac{\beta(\omega + v_F q)}{2}\right) \\
&\quad |q| \left(\Theta_q \delta(\omega + qv_F - \omega_{|q|}) - \Theta_{-q}\delta(\omega + qv_F + \omega_{|q|})\right) \\
&= \frac{1}{2\pi}\int_0^\infty (dq)\, U_q^2 q \coth\left(\frac{\beta\omega_q}{2}\right) \left[\frac{2\pi}{U_q q}\right]^2 \\
&= \int_0^\infty \frac{dq}{q} \coth\left(\frac{\beta\omega_q}{2}\right).
\end{aligned}
\tag{5.20}
$$

Calculation of F_3 We proceed with the evaluation of the third contribution F_3. For this we make use of the result for $\langle\hat{V}\hat{V}\rangle_\omega^{(1)}$ in Eq. (5.17). It follows

$$
\begin{aligned}
F_3 &= -\frac{1}{2}\int \frac{(d\omega)}{\omega^2} \int (dq)\, e^{iq\delta x - i\omega t} U_q^2 \left(1 + \coth\left(\frac{\beta(\omega + qv_F)}{2}\right)\right) \times \\
&\quad |q| \left(\Theta_q \delta(\omega + qv_F - \omega_{|q|}) - \Theta_{-q}\delta(\omega + qv_F + \omega_{|q|})\right) \\
&= -\frac{1}{8\pi^2}\int_0^\infty dq\, e^{iqx - i\omega_q t} U_q^2 |q| \left[\frac{2\pi}{U_q q}\right]^2 \left(1 + \coth\left(\frac{\beta\omega_q}{2}\right)\right) \\
&\quad +\frac{1}{8\pi^2}\int_0^\infty dq\, e^{-iqx + i\omega_q t} U_q^2 |q| \left[\frac{2\pi}{-U_q q}\right]^2 \left(1 - \coth\left(\frac{\beta\omega_q}{2}\right)\right) \\
&= -\int_0^\infty \frac{dq}{q} \left(\cos(qx - \omega_q t)\coth\left(\frac{\beta\omega_q}{2}\right) + i\sin(qx - \omega_q t)\right).
\end{aligned}
$$

Summing up all the different parts gives us the final expression for the Green's function of an electron subjected to a bath of plasmons, whose dynamics are governed by the dispersion relation $\omega_q = v_F q[1 + \frac{U_q}{2\pi v_F}]$. After this lengthy calculation the ansatz in Eq. (5.2) yields:

$$
\begin{aligned}
\left\langle \hat{\psi}(x,t)\hat{\psi}^\dagger \right\rangle &= -i \lim_{t_i \to -\infty} \left\langle \hat{\psi}(\delta x + v_F t_i, t_i)\hat{\psi}^\dagger(v_F t_i, t_i) \right\rangle_{\text{el}} e^{-F(x,t)} \\
&= -i \lim_{t_i \to -\infty} \left\langle \hat{\psi}(\delta x + v_F t_i, t_i)\hat{\psi}^\dagger(v_F t_i, t_i) \right\rangle_{\text{el}} e^{i\left[\frac{U(x=0)}{2}\right]t} \times \\
&\quad \exp\left[\int_0^\infty \frac{dq}{q} \left\{ \coth\left(\frac{\beta\omega_q}{2}\right)(\cos(qx - \omega_q t) - 1) + i\sin(qx - \omega_q t) \right\} \right]. \quad (5.21)
\end{aligned}
$$

In order to compare this result to the full bosonization solution, there is only one last question to answer: What are the correlations of the electrons at $t_i \to -\infty$? Equivalently, one could ask for the appropriate initial conditions of the Green's function, which is represented by the first term in Eq. (5.21). Postponing the discussion of this subtle and very important point to section 5.3, first of all, we note what the initial condition should look like in order to reproduce the bosonization result. Namely, a comparison of Eq. (5.21) with Eq. (3.30) yields

$$
\lim_{t_i \to -\infty} \left\langle \hat{\psi}(\delta x + v_F t_i, t_i)\hat{\psi}^\dagger(v_F t_i, t_i) \right\rangle = \frac{-i}{2\pi a}. \quad (5.22)
$$

Equation (5.22) states that if we start with a perfectly correlated electron system, i.e. the correlation between the electrons for $t_i \to -\infty$ is independent of its relative distance, the semiclassical calculation gives the correct result (up to the trivial phase factor $e^{-i\left[\frac{U(x=0)}{2}\right]t}$ which we already discussed in Chapter 4, cf. Eq. (4.15)).

However, usually (coupling the electron to some external bath) one identifies the initial condition with the non-interacting Green's function $g^>(x,t)$. Therefore, Eq. (4.17) might indicate the failing of the semiclassical method for arbitrary energies.

5.2.3 Discussion of the additional terms

Here we show the vanishing of the additional terms rising up in the calculations of the semiclassical model due to the adiabatic switching on of the fluctuations. For this we discuss the contributions related to the commutator parts of the correlators $\langle \hat{V}\hat{V} \rangle_\omega^{(0)}$ and $\langle \hat{V}\hat{V} \rangle_\omega^{(1)}$ and those which emerges together with the corresponding anti-commutator parts, separately. The reason for this is that the commutator part does not depend on temperature, while the symmetrised correlator does. The temperature dependence of the latter results from the fluctuation-dissipation theorem, relating the linear response of the bath ($\sim \langle [\hat{V}, \hat{V}] \rangle_\omega$) to its fluctuations ($\sim \langle \{\hat{V}, \hat{V}\} \rangle_\omega$) at a certain temperature T: $\langle \{\hat{V}, \hat{V}\} \rangle_\omega = \coth(\frac{\beta\omega}{2})\langle [\hat{V}, \hat{V}] \rangle_\omega$. The point is that, as discussed above, the ohmic spectrum at zero temperature turns into a white-noise spectrum at low frequencies. One observes a cancellation mechanism, suppressing the contributions even for $T \neq 0$.

Additional terms coming up with Anti-commutator part   Starting from Eqs. (5.13) and (5.15) and plugging in the result for the correlation functions (see Eq. (5.17)), the calculation of the t_0-dependent terms coming up together with the anti-commutator part yields

$$
\begin{aligned}
&\int (d\omega)\, \delta(\omega) \frac{\pi}{2} (t - 2t_0) \left(\left\langle \left\{ \hat{V}, \hat{V} \right\} \right\rangle_\omega^{(0)} - e^{-i\omega t} \left\langle \left\{ \hat{V}, \hat{V} \right\} \right\rangle_\omega^{(1)} \right) \\
&\approx \quad \frac{(t - 2t_0)}{4} \lim_{\omega \to 0^+} \left(\left\langle \left\{ \hat{V}, \hat{V} \right\} \right\rangle_\omega^{(0)} - e^{-i\omega t} \left\langle \left\{ \hat{V}, \hat{V} \right\} \right\rangle_\omega^{(1)} \right) \\
&= \quad \frac{(t - 2t_0)}{4} \lim_{\omega \to 0^+} \left(\int_0^\infty (dq)\, (1 - e^{-i\omega t + iq\delta x}) |U_q|^2 q \coth \left[\frac{\beta \omega_q}{2} \right] \delta \left(\omega - \frac{U_q q}{2\pi} \right) \right) \\
&= \quad -i\pi (t - 2t_0) \lim_{\omega \to 0^+} \left[\delta x \cdot \omega \left\{ \begin{array}{ll} T = 0 : & \pi\omega / U_0 \\ T > 0 : & \frac{T}{(v_F + \frac{U_0}{2\pi})} \end{array} \right\} \right] \\
&= \quad 0.
\end{aligned}
\tag{5.23}
$$

Here we set $\omega \to 0^+$, which is not of importance as $\langle \{\hat{V}, \hat{V}\} \rangle_\omega^{(1)} = (\langle \{\hat{V}, \hat{V}\} \rangle_{-\omega}^{(1)})^*$. Therefore, as a result even at non-zero temperature those extra contribution vanishes.

Additional terms arising with commutator part   To conclude this brief subsection we check the contributions arising together with the commutator parts of the correlation function. Here we do not have to care about temperature, as the commutator part is temperature independent. Realizing that $\langle [\hat{V}, \hat{V}] \rangle_{\omega \to 0^+}^{(1)} = 2\pi\omega e^{iq\delta x 2\pi / U_0 \omega}$, it follows:

$$
\begin{aligned}
&- \int (d\omega) \left(e^{-i\omega t} \left\langle \left[\hat{V}, \hat{V} \right] \right\rangle_\omega^{(1)} \right) \\
&= \quad \lim_{\omega \to 0^+} \left[-\frac{(t - 2t_0)}{4} e^{-i\omega t} \left\langle \left[\hat{V}, \hat{V} \right] \right\rangle_\omega^{(1)} \right] \\
&= \quad 0.
\end{aligned}
\tag{5.24}
$$

5.3   Interpretation of the results

This section is meant to give a phenomenological interpretation of the central result of this Chapter, namely of the mathematical identity Eq. (5.22). First of all we have to discuss the appropriate initial condition of the Green's function, followed by a short discussion of the consequences of the semiclassical approach.

5.3.1 Initial condition

The comparison of the Green's function derived within the semiclassical model Eq. (5.21) and the bosonization solution in Eq. (3.30) shows that both coincides, assuming

$$\lim_{t_i \to -\infty} \left\langle \hat{\psi}(\delta x + v t_i, t_i) \hat{\psi}^\dagger(v_F t_i, t_i) \right\rangle = \frac{-i}{2\pi a}. \tag{5.25}$$

At first sight, such a choice may seem to be rather unmotivated. Instead, one expects the non-interacting Green's function $g^>(x,t)$ to show up here. Particularly, as per construction of the semi-classical solution at $t_i \to -\infty$ the influence of the fluctuating potential vanishes. Namely, in Eqs. (5.3) and (5.4) we multiply the potential $\hat{V}$ with a factor $\lambda(t)$, decaying exponentially for $t < t_0$. As a result the influence of the fluctuations is switched off adiabatically, while the coupling constant α itself remains constant. It is the last statement which may be of crucial importance here.

We start the discussion expressing the Green's function in terms of the bosonization phase field $\hat{\Phi}$ (Eq. (3.30)). Setting $\mu = 0$ leads to

$$G^>(x,t) = \frac{-i}{2\pi a} \left\langle e^{-i\hat{\Phi}(x,t)} e^{i\hat{\Phi}(0,0)} \right\rangle. \tag{5.26}$$

Most remarkably, the correlator of the bosonic field $\hat{\Phi} = -i \sum_{q>0} \sqrt{\frac{2\pi}{Lq}} \left[\hat{b}_q e^{iqx} - h.c. \right]$ turns out to be identical to the correlator of the phase $\hat{\phi}_{SC}(x,t) \equiv \int_{-\infty}^t dt' \, \hat{V}(\delta x + v t', t')$ an electron collects propagating along its classical trajectory

$$
\begin{aligned}
\left\langle \hat{\phi}_{SC} \hat{\phi}_{SC} \right\rangle_{\omega,q} &= \frac{\left\langle \hat{V}\hat{V} \right\rangle_{\omega,q}}{[\omega - q v_F]^2} \\
&= \frac{4\pi^2}{|q|} \left(\Theta_q(\bar{n}(\omega_q) + 1)\delta(\omega - \omega_q) + \Theta_{-q}\bar{n}(\omega_q)\delta(\omega + \omega_{|q|}) \right).
\end{aligned}
\tag{5.27}
$$

An important feature of the correlation function $\langle \hat{\phi}_{SC}\hat{\phi}_{SC} \rangle_{q\omega}$ is that the strength of the fluctuations are not related to the coupling constant directly, but the latter only changes the dispersion relation of the plasmons ω_q. Even for $\alpha = 0$ the fluctuations remains finite. A comparison with Eq. (C.4) yields

$$\boxed{\left\langle \hat{\Phi}\hat{\Phi} \right\rangle_{q\omega} = \left\langle \hat{\phi}_{SC}\hat{\phi}_{SC} \right\rangle_{q\omega}}. \tag{5.28}$$

This is a very important observation confirming that the semiclassical ansatz we employ here is closely related to the bosonization solution. The identity suggests the following interpretation of the Green's function within the frame-work of bosonization. The Green's function factorizes into two different parts. Firstly, there is constant prefactor $\frac{1}{2\pi a} \sim \bar{\rho}$, which is directly related to the mean electron density $\bar{\rho}$ of the Luttinger liquid. This factor tells us that there are only collective

excitations in the Luttinger liquid, i.e., initially all the electrons are perfectly correlated. Therefore the amplitude of extracting an electron, which is coherent with the electron inserted into the liquid at $(x = 0, t = 0)$ is nothing but the mean electron density $\bar{\rho}$. But this is not the whole story. In addition there are fluctuations of the phase field $\hat{\Phi}(x, t)$ leading to a decay of the coherence between the electrons (and therefore to a decay of the Green's function). As the bosonization remains valid even for $\alpha = 0$, it is amazing that this mechanism still works, producing the non-interacting Green's function $g^>(x, t)$. In the non-interacting case, the fact that $\langle \hat{\phi}\hat{\phi} \rangle_{q\omega} = [\omega - qv_F]^{-2} \langle \hat{V}\hat{V} \rangle_{\omega, q}$ seems to be somehow counterintutitive, suggesting the need for a fluctuating potential $\hat{V}$ (which itself vanishes for α) in order to arrive at the non-interacting Green's function. The solution to this puzzle is that the strength of the fluctuations of $\langle \hat{\Phi}\hat{\Phi} \rangle_{q\omega}$ does not depend on α itself (see Eq. (5.27)) and the fluctuations do not vanish at all, even for $\alpha = 0$. As a result, the bosonization solution can be derived starting from perfectly correlated electrons experiencing the fluctuations of the plasmonic bath.

In the semiclassical approach, we actually assume the fluctuations of $\langle \hat{\phi}_{SC}\hat{\phi}_{SC} \rangle_{q\omega}$ (not the coupling strength α) to vanish in the limit $t_i \to -\infty$. For an arbitrary external bath potential this does not have any consequences for the initial Green's function and the initial condition is given by the non-interacting Green's function $g^>(x, t)$. However, applying the theory to an electronic bath and forcing the fluctuations to vanish in the limit $t_i \to -\infty$, one has to be more careful. At this point the fact that $\langle \hat{\phi}_{SC}\hat{\phi}_{SC} \rangle_{q\omega} = \langle \hat{\Phi}\hat{\Phi} \rangle_{q\omega}$ is of crucial importance. Demanding the fluctuations $\langle \hat{\phi}_{SC}\hat{\phi}_{SC} \rangle_{q\omega}$ to vanish, from Eq. (5.26) we get

$$\lim_{t_i \to -\infty} \left\langle \hat{\psi}(\delta x + vt_i, t_i)\hat{\psi}^\dagger(v_F t_i, t_i) \right\rangle = g(x, t)^> \Big|_{\langle \hat{\Phi}\hat{\Phi} \rangle \equiv 0}$$
$$= \frac{-i}{2\pi\alpha}, \tag{5.29}$$

i.e., neglecting the phase fluctuations the non-interacting Green's function turns into $g^>(x, t) \to \frac{-i}{2\pi a}$. But this is exactly the required initial condition for the Green's function in the limit $t_i \to -\infty$ yielding a coincidence of the semiclassical ansatz and the bosonization solution.

As the discussion given here is based on rather phenomenological arguments, there is still some need for a more rigorous explanation for the mathematical identity in Eq. (5.22).

5.3.2   The semiclassical approach - an alternative point of view?

This short section is meant to consider the Green's function $G^>(x, t)$ from the semiclassical point of view. While, the semiclassical ansatz was shown to fail (the required initial condition seems to be rather unphysical), nevertheless it may serve as an alternative way of understanding the physical situation of chiral interacting electron systems. In Fig. 5.2a we pictorially show the Green's function evolving in time. At $t_i \to -\infty$, one starts with a one-dimensional system of perfectly correlated electrons. For $t > t_i$ the electrons start to propagate with the unrenormalized Fermi velocity v_F

collecting a random phase due to the potential background stemming from the plasmonic excitations. At $t = 0$, the full fluctuations are present and the interacting single particle Green's function has built up. The usual interpretation of the single particle Green's function $G^>(x, t)$ assumes that there is no phase correlation between the electron injected at $t = 0$ and the electrons from the Fermi sea. Therefore, in order to re-extract an electron at (x, t) which is phase coherent with the inserted one, we have to annihilate exactly the same particle again. In the non-interacting case, the only influence of the Fermi sea electrons relies on the Pauli principle. As one can insert the electron (at $T = 0$) only with momenta $k > 0$, naturally an uncertainty in position arises. The Green's function $g^>(x, t = 0)$ gets broadened in x (its absolute value decays like $1/x$, rather to show a δ-peak at $x = 0$). Therefore, the Pauli blocking determines the shape of the Green's function.

In contrast, starting from the perfectly coherent electron system (this is the initial condition the semiclassical ansatz requires to become exact), in principle there are contributions to the Green's function from all the electrons propagating through the one-dimensional channel. From this point of view, the Green's function $G^>(x, t)$ can be interpreted as a measure of how coherent two electrons, one at $(x = 0, t = 0)$ and the other one at (x, t), actually are.

We already mentioned in Chapter 4 that usually one considers the chiral Luttinger liquid to be equivalent with a Fermi liquid at low energies. The only effect of the interaction shows up in a certain velocity renormalization. Indeed, the tunnel density of states shows a dip in the close vicinity to the Fermi edge (for repulsive interactions) (cf. Fig. 3.3). Furthermore, considering the Green's function $G^>(x, t)$ two peaks emerge, propagating with v_F and $\bar{v}$ (cf. Fig. 3.2). The most natural interpretation (see Chapter 3) of this is given within the Fermi liquid picture. The low-energy quasi-particles fly with $\bar{v}$, while the velocity of the electrons with large energies is not effected. Therefore, the latter give rise to the sharp peak moving with v_F.

The double peak structure seems to contradict the main assumption of the semiclassical ansatz that regardless of its particular energy all electrons fly with the bare velocity v_F. However, there is a simple way to understand the additional peak in $G^>(x, t)$ at $x = \bar{v}t$ without assuming the renormalization of the velocity. The idea is shown in Fig. 5.2b. There, one assumes all electrons to move with v_F feeling the influence of the plasmonic background potential. Then we insert an electron at $(x = 0, t = 0)$ which is equivalent to annihilating the corresponding hole. The point is that, in the moment an arbitrary electron crosses the line $x = \bar{v}t$ the phase it has accumulated is identical to the phase the hole collected propagating from t_i to $t = 0$ (with an inverted sign). Therefore one can oberserve a 'coherence revival' which shows up as peak in the Green's function, propagating with $\bar{v}$.
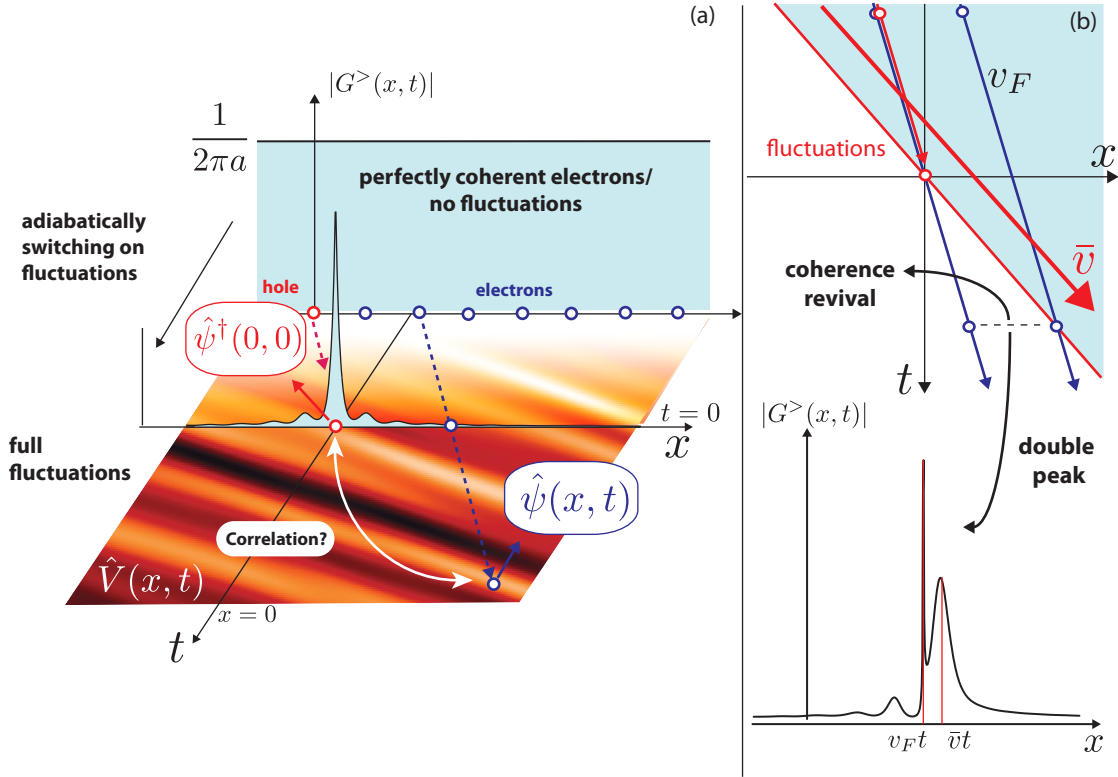
Figure 5.2: (a) Pictorial plot of the electrons propagating with v_F over the fluctuating potential background $\hat{V}(x,t)$. The latter is switched of adiabatically for $t < t_0$, such that the fluctuations vanish for $t_i \rightarrow = -\infty$. At t_i, we assume the electrons to be perfectly phase correlated, following the assumptions made in the main text concerning the interpretation of the semiclassical approach, namely: $\lim_{t_i \to -\infty} \left\langle \hat{\psi}(\delta x + v t_i, t_i) \hat{\psi}^\dagger(v_F t_i, t_i) \right\rangle = \frac{-i}{2\pi a}$. (b) Pictorial plot showing an alternative way explaining the additional peak in $G^>(x,t)$ at $x = \bar{v}t$, without assuming the velocity renormalization at low energies. For a detailed explanation see subsection 5.3.2.

Chapter 6

Keldysh perturbation theory

In this short chapter we employ perturbation theory to discuss the behaviour of the single-particle Green's function at short propagation distances and weak coupling for all energies. This includes the low energy regime, where the influence of the Fermi edge becomes important. Here, we apply Keldysh (i.e., nonequilibrium) perturbation theory up to second order in the interaction strength α. As in the previous chapters, with the semiclassical method we introduced an effective and transparent tool describing the coherence properties of high-energy electrons, in this Chapter we focus especially on the low-energy regime.

The main advantage of the perturbation theory in Keldysh time is that it applies even in a non-equilibrium situation. The bosonization solution showed that the characteristic visibility oscillations, the "lobe structure" can not be explained in the weak-tunneling limit between the interferometer arms. Unfortunately, in the framework of bosonization the current can only be evaluated perturbatively. In contrast, treating the electron-electron interactions perturbatively, in principle one is not restricted to weakly tunnel-coupled interferometers. Therefore, the results in this Chapter may serve as a starting point for the latter approach.

The main outcome of the perturbation theory is that the tunnel density of states is affected by renormalization effects while the decay of the Green's function in close vicinity of the Fermi edge is suppressed. We will find that the suppression of decoherence is brought about by a cancellation between two second order diagrams near the Fermi edge as well as by Pauli blocking.

After a short introduction in Section 6.1, we calculate the relevant diagrams up to second order and compare the resulting Green's function to the bosonization solution (Section 6.2). We end with a short summary of the results in Section 6.3.

6.1   Perturbation theory on the Keldysh contour

In this section we fix the notation, following the review [19]. Using the Keldysh time leads to an additional matrix structure of the GF which reflects the fact that one has to differentiate between points in time which lie on the backward or the forward branch of the Keldysh contour. Beyond this additional structure, all the known Feynman rules remain exactly the same. After performing the rotation in Keldysh space [19], the representation of the matrix GF G and the related matrix self-energy is given by

$$G \equiv \left[\begin{array}{cc} G^R & G^K \\ 0 & G^A \end{array} \right] \qquad \Sigma \equiv \left[\begin{array}{cc} \Sigma^R & \Sigma^K \\ 0 & \Sigma^A \end{array} \right], \tag{6.1}$$

where we introduce the Keldysh GF, $G^K(x, t, x', t') \equiv -i\langle [\hat{\psi}(x, t), \hat{\psi}^\dagger(x', t')] \rangle$. First, we will derive an expression for the retarded self-energy $\Sigma^R(\epsilon.k)$, which will be used to calculate G^R that can be related to the single particle propagator $G^>$ in equilibrium using the fluctuation-dissipation theorem in Eq. (2.13). Starting from the matrix Dyson equation $G(\epsilon, k) = G_0(\epsilon, k) + G_0(\epsilon, k) \cdot \Sigma(\epsilon, k) \cdot G(\epsilon, k)$, one finds that the retarded Green's function only depends on the retarded self-energy:

$$G^R(\epsilon, k) = \frac{1}{[\epsilon - \epsilon_0(k) + i0^+] - \Sigma^R(\epsilon, k)}. \tag{6.2}$$

In the following, we calculate the diagrams up to second order for a linearized dispersion relation, but for finite temperature and for an arbitrary interaction potential. In the end, we compare the results of the perturbation theory with the results of the bosonization technique. The relevant processes are shown in Fig. 6.1. There are two second order diagrams, which can be identified as the interaction with a plasmonic excitation and a corresponding diagram containing an additional exchange process (that can be viewed as a vertex correction diagram). The crucial point is that the vertex correction counteracts the plasmonic processes in the vicinity of the Fermi edge, leading to a suppression of the decay of the GF.

6.2   Evaluation of the diagrams

The starting point of the calculation is the evaluation of the the unperturbed electronic propagator matrix G_0. In addition to the usual retarded and advanced [Eq. (2.12)] Green's functions of free electrons

$$G_0^{R/A}(\omega, k) \;\; = \;\; \frac{1}{\omega - v_F k \pm i0^+}, \tag{6.3}$$
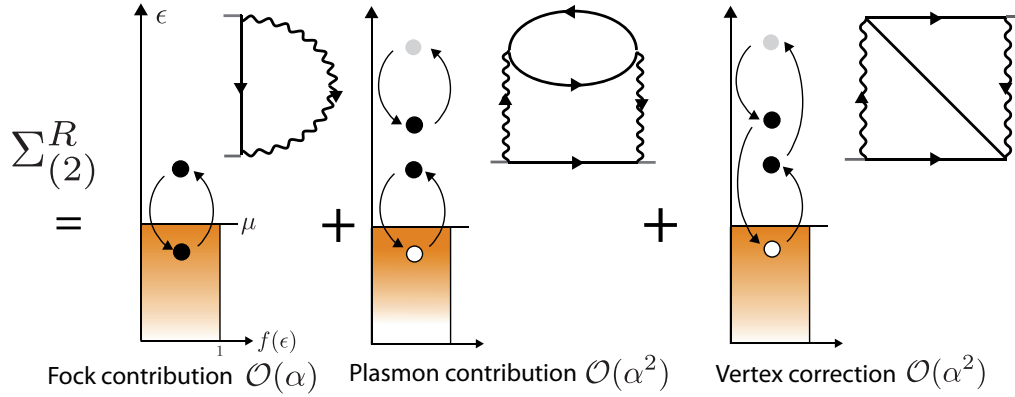
Figure 6.1: The relevant processes which contribute to the self-energy up to second order in the coupling. The wiggly lines indicate the interaction. Note that the plasmonic diagram and the vertex correction differ only by an additional exchange process. That produces a minus sign, such that the diagrams tend to cancel each other at low momenta.

in equilibrium the Keldysh propagator G_0^K is given by [see Eq. (B.2)]

$$G_0^K(\omega, k) = -2\pi i \tanh(\frac{\beta\omega}{2}) \cdot \delta(\omega - v_F k). \tag{6.4}$$

In contrast to the advanced and retarded GFs, the Keldysh propagator contains information about the electronic spectrum as well as about the occupation of those states. Therefore, at this point one could introduce arbitrary non-equilibrium states, which is the main advantage of working on the Keldysh contour. However, as we are describing channels which are only weakly tunnel-coupled to each other, here we are interested in equilibrium Green's functions.

As in second order we explicitly include interactions with free plasmons, we also derive their propagators here. To this end we identify the bosonic field with the potential $\hat{V}(x,t) = \int dx' \, U(x-x')\hat{\rho}(x',t)$. This is identical to the potential we introduced in the semiclassical description (although in the latter case we specialized to $x \equiv v_F t$). The bosonic propagators are defined as

$$D^{R/A}(x,t) = \mp i\Theta(\pm t)\left\langle\left[\hat{V}(x,t),\hat{V}(0,0)\right]\right\rangle$$
$$D^K(x,t) = -i\left\langle\left\{\hat{V}(x,t),\hat{V}(0,0)\right\}\right\rangle. \tag{6.5}$$

A straightforward calculation yields for the retarded and advanced propagators (the short calculation is attached in Appendix B.1.2)

$$D^{R/A}(\omega, q) = |U_q|^2 \cdot \int \frac{dk}{2\pi} \frac{f(k) - f(q+k)}{(\omega + \epsilon_0(k) - \epsilon_0(k+q)) \pm i0^+} = |U_q|^2 \frac{q}{2\pi} \cdot G^{R/A}(\omega, q). \tag{6.6}$$

As we assume the system to be in equilibrium, we use the fluctuation-dissipation theorem in Eq. (4.8) to obtain the plasmonic Keldysh propagator:

$$D^K(\omega, q) = 2i \coth(\beta\omega/2)\text{Im}[D^R(\omega, q)]. \tag{6.7}$$

Now we can proceed calculating the various contributions to the self-energy up to $\mathcal{O}(\alpha^2)$. Considering all the possible Feynman diagrams, we are left with the first order Hartree-Fock diagrams and in second order with the plasmon diagram and the vertex correction (see Fig.6.1). Thus, we can express the self-energy as $\Sigma_{(2)}^R = \Sigma_{\text{Hartree}} + \Sigma_{\text{Fock}} + \Sigma_{\text{Plasmon}} + \Sigma_{\text{Vertex}}$.

These contributions can be evaluated according to the rules given in [19]. The diagrammatic calculation in Keldysh time follows the ordinary Feynman rules (including additional minus signs for electron bubbles, etc.), with the only difference that one has to take care of the additional matrix structure of the propagator functions (cf. Fig. B.1). We use the equal-time interaction propagators $U^{R/A}(q) \equiv U_q$ and set $U^K \equiv 0$, as usual.

In the following, we already present the final results of the diagrammatic calculations. All the calculations are attached in Appendix B.2.

6.2.1   First-order contributions: Hartree-Fock diagrams

The Hartree diagram yields a global energy renormalization $\Delta E_{\text{Hartree}} = U(q = 0)\bar{\rho}$. In the framework of the Luttinger model the electron density diverges as there is no lower boundary of the electron spectrum. However, formally one can include the energy shift into the definition of the chemical potential (see Subsection 3.1.1). In the following we omit the Hartree contribution.

The self-energy contribution due to the Fock diagrams is

$$\Sigma_F^R(\omega, k) = -\frac{1}{2\pi} \int dq\, U_q f(k - q), \tag{6.8}$$

which for zero temperature yields $\Sigma_{F,T\equiv0}^R(k) = -\frac{1}{2}U(x = 0) + \frac{1}{2\pi} \int_0^{|k|} dq\, U_q$ [see Fig. 6.2b].

The resulting k-dependent energy shift describes, in particular, the renormalization of the electron velocity near the Fermi edge. This also affects the tunneling density of states, leading to a suppression (for repulsive interactions, $\alpha > 0$) or enhancement ($\alpha < 0$). This can be seen in Fig.3.3. Again, the constant shift can be incorporated in the definition of the chemical potential.

6.2.2   Second-order contributions: Plasmonic excitations and vertex correction

The electron's coherence decays by interacting with the plasmons, i.e. the density fluctuations of the other electrons. The plasmon diagram (see Fig. 6.1) represents one of the contributions describing

this physics. It yields

$$\Sigma_P^R(\epsilon, k) = \frac{i}{2} \int (dq) \int (d\omega) \left[G_0^R(\epsilon - \omega, k - q) \cdot D_0^K(\omega, q) + G_0^K(\epsilon - \omega, k - q) \cdot D_0^R(\omega, q) \right], \quad (6.9)$$

where the second term contains the Fermi function, which introduces the effects of the Fermi edge on the coherence. Inserting the propagators, the contribution can be written in a compact form

$$\Sigma_P^R(\epsilon, k) = \frac{G_0^R(\epsilon, k)}{8\pi^2} \cdot \int_{-\infty}^{\infty} dq \quad U_q^2 q \cdot [\coth(\beta \hbar v_F q / 2) + \tanh(\beta \hbar v_F (k - q) / 2)], \quad (6.10)$$

which for $T = 0$ reduces to $\Sigma_P^R(\epsilon, k) = G_0^R(\epsilon, k) \cdot \frac{1}{4\pi^2} \int_0^{|k|} dq\, U_q^2 q$. Thus, at $T = 0$ this contribution vanishes for $k \to 0$. We note in passing that the structure "coth + tanh" generically occurs in discussions of dephasing, where it describes both the strength of the thermal fluctuations and the influence of the Fermi function, i.e., the physics of Pauli blocking. In the limit of high energies, the result of Eq. (6.10) can be rewritten in terms of the potential fluctuations at the particle position, as discussed in Chapter 4. Specifically, we have $\lim_{k \to \infty} \Sigma_{P,T \equiv 0}^R = G_0^R \cdot \langle \hat{V}(x = 0, t = 0)^2 \rangle$. For a plot of the function $\Sigma_{P,T=0}^R$, see Fig. 6.2c.

Finally, we derive the vertex correction, mentioned above, which after a rather lengthy calculation yields

$$\Sigma_V^R(\epsilon, k) = \left[\frac{G_0^R(\epsilon, k)}{16\pi^2} \right] \int_{-\infty}^{\infty} dq_1 \int_{-\infty}^{\infty} dq_2 U_{q_1} U_{q_2}$$

$$\times \left[\tanh(\frac{\beta v_F(k - q_1 - q_2)}{2})) \cdot \left[\tanh(\frac{\beta v_F((k - q_1))}{2}) + \tanh(\frac{\beta v_F((k - q_2))}{2})) \right] - \right.$$

$$\left. - \tanh(\frac{\beta v_F((k - q_2))}{2}) \, \tanh(\frac{\beta v_F((k - q_1))}{2}) - 1 \right] \quad (6.11)$$

This expression simplifies for $T = 0$ to $\Sigma_{V,T=0}^R = -G_0^R \cdot \frac{1}{4\pi^2} \int_0^{|k|} dq_1 \int_{|k|-q_1}^{|k|} dq_2 U_{q_1} U_{q_2}$. The contribution from the vertex correction as well as the total second order correction to the self-energy $\Sigma_{P+V}^R \equiv \Sigma_P^R + \Sigma_V^R$ are shown in Fig. 6.2. The crucial feature is that up to second order in momentum k the plasmon diagram and the vertex correction cancel exactly against each other, whereas for high momenta $[k \gg q_c]$ only the plasmon contribution remains while the vertex correction tends to zero. In summary, when calculating up to second order in the coupling, we already see that the dephasing is suppressed in the vicinity of the Fermi edge. As the comparison with the exact bosonization solution shows, this conclusion holds true qualitatively to all orders. We can use the preceding expressions to evaluate the retarded Green's function G^R and from this the propagator $G^>$. The final results has been evaluated numerically. The results are illustrated in Fig. 6.2. Expanding the Green's function

for small propagation distance $x \ll v_F \left(2\sqrt{\langle \hat{V}(0)^2 \rangle} \right)^{-1}$ yields:

$$|G^>(\epsilon \to \infty, x)|v_F \approx 1 - \frac{1}{2}\langle \hat{V}(0)^2 \rangle (\frac{x}{v_F})^2 + \ldots, \tag{6.12}$$

which coincides with the expanded exact result. The good agreement of the bosonization result and the Keldysh perturbation theory for small $|\alpha|$ is shown in Fig. 6.2. However, for large x the perturbation theory fails. For a detailed study of the spectrum of chiral interacting electrons in $(\epsilon - k)$-space, starting from the bosonization result, the reader is referred to [43].
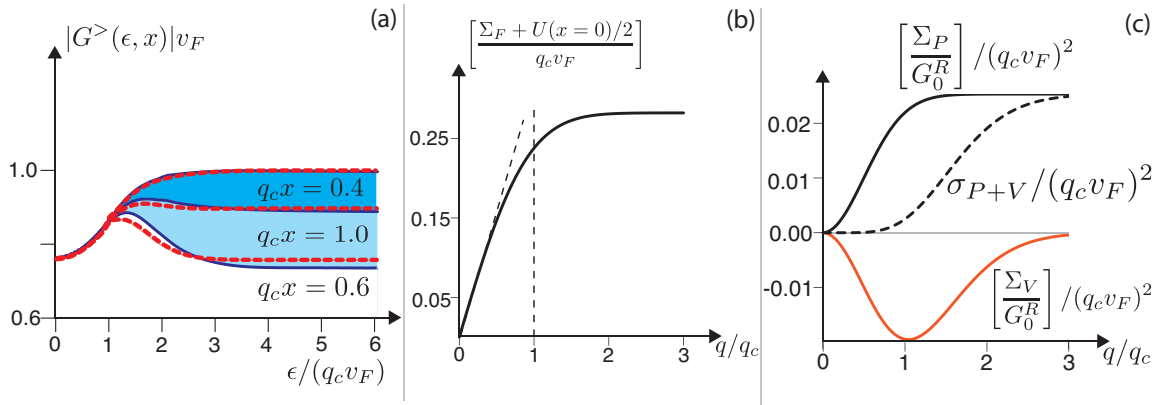
Figure 6.2: (a) The GF from bosonization (solid blue lines) vs. the results from second-order Keldysh pertubation theory (dashed red lines) for different propagation distances as a function of energy. Note the fairly good agreement. (b) Fock contribution to the self-energy $\Sigma_F^R(k)$, which starts with a linear slope (corresponding to the electron velocity renormalization) and then saturates for large momenta. (c) Total second order contribution to the self-energy (dashed black line); plasmonic (solid black line) and vertex correction (lower red line) separately. The cancellation for small momenta is discussed in detail in the text (in all figures $U_q = U_0 \exp(-(q/q_c)^2)$ and $2\pi\alpha = U_0/v_F = 2$).

6.3   Summary of the Keldysh perturbation theory

To summarize, the perturbation theory shows that there are two different energy regimes: In general, the GF decays as a function of propagation distance due to the interaction with the density fluctuations. This is particularly pronounced at high energies $\epsilon \gg v_F q_c$, where we have also shown that the Keldysh result and the semiclassical (or bosonization) approach coincide at short distances. For low energies $\epsilon \ll v_F q_c$, the decay is suppressed. On the other hand, at low energies the Fermi velocity is renormalized due to virtual processes, leading to a modification of the tunneling density of states. It is important to note that these two different energy regimes only emerge since we are dealing with

interaction potentials of finite range.

Chapter 7

Four-point correlation function

This chapter is meant to give an outlook on how to proceed further for a deeper understanding of the decoherence in one-dimensional electron systems in general and in the Mach-Zehnder interferometer in particular. As the foregoing analysis showed, some of the most prominent features of the Mach-Zehnder interferometer, e.g., the lobe-structure in the visibilty [27, 39], can not be described by the present theory. Neither the influence of an external quantum bath [36, 32, 31], nor the intrinsic electron-electron interactions [6] offer an explanation of these effects. Analyzing the effect of the electron-electron interactions in the frame-work of bosonization, the main restriction is that the theoretical description is valid only for weakly tunnel-coupled interferometer arms (cf. Chapter 2). As in the experiment the situation is quite the opposite, the lobe structure becomes more pronounced increasing the tunnel coupling of the interferometer arms, an extension of the theoretical description to higher orders in the coupling seems to be fruitful. In particular, this is motivated by the proposal in [40, 39], where the authors investigate the influence of non-Gaussian shot noise on the interferometer visibility, while the noise has its origin in an external electron channel coupled to one of the interferometer arms. The number of electrons in the external channel is assumed to be such small that the corresponding random potential can not assumed to be Gaussian anylonger. The resulting oscillations in the visibility as a function of the applied bias voltage shows a striking similarity with the reported lobe-structure. Unfortunately, the effect of shot noise on the coherence properties can not be described in the lowest order in tunneling, i.e., with the theory presented in this work. There are two main approaches to proceed further. On the one hand, one can choose to take into account the tunnel coupling exactly but treat the intrinsic interactions only perturbatively. Our perturbative expansion in Keldysh time should be an appropriate starting point following these lines. On the other hand, one can stay in the frame-work of bosonization but takes into account the next non-vanishing order in the tunnel coupling ($\mathcal{O}(t_A^4)$), contributing to the current trough the interferometer. It turns out that in the next highest order, the current depends on two-particle Green's functions (equivalently, we refer to them as four-point correlation functions). These show up naturally in this context,

as the stronger coupling between the interferometer arms drives them out of equilibrium. To put it different: Now, an electron hopping into the opposite interferometer arm, knows whether there is another electron already propagating through this arm or not. Therefore, the electron experiences the simplest possible form of non-Gaussian shot noise.

Here we study some four-point correlation functions of particular interest, reflecting the non-equilibrium energy- and momentum distribution of a chiral one-dimensional electron system after the injection of an extra electron. For this we start from the formal solution via the bosonization technique. After some general remarks on the construction scheme of four-point correlation functions in the frame-work of bosonization (section 7.1), we proceed with the explicit calculation and the numerical evaluation (sections 7.2 and 7.3).

Most interestingly, it turns out that after some transient behaviour there is no further energy and momentum transfer between the injected electron and the electrons from the Fermi sea. This feature is in agreement with the known fact that in clean Luttinger liquids, i.e., in the absence of impurities, the scattering rates for inelastic processes, where electrons relax its energy transfering energy to the plasmonic bath, vanish [3]. Besides these interesting physical results, the second message of this section is that the numerical evaluation of four-point functions in principle is possible. However, one has to increase further the numerical precision, especially to analyze reliably the non-equilibrium energy distribution in the close vicinity to the Fermi edge.

7.1 Four-point correlators

In general, calculating observables of the system after the insertion of an extra electron leads to the analysis of four-point correlation functions. This s due to the fact that the creation of an electron drives the system out of equilibrium, such that we have to evaluate the expectation values of the observables of interest with respect to the excited state of the system. Thus, the expectation value of an arbitrary observable $\hat{O}$ after the insertion at $(x = 0, t = 0)$ is given by $\langle\hat{O}\rangle_{\text{excited}} = \left[\langle\text{vac}|\,\hat{\psi}(0,0)\right]\hat{O}\left[\hat{\psi}^\dagger(0,0)\,|\text{vac}\rangle\right]$, where $|\text{vac}\rangle$ denotes the vacuum state of the system. We define an arbitrary four-point correlator as

$$C^4(r_1, r_2, r_3, r_4) \equiv \langle\hat{\psi}^{(\dagger)}(r_1)\hat{\psi}^{(\dagger)}(r_2)\hat{\psi}^{(\dagger)}(r_3)\hat{\psi}^{(\dagger)}(r_4)\rangle, \tag{7.1}$$

with the collective coordinate $r \equiv (x, t)$. Using the bosonization identity $\hat{\psi}_R = \frac{F}{\sqrt{2\pi a}}e^{ik_F x}e^{-i\hat{\phi}_R}$, where $\hat{\phi}(x,t) \equiv i\sum_{q>0}\sqrt{\frac{2\pi}{Lq}}\left(e^{iqx-aq}\hat{b}_q(t) - h.c.\right)$, its calculation is a straight forward task. The reason is that the correlation function can be written as a product over exponentials of the bosonic fields $\hat{\phi}$ (here $\mu \equiv 0$) :

$$C^4 = \frac{1}{(2\pi a)^2}\cdot\langle\prod_j e^{-iA_j\hat{\phi}(r_j)}\rangle, \tag{7.2}$$

The coefficients $A_i = \pm 1$ depend on the nature of the fermionic operator $\hat{\psi}_i^{(\dagger)}$ (the minus signs represents annihilation operators and vice versa) and we restrict the consideration to chiral (right moving) electrons. As the electronic Hamiltonian is quadratic in the bosonic operators, the average can be evaluated using the Baker-Hausdorff identity $e^A e^B = e^{A+B} e^{\frac{1}{2}[A,B]}$. Thus, we can make use of the identity, valid for Gaussian random variables : $\left\langle e^{-i\hat{\phi}} \right\rangle = e^{\frac{1}{2}\left\langle \hat{\phi}^2 \right\rangle}$. The calculation of Eq. (7.2) yields (for reasons of brevity we set $\hat{\phi}_j \equiv A_j \hat{\phi}(r_j)$ and $\phi_{ij} \equiv \left\langle \hat{\phi}_i \hat{\phi}_j \right\rangle$)

$$
\begin{aligned}
\left\langle \Pi_j e^{-iA_j \hat{\phi}(r_j)} \right\rangle &= e^{-\frac{1}{2}\left\langle [\hat{\phi}_1, \hat{\phi}_2] \right\rangle} \left\langle e^{-i(\hat{\phi}_1+\hat{\phi}_2)} \prod_{j>2} e^{-iA_j \hat{\phi}(r_j)} \right\rangle \\
&= e^{-\frac{1}{2}\left\langle [\hat{\phi}_1, \hat{\phi}_2] \right\rangle - \frac{1}{2}\left\langle [\hat{\phi}_1+\hat{\phi}_2, \hat{\phi}_3] \right\rangle} \left\langle e^{-i(\hat{\phi}_1+\hat{\phi}_2+\hat{\phi}_3)} \prod_{j>3} e^{-iA_j \hat{\phi}(r_j)} \right\rangle \\
&= \exp\left[-\frac{1}{2} \sum_{i<j,j>2} (\phi_{ij} - \phi_{ji}) - \frac{1}{2}\left\langle \left(\sum_{i=1}^{4} \hat{\phi}_i \right)^2 \right\rangle \right] \\
&= \exp\left[-2\left\langle \hat{\phi}^2(0,0) \right\rangle - \sum_{i<j,j>2} A_i A_j \left\langle \hat{\phi}(r_i)\hat{\phi}(r_j) \right\rangle \right].
\end{aligned}
\tag{7.3}
$$

The emerging correlators $\left\langle \hat{\phi}(r_i)\hat{\phi}(r_j) \right\rangle$ where already discussed in Chapter 3

$$
\tilde{S}(x,t) = \langle \hat{\phi}(x,t)\hat{\phi}(0,0) \rangle = \int_0^\infty \frac{dq}{q}\left((\bar{n}_q+1)e^{i(qx-\omega_q t)} + \bar{n}_q e^{-i(qx-\omega_q t)} \right).
\tag{7.4}
$$

To ensure a fast convergence of the momentum integrals, as in the case of the single particle Green's function (cf. Eq. (3.30)) we substract the non-interacting correlation function. For this we define $S(r_i - r_j) \equiv S_{ij} \equiv \langle \hat{\phi}(r_i)\hat{\phi}(r_j) \rangle - \langle \hat{\phi}_0(r_i)\hat{\phi}_0(r_j) \rangle$, where $\hat{\phi}_0$ denotes the non-interacting bosonic field. Furthermore, due to the equal number of annihilation and creation operators involved in the four-point correlation function, it can be written as a product of single particle Green's functions:

$$
\begin{aligned}
C^4 &= -\prod_{i<j,j>2} (G_{ij}^>)^{-A_i A_j} \\
&= -\prod_{i<j,j>2} (g_{ij}^>)^{-A_i A_j} \exp\left(-\sum_{i<j,j>2} A_i A_j (S_{ij} - S_{ij}^0) \right).
\end{aligned}
\tag{7.5}
$$

Here we introduce the abbreviations $G^>(r_i - r_j) \equiv G_{ij}^> = \frac{-i}{2\pi a}\exp[S_{ij} - S_{ij}^0]$ and let $g_{ij}^>$ denote the unperturbed single particle Green's functions, i.e., $g_{ij}^> \equiv G_{ij}^>(\alpha = 0)$. In addition the function $S_{ij}^0 \equiv S_{ij}(\alpha = 0)$ vanishes at zero temperature $T = 0$. The pole structure of the two-particle Green's function, whose knowledge is essentially for the numerical evaluation, is determined by the product of non-interacting Green's functions. Thus, the calculation of a particular four-point function always

starts with the analysis of its pole structure, i.e., of the non-interacting case.

Density after injection of electron In order to check the consistency of expression Eq. (7.5), we start with a simple task. Namely, one could ask how the plasmons evolve in time when an additional electron was inserted at $r = 0$. For this we have to introduce the correlation function

$$C_\rho(x,t) \quad \equiv \lim_{\epsilon \to 0} \quad \left\langle \hat{\psi}(0,0) \left(\hat{\psi}^\dagger(x,t+\epsilon)\hat{\psi}(x,t-\epsilon) \right) \hat{\psi}^\dagger(0,0) \right\rangle \tag{7.6}$$

where we explicitly denote the point splitting by the infinitesimal time-shift $\epsilon \to 0$. First of all, we want to check the expression Eq. (7.5) for the non-interacting case. Dealing with non-interacting systems in the Luttinger approximation is somehow feasible, as there is no natural length scale besides the cutoff parameter a itself, which should be send to zero in the end (in the presence of an interaction potential with a finite range the length scale is set by q_c^{-1}). Therefore, in a non-interacting consideration we always keep a finite, realizing that it is closely connected to the inverse Fermi momentum $a \sim k_F^{-1}$ and therefore to the mean density $\bar{\rho}$. Making use of Wick's theorem $C_\rho^0 \equiv C_\rho(\alpha \to 0)$ can be calculated to yield (here for $T = 0$)

$$\begin{aligned} C_\rho^0(x,t) \quad &= \quad g^>(x,t)g^<(x,t) + g^>(0,0)g^<(0,0) \\ &= \tfrac{1}{4\pi^2} \quad \left(\frac{1}{(x - v_F t)^2 + a^2} + \frac{1}{a^2} \right), \end{aligned} \tag{7.7}$$

where the unperturbed, zero temperature Green's function is given by $g_{ij}^{>/<} = \frac{1}{2\pi}[(x_i - x_j) - v_F(t_i - t_j) \pm ia]^{-1}$. Alternatively, evaluating Eq. (7.5) leads to

$$\begin{aligned} C_\rho^0 \quad (x,t) = \quad &\lim_{\epsilon \to 0} \left(-\frac{g^<(x,t+\epsilon)g^>(x,t-\epsilon)}{g^<(x,t-\epsilon)g^>(x,t+\epsilon)} \cdot g^>(0,0)g^>(0,2\epsilon) \right) \\ = \quad &\frac{1}{4\pi^2} \lim_{\epsilon \to 0} \left(\frac{(x - v_F t)^2 - \epsilon_+^2}{(x - v_F t)^2 - \epsilon_-^2} \cdot \frac{1}{a^2 + 2i\epsilon a} \right) \\ = \quad &\frac{1}{4\pi^2} \left(\frac{1}{(x - v_F t)^2 + a^2} + \frac{1}{a^2} \right), \end{aligned} \tag{7.8}$$

which serves as a consistency check, as the result is identical with Eq. (7.7). Clearly, C_ρ^0 consists of two contributions, the equilibrium density and the part representing the response of the electron density to the insertion of the extra electron at $r = 0$.

7.2   Energy relaxation

Dealing with two-particle Green's functions provides us with the local non-equilibrium energy and momentum distribution of the system as a function of x and t. The injection of an extra electron

drives the system out of equilibrium. Therefore, the analysis of the corresponding four-point functions is closely related to the question how the energy of the additional electron relaxes with increasing propagation time. It is a known, but nevertheless amazing fact that for Luttinger liquids in the absence of impurities, inelastic scattering processes are precluded. To be precise, in an equilibrium situation the rate of an electron to be scattered out of its initial state turns out to be zero. However, here we are dealing with the simplest possible non-equilibrium situation as we inject an electron on top of the Fermi sea. As a consequence, we expect some transient behaviour where the bath electrons and the inserted electron re-arrange thereby minimizing its energy. However, in the long-time limit there should be no further energy transfer between the additional electron and the electrons stemming from the Fermi sea. In the following we consider the local energy distribution after the creation of an electron at $(x = 0, t = 0)$.

7.2.1   Initial energy unknown

For the remainder of this chapter we restrict the analysis to $T = 0$, while the non-zero temperature case is easily established following the same lines. As a starting point we consider an electron with an arbitrary initial energy inserted into the liquid at $(x = 0, t = 0)$ and ask for the energy distribution for $t > 0$. We consider the correlation function

$$W_t(\epsilon, x) \equiv \int dt_1\, e^{i\epsilon t_1} \left\{ \frac{\left\langle \hat{\psi}(0,0) \left(\hat{\psi}^\dagger \left(x, t - \frac{t_1}{2}\right) \hat{\psi} \left(x, t + \frac{t_1}{2}\right) \right) \hat{\psi}^\dagger(0,0) \right\rangle}{\left| \left\langle \hat{\psi}(0,0) \hat{\psi}^\dagger(0,0) \right\rangle \right|} \right\}. \tag{7.9}$$

which is purely real but can take negative values. This function, which is directly related to the Wigner density [30], in energy and real space is a measure of the average electron number at (x, t) with energy ϵ. However, as soon as W_t becomes negative this physical interpretation fails. This is a well known problem considering quasiclassical distribution functions as the Wigner density. Usuallly, one interprets the appearance of those negative values as the signature of purely quantum mechanical interference phenomena. To motivate the structure of Eq. (7.9) one has to think of how to fix the final energy of the electron? After insertion, due to the uncertainity principle, the energy of the electron is completly undetermined, i.e., a superposition of all possible energy eigenstates builds up. The injection of the electron preparates the system in an excited, non-equilibrium state: $\hat{\psi}^\dagger(x = 0, t = 0) \left|\text{vac}\right\rangle$. At (x, t) we pick up an arbitrary electron and ask for its energy ϵ. This is done by introducing an internal time t_1 in order to test the phase of the annihilated electron. Then, the Fourier tranformation with respect to t_1 filters out those contributions where an electron with ϵ is present at (x, t).

Non-interacting case   To start the analysis of Eq. (7.9) we consider the non-interacting case. One expects two main features to arise. First of all, we expect two contributions to show up in $W_t(\epsilon, x)$

stemming from the inserted electron as well as from the electrons present in the Fermi sea. Secondly, the Pauli principle should play an important role even in the non-interacting case. Namely, after the insertion a superposition consisting of all accessible energy eigenstates builds up. Here, the Pauli principle comes into play as it allows the electron to tunnel only in unoccupied states.

The foregoing analysis of chiral one-dimensional electrons has shown that electrons flying high above the Fermi sea move with the bare Fermi velocity v_F. Therefore, the naive expectation is that this single electron shows up in the local energy distribution $W(\epsilon, x, t)$ mainly at $x = v_F t$, contributing (for $T = 0$) essentially to energies $\epsilon > \epsilon_F$. However, as already mentioned the Pauli principle restricts the initial energy of the single electron to a certain set of eigenstates. As a result the energy-time uncertainty relation $\Delta\epsilon\Delta t \sim 1$, even in the non-interacting case, leads to some spreading of this single-particle peak in W, centered at $x = v_F t$. It will turn out that an interference pattern arises reflecting this kind of physics. The non-interacting case can easily be evaluated with help of Wick's theorem. At zero temperature Eq. (7.9) gives (where we set $\delta x \equiv x - v_F t$ and use the non-interacting Green's function at zero temperature $g^>(x, t) = \frac{1}{2\pi}[\delta x + ia]^{-1}$)

$$
\begin{aligned}
W_t^0(\epsilon, x) &= \frac{1}{\bar{\rho}} \int dt_1\, e^{i\epsilon t_1} \left(g^>(x, t + \frac{t_1}{2}) g^<(x, t - \frac{t_1}{2}) + g^>(0, 0) g^<(0, t_1) \right) \\
&= \frac{1}{4\pi^2\bar{\rho}} \int dt_1\, e^{i\epsilon t_1} \frac{1}{\delta x - v_F t_1/2 + ia} \frac{1}{\delta x + v_F t_1/2 - ia} \\
&\quad + \frac{i}{4\pi^2 a} \int dt_1\, e^{i\epsilon t_1} \frac{1}{v_F t_1 + ia} \\
&= \underbrace{\frac{\sin(2\delta x/v_F \epsilon)}{\pi\bar{\rho}v_F\delta x} e^{-2a\epsilon/v_F}\Theta(\epsilon)}_{\text{extra electron}} + \underbrace{\frac{e^{a\epsilon/v_F}}{v_F}\Theta(-\epsilon)}_{\text{Fermi sea}}.
\end{aligned}
\tag{7.10}
$$

After inserting the electron, compared to the equilibrium situation, the amplitude of extracting an electron at (x, t) with $\epsilon > 0$ is increased. The first term in the integrand of Eq. (7.10) takes care of this contribution. Naturally, it is closely related to the single particle Green's function $g^>(x, t)$ itself. The first term vanishes for $\epsilon < 0$ vanishes as at $T = 0$, in the absence of interactions, it is not possible to create an extra electron below the Fermi edge. The oscillating prefactor in the single particle contribution is responsible for the interference pattern resulting from the interplay between the time-energy uncertainty relation and the Pauli principle we discussed above. In addition, there is a contribution from the filled Fermi sea as well, represented by the second part of the integrand (besides re-extracting the inserted electron itself, we can pick up an arbitrary electron with $\epsilon < 0$ from the Fermi sea).

Fig. 7.1 shows a plot of $W_t^0(\epsilon, x)$. One can observe the non-interacting electron with unknown initial energy (sharp peak) flying above the Fermi sea and the Fermi edge, while the mentioned interference fringes show up.

Interacting case Now, we turn on the electron-electron interactions. For this, we only have to multiply the integrand in Eq. (7.10) by some extra factor. Starting from the general expression in Eq. (7.5), we derive

$$W_t(\epsilon, x) \;\; = \;\; \int dt_1 \, e^{i\epsilon t_1} \left(g^>(x, t + \frac{t_1}{2}) g^<(x, t - \frac{t_1}{2}) + g^>(0,0) g^<(0, t_1) \right) \times e^{S(x,t,t_1)}, \quad (7.11)$$

with

$$S(x, t, t_1) \;\; = \;\; \int_0^\infty \frac{dq}{q} \left(-4i \sin\left(\frac{\omega_q t_1}{2}\right) \cos(qx - \omega_q t) + e^{i\omega_q t_1} \right) - (\alpha = 0'),$$

where in the exponent the integral is regularized substracting the non-interacting expression (cf. the construction of the single particle Green's function in Chapter 3).

Discussion of the numerical results Fig. 7.1(b-d) shows $W_t(\epsilon, x)$ as a function of x for various times. One can observe the two contributions, stemming from the extra particle and from the electrons of the Fermi sea. The former shows up as a vertical line at $x = v_F t$, while in the insets we focus on $W_t(\epsilon, x = v_F t)$ at the classical particle position $x = v_F t$. The important feature is that compared to the non-interacting result (dashed white lines) the weight of the single particle peak does not decay significantly with increasing propagation time, i.e., obviously the inserted electron does not thermalize. This is in agreement with the mentioned fact [3] that in the absence of impurities, in Luttinger liquids any inelastic relaxation processes are precluded.

Injecting an electron at $(x = 0, t = 0)$ into the liquid creates a density pulse, while the energy for this is brought up by the electron itself. Therefore, only in the very beginning there is an energy transfer between the inserted electron and the plasmonic bath (exciting the bosonic modes $\hat{b}_q$) related to the tunnel event. After this, the deformation of the electron density propagates through the liquid thereby shifting the energy distribution as a whole, i.e., the position of the "local" Fermi edge. This general feature can be understood realizing that the energy of any electron at a certain position x is affected in the same manner by a perturbation of the local liquid density. In addition, one observes an interference pattern (including negative values of $W_t(\epsilon, x)$), reflecting the interference between the extra electron and those stemming from the Fermi sea.

7.2.2   Initial energy known

As in the previous section the initial energy of the inserted electron was unknown, in a next step one can ask for the number of electrons at (x, t) with energy ϵ_f after the insertion of an electron with a certain energy ϵ_i at $(x = 0, t = 0)$. Extending the definition of $W_t(\epsilon, x)$ in Eq. (7.9) by a further internal time (and the corresponding Fourier transformation) meant to fix the initial energy ϵ_i, for
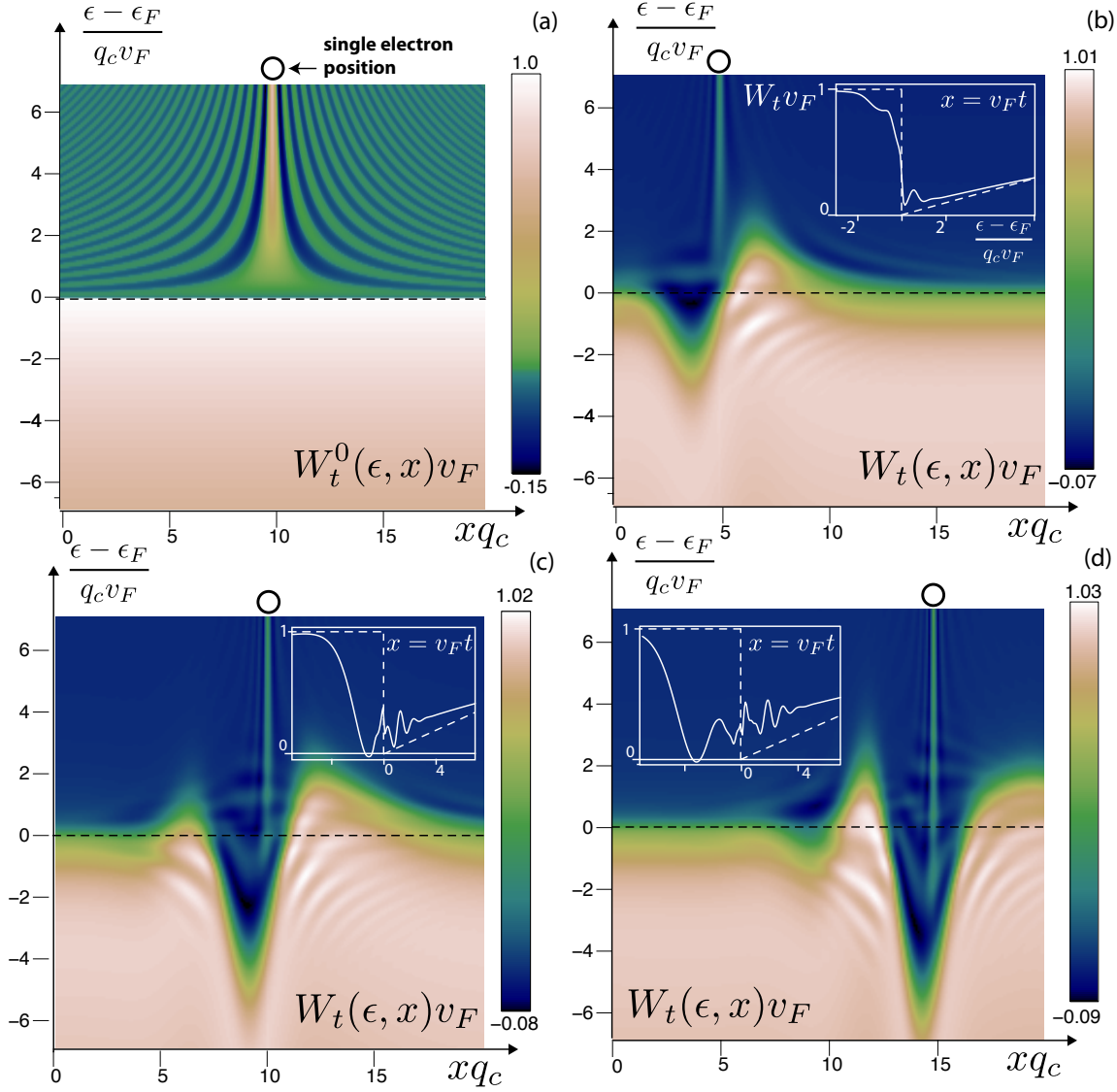
Figure 7.1: (a) Non-interacting four-point correlation function $W_t^0(\epsilon, x)$ for $tq_c v_F = 5$ and $T = 0$. It consists of two parts stemming from the electrons of the Fermi sea $\epsilon \leq 0$ and the inserted extra electron ($\epsilon > 0$) moving with v_F. One observes the interference fringes reflecting the Pauli principle (see main text). (b-d) Interacting case: Plot of $W_t(\epsilon, x)$ at $T = 0$ with $U_q = 2\pi\alpha v_F e^{-(q/q_c)^2}$ ($\alpha = 0.5$) for various times (from left to right): $tq_c v_F = 5, 10, 15$. One may note the vertical line at $x = v_F t$ representing the extra electron inserted at ($x = 0, t = 0$). Insets: Interested in the momentum distribution of the injected electron we focus on the classical particle position $x = v_F t$, i.e., the plot shows $W_t(\epsilon, x = v_F t)$ (solid white lines) and the non-interacting function $W_t^0(\epsilon, x)$ (white dashed lines). A comparison of both shows that the momentum distribution of the injected electron does not thermalize.

this purpose we propose the real function

$$
\begin{aligned}
C_\epsilon(x,t;\epsilon_i,\epsilon_f) &\equiv c^{-1}\int dt_1 \int dt_2\, e^{i\epsilon_i t_1} e^{i\epsilon_f t_2} \times \\
&\left\langle \hat{\psi}(0,\tfrac{t_1}{2})\left(\hat{\psi}^\dagger(x,t-\tfrac{t_2}{2})\hat{\psi}(x,t+\tfrac{t_2}{2})\right)\hat{\psi}^\dagger(0,-\tfrac{t_1}{2})\right\rangle,
\end{aligned}
\tag{7.12}
$$

where c is a normalization constant which we will fix with help of the non-interacting solution. To motivation this definition one can follow the same lines as in the case of $W_t(\epsilon,x)$. Comparing Eqs. (7.12) and (7.12), the only difference is that with help of the additional Fourier transformation we project out the arriving electrons at (x,t) with energy ϵ_f. To be precise, this definition has the status of a first idea how to construct a correlation function with the demanded properties. The problem is that C_ϵ can not be interpreted without any doubt in the same fashion as the correlation functions $C_\rho(x,t)$ and $W_t(\epsilon,x)$, introduced earlier. Namely, due to the additional internal time t_1, distinguishing the operators $\hat{\psi}^\dagger(0,-\tfrac{t_1}{2})$ and $\hat{\psi}(0,\tfrac{t_1}{2})$, one can not consider the operator $\int dt_2\, e^{i\epsilon_f t_2}\hat{\psi}^\dagger(x,t-\tfrac{t_2}{2})\hat{\psi}(x,t+\tfrac{t_2}{2})$ to be averaged over the non-equilibrium state after the insertion of the extra electron. Even so, the definition of C_ϵ seems to be reasonable enough to study this correlation function with some reservation concerning its physical interpretation.

Non-interacting case Again, we start with the analysis considering the non-interacting function at zero temperature, C_ϵ^0. Wick's theorem provides us with the pole structure of the correlation function (here $\bar{t}\equiv\tfrac{t_1+t_2}{2}$ and $\delta t\equiv\tfrac{t_1-t_2}{2}$):

$$
C_\epsilon^0 = \int dt_1\, e^{i\epsilon_i t_1}\int dt_2\, e^{i\epsilon_f t_2}\left(\underbrace{g^>(x,t+\bar{t})g^<(x,t-\bar{t})}_{\text{Extra electron}}+\underbrace{g^>(0,t_1)g^<(0,t_2)}_{\text{Fermi sea}}\right).
\tag{7.13}
$$

After inserting the electron with energy ϵ_i, compared to the equilibrium situation the amplitude of extracting an electron at $r=(x,t)$ with $\epsilon_f\approx\epsilon_i$ is increased. In addition, there is a contribution from the filled Fermi sea as well. The expression yields:

$$
\begin{aligned}
C_\epsilon^0 &= c^{-1}\int dt_1\, e^{i\epsilon_i t_1}\int dt_2\, e^{i\epsilon_f t_2}\left(g^>(x,t+\tau)g^<(x,t-\tau)+g^>(0,t_1)g^<(0,t_2)\right) \\
&= -\frac{2}{4\pi^2 v_F^2 c}\int d[\delta t]\, e^{i(\epsilon_i-\epsilon_f)\delta t}\int d\bar{t}\,\frac{e^{i(\epsilon_i+\epsilon_f)\bar{t}}}{[\bar{t}_- - \delta x/v_F][\bar{t}_- + \delta x/v_F]} \\
&\quad +\frac{e^{-a/v_F(\epsilon_i-\epsilon_f)}}{cv_F^2}\Theta(\epsilon_i)\Theta(-\epsilon_f) \\
&= \frac{1}{v_F^2 c}\delta(\epsilon_i-\epsilon_f)\Theta(\epsilon_i+\epsilon_f)\frac{2\sin((\epsilon_i+\epsilon_f)\delta x/v_F)e^{-a/v_F(\epsilon_i+\epsilon_f)}}{\delta x/v_F} \\
&\quad +\frac{e^{-a/v_F(\epsilon_i-\epsilon_f)}}{cv_F^2}\Theta(\epsilon_i)\Theta(-\epsilon_f),
\end{aligned}
\tag{7.14}
$$

where $\bar{t}_- \equiv \bar{t} - ia$. In the first term, which is directly related to the extra electron, the expected δ-peak at $\epsilon_f = \epsilon_i$ appears. However, the probability of finding an electron with $\epsilon_f = \epsilon_i$, centered at the classical particle position $x = v_F t$, is spreaded over the whole time axis, such that the energy-time uncertainty relation is fulfilled. For $\epsilon_i < 0$ the whole amplitude vanishes, as it is not possible to create an electron in the Fermi sea for $T = 0$. As the integration of the second term over all initial and final energies should give the mean electron density $\bar{\rho}$, i.e., $(2\pi v_F)^{-2}c^{-1}\int_0^\infty d\epsilon_i \int_{-\infty}^0 d\epsilon_f \exp\left(-a/v_F(\epsilon_i - \epsilon_f)\right) = \bar{\rho}$, for c it follows: $c = \bar{\rho}$.

Interacting case Turning on the electron-electron interactions leads to

$$
\begin{aligned}
C_\epsilon &= \int dt_1 \int dt_2\, e^{i\epsilon_i t_1} e^{i\epsilon_f t_2} \\
&\quad \left\{ g^>(x, t+\bar{t})g^<(x, t-\bar{t}) + g^>(0, t_1)g^<(0, t_2) \right\} e^S \\
S &= \int_0^\infty \frac{dq}{q} \left(2\cos(qx - \omega_q t)\left(e^{-i\omega_q \bar{t}} - e^{-i\omega_q \delta t}\right) + \left(e^{i\omega_q t_2} + e^{-i\omega_q t_1}\right)\right) \\
&\quad -(\alpha \to 0).
\end{aligned}
\tag{7.15}
$$

We note that the numerical evaluation of Eq. (7.15) involves a double Fourier transformation with respect to time. More importantly, for $\delta x = 0$ the integrand has a branch-cut for $\bar{t} = 0$ and for $t_1, t_2 = 0$, and therefore does not converge to zero. Thus the numerical evaluation of C_ϵ is rather difficult and can only be performed to a limited numerical precision, restricted by the finite time-integration intervall. Nevertheless it can be done, realizing that the branch-cuts are related to the step functions (for $T = 0$) reflecting the Pauli principle as well as to the delta function representing the injected particle (see Eq. (7.14)). Introducing an artificial cutoff function $\exp\left(-\tilde{\gamma}\sqrt{t_1^2 + t_2^2}\right)$ enables the integration and only leads to some smearing of the Fermi edge and to a numerical broadening of the sharp single particle peak. As a consequence, especially considering initial energies in the close vicinity to the Fermi edge the numerical results have to be handled with some care.

Numerical evaluation of C_ϵ Particularly, we are interested in the energy of the injected particle as a function of propagation time. Therefore, in Fig. 7.2 we evaluate C_ϵ for $x = v_F t$, i.e., at the classical position of the inserted electron moving with v_F (in the high-energy limit this can be taken for granted). Fig. 7.2 shows C_ϵ at $T = 0$ as a function of propagation distance x and final energy ϵ_f for various initial energies. Some obvious features can directly be observed. In agreement with Fig. (7.1), the whole energy distribution oscillates with increasing propagation distance. The period is approximatively given by $\frac{2\pi v_F}{\omega_{max}}$ (see Fig. 7.3). Besides those oscillations the width of the main peak, representing the injected particle oscillates with the same frequency. This can be understood in the framework of the semiclassical picture (which gets exact for energies $\epsilon \gg q_c v_F$), taking into account the zero point fluctuations of the plasmonic quantum bath, present even at $T = 0$. Due to the fluctuations, the energy of an electron flying over the potential landscape gets smeared out. In
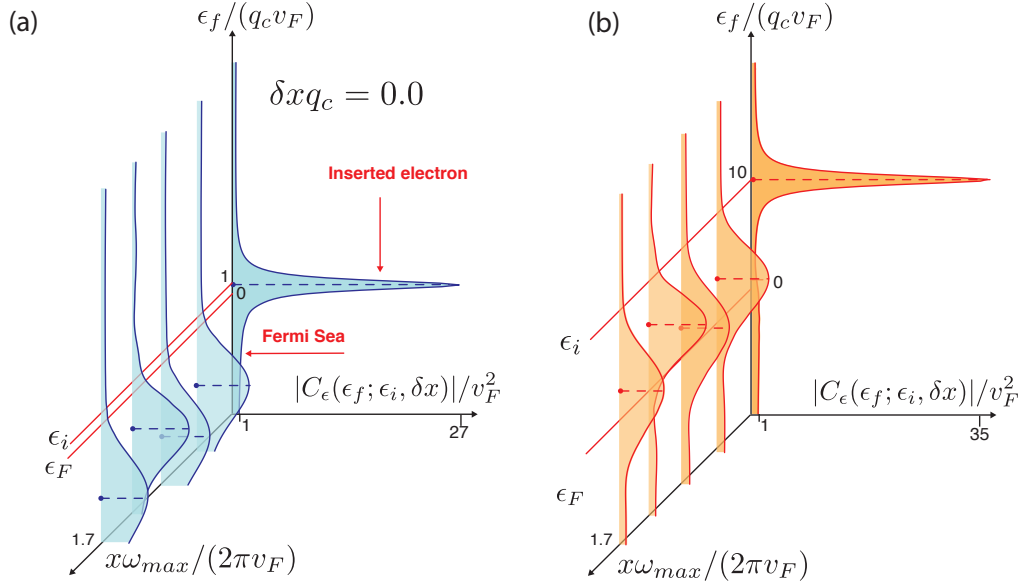
Figure 7.2: Plot of $|C_\epsilon(\epsilon_f; \epsilon_i, \delta x = 0)|$ as a function of the final energy ϵ_f and propagation distance x for two different initial energies $\epsilon_i/(q_c v_F) = 1, 8$ (from left to right). Here we set $T = 0$, $\delta x = x - v_F t = 0$ and $U_q = 2\pi\alpha v_F e^{-(q/q_c)^2}$, with $2\pi\alpha = 8.0$. As the integrand converges only very slowly, the double Fourier transformation with respect to the time-arguments was done by convoluting the integrand of Eq. (**??**) with an exponential $e^{-\tilde{\gamma}t}$ (here $\gamma = 0.5$). This leads to an artificial broadening of the main peak of the order $\mathcal{O}(\gamma)$, while the Fermi edge is smeared out (the finite width of the peak at $t = 0$ is only related to this numerical broadening). The whole energy distribution is shifted periodically, but the main peak does not decay for large times. In addition, the width of the main peak oscillates with the same period, which is approximatively given by $\frac{2\pi v_F}{\omega_{max}}$.

Chapter 4 it was shown that in the electron frame-of-reference the effective noise spectrum $\left\langle \hat{V}\hat{V} \right\rangle_\omega$ has a square-root singularity at $\omega = \omega_{\max}$, resulting in a nearly periodic random potential. It is a well known fact that the coherence of a particle subjected to a periodic noise potential, shows local maxima after propagation times which are multiples of the corresponding period. The reason for this is that the random phases which are accumulated, integrated over a full period, tends to cancel out. Therefore, the coherence is periodically recovered up to some amount. Note, that the single particle Green's function $G^>(\epsilon, x)$ in the high-energy limit displays exactly that kind of 'echos' as a function of time-of-flight (cf. Fig. (4.2)).

As a measure for the energy of the injected electron we define $\epsilon_{\max}(x)$, so that

$$\max\left(C_\epsilon(\delta x = 0, \epsilon_i, \epsilon_f)\right) = C_\epsilon(\delta x = 0, \epsilon_i, \epsilon_{\max}). \tag{7.16}$$

Fig. 7.3 shows $\epsilon_{\max}(x)$ for various initial energies. After some transient decay, it turns into the mentioned oscillation whose amplitude decays for $x \to \infty$. Thus, it follows that the single electron does not thermalize, transfering its initial energy completly to the bath, but propagates in the long-time limit without any further perturbation. This remarkable property is in complete agreement with [3] and with the semiclassical approach we introduced earlier. One of the most important implications following from the corectness of the semiclassical approach (see Chapter 4) at high energies is that the injected electron, despite of the electron-electron interactions, flys ballistically with velocity v_F. During its propagation it experiences a background potential, stemming from the density fluctuations of all the other electrons. In Chapter 4 we were mainly interested in the fluctuations of this plasmonic bath, leading to the decoherence of the single particle Green's function. As we already mentioned in subsection 7.2.1 the injection of the electron creates a density pulse in the liquid, $\delta\rho_{\rm cl}(x) = \delta(x)$. For a classical liquid one would expect the δ-peak to evolve in time according to the plasmonic dispersion relation ω_q: $\delta\rho_{\rm cl}(x, t) = \int \frac{dq}{2\pi} e^{iqx - i\omega_q t}$. This propagating density pulse gives reason for a potential V_{cl}, which can be obtained convoluting the plasmon density with the interaction potential U_q: $V_{\rm cl}(x, t) = \int \frac{dq}{2\pi} U_q e^{iqx - i\omega_q t}$ In the absence of fluctuations, the electron would only experience a capacitive energy shift due to the background potential $V_{\rm cl}$ without being scattered out of its original state. In Fig. 7.3b we show this classical potential landscape and compare the potential evaluated at the classical electron position $V_{\rm cl}(x = v_F t)$ with the electron energy in Fig. 7.3a. As a result one can observe that $V(x = v_F t)$ and $\epsilon_{\max}(x)$ qualitatively agree quite well.

Interestingly, the energy dependence of the injected electron is nearly the same, irrespective of the particular initial energy. While this was expected for high-energy electrons (the single particle Green's function $G^>(\epsilon, x)$ saturates for $\epsilon \to \infty$, cf. Fig. 3.3) , surprisingly even for small energies like $\epsilon_i = q_c v_F$ the behaviour seems to be identical. However, due to the numerical smearing of the distribution function in energy this result has to considered with some reservation.
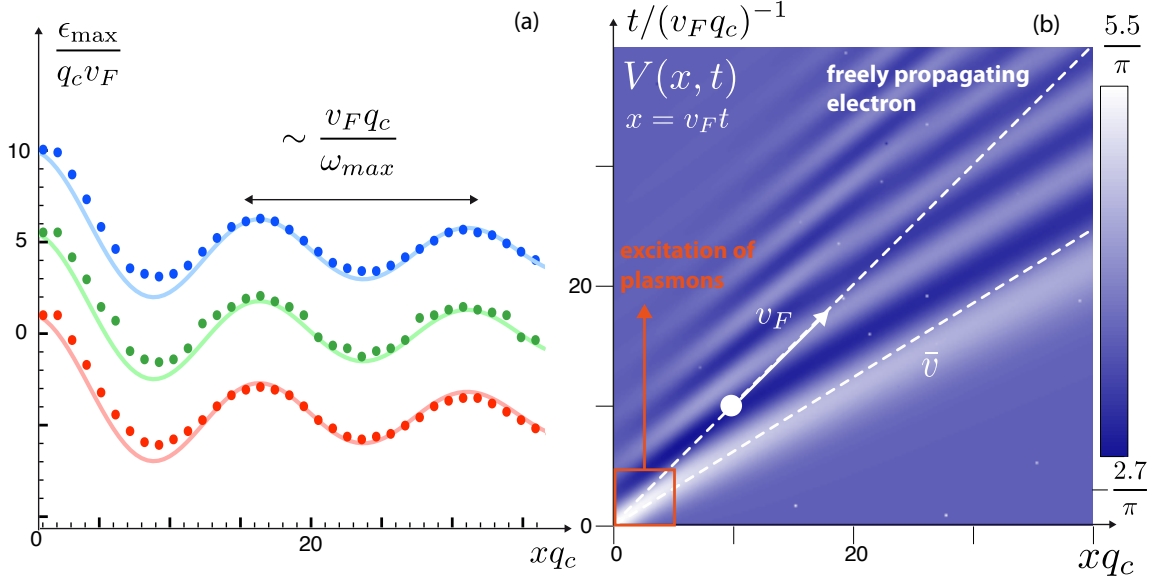
Figure 7.3: (a)Plot of ϵ_{max} as a measure for the energy of the injected electron, as a function of propagation distance x for various initial energies $\epsilon_i = 1.0, 5.5, 10.0$ (from bottom to top) and $T = 0$. The interaction potential is $U_q = 2\pi v_F \alpha e^{-(q/q_c)^2}$ where $\alpha = 1.0$. The solid points represent the numerical evaluation of the correlation function C_ϵ. The solid lines are proportional to the classical potential $V_{\mathrm{cl}}(x, t = \frac{x}{v_F})$ mentioned in the main text resulting from a pulse in a classical liquid at $(x = 0, t = 0)$ shifted by the particular initial energies ϵ_i (for better comparison to the numerical results we plot πV). Obviously, the qualitative behaviour can be understood rather well by thinking of a single electron whose energy is modulated due to the influence of the classical background potential $V_{\mathrm{cl}}(x, t)$ shown in Fig. 7.3(b). One may note that the electron energy as a function of propagation distance appears to be independent from ϵ_i (up to the difference in the initial energy ϵ_i).

7.3 Momentum distribution

To conclude this section we calculate the number of electrons at (x, t) with momentum k in a chiral interacting system after the injection of an additional electron whose initial momentum is unknown. For this we define

$$W_t(x, k) \equiv \int dx' \, e^{-ikx'} \left\{ \frac{\left\langle \hat{\psi}(0,0) \left(\hat{\psi}^\dagger(x - \frac{x'}{2}, t)\hat{\psi}(x + \frac{x'}{2}, t) \right) \hat{\psi}^\dagger(0,0) \right\rangle}{\left| \left\langle \hat{\psi}(0,0)\hat{\psi}^\dagger(0,0) \right\rangle \right|} \right\}, \qquad (7.17)$$

which is up to the normalization constant identical to the non-equilibrium Wigner density (see for instance [30]). The normalization constant follows from the single particle Greens function:

$\left|\left\langle \hat{\psi}(0,0)\hat{\psi}^\dagger(0,0)\right\rangle\right| = \frac{1}{2\pi a} = \bar{\rho}$. The non-interacting case yields:

$$
\begin{aligned}
W_t^0(x,k) &= \frac{1}{\bar{\rho}}\int dx'\, e^{-ikx'}\left(g^>(x+\frac{x'}{2},t)g^<(x-\frac{x'}{2},t)+g^>(0,0)g^<(x',0)\right)\\
&= \frac{1}{\bar{\rho}\pi}\Theta(k)\frac{\sin(2k\delta x)e^{-2ak}}{\delta x}+\Theta(-k)e^{ak}.
\end{aligned}
\tag{7.18}
$$

Switching on the coupling between the electrons turns the Wigner density into

$$
\begin{aligned}
W_t(x,k) = \frac{1}{\bar{\rho}}\quad \int dx'\, e^{-ikx'}&\left(g^>(x+\frac{x'}{2},t)g^<(x-\frac{x'}{2},+t)+g^>(0,0)g^<(x',0)\right)\times\\
&\exp\left\{4i\int_0^\infty \frac{dq}{q}\,\sin\left(\frac{qx'}{2}\right)\left(\cos\left(qx-\omega_q t\right)-\cos(qx-v_F q t)\right)\right\}.
\end{aligned}
\tag{7.19}
$$

The results of the numerical evaluation of Eq. (7.19) are shown in Fig. 7.4. Before we start with the analysis of the most obvious results, we notice an important relation between the electronic distribution in momentum space and the mean density. For this think of a non-interacting, homogeneous one-dimensional electron system with Fermi momentum k_F. For $T=0$ the density is directly related to the Fermi momentum, as: $\bar{\rho} = L\int_{-\infty}^\infty (dk)\, f_k/L = k_F/(2\pi)$. If the system suffers a perturbation, in the present case the insertion of the extra electron, the distribution function changes to $f(k,x,t)\equiv f_k + \delta f_k(x,t)$, such that the average electron density $\rho(x,t)\equiv \bar{\rho}+\delta\rho(x,t)$ gets distorted, with $\delta\rho(x,t) = \frac{1}{2\pi}\int_{-\infty}^\infty dk\,\delta f_k(x,t)$. If the non-equilibrium distribution function still shows some pronounced step like behaviour, it is reasonable to introduce a local 'Fermi momentum' $k_{\max}(x,t)$ which is in this case directly related to the deviation in the electron density: $\delta\rho(x,t)\approx\frac{1}{2\pi}k_{\max}(x,t)$. Obviously, we can observe that while the distribution function gets distorted rather drastically, still one can identify a sharp step. Following, the previous arguments this step, i.e., $k_{\max}(x,t)\sim\delta\rho(x,t)$ can be interpreted as a direct measure of the deviations from the mean electron density $\delta\rho(x,t)$ itself. Thus, besides some complex interference pattern resulting from the interference between the additional electron injected at $(x=0,t=0)$ and the electrons stemming from the Fermi sea, Fig. 7.4 essentially displays the distortion of the liquid density propagating through the channel. The sharp (red) peak at $x = v_F t$ represents the single electron. One may note that its contribution survives even for large propagation times, reflecting the fact that there is no finite scattering rate of electrons in a chiral interacting electron system. Once again, we point out the amazing fact that in the absence of impurities a one-dimensional electron can not relax its energy, being scattered out of its original state. Most naively one would expect that the electron density displays the propagation of the initial pulse, resulting from the injection of the additional electron into the system, i.e., $\delta\rho_{\mathrm{cl}}(x,t) = \int\frac{dq}{2\pi}\,e^{iqx-i\omega_q t}$. Indeed, a comparison of this propagating density pulse $\delta\rho_{\mathrm{cl}}(x,t)$ with the density resulting from the Wigner function $\int\frac{dk}{2\pi}\,W_t(x,k)$ show that they do agree quite well (inset Fig. 7.4), reflecting the fact that up to a certain extent one can understand a chiral interacting fermion system in terms of a classical liquid.
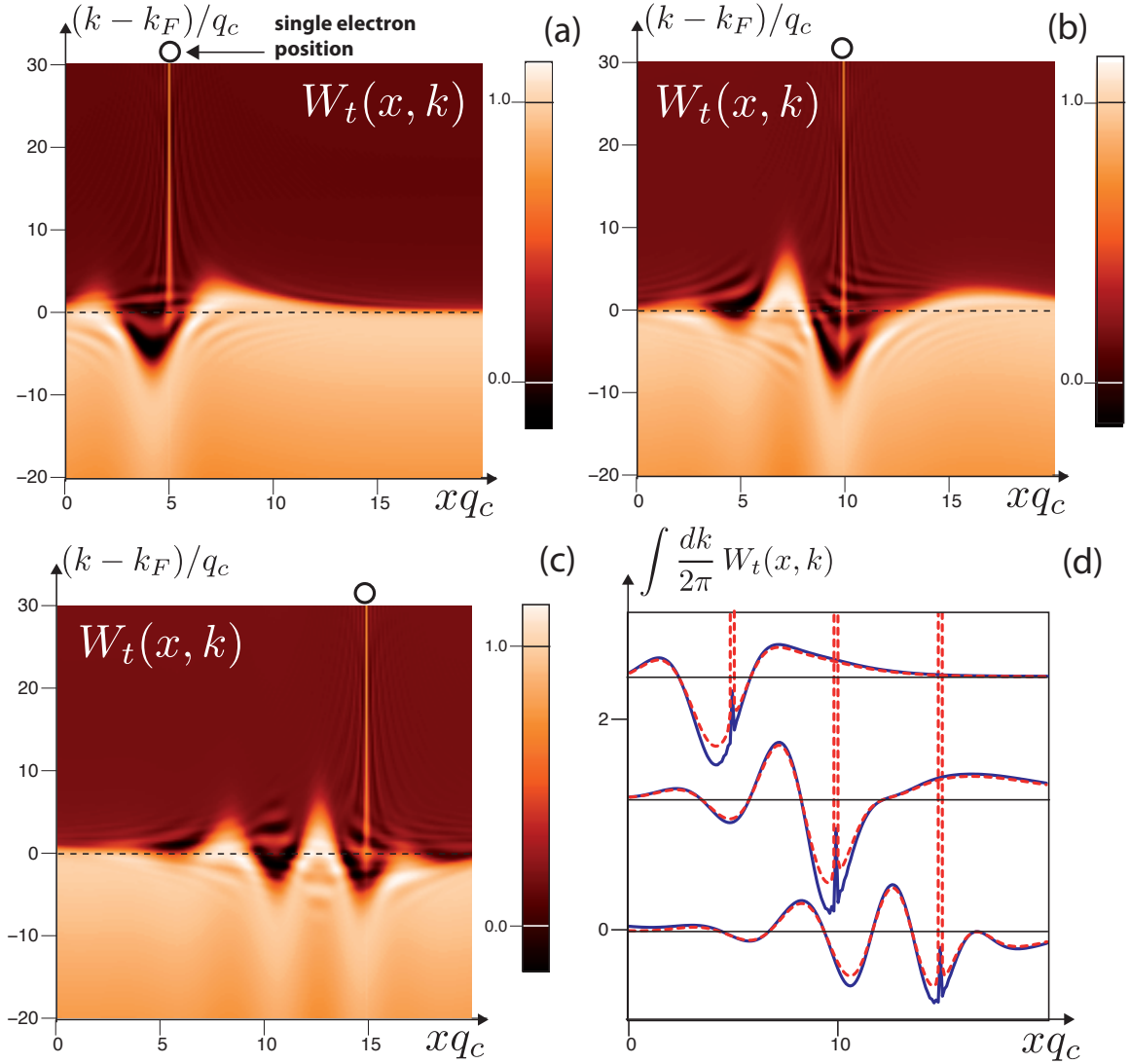
Figure 7.4: (a-c) $W_t(k, x)$ as a function of propagation distance x for various times (from a to c): $tq_c v_F = 5, 10, 15$. The dot on top of the plot indicates the classical electron position $x = v_F t$. Here the interaction potential is $U_q = 2\pi\alpha v_F e^{-(q/q_c)^2}$ with $\alpha = 2.0$. The sharp peak at $x = v_F t$ represents the additional electron injected at $(x = 0, t = 0)$, which does not decay significantly for large t. In addition, one can observe the distortion of the electron density $\delta\rho(x, t)$, i.e., the local shift of the Fermi edge $k_{\max}(x, t)$ (in the main text we argue that $\delta\rho(x, t) \sim k_{\max}(x, t)$). Thus, to some extent the plot can be read as a density profile of a chiral electron system. (d) Deviation from the mean density $\delta\rho_{\mathrm{cl}}(x, t) = \int \frac{dq}{2\pi} e^{iqx - i\omega_q t}$ of a classical liquid after creation of a density pulse $\delta\rho_{\mathrm{cl}}(x, t = 0) = \delta(x)$ for the same times as in (a) (dashed, red line). This is compared to the electron density resulting from the Wigner density integrated over all momenta $\int \frac{dk}{2\pi} W_t(x, k)$ (solid, blue line). For better clarity the plots are shifted vertically. Obviously, they fit rather well, except from the single particle contribution $(x = v_F t)$ in $\int \frac{dk}{2\pi} W_t(x, k)$, which is much smaller than expected. The reason for this might lie in the finite integration intervall for positive k.

Chapter 8

Open Luttinger liquids

Up to now, we focussed exclusively on the effect of the electron-electron interaction on the coherence properties of a one-dimensional electron system. In this Chapter, we extend the description by taking into account the coupling to an arbitrary harmonic oscillator bath. This includes the interaction with a two-dimensional bath of acoustical or optical phonons, which are always present in the 2DEG's and lead to an additional decoherence of the electrons. However, the purpose of this Chapter is two-fold.

On the one hand, the discussion of the coherence properties of a one-dimensional electron system, studied in the MZI is extended taking into account an external bosonic bath. For this, we analyze the influence of the coupling on the electron's Green's function $G^>(\epsilon, x)$. In passing, we consider some interesting properties of "open" chiral electron systems, like the occurence of "polaron clouds", i.e., the collective movement of a pulse in the electronic density $\hat{\rho}$ and a distortion of the crystal lattice. Coupling the electrons to a two-dimensional phonon bath leads to an effective electron-electron interaction, which can become attractive. It seems that the loss of coherence is related to the excitation of phonons by the inserted electron, if initially its energy was large enough (here, the energy has to be compared to the phonon energy). In contrast, the decoherence for low-energy electrons is strongly suppressed.

On the other hand, we are interested in how Pauli blocking (PB), which becomes important for the coherence of low-energy electrons [31, 32, 11], is included in the framework of bosonization. Up to now, there where only a few attempts to include many-body effects, as the Pauli blocking and renormalization effects into the description of decoherence. For instance, in [31, 32, 11] the semiclassical equations of motion approach (see Section 4.4) was proposed to describe the influence of an external quantum bath on the coherence of ballistically propagating electrons. There, the decoherence is related to the spectrum of the bath fluctuations. Including the backaction of the electron onto the bath, the PB is introduced. As a result the noise spectrum is substituted by a "Pauli blocked" version leading to a suppression of the decoherence of low-energy electrons in the

close vicinity to the Fermi edge. It was shown that in the context of weak localization the results are in agreement with the corresponding second order Keldysh perturbation theory. However, up to now all attempts to understand in more detail the influence of PB on the decoherence remained of perturbative nature. In contrast, in this Chapter we will use the exact bosonization solution for the electron Green's function $G^>$ of an "open Luttinger liquid" (i.e., coupled to a quantum environment) in order to come to a better understanding of these questions. In particular, we perform a weak-coupling expansion of the bosonization solution and identify the decay rate of the coherence with the expected rates resulting from a simple Fermi's golden rule calculation.

From a technical point of view starting from standard bosonization the coupling to an harmonic oscillator bath can be achieved rather easily. The reason for this is that the total Hamiltonian remains quadratic in bosonic operators. In contrast to the coupling to an arbitrary linear bath, the interaction between (chiral) Luttinger liquids and one-dimensional phonons was studied extensively, for example in [9, 47, 38, 17]. In the present case, it turns out that the most difficult aspect is the coupling of the chiral electron system to the non-chiral bath modes.

In Section 8.1 we introduce the Hamiltonian of a chiral interacting electron system coupled to an arbitrary harmonic oscillator bath. Especially, we are interested in the electronic Green's function $G^>(x,t)$. It turns out that for this purpose we only have to calculate the plasmonic spectrum, i.e., the spectrum of the bosonic modes related to modulations in the electron density, in presence of the linear bath. Two different approaches are presented to derive this plasmonic spectral density. In Section 8.2 we bring the Hamiltonian to a quadratic form and solve the problem introducing an appropriate resolvent [37, 35]. Then, we re-derive the plasmonic spectrum in the framework of the functional field integral technique [22, 5] (Section 8.3). In Section 8.4 we derive the main result of this Chapter: expanding the bosonization solution up to second order in the coupling strength we calculate the decoherence rates of electrons subjected to an harmonic oscillator bath. Then, we apply the developed tools on the coupling to two-dimensional phonons and evaluate numerically the corresponding coherence $G^>(\epsilon, x)$ (Section 8.5) and the mentioned "polaron cloud" (Section 8.6).

8.1   Hamiltonian and model

In order to couple the chiral (right-moving) one-dimensional electron system to some external quantum bath, one starts with the usual bosonized Hamiltonian, which is already diagonal in the bosonic operators related to the electronic degrees of freedom $\{\hat{b}_q\}$: $\hat{H}_{\text{el}} = \sum_{q>0} \omega_q \hat{b}_q^\dagger \hat{b}_q$. The dynamics of the bath of harmonic oscillators is assumed to be governed by the Hamiltonian: $\hat{H}_{\text{bath}} = \sum_{j,q} \Omega_{j,q} \hat{a}_{j,q}^\dagger \hat{a}_{j,q}$, where the operators $\{\hat{a}_{j,q}, \hat{a}_{j,q}^\dagger\}$ correspond to the various oscillator modes with dispersion relation $\Omega_{j,q}$. We assume the interaction between the chiral electron system and the harmonic oscillator bath

to be linear, i.e., the electron density is assumed to couple to some potential $\hat{V}$

$$\hat{H}_{\text{int}} \equiv \int dx\, \hat{\rho}(x)\hat{V}(x) = \frac{1}{L}\sum_q \hat{V}_q \hat{\rho}_{-q}, \tag{8.1}$$

where $\hat{V}(x) = \frac{1}{L}\sum_q \hat{V}_q e^{iqx}$ is hermitian and a linear function of the bosonic operators $\{\hat{a}_{j,q}, \hat{a}_{j,q}^\dagger\}$. From the hermiticity of $\hat{V}(x)$ it follows: $\hat{V}_q = \hat{V}_{-q}^\dagger$. This condition is fulfilled by the most general expression

$$\hat{V}_q = \sum_{j=1}^N g_{j,q}(\hat{a}_{j,q} + \hat{a}_{j,-q}^\dagger) \text{ with } g_{jq} = g_{j,-q}^*. \tag{8.2}$$

In total, the interaction of a Luttinger liquid with some linear bath leads to the usual problem of coupled harmonic oscillators:

$$\begin{aligned}
\hat{H} &= \hat{H}_{\text{el}} + \hat{H}_{\text{bath}} + \hat{H}_{\text{int}} \\
&= \sum_{q>0} \omega_q \hat{b}_q^\dagger \hat{b}_q + \sum_{j,q} \Omega_{j,q} \hat{a}_{j,q}^\dagger \hat{a}_{j,q} + \sum_j M_{j,q}(\hat{a}_{j,q} + \hat{a}_{j,-q}^\dagger)\hat{b}_{-q},
\end{aligned} \tag{8.3}$$

where we substituted the electron density $\hat{\rho}_q$ by the bosonic operators $\hat{b}_q$ and introduced the effective coupling coefficient $M_{j,q} \equiv \sqrt{\frac{|q|}{2\pi L}}g_{j,q}$. As the electronic system is coupled differently to each of the bosonic modes it is hard to give an adequate definition of a dimensionless coupling strength between bath and electrons. However, in the folllowing we understand the dimensionless constant g as a parameter which is proportional to the mean coupling strength and when introducing the explicit form of the bath and the interaction, g will be defined precisely. Our main interest is directed towards the single particle Green's function $G^>(x,t)$ of an electron propagating coherently through a one-dimensional system. As the bosonization identity introduced earlier (cf. Eq. (3.26)) yields: $G^>(x,t) = \frac{-i}{2\pi a}\langle e^{-i\hat{\Phi}(x,t)} e^{i\hat{\Phi}(0,0)}\rangle$ with $\hat{\Phi}(x,t) = i\sum_{q>0}\sqrt{\frac{2\pi}{Lq}}[\hat{b}_q(t)e^{iqx} - \hat{b}_q^\dagger(t)e^{-iqx}]$, for this we only have to calculate the plasmonic correlation functions $\langle \hat{b}_q(t)\hat{b}_q^\dagger\rangle$ and $\langle \hat{b}_q^\dagger(t)\hat{b}_q\rangle$. For later purpose, we define the plasmonic Green's functions for $q>0$ here as

$$\begin{aligned}
B_q^>(t) &= -i\left\langle \hat{b}_q(t)\hat{b}_q^\dagger \right\rangle \\
B_q^<(t) &= -i\left\langle \hat{b}_q^\dagger \hat{b}_q(t) \right\rangle \\
B_q^R(t) &= -i\Theta(t)\left\langle \left[\hat{b}_q(t), \hat{b}_q^\dagger\right] \right\rangle.
\end{aligned} \tag{8.4}$$

Fortunately, there are several techniques which enable its evaluation. In particular, the fact that for every momentum q there is only a single harmonic oscillator which is coupled to all the others simplifies the problem crucially. The main question is: how to calculate the correlators without explicitly diagonalizing the problem?

First of all, this problem can be solved by a direct calculation of the plasmonic spectral density

$$\mathcal{B}_{q\omega} \;\; \equiv \;\; -\frac{1}{\pi}\mathrm{Im}B_{q\omega}^R, \tag{8.5}$$

as the plasmonic propagator functions are connected to the spectral density via the fluctuation-dissipation theorem in Eq. (2.13). In addition, one can make use of the functional field integral method (for instance see [2]) and trace out the bath degrees of freedom. We are not solely interested in the single particle Green's function, but in correlation functions involving both the electronic and the external bath fields (e.g., for the calculation of the plasmon cloud), as well. For this purpose, the functional field integral technique turns out to be a very powerful tool. In the whole chapter, the bosonsic modes related to the electronic density fluctuations, $\{\hat{b}_q\}$, are denoted as plasmonic modes in order to distinct them from the bath modes $\{\hat{a}_{qj}\}$.

8.2   Solution via the resolvent method

The purpose of this section is the calculation of the correlation functions $\langle \hat{b}_q(t)\hat{b}_q^\dagger \rangle$ and $\langle \hat{b}_q^\dagger(t)\hat{b}_q \rangle$. For this we calculate the spectral density $\mathcal{B}_{q\omega}$ of the plasmonic modes. This can be done with help of a "resolvent", we introduce below. Before the explicit calculation of $\mathcal{B}_{q\omega}$, some preliminary remarks are in order. The Hamiltonian (Eq. (8.3)) of the one-dimensional electrons system coupled to some linear environment is equivalent to the standard problem of a set of coupled, harmonic oscilators. To simplify the further discussion, we introduce a compact notation: $\vec{a}_q$ denotes a column vector whose entries are the operators $\hat{a}_{j,q}$ and whose zeroth component is given by $\hat{b}_q$. Analogously, $\vec{a}_q^\dagger$ is defined as the corresponding row vector with the hermitian conjugate entries. The solution of the system of coupled harmonic oscillators provides a set of normal modes $\hat{d}_{j,q}$ such that: $\hat{H} = \sum_{q,j} \tilde{\Omega}_{j,q}\hat{d}_{j,q}^\dagger \hat{d}_{j,q}$, where $\tilde{\Omega}_{j,q}$ denotes the corresponding eigenfrequencies. If we already had diagonalized the Hamiltonian, we would only have to express the operators $\hat{b}_q$ by a linear combination of the normal modes: $\hat{b}_q = \sum_j \lambda_{j,q}\hat{d}_{j,q}$. Then, the time evolution of the electronic, bosonic operators would become trivial, $\hat{b}_q(t) = \sum_j \lambda_{j,q}\hat{d}_{j,q}e^{-i\tilde{\Omega}_{j,q}t}$. In terms of the normal modes we could write:

$$\begin{aligned}
\left\langle \hat{b}_q \hat{b}_q^\dagger \right\rangle_\omega &= 2\pi \sum_j |\lambda_{j,q}|^2 \,\delta(\omega - \tilde{\Omega}_{j,q}) \cdot (1 + \bar{n}(\tilde{\Omega}_{j,q})) \\
&= 2\pi(1 + \bar{n}(\omega)) \sum_j |\lambda_{j,q}|^2 \,\delta(\omega - \tilde{\Omega}_{j,q}).
\end{aligned} \tag{8.6}$$

Equation 8.6 is nothing than the fluctuation-dissipation theorem in Eq. (2.13) and the sum emerging in Eq. (8.6) can be identified with the plasmonic spectral density $\mathcal{B}(\omega, q)$. However, before we can proceed with the direct calculation of the spectral density, in a preliminary step we have to bring the Hamiltonian into a sligthly different form.

Hamiltonian in terms of bosonic excitations and holes The crucial point about the Hamiltonian in Eq. (8.3) is that is couples the chiral electronic modes to non-chiral excitations, e.g., left-and right-moving phonons. The Hamiltonian can be re-written as follows:

$$
\begin{aligned}
\hat{H} &= \sum_{q>0} \omega_q \hat{b}_q^\dagger \hat{b}_q + \sum_{j,q} \Omega_{j,q} \hat{a}_{j,q}^\dagger \hat{a}_{j,q} \\
&+ \sum_{jq>0} \left\{ \left(M_{j,q} \hat{a}_{j,q} \hat{b}_q^\dagger + M_{j,q}^* \hat{a}_{j,q}^\dagger \hat{b}_q \right) + \left(M_{j,q}^* \hat{a}_{j,-q} \hat{b}_q + M_{j,q} \hat{a}_{j,-,q}^\dagger \hat{b}_q^\dagger \right) \right\}.
\end{aligned}
\tag{8.7}
$$

Here, we made use of the identity for $q > 0 : \hat{b}_q = \hat{b}_{-q}^\dagger$. Obviously, the momentum conservation leads to an asymmetric coupling of the electronic mode to the bath modes with $q > 0$ and $q < 0$. For chiral moving electrons there are no processes coupling them to bath modes with opposite chirality, which fulfill energy and momentum conservation simultaneously. Therefore, the second term (coupling the right moving plasmons and the left moving bath modes) in Eq. (8.7) contains only "virtual processes", where an electronic mode and a bath mode are (de)excited at the same time. Introducing "hole operators" $\hat{h}_{jq}^\dagger \equiv \hat{a}_{j,-q}$ and substituting $\sum_{j,q<0} \omega_{jq} \hat{a}_{jq}^\dagger \hat{a}_{jq} \sim \sum_{j,q>0} \omega_{jq} \hat{h}_{jq}^\dagger \hat{h}_{jq}$, up to a constant the Hamiltonian can be written as

$$
\hat{H} \sim \sum_{q>0} \vec{a}_q^\dagger \hat{\Omega}_q \vec{a}_q,
\tag{8.8}
$$

where $\vec{a}_q \equiv (\hat{b}_q, \hat{a}_{1,q}, \ldots, \hat{a}_{N,q}, \ldots, \hat{h}_{1,q}, \ldots \hat{h}_{N,q})^T$ denotes a $2N + 1$-dimensional column vector containing all the different modes and the $(2N + 1) \times (2N + 1)$ matrix $\hat{\Omega}_q$ is given by

$$
\hat{\Omega}_q = \begin{pmatrix}
\omega_q & M_{1,q} & \cdots & M_{N,q} & M_{1q}^* & \cdots \\
M_{1,q}^* & \omega_{1,q} & \cdots & 0 & 0 & \cdots \\
\vdots & \vdots & \ddots & \cdots & \cdots & \cdots \\
M_{N,q}^* & 0 & 0 & \omega_{N,q} & 0 & \cdots \\
M_{1,q} & 0 & 0 & 0 & \omega_{1,q} & \cdots \\
\vdots & \vdots & \vdots & \vdots & \vdots & \ddots
\end{pmatrix}.
\tag{8.9}
$$

A diagonalization of the matrix leads to eigenmodes, which contain hole-contributions as well. At first sight, dealing with a combination of hole and ordinary modes seems to be a difficult task: however, it will turn out that the resolvent method takes care of this fact nearly automatically.

Introduction of the resolvent In this paragraph, with $|j, q\rangle$ we denote the j-th eigenvector of the matrix $\hat{\Omega}_q$ and $|0\rangle$ represents the $(1, 0, 0, \ldots)^T$-vector. Furthermore, we can identify the coefficients $\lambda_{j,q}$ in Eq. (8.6) with: $\lambda_{j,q} = \langle j, q|0\rangle$.

To proceed further, we consider the matrix $\hat{B}_{q\omega} \equiv [\omega_+ - \hat{\Omega}_q]^{-1}$. The special matrix element $\langle 0| \hat{B}_{q\omega} |0\rangle$ is also called the "resolvent", which is nothing than the retarded plasmonic Green's function $B^R_{q\omega}$. Namely, it follows (cf. Eq. (8.5))

$$
\begin{aligned}
\mathcal{B}_{q\omega} = -\frac{1}{\pi}\mathrm{Im}\left\{ \langle 0| \frac{1}{\omega - \hat{\Omega}_q + i0^+} |0\rangle \right\} &= -\frac{1}{\pi}\mathrm{Im}\left\{ \sum_j \langle 0|j,q\rangle\langle j,q| \frac{1}{\omega - \hat{\Omega}_q + i0^+} |0\rangle \right\} \\
&= -\frac{1}{\pi}\mathrm{Im}\left\{ \sum_j \frac{|\langle 0|j,q\rangle|^2}{\omega - \tilde{\Omega}_{j,q} + i0^+} \right\} \\
&= \sum_j |\lambda_{j,q}|^2 \delta(\omega - \tilde{\Omega}_{j,q}),
\end{aligned}
\tag{8.10}
$$

where $\tilde{\Omega}_{jq}$ denotes the frequencies of the eigenmodes after diagonalization of the Hamiltonian in Eq. (8.8).

Calculation of the retarded plasmonic Green's function   Here, the fact that there is one single harmonic oscillator, which couples to a set of bath oscillators, is of crucial importance. Before starting the calculation, we mention that for this paragraph matrices are denoted with a hat on top of the variable.

In a first step, we rewrite the retarded plasmonic Green's function as $B^R_{q\omega} = \langle 0|[(\omega_+ - \hat{\Omega}^0_q) - \hat{V}_q]^{-1}|0\rangle$. The matrix $\hat{\Omega}^0_q$ contains only the diagonal elements of $\hat{\Omega}_q$ while $\hat{V}_q$ contains the off-diagonal elements, such that: $\hat{\Omega}_q = \hat{\Omega}^0_q + \hat{V}_q$. Furthermore, we set: $V_{ij}(q) \equiv \langle i,q;0| \hat{V} |j,q;0\rangle$, $\hat{B}^0_{q\omega} \equiv [\omega_+ - \hat{\Omega}^0_q]^{-1}$ and $b_{ij} \equiv \langle i,q;0| \hat{B}^0_{q\omega} |j,q;0\rangle \delta_{ij}$, where the vectors $\{|j,q;0\rangle\}$ denote the original basis of the free Hamiltonian, i.e., $\hat{H}_0 = \sum_{q>0} \vec{a}^\dagger_q \hat{\Omega}^0_q \vec{a}_q$.

After these preliminary definitions, we can now expand $B^R_{q\omega}$ as

$$
B^R_{q\omega} = \langle 0|\hat{B}^0_{q\omega} + \hat{B}^0_{q\omega}\hat{V}_q\hat{B}^0_{q\omega} + \hat{B}^0_{q\omega}\hat{V}_q\hat{B}^0_{q\omega}\hat{V}_q\hat{B}^0_{q\omega}\hat{V}_q\hat{B}^0_{q\omega} + \dots |0\rangle,
\tag{8.11}
$$

where we already omit terms which are even in the operator $\hat{V}_q$, as due to the diagonality of b_{ij} and the fact that $V_{ii} = 0$ these terms vanish. In addition, all the matrix elements of $\hat{V}_q$ vanish, except from V_{0j} and V_{j0}. One arrives at:

$$
\begin{aligned}
B^R_{q\omega} &= b_{00} \sum_{n=0}^{\infty} \left[b_{00} \sum_{j=1}^{2N} |V_{0j}|^2 b_{jj} \right]^n \\
&= \frac{1}{b_{00}^{-1} + \Sigma_{q\omega}},
\end{aligned}
\tag{8.12}
$$

where the self-energy $\Sigma_{\omega q} = -\sum_{j=1}^{2N} |V_{0j}|^2 b_{jj}$ has to be calculated carefully, as the Hamiltonian

contains also the hole-modes $\hat{h}_{jq}$, which need some special treatment. The first part $(1 \leq j \leq N)$ of the sum treats all contributions stemming from the bath modes $\hat{a}_{j,q}$ itself, while the second part $(N < j \leq 2N)$ takes care of terms related to the hole modes $\hat{h}_{j,q}$. In the calculation of the sum occurs the non-interacting retarded Green's function b_{jj} evaluated for the j-th bath mode (including the holes as well). At this point, the fact that for $j > N$ we are dealing with the non-interacting, retarded Green's function of the hole-modes becomes important. Namely, the Fourier transform of the latter, $b_{jj}(q, \omega)$, can be written as (for $j > N$):

$$
\begin{aligned}
b_{jj}(q, \omega) &= -i \int_{-\infty}^{\infty} dt \, e^{i\omega t} \Theta(t) \left\langle \left[\hat{h}_{j-N,q}(t), \hat{h}_{j-N,q}^{\dagger}(0) \right] \right\rangle \\
&= i \int_{-\infty}^{\infty} dt \, e^{i\omega t} \Theta(t) \left\langle \left[\hat{a}_{j-N.q}(0), \hat{a}_{j-N.q}^{\dagger}(t) \right] \right\rangle \\
&= -\frac{1}{\omega_+ + \omega_{j-N,q}},
\end{aligned} \tag{8.13}
$$

while for the bath modes, the Fourier transform of the non-interacting retarded Green's function b_{jj} simply gives ($j \leq N$): $b_{jj} = [\omega_+ - \omega_{j,q}]^{-1}$. The self-energy yields:

$$
\begin{aligned}
\Sigma_{q\omega} &= -\sum_{j=1}^{N} |V_{0j}|^2 \, b_{jj} - \sum_{j>N}^{2N} |V_{0j}|^2 \, b_{jj} \\
&= -\sum_{j=1}^{N} |M_{j,q}|^2 \left(\frac{1}{\omega_+ - \omega_{jq}} - \frac{1}{\omega_+ + \omega_{jq}} \right) \\
&= -2 \sum_{j=1}^{N} |M_{j,q}|^2 \frac{\omega_{j,q}}{\omega_+^2 - \omega_{j,q}^2}.
\end{aligned} \tag{8.14}
$$

Finally, for the plasmonic propagator functions $B_q^{>/<}$ it follows

$$
\begin{aligned}
iB_{q\omega}^{>} &= 2\pi \mathcal{B}(\omega, q)(1 + \bar{n}(\omega)) \\
iB_{q\omega}^{<} &= 2\pi \mathcal{B}(\omega, q)\bar{n}(\omega) \\
\mathcal{B}(\omega, q) &= -\frac{1}{\pi} \text{Im} \left\{ \frac{1}{\omega_+ - \omega_q + \Sigma_{q\omega}} \right\}.
\end{aligned} \tag{8.15}
$$

As a result, we succesfully calculated the plasmonic spectral density of electrons coupled to an arbitrary linear bath. In the next section, we employ the functional field integral formalism to re-derive the self-energy $\Sigma_{q\omega}$ and the electronic single particle Green's function.

8.3   Field theoretical approach

In this section we turn to the description of the open chiral electron system, using the functional field integral technique. While the calculation of the plasmonic Green's functions $B_{q\omega}^{>}$ and $B_{q\omega}^{<}$ could be performed straightforwardly with the resolvent method, the calculation of more complicated correlation functions is most easily done in the framework of functional field integrals. This section starts with a short reminder of the main ideas behind the method of functional field integrals [2]. After the re-expression of the Hamiltonian (Eq. (8.1)) in terms of coherent state amplitudes, we start with the tracing-out procedure of the bath degrees of freedom, thereby deriving the plasmonic self-energy $\Sigma_{q\omega}$. As demanded, the self-energy turns out to be identical to the one resulting from the resolvent method, which serves as a consistency check. The following calculation of the plasmonic Green's functions gives the exact solution of the electronic single particle Green's function under the influence of an external harmonic oscillator bath.

8.3.1   General remarks

The functional field integral method is based on the description in terms of the coherent state amplitudes ϕ, which are defined as:

$$|\phi\rangle \equiv \exp\left(\sum_i \phi_i \hat{a}_i^\dagger\right)|0\rangle \Rightarrow \hat{a}_i |\phi\rangle = \phi_i |\phi\rangle. \tag{8.16}$$

These can be ordinary complex fields, for bosonic operators $\{\hat{a}_i\}$, or Grassman fields if they represent fermionic operators. The partition sum $\mathcal{Z}$ can be expressed in terms of functional field integrals, where the corresponding weight is determined by the action $S[\phi]$. Introducing the imaginary time $\tau \equiv it$, and the fields $\phi(\tau, x)$, it is given by:

$$\mathcal{Z} \equiv \int D(\phi, \bar{\phi})\, e^{-S[\phi,\bar{\phi}]} \tag{8.17}$$

$$S[\phi, \bar{\phi}] \equiv \int_0^\beta d\tau \int_{-\infty}^\infty dx\, \bar{\phi}(x,\tau)\partial_\tau \phi(x,\tau) + H[\phi, \bar{\phi}]. \tag{8.18}$$

Here, $\bar{\phi}$ denotes the conjugated field, which for bosonic fields is identical to the complex conjugated of ϕ. This is in contrast to the case of Grassman fields, where the field and its conjugated are independent of each other. Conveniently, one transforms to the Matsubara frequency and momentum representation. For this we introduce the definitions[1]:

$$\phi(\tau) \equiv \frac{1}{\beta}\sum_n e^{-i\omega_n \tau}\phi(i\omega_n) \qquad \phi(i\omega_n) \equiv \int_0^\beta d\tau\, e^{i\omega_n \tau}\phi(\tau). \tag{8.19}$$

---

[1] Note that $\frac{1}{\beta}\int_0^\beta d\tau\, e^{i\omega_n \tau} = \delta_{n0}$

Here, one has to be careful, as $(\bar{\phi})_{-n} = \bar{\phi}_n$ and in the following we always set $\bar{\phi}_n \equiv (\phi_n)^*$. The Matsubara frequencies ω_n are quantized due to the finite temperature which determines the length of the imaginary time interval. For fermionic and bosonic fields, these eigenfrequencies are given by $\omega_n \equiv \frac{2\pi}{\beta}\{2n+1\}$ and $\omega_n \equiv \frac{2\pi}{\beta}\{2n\}$ respectively. The Matsubara action yields (where $\phi(i\omega_n) = \phi_n$):

$$S[\phi_n, \bar{\phi}_n] = \frac{1}{L\beta}\sum_{n,q}\bar{\phi}_{qn}(-i\omega_n)\phi_{qn} + H(\{\phi_{nq}, \bar{\phi}_{n'q'}\}). \tag{8.20}$$

The calculation of an arbitrary correlation function, initially given in its operator version, is done substituting the operators by the corresponding fields

$$\left\langle T_\tau \hat{\phi}_i(\tau)\hat{\phi}_j^\dagger \right\rangle = \left\langle \phi_i(\tau)\bar{\phi}_j \right\rangle$$
$$= \frac{1}{\mathcal{Z}} \cdot \int D(\phi, \bar{\phi})\, e^{-S[\phi,\bar{\phi}]}\phi_i(\tau)\bar{\phi}_j \tag{8.21}$$

Here, one has to have in mind that evaluating a correlator with the help of the functional field technique actually means calculating its imaginary time-ordered version. This is a direct consequence following from the construction principle of the path integral itself. The explicit calculation of the correlation function can in many important cases be done only by making use of the integration rules of complex, Gaussian integrals. Finally, one has to perform the analytic continuation, which relates the imaginary time-ordered correlator to the corresponding retarded Green's function in real-time (or rather to its Fourier transform).

8.3.2 Action of an open Luttinger liquid

In the framework of bosonization, one can implement any bath of harmonic oscillators, coupled linearly to the chiral interacting electron system. The main feature is that the resulting Hamiltonian remains quadratic in bosonic operators. Therefore, the model can be solved exactly by tracing out the bath degrees of freedom as we will show below. Using the functional field integral technique, the tracing-out procedure can be performed easily. For this, we translate the Hamiltonian in Eq. (8.3) into the language of function field integrals. Starting from Eq. (8.3)

$$\hat{H} = \sum_{q>0}\omega_q \hat{b}_q^\dagger \hat{b}_q + \sum_{j,q}\Omega_{j,q}\hat{a}_{j,q}^\dagger \hat{a}_{j,q}$$
$$+ \sum_{jq>0}\left(M_{j,q}\hat{a}_{j,q}\hat{b}_q^\dagger + M_{j,q}^*\hat{a}_{j-,q}\hat{b}_q + M_{j,q}\hat{a}_{j,-q}^\dagger \hat{b}_q^\dagger + M_{j,q}^*\hat{a}_{jq}^\dagger \hat{b}_q\right) \tag{8.22}$$

and Eq. (8.20), the corresponding action yields:

$$
\begin{aligned}
S[\varphi_j, \phi] &\equiv S_{\text{el}} + S_{\text{bath}} + S_{\text{int}} \\
&= \frac{1}{\beta} \sum_{q>0,n} \bar{\phi}_{qn}(-i\omega_n + \omega_q)\phi_{qn} + \frac{1}{\beta} \sum_{q,n,j} \bar{\varphi}_{j,qn}(-i\omega_n + \omega_{j,q})\varphi_{j,qn} + \\
&\quad \frac{1}{\beta} \sum_{jq>0} \left(M_{j,q} \left[\varphi_{j,qn}\bar{\phi}_{qn} + \bar{\varphi}_{j,-q,n}\bar{\phi}_{q,-n} \right] \right. \\
&\quad \left. + M_{j,q}^* \left[\varphi_{j,-q,n}\phi_{q,-n} + \bar{\varphi}_{j,qn}\phi_{qn} \right] \right)
\end{aligned}
\tag{8.23}
$$

Here, the field ϕ represents the plasmonic modes, while $\{\varphi_j\}$ denote the modes of the external bath. Obviously, the action is quadratic in the bosonic (complex) fields. This fact will be of crucial importance when calculating the various correlation functions of interest.

8.3.3 Electron Green's function

The electronic single particle Green's function can be calculated by tracing out the bath degrees of freedom. As noted above, the great advantage of the functional field integral formalism is that this can be done easily. Starting from the bosonization identity we only have to calculate the propagator functions $B_{q\omega}^{>/<}$. As we have already seen in Subsection 8.2, the fluctuation-dissipation theorem connects the propagator function with the spectral density and thus with the retarded Green's function. Therefore, our concern here is the calculation of the retarded Green's function for the plasmonic modes $\hat{b}_q$. As usual, first one derives the imaginary-time ordered correlation function from which the retarded Green's function follows via the analytical continuation $i\omega_n \to \omega + i0^+ \equiv \omega_+$. Making use of the identity for complex, Gaussian integrals

$$
\int D(\varphi, \bar{\varphi}) e^{-\bar{\varphi}A\varphi + \bar{\varphi}\chi' + \varphi\bar{\chi}} = \det(A) \cdot e^{\bar{\chi}A^{-1}\chi'},
\tag{8.24}
$$

the bath modes can be integrated out. As the plasmonic fields ϕ_{qn} are only well defined for $q > 0$, the tracing out is separately done for the left- and the right moving bath modes. The bath- and the interacting part of the action in Eq. (8.23) can be written as a sum

$$
\begin{aligned}
&\frac{1}{\beta} \sum_{q>0,n,j} \bar{\varphi}_{j,qn}(-i\omega_n + \omega_{j,q})\varphi_{j,qn} + \frac{1}{\beta} \sum_{q>0,nj} \left(M_{jq}^+ \varphi_{j,qn}\bar{\phi}_{qn} + (M_{jq}^+)^* \bar{\varphi}_{qn}\phi_{qn} \right) \quad + \\
&\frac{1}{\beta} \sum_{q<0,n,j} \bar{\varphi}_{j,qn}(-i\omega_n + \omega_{j,q})\varphi_{j,qn} + \frac{1}{\beta} \sum_{q<0,nj} \left((M_{jq}^-)^* \bar{\varphi}_{jqn}\bar{\phi}_{|q|,-n} + M_{jq}^- \varphi_{qn}\phi_{|q|,-n} \right),
\end{aligned}
\tag{8.25}
$$

such that we can perform the integration over the bath fields with $q < 0$ and $q > 0$ separately. For later purposes, we formally introduced coupling amplitudes M^+ and M^- labeling the terms stemming from energy (non-)conserving processes. With help of equation Eq. (8.24), the effective electronic action

becomes

$$
\begin{aligned}
S_{\text{eff}} \quad = \frac{1}{\beta} \quad \sum_{q>0,n} \bar{\phi}_{qn}(-i\omega_n + \omega_q)\phi_{qn} - \\
\frac{1}{\beta} \left\{ \sum_{q>0,n} \bar{\phi}_{qn} \left[\sum_j \frac{|M_{jq}^+|^2}{-i\omega_n + \omega_{jq}} \right] \phi_{qn} - \sum_{q>0,n} \bar{\phi}_{q,-n} \left[\sum_j \frac{|M_{jq}^-|^2}{-i\omega_n + \omega_{jq}} \right] \phi_{q,-n} \right\} \\
= \frac{1}{\beta} \quad \sum_{q>0,n} \bar{\phi}_{qn} \underbrace{(-i\omega_n + \omega_q - \Sigma_{qn})}_{A_{qn}^{-1}} \phi_{qn},
\end{aligned}
\tag{8.26}
$$

where in the last line we used the identity (valid only for the plasmonic field and for $q > 0$) : $\phi_{-q,-n} = \bar{\phi}_{qn}$. Furthermore, we defined the self-energy as

$$
\Sigma_{qn} \quad \equiv \quad \sum_j \frac{|M_{jq}^+|^2}{-i\omega_n + \omega_{jq}} + \sum_j \frac{|M_{jq}^-|^2}{i\omega_n + \omega_{jq}}
\tag{8.27}
$$

$$
= \quad \sum_j |M_{jq}|^2 \frac{2\omega_{jq}}{\omega_n^2 + \omega_{jq}^2}.
\tag{8.28}
$$

The imaginary time-ordered correlator $B^\tau(x,\tau) \equiv - \langle \phi(x,\tau)\bar{\phi}(0,0) \rangle$ follows directly from the corresponding matrix element in the action. It is given by

$$
B_{qn}^\tau = -\frac{1}{\beta} \langle \phi_{qn}\bar{\phi}_{qn} \rangle \quad = - \quad A_{qn}.
\tag{8.29}
$$

Thus the retarded Green's function $B_{q\omega}^R$ yields

$$
\begin{aligned}
B_{q\omega}^R \quad &= \quad B_{qn}^\tau \big|_{\omega_n \to \omega_+} \\
&= \quad \frac{1}{\omega_+ - \omega_q + \Sigma_{q\omega}}
\end{aligned}
\tag{8.30}
$$

Finally, the spectral density is given by $\mathcal{B}_{q\omega} = -\frac{1}{\pi}\text{Im}\{[\omega_+ - \omega_q + \Sigma_{q\omega}]^{-1}\}$, where the self-energy is identical to that we calculated via the resolvent method in Eq. (8.14). After the standard analytic continuation, the self-energy is given by: $\Sigma_{q\omega} = -\sum_j |M_{jq}|^2 2\omega_{jq}[\omega_+^2 - \omega_{jq}^2]^{-1}$.

8.3.4 The bath in terms of its spectrum

For later purposes we re-write the self-energy of the plasmonic modes in terms of the spectrum of the external bath. For this, we realize that the Fourier transform of the retarded Green's function of the

bath potential $\hat{V}$

$$D_q^R(t) \equiv -i\Theta(t)\left\langle \left[\hat{V}_q(t), \hat{V}_{-q}\right]\right\rangle \tag{8.31}$$

is given by

$$
\begin{aligned}
D_{q\omega}^R &= \int dt\, e^{i\omega t} D_q^R(t) \\
&= -\int (d\omega') \frac{\left\langle \left[\hat{V}, \hat{V}\right]\right\rangle_{q\omega'}}{\omega_+ - \omega'}.
\end{aligned}
\tag{8.32}
$$

We not that $\mathrm{Im}D_{q\omega}^R = \frac{1}{2}\langle[\hat{V}, \hat{V}]\rangle_{q\omega}$, while the correlation function $\langle[\hat{V}, \hat{V}]\rangle_{q\omega}$ can be evaluated starting from the definition of the potential $\hat{V}_q$ in Eq. (8.59). Namely, we get

$$\left\langle \left[\hat{V}, \hat{V}\right]\right\rangle_{q\omega} = \sum_j |g_{jq}|^2 \left\{\delta(\omega - \omega_{jq}) - \delta(\omega + \omega_{jq})\right\} \tag{8.33}$$

so that for the retarded Green's function it follows: $D_{q\omega}^R = -\sum_j \frac{2|g_{jq}|^2 \omega_{jq}}{\omega_+^2 - \omega_{jq}^2}$. A comparison to Eq. (8.27) shows that it is directly proportional to the self-energy derived in the preceding paragraph, $D_{q\omega}^R = \frac{2\pi L}{|q|}\Sigma_{q\omega}$. The imaginary part of $D_{q\omega}^R$ is asymmetric in ω, i.e., $\mathrm{Im}D_{-q,-\omega}^R = -\mathrm{Im}D_{q\omega}^R$, while the real part turns out to be a symmetric function in ω.

8.3.5   The single particle Green's function

With the results from the preceding subsection, the single-particle Green's function $G^>(x,t)$ of electrons coupled to an external harmonic oscillator bath can be calculated formally. For this we note that (where we omit the time-arguments for $t = 0$)

$$
\begin{aligned}
G^>(x,t) &= \frac{-i}{2\pi a}\exp\left(\int_0^\infty \frac{dq}{q}\, e^{iqx}\left\langle \hat{b}_q(t)\hat{b}_q^\dagger\right\rangle + e^{-iqx}\left\langle \hat{b}_q^\dagger(t)\hat{b}_q\right\rangle \right.\\
&\qquad\qquad \left. -\left[\left\langle \hat{b}_q\hat{b}_q^\dagger\right\rangle + \left\langle \hat{b}_q^\dagger\hat{b}_q\right\rangle\right]\right)\\
&= \frac{-i}{2\pi a}\exp\left(\int_{-\infty}^\infty \frac{d\omega}{2\pi}\int_0^\infty \frac{dq}{q}\left[(e^{iqx-i\omega t}-1)\left\langle \hat{b}_q\hat{b}_q^\dagger\right\rangle_\omega + \right.\right.\\
&\qquad\qquad \left.\left. (e^{-iqx-i\omega t}-1)\left\langle \hat{b}_q^\dagger\hat{b}_q\right\rangle_\omega\right]\right).
\end{aligned}
\tag{8.34}
$$

Making use of the fluctuation-dissipation theorem in Eq.(8.15), the expression can be written in terms of the plasmonic spectral density $\mathcal{B}_{q\omega}$ as well,

$$
\begin{aligned}
G^>(x,t) &= \frac{-i}{2\pi a} e^{S(x,t)} \\
S(x,t) &= \int_{-\infty}^{\infty} d\omega \int_0^{\infty} \frac{dq}{|q|} \left[(e^{iqx-i\omega t} - 1)(1+\bar{n}(\omega))\mathcal{B}(\omega,q) + \right. \\
&\qquad \left. (e^{-iqx+i\omega t} - 1)\bar{n}(\omega)\mathcal{B}(\omega,q) \right]
\end{aligned}
\tag{8.35}
$$

As an intermediate conclusion, it was shown that the whole effect of the linear coupling between the electrons and the external bath on the single particle Green's function $G^>(x,t)$ is encoded in the effective plasmonic spectrum $\mathcal{B}(\omega,q)$. Based on this result, in section 8.5 we study the influence of a bath consisting of two-dimensional phonons on the coherence properties of the one-dimensional electron system.

8.4   Weak coupling expansion

In this section we expand the bosonization solution Eq. (8.34), assuming the electrons and the bath to be only weakly coupled, i.e., we consider the self-energy Σ to be a small parameter. In the end we are interested in the decay of the Green's function $G^>(\epsilon,x)$, as it is a direct measure for the coherence properties of the system. The main purpose of this section is to illustrate in more detail how bosonization brings the Pauli blocking into play. The latter has important consequences, e.g., in the weak-coupling limit for the decay rates of the electron's coherence. We will show that the calculated decay rate is in agreement with the rate resulting from a simple Fermi's golden rule consideration and coincides with the results derived in [31, 36, 32, 11] with help of the equations of motion approach. For the purpose of calculatory simplicity we assume the self-energy not to depend on q, i.e., $\Sigma_{q\omega} = \Sigma_{\omega}$ and neglect the electron-electron interactions, i.e., $\omega_q = v_F q$. Approximatively, this is the case for a bath consisting of optical phonons, while the phonon-electron interaction is assumed to be point-like. The expansion in the coupling strength g between the bath and the plasmonic modes is done by expanding the spectral density itself:

$$
\begin{aligned}
\mathcal{B}(\omega,q) &= -\frac{1}{\pi}\text{Im}\left\{ \frac{1}{\omega_+ - \omega_q + \Sigma_{\omega q}} \right\} \\
&\approx -\frac{1}{\pi}\text{Im}\left\{ \frac{1}{\omega_+ - \omega_q} - \frac{\Sigma_{\omega q}}{(\omega_+ - \omega_q)^2} + \mathcal{O}(g^4) \right\} \\
&= \mathcal{B}^0(\omega,q) + \mathcal{B}^1(\omega,q) + \mathcal{O}(g^4).
\end{aligned}
\tag{8.36}
$$

Thus, the exponent in powers of g is given by $S(x,t) \approx S^0(g^0) + S^1(g^2) + \mathcal{O}(g^4)$, where the first correction S^1 yields:

$$
\begin{aligned}
S^1 \quad = \quad & \int_{-\infty}^{\infty} d\omega \int_0^{\infty} \frac{dq}{|q|} \left[(e^{iqx-i\omega t} - 1)(1 + \bar{n}(\omega))\mathcal{B}^1(\omega, q) + \right. \\
& \left. (e^{-iqx+i\omega t} - 1)\bar{n}(\omega)\mathcal{B}^1(\omega, q) \right].
\end{aligned}
\tag{8.37}
$$

The calculation of the first correction to S is a straightforward, but rather tedious task.

8.4.1   Calculation of S^1

Before we start with the explicit calculation, we define, for the purpose of brevity, the functions $\sigma_\omega \equiv \Sigma_\omega/|q| = \frac{1}{2\pi L} D_{q\omega}^R$ and $Y(\omega, q) \equiv \frac{\sigma_\omega}{(\omega_+ - v_F q)^2}$. Furthermore, in the following we will frequently make use of the identity: $Y(\omega, q) = Y^*(-\omega, -q)$. Then, Eq. (8.37) yields

$$
\begin{aligned}
S^1 \quad &= \quad S_A^1 + S_B^1 \\
S_A^1 \quad &\equiv \quad \frac{1}{\pi} \int_{-\infty}^{\infty} d\omega \int_0^{\infty} dq \left\{ \left(e^{iqx-i\omega t}(1 + \bar{n}(\omega)) + e^{-iqx+i\omega t}\bar{n}(\omega) \right) \right. \\
& \qquad \left. \times \frac{Y(\omega, q) - Y(-\omega, -q)}{2i} \right\} \\
S_B^1 \quad &\equiv \quad \frac{1}{\pi} \int_{-\infty}^{\infty} d\omega \int_0^{\infty} dq \left\{ \coth\left[\frac{\beta\omega}{2} \right] \frac{Y(\omega, q) - Y(-\omega, -q)}{2i} \right\}
\end{aligned}
\tag{8.38}
$$

Calculation of S_A^1:   In a first step we re-arrange the integrand so that we can extend the momentum integration over the whole real axis, $\int_0^{\infty} dq \to \int_{-\infty}^{\infty} dq$.

$$
\begin{aligned}
S_A^1 \quad = \quad & \frac{1}{\pi} \int_{-\infty}^{\infty} d\omega \int_0^{\infty} dq \left\{ \cos(qx - \omega t) \coth\left[\frac{\beta\omega}{2} \right] \frac{Y(\omega, q) - Y(-\omega, -q)}{2i} + \right. \\
& \left. i\sin(qx - \omega t) \frac{Y(\omega, q) - Y(-\omega, -q)}{2i} \right\} \\
= - \quad & \frac{i}{2\pi} \int_{-\infty}^{\infty} d\omega \int_{-\infty}^{\infty} dq \left\{ \cos(qx - \omega t) \coth\left[\frac{\beta\omega}{2} \right] Y(\omega, q) + \right. \\
& \left. i\sin(qx - \omega t)Y(\omega, q) \right\} \\
= - \quad & \frac{i}{4\pi v_F^2} \left\{ \int_{-\infty}^{\infty} d\omega \, \coth\left[\frac{\beta\omega}{2} \right] \sigma_\omega \int_{-\infty}^{\infty} dq \, \frac{e^{iqx-i\omega t} + e^{-iqx+i\omega t}}{(q - \frac{\omega}{v_F} - i0^+)^2} + \right. \\
& \left. \int_{-\infty}^{\infty} d\omega \, \sigma_\omega \int_{-\infty}^{\infty} dq \, \frac{e^{iqx-i\omega t} - e^{-iqx+i\omega t}}{(q - \frac{\omega}{v_F} - i0^+)^2} \right\}.
\end{aligned}
\tag{8.39}
$$

In order to evaluate the integral, one may note that the residue of the twofold pole at $q = \omega/v_F + i0^+$ can be evaluated with the help of the general formula for the residue of an n-fold pole at z_0: $\text{Res}(f, z_0) = \frac{1}{n!}\left[(z - z_0)^n f(z)\right]^{n-1}$. In the following, we restrict the considerations to $x \geq 0$. Then Eq. (8.39) yields

$$S_A^1(x > 0, t) = \frac{xi}{2v_F^2} \int_{-\infty}^{\infty} d\omega \, \sigma_\omega e^{i\frac{\omega}{v_F}\delta x} \left\{\coth\left[\frac{\beta\omega}{2}\right] + 1\right\} \tag{8.40}$$

$$S_A^1(x > 0, \epsilon) = \frac{ix}{2v_F^2} \frac{1}{L} D_\omega^R e^{i\epsilon\frac{x}{v_F}} \left(\coth\left[\frac{\beta\epsilon}{2}\right] + 1\right). \tag{8.41}$$

Calculation of S_B^1: The third term in Eq. (8.38) vanishes, as a short calculation shows:

$$\begin{aligned}
S_B^1 &= -\frac{i}{2\pi} \int_{-\infty}^{\infty} d\omega \coth\left[\frac{\beta\omega}{2}\right] \int_{-\infty}^{\infty} dq \frac{1}{(\omega_+ - v_F q)^2} \\
&= 0,
\end{aligned} \tag{8.42}$$

because the momentum integral is identical to zero.

8.4.2   Decay rate and phase shift

With the results from the preceding subsection we are now in the position to evaluate the Green's function up to second order in the coupling strength g. The Fourier transformation of the expanded Green's function $G^>(\epsilon, x) = \int dt \, e^{i\epsilon t} \left\{g^>(x, t)\left(1 + S^1(x, t) + \mathcal{O}(g^4)\right)\right\}$ yields

$$G^>(\epsilon, x) = g^>(\epsilon, x)\left[1 + \int (d\omega) S^1(x, \omega)\frac{g^>(x, \epsilon - \omega)}{g^>(x, \epsilon)} + \mathcal{O}(x^2, g^4)\right], \tag{8.43}$$

where the emerging convolution $\int (d\omega) S^1(\omega, x) g^>(\epsilon - \omega, x)$ gives (for $x > 0$):

$$\begin{aligned}
\int (d\omega) S^1(\omega, x)\frac{g^>(\epsilon - \omega, x)}{g^>(\epsilon, x)} &= \frac{ix}{v_F^2} \int (d\omega) \frac{1}{L} D_\omega^R \left(\bar{n}(\omega) + 1\right)\left[\frac{1 - f(\epsilon - \omega)}{1 - f(\epsilon)}\right] \\
&= -\Gamma(\epsilon)\frac{x}{v_F} - i\varphi(\epsilon)\frac{x}{v_F}.
\end{aligned} \tag{8.44}$$

Using the (a)symmetry of $\text{Re}D_{q\omega}^R$ ($\text{Im}D_{q\omega}^R$) in ω, the decay rate $\Gamma(\epsilon)$ yields

$$\Gamma(\epsilon) = \frac{\text{DOS}_{\text{el}}}{[1 - f_\epsilon]} \int_0^\infty d\omega \, \text{Im}\bar{D}_\omega^R \left\{2\bar{n}_\omega + 1 - [\bar{n}_\omega + 1]f_{\epsilon-\omega} - \bar{n}_\omega f_{\epsilon+\omega}\right\}, \tag{8.45}$$

where we set $\bar{D}_\omega^R = \frac{1}{L}D_\omega^R$, and the phase shift is:

$$\varphi(\epsilon) = -\frac{\text{DOS}_{\text{el}}}{[1 - f_\epsilon]} \int_0^\infty d\omega \, \text{Re}\bar{D}_\omega^R \left\{1 - [\bar{n}_\omega + 1]f_{\epsilon-\omega} + n_\omega f_{\epsilon+\omega}\right\}, \tag{8.46}$$

where we introduced the electronic density of states $\mathrm{DOS}_{\mathrm{el}} = (2\pi v_F)^{-1}$. In order to clarify the physical meaning of the expressions in Eqs. (8.45) and (8.46) in the next subsection we compare them to a simple Fermi's golden rule calculation.

8.4.3 Comparison to Fermi's golden rule approach

The weak coupling expansion of the bosonization solution for the coherence provides us with a decay rate and a phase shift which can be compared to the results stemming from the equations of motion approach [11, 31, 36]. There, the authors studied the influence of decoherence due to an external quantum bath on the weak localization of electrons and compared the resulting dephasing rate Γ_φ with a simple Fermi's golden rule calculation. It was shown that the dephasing rate of an electron subjected to quantum noise is not simply given by the electronic decay rate Γ^{el}. In addition, the coherence of the electronic Green's function is sensitive to the scattering of the corresponding holes (Γ^{h}) as well. For a detailed explanation of this fact we refer the reader to [36, 11]. However, the main idea is to re-express the Green's function $G^>(k,t) = -i \left\langle \hat{c}_k(t)\hat{c}_k^\dagger(0) \right\rangle$ as (where we introduce the time evolution operator $\hat{U}_t = \exp(-i \int_0^t dt'\, \hat{H}(t'))$)

$$
\begin{aligned}
G^>(x,k) &= -i \left\langle \mathrm{vac} \right| \hat{U}_t^\dagger \hat{c}_k \hat{U}_t \hat{c}_k^\dagger \left| \mathrm{vac} \right\rangle \\
&= -i \left\langle \hat{c}_k^\dagger \hat{U}_t \mathrm{vac} \right| \hat{U}_t \hat{c}_k^\dagger \mathrm{vac} \right\rangle .
\end{aligned}
\tag{8.47}
$$

The overlap in the second line in Eq. (8.47) can decay by two processes: either the ket state changes (i.e., the electron created at $t = 0$ can be scattered during its propagation), or the bra state changes after time t (i.e., the hole with momentum k is annihilated). Thus, the total decay rate is a sum of the electron and the hole scattering rates. These can be calculated with help of Fermi's golden rule, valid in the weak coupling limit. The rate of emmiting (absorbing) the energy ω into (from) the bath is given by $\Gamma^{\mathrm{el}}(\epsilon \to \epsilon \pm \omega) = 2\pi \mathrm{DOS}_{\mathrm{el}} \left\langle \hat{V}\hat{V} \right\rangle_{\mp\omega}$, where we set $\mathrm{DOS}_{\mathrm{el}} = (2\pi v_F)^{-1}$. As both, emission and absorbtion of energy leads to decoherence of the electron, the electronic scattering rate is the sum of both $\Gamma^{\mathrm{el}}(\epsilon) = \Gamma^{\mathrm{el}}_\uparrow(\epsilon) + \Gamma^{\mathrm{el}}_\downarrow(\epsilon)$, where

$$
\begin{aligned}
\Gamma^{\mathrm{el}}_\downarrow(\epsilon) &= \mathrm{DOS}_{\mathrm{el}} \int_0^\infty d\omega \left\langle \hat{V}\hat{V} \right\rangle_\omega \cdot [1 - f_{\epsilon - \omega}] \\
\Gamma^{\mathrm{el}}_\uparrow(\epsilon) &= \mathrm{DOS}_{\mathrm{el}} \int_0^\infty d\omega \left\langle \hat{V}\hat{V} \right\rangle_{-\omega} \cdot [1 - f_{\epsilon + \omega}] .
\end{aligned}
\tag{8.48}
$$

Now, with help of the fluctuation-dissipation theorem we can sum up the two contributions, yielding:

$$
\begin{aligned}
\Gamma^{\text{el}}(\epsilon) &= \text{DOS}_{\text{el}} \int_0^\infty d\omega \left\langle [\hat{V}, \hat{V}] \right\rangle_\omega \left\{ \frac{1 + \coth(\frac{\beta\omega}{2})}{2} \cdot [1 - f_{\epsilon - \omega}] \right. \\
&\qquad \left. - \frac{1 - \coth(\frac{\beta\omega}{2})}{2} \cdot [1 - f_{\epsilon + \omega}] \right\} \\
&= 2\text{DOS}_{\text{el}} \int_0^\infty d\omega \, \text{Im} D_\omega^R \left\{ 2\bar{n}_\omega + 1 - \bar{n}_\omega f_{\epsilon + \omega} - [\bar{n}_\omega + 1] f_{\epsilon - \omega} \right\}.
\end{aligned} \tag{8.49}
$$

The corresponding hole decay rates are given by

$$
\begin{aligned}
\Gamma_\uparrow^{\text{h}}(\epsilon) &= \text{DOS}_{\text{el}} \int_0^\infty d\omega \left\langle \hat{V}\hat{V} \right\rangle_\omega \cdot f_{\epsilon + \omega} \\
\Gamma_\downarrow^{\text{h}}(\epsilon) &= \text{DOS}_{\text{el}} \int_0^\infty d\omega \left\langle \hat{V}\hat{V} \right\rangle_{-\omega} \cdot f_{\epsilon - \omega},
\end{aligned} \tag{8.50}
$$

and result in the total hole scattering rate

$$
\Gamma^h(\epsilon) = 2\text{DOS}_{\text{el}} \int_0^\infty d\omega \, \text{Im} D_\omega^R \left\{ [\bar{n}_\omega + 1] f_{\epsilon + \omega} + \bar{n}_\omega f_{\epsilon - \omega} \right\}. \tag{8.51}
$$

Following [11, 31, 36], the total dephasing rate is given by $\Gamma_\varphi(\epsilon) = \frac{\Gamma^{\text{el}} + \Gamma^{\text{h}}}{2}$. The factor $\frac{1}{2}$ reflects the fact that Fermi's golden rule gives the probability of a scattering event per time unit. Therefore, the decay of the Green's function, which is the amplitude of an electron to propagate coherently, is related to exactly the half of the rate stemming from a Fermi's golden rule calculation. One gets:

$$
\begin{aligned}
\Gamma_\varphi(\epsilon) &= \frac{\Gamma^{\text{el}}(\epsilon) + \Gamma^h(\epsilon)}{2} \\
&= \text{DOS}_{\text{el}} \int_0^\infty d\omega \, \text{Im} D_\omega^R \left\{ 2\bar{n}_\omega + 1 + f_{\epsilon + \omega} - f_{\epsilon - \omega} \right\}.
\end{aligned} \tag{8.52}
$$

The dephasing rate Γ_φ can now be compared to the rate Γ in Eq. (8.45) resulting from the weak coupling expansion of the exact bosonization result (Eq. (8.34)). While at first sight the results seem to differ crucially, a closer look shows that indeed they are identically the same. This follows from the identity

$$
\begin{aligned}
\frac{2\bar{n}_\omega + 1 - [\bar{n}_\omega + 1] f_{\epsilon - \omega} - \bar{n}_\omega f_{\epsilon + \omega}}{1 - f_\epsilon} &= 2\bar{n}_\omega + 1 + f_{\epsilon + \omega} - f_{\epsilon - \omega} \\
e^{-\epsilon\beta} \left(2 + \bar{n}_\omega^{-1} - [\bar{n}_\omega^{-1} + 1] f_{\epsilon - \omega} - f_{\epsilon + \omega} \right) &= f_{\epsilon - \omega} + [\bar{n}_\omega^{-1} + 1] f_{\epsilon + \omega} \\
e^{-\epsilon\beta} \left(1 + e^{\beta\omega} - f_{\epsilon - \omega}(e^{\beta\omega} + e^{\epsilon\beta}) - f_{\epsilon + \omega}(1 + e^{\beta(\epsilon + \omega)}) \right) &= 0 \\
e^{-\epsilon\beta} \left(e^{\beta\omega} - e^{\beta\omega} \right) &= 0.
\end{aligned} \tag{8.53}
$$

Therefore, as a final result the decay rate $\Gamma(\epsilon)$ determing the decay of the single particle Green's function in the weak-coupling limit is given by

$$\boxed{\Gamma(\epsilon) = \text{DOS}_{\text{el}} \int_0^\infty d\omega \, \text{Im} \bar{D}_\omega^R \{ \underbrace{2\bar{n}_\omega + 1}_{\text{fluctuations}} + \underbrace{(f_{\epsilon+\omega} - f_{\epsilon-\omega})}_{\text{Pauli blocking}} \}.} \tag{8.54}$$

Equation (8.54) proofs that the bosonization solution contains the effect of Pauli blocking. This is a non-trivial fact, as here we start from an exact solution for the Green's function. The resulting dephasing rate is identical to that evaluated in the framework of the semiclassical equations of motion approach [31, 36, 32, 11]. While, the exponent in the bosonization solution for $G^>(\epsilon, x)$ in Eq. (8.35) only depends on the plasmonic spectrum, the Fermi functions enter the calculation via the non-interacting Green's function $g^>(\epsilon, x)$ (cf. Eq. 8.43).

8.5   Coupling to two-dimensional phonons

In this section we study the coherence properties of one-dimensional electrons interacting with a bath of two-dimensional phonons. We are particularly interested in how the influence of an external bosonic bath compares to that of intrinsic electron-electron interaction studied in Chapter 3. In the latter case, at least for high-energy electrons we could show that the decoherence simply relies on a pure dephasing process. In contrast, for electrons with high energies (compared to the energy, related to the excitation of a phonon) we expect to observe decoherence processes which rely crucially on the scattering between electrons and phonons. In addition, at small energies, as an effect of the electron-phonon interaction, even for non-interacting electrons there should show up some effective electron-electron coupling mediated by the phonon field. One may note that this effective (and in some frequency regime attractive) interaction is at the heart of the theory of superconductors.

8.5.1   Coupling between phonons and electrons

In Section 8.1 we introduced the most general coupling of the electron density to a potential $\hat{V}$ resulting from the interaction with an arbitrary harmonic oscillator bath (see Eq. (8.1)). In addition, the potential was assumed to be a linear function of the bath modes $\{\hat{a}_{j,q}\}$: $\hat{V}_q = \sum_{j=1}^N \alpha_{j,q}(\hat{a}_{j,q} + \hat{a}_{j,-q}^\dagger)$. For the case of electron-phonon interaction, the potential $\hat{V}$ is given by a convolution between the density of the ions $\hat{\rho}_{\text{ph}}$ and the screened Coulomb potential $\tilde{U}$: $\hat{V}_q = \tilde{U}_q \hat{\rho}_{\text{ph},q}$. As usual, one defines a displacement field $\vec{u}(x, t)$ denoting the deviations of the ion-cores from its rest position [30]:

$$\vec{u}_{\vec{q}} = \frac{-i\hat{\epsilon}_{\vec{q}}}{\sqrt{2V^{-1}\rho_c \omega_{\vec{q}}}} \cdot \left[\hat{a}_{\vec{q}} + \hat{a}_{-\vec{q}}^\dagger\right]. \tag{8.55}$$

Here, $\hat{\epsilon}_{\vec{q}}$ stands for the polarization vector of the phonon mode $\hat{a}_{\vec{q}}$, whose dispersion relation is denoted by $\omega_{\vec{q}}$. V is the two-dimensional volume and ρ_c is the density of the ion cores. In two dimensions, there exist two normal modes, namely the longitudinal and the transversal mode. As we assume the phonons to be coupled to the chiral electron system via a density-density interaction, we can neglect the transversal phonons, which do not lead to a deformation of the ion density. These deformations are given by: $\hat{\rho}_{ph}(x) \equiv -\nabla \vec{u}(x)$, where $\vec{u}(x)$ is the Fourier transformed of $\vec{u}_{\vec{q}}$. For longitudinal phonons the polarization vector is given by $\hat{\epsilon}_{\vec{q}} = \frac{\vec{q}}{q}$ and the density operator yields

$$\hat{\rho}_{ph,\vec{q}} = \frac{|\vec{q}|}{\sqrt{2V^{-1}\rho_c\omega_{\vec{q}}}} \left[\hat{a}_{\vec{q}} + \hat{a}_{-\vec{q}}^{\dagger} \right], \qquad (8.56)$$

while the corresponding free bath Hamiltonian is given by $\hat{H}_{\text{bath}} = \sum_{\vec{q}} \omega_{\vec{q}} a_{\vec{q}}^{\dagger} a_{\vec{q}}$. We assume the electron system to be orientated in x-direction and denote the finite width of the 2DEG in y-direction as W. Thus, we can introduce an additional quantum number Q, labelling the perpendicular momentum of the phonons y-direction. For this we set $\vec{q} = (q, Q)$. This yields an effective bath Hamiltonian of the form we used in the previous calculations

$$
\begin{aligned}
\hat{H}_{\text{bath}} &= \sum_{jq} \omega_{jq} \hat{a}_{jq}^{\dagger} \hat{a}_{jq} \\
\omega_{\vec{q}} &= \omega\left(\sqrt{q^2 + Q^2} \right).
\end{aligned}
\qquad (8.57)
$$

The density-density coupling, defined as

$$\hat{H}_{\text{int}} = \int dx \left(\int dx'^2 \, \tilde{U}(\vec{x'} - \hat{e}_x x) \hat{\rho}_{\text{ph}}(\vec{x'}) \right) \cdot \hat{\rho}(x), \qquad (8.58)$$

after the Fourier transformation to momentum space, yields $\hat{H}_{\text{int}} = \frac{1}{V} \sum_{\vec{q}} \tilde{U}_{\vec{q}} \hat{\rho}_{\text{ph},\tilde{q}} \hat{\rho}_{-q}$, where the potential $\hat{V}_{\vec{q}}$ follows from Eq. (8.56):

$$
\begin{aligned}
\hat{V}_q &= \sum_Q \tilde{U}_{\vec{q}} \frac{|\vec{q}|}{\sqrt{2\rho_c V^{-1}\omega_{jq}}} \left[\hat{a}_{jq} + \hat{a}_{j,-q}^{\dagger} \right]. \\
&= \sum_Q g_{\vec{q}} \left[\hat{a}_{\vec{q}} + \hat{a}_{\vec{q}}^{\dagger} \right].
\end{aligned}
\qquad (8.59)
$$

Electronic self-energy As we already mentioned, the effect of the coupling between electrons and phonons on the electronic single-particle Green's function is completely encoded in the resulting self-energy $\Sigma_{q\omega}$ (Eq. (8.27)). In the continuum limit, i.e., $W \to \infty$, it follows (note that $M_{j,q} \equiv$

$\frac{1}{W} \sqrt{\frac{|q|}{2\pi L}} \alpha_{j,q})$:

$$
\begin{aligned}
\Sigma_{q\omega} &= -\sum_{Q} \frac{2\omega_{jq}|M_{jq}|^2}{\omega_+^2 - \omega_{jq}^2} \\
&\approx -|q| \int_0^\infty dQ \, \frac{\bar{U}^2 \left(\sqrt{q^2+Q^2}\right) \cdot \left(q^2+Q^2\right)}{\omega_+^2 - \omega^2(\sqrt{q^2+Q^2})},
\end{aligned} \tag{8.60}
$$

where we included several constants into the function $\bar{U}_{q,Q} \equiv \frac{\tilde{U}_{q,Q}}{8\pi^2 \rho_c}$ and Q denotes the momentum perpendicular to the electronic flight-direction. As in the case of the intrinsic electron-electron interaction, we assume $\bar{U}$ to be cutoff for $q \gg q_c'$ and denote the dimensionless coupling strength as $g \equiv \lim_{q,Q \to 0} \bar{U}_{q,Q}/(2\pi v_F)$. Before we start with the calculation of the Green's function, some further remarks are in order. Obviously, the coupling constant g is a free parameter of the theory. For acoustical phonons, we treat the dispersion relation $\omega(\vec{q})$ in the Debye approximation, where we assume the Debye frequency ω_c to be much larger than the high-energy cutoff underlying the Luttinger approximation, i.e., $v_F k_F \ll \omega_c$. Therefore, in the following we use the linearised phonon dispersion relation $\omega(\vec{q}) = v_s |\vec{q}|$, where v_s denotes the sound velocity of the acoustical phonons. For the coupling to acoustical phonons, the dimensionless ratio v_s/v_F is the second free parameter of theory. Instead, considering optical phonons with the dispersion relation $\omega(\vec{q}) \equiv \omega_0$, the second dimensional parameter is given by $\omega_0/v_F q_c'$.

Plasmonic spectrum and $G^>(\epsilon, x)$ for electron-phonon coupling   Here, we mention only the most obvious features of the plasmonic spectrum and the corresponding Green's function of electrons coupled to a two-dimensional phonon bath. Fig. 8.1 shows the plasmonic spectral density for one-dimensional electrons (in the absence of intrinsic interactions) coupled to a bath consisting of two-dimensional, either acoustical or optical phonons. As a result of the coupling to acoustical phonons, an attractive electron-electron interaction is mediated by the phonon-field. This follows from the observation that at low frequencies the plasmonic velocity is lowered compared to the non-interacting case. In Fig. 8.2 we show the corresponding Green's function (for coupling to optical phonons). Obviously, there are two distincy energy regimes. The decoherence of electrons with $\epsilon \ll \omega_0$ is strongly suppressed, as these can not excite optical phonons of energy ω_0. This is in contrast to high-energy electrons with $\epsilon \gg \omega_0$. These can excite phonons, thereby suffering decoherence.

8.6   Polaron cloud

As a further application of the formalism developed above, we are interested in the correlation between the electron and the phonon density. For example, one can ask, what is the amplitude of detecting a deformation in the two-dimensional crystal structure at position $\vec{x} = (x, y)$ and time t, if an electron
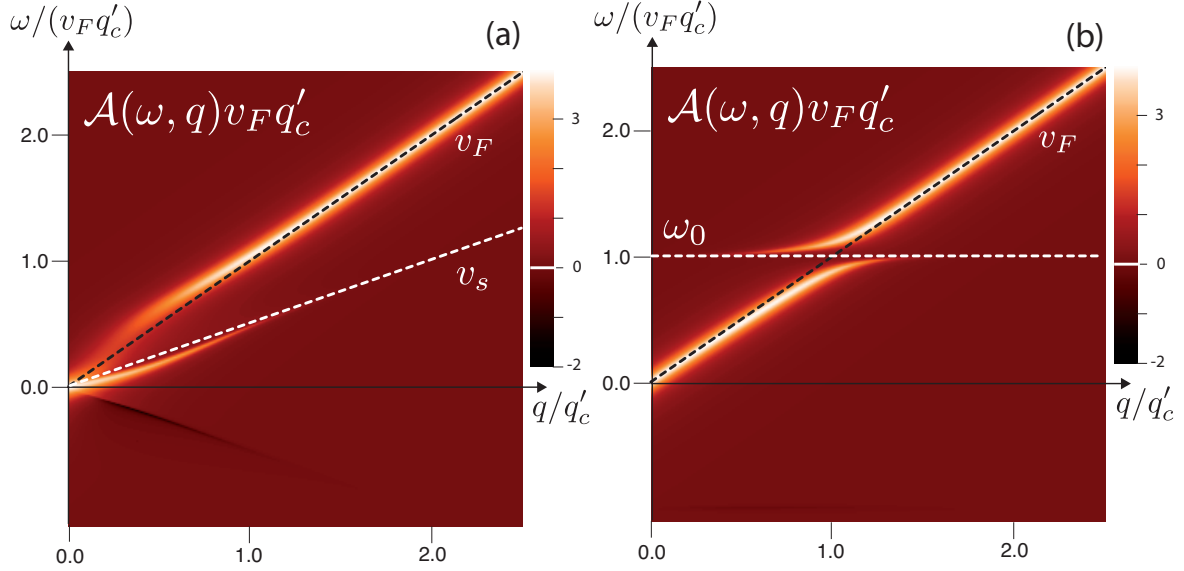
Figure 8.1: (a) Plasmonic spectral density of one-dimensional electrons (in the absence of intrinsic interactions) coupled to two-dimensional acoustical phonons with velocity $v_s/v_F = 0.5$; here the interaction potential is $\bar{U}_{\vec{q}} = 2\pi v_F g \exp(-(|\vec{q}|/q_c')^2)$ with $g = 0.5$; Obviously, at small frequencies the plasmon velocity is lowered indicating the effective, attractive, electron-electron interaction mediated by the phonon field. (b) Plasmonic spectral density for one-dimensional electrons coupled to two-dimensional optical phonons with $\omega_0/(q_c' v_F) = 1$ for the same interaction potential as in (a).

was inserted at $t = 0$ and $x, y = 0$. A collective movement of a pulse in the electronic density $\hat{\rho}$ and a distortion of the crystal lattice, usually is called a "polaron". This amplitude can be obtained by calculating the correlation function $C(x,t) \equiv \langle \hat{\rho}_{ph}(x,t)\hat{\rho}(0,0)\rangle$. It yields (we set $\vec{q} = (q_x, q_y) = (q, Q)$):

$$
\begin{aligned}
\langle \hat{\rho}_{ph}(\vec{x},t)\hat{\rho}(0,0)\rangle &= -\left\langle \nabla\hat{\vec{u}}(\vec{x},t)\hat{\rho}\right\rangle \\
&= \sum_{\vec{q},q'>0} e^{i\vec{q}\vec{x}} M_{\vec{q}} \left\langle \left(\hat{a}_{\vec{q}}(t) + \hat{a}^\dagger_{-\vec{q}}(t)\right)\left(\hat{b}_{q'} + \hat{b}^\dagger_{q'}\right)\right\rangle,
\end{aligned}
\tag{8.61}
$$

where $M_{\vec{q}} = \frac{|\vec{q}|}{W}\sqrt{\frac{|q|}{2\pi L}}U(\vec{q})\cdot(2V^{-1}\rho_c\omega(\vec{q}))^{-1/2}$. From the interacting part of the action S in Eq. (8.26) one can directly derive the selection rules for the correlation functions emerging in Eq. (8.61). As discussed above, the action includes processes which violate the energy conservation and therefore we call them "virtual processes". In order to take care of those processes, we formally labelled the corresponding coupling coefficients with $M_{\vec{q}}^-$ and $(M_{\vec{q}}^-)^*$ (the coefficients, related to the energy and momentum conserving interactions between bosons of same chirality are denoted by $M_{\vec{q}}^+$ and $(M_{\vec{q}}^+)^*$).
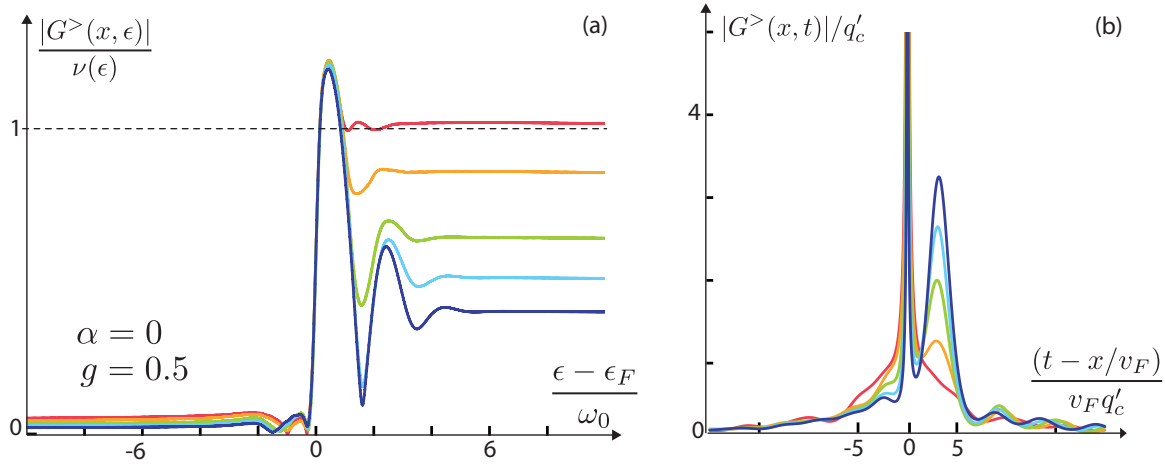
Figure 8.2: (a) Plot of the electronic Green's function $|G^>(\epsilon, x)|$ under the influence of optical two-dimensional phonons with $\omega_0/(q_c' v_F) = 1$ for various propagation lengths (from top to bottom): $x q_c' = 0, 3.3, 6.6, 10, 13.3$. The coupling between the electrons and phonons is given by $\bar{U}_{\vec{q}} = 2\pi v_F g \exp((|\vec{q}|/q_c')^2)$ with $g = 0.5$, while the internal interaction is set to zero, i.e., $\alpha = 0$ and we restrict the considerations to $T = 0$. As the Fourier transform into frequency space involves an integration with a slowly decaying integrand, we introduced an artificial exponential cutoff ($\sim e^{-\gamma|t|}$ with $\gamma = 0.1$), leading to a certain smearing of $|G^>(\epsilon, x)|$ in ϵ (e.g., near the Fermi edge this can be seen clearly). (b) Corresponding Green's function $|G^>(x, t)|$.

For the correlation function $C(x, t)$ it follows that

$$
\begin{aligned}
C(\vec{x}, t) = & \; i \sum_{Q, q > 0} e^{iQy} \left\{ M_{qQ} \left[-i \left\langle \hat{a}_{qQ}(t) \hat{b}_q^\dagger \right\rangle \right] e^{iqx} + M_{qQ}^* \left[-i \left\langle \hat{a}_{qQ}^\dagger(t) \hat{b}_q \right\rangle \right] e^{-iqx} \right. \\
& \left. M_{qQ} \left[-i \left\langle \hat{a}_{-q,Q}^\dagger(t) \hat{b}_q^\dagger \right\rangle \right] e^{iqx} + M_{qQ}^* \left[-i \left\langle \hat{a}_{-q,Q}(t) \hat{b}_q \right\rangle \right] e^{-iqx} \right\}.
\end{aligned}
\tag{8.62}
$$

As the bosonic operators $\hat{a}_{\vec{q}}$ and $\hat{b}_q$ commute, we can simplify the expression by introducing the time-ordered correlation functions $C_+^T(\vec{q}, t) \equiv -i \left\langle T \hat{a}_{\vec{q}}(t) \hat{b}^\dagger \right\rangle$ and $C_-^T(\vec{q}, t) \equiv -i \left\langle T \hat{a}_{-\vec{q}}^\dagger(t) \hat{b}^\dagger \right\rangle$, restricting the considerations to positive times $t > 0$:

$$
\begin{aligned}
C(\vec{x}, t) = & \; i \sum_{Q, q > 0} e^{iQy} \left\{ \left[M_{qQ} e^{iqx} C_+^T(q, Q, t) - c.c \right] + \left[M_{qQ} e^{iqx} C_-^T(q, Q, t) - c.c \right] \right\} \\
= & \; -2 \int (dQ) e^{iQy} \times \\
& \; \text{Im} \left\{ \int_0^\infty (dq) \int_{-\infty}^\infty (d\omega) \, e^{iqx - i\omega t} M_{qQ} \left[C_+^T(q, Q, \omega) + C_-^T(q, Q, \omega) \right] \right\}
\end{aligned}
\tag{8.63}
$$

8.6.1 Calculation of the time-ordered correlation functions

In a next step one has to derive the correlation function C_+^T and C_-^T in frequency representation. Here, the functional field integral approach shows its full power. One calculates the imaginary time-ordered version of $C_{+,-}^T$, which after a analytical continuation yields the corresponding retarded Green's functions. The latter is related to the time-ordered correlation functions via the identity

$$C_{+/-}^T(\vec{q}, \omega) = \mathrm{Re}[C_{+/-}^R(\vec{q}, \omega)] + i \coth\left[\frac{\beta\omega}{2}\right] \mathrm{Im}[C_{+/-}^R(\vec{q}, \omega)], \tag{8.64}$$

where $C_+^R(\vec{q}, t) \equiv -i\Theta(t)\left\langle \left[\hat{a}_{\vec{q}}(t), \hat{b}_q^\dagger\right]\right\rangle$ and C_-^R is defined analogously. The imaginary time-ordered correlation functions $C_+^\tau(\vec{q}, \tau) \equiv -\left\langle T_\tau \hat{a}_{\vec{q}}(\tau)\hat{b}_q^\dagger\right\rangle$ and $C_-^\tau(\vec{q}, \tau) \equiv -\left\langle T_\tau \hat{a}_{-\vec{q}}^\dagger(\tau)\hat{b}_q^\dagger\right\rangle$ can be translated into the field theoretical description be expressing the involved operators by the corresponding fields φ and ϕ (for brevity here we already show the correlators in the Matsubara representation) :

$$C_+^\tau(\vec{q}, i\omega_n) = -\frac{1}{\beta}\left\langle \varphi_{n\vec{q}}\bar{\phi}_{qn}\right\rangle$$

$$C_+^\tau(\vec{q}, i\omega_n) = -\frac{1}{\beta}\left\langle \bar{\varphi}_{-\vec{q}n}\bar{\phi}_{q,-n}\right\rangle. \tag{8.65}$$

Now, the explicit calculation of the correlators is rather simple, realizing that

$$C_+^\tau(\vec{q}, i\omega_n) = \partial_{M_{\vec{q}}^+} \ln \mathcal{Z}$$

$$C_-^\tau(\vec{q}, i\omega_n) = \partial_{M_{\vec{q}}^-} \ln \mathcal{Z}, \tag{8.66}$$

and remembering the fact that the self-energy emerging in the effective plasmonic action (Eq. (8.27)) is a sum of the two contributions stemming from the right- and the left-moving phonons. Then, it directly follows

$$C_{+/-}^\tau(\vec{q}, i\omega_n) = \mp\frac{1}{2} \quad \frac{1}{i\omega_n - \Omega_q + \Sigma_{qn}} \cdot \frac{M_{\vec{q}}^*}{i\omega_n \mp \omega_{\vec{q}}}. \tag{8.67}$$

In a last step, performing the analytic continuation we derive the retarded Green's functions: $C_{+/-}^R(\vec{q}, \omega) = C^\tau(\vec{q}, i\omega_n \to \omega_+)$. Finally, employing Eq. (8.64), the correlation function $C(\vec{x}, t)$ turns out to be real

and yields for $t > 0$:

$$
\begin{aligned}
C_{\vec{x},t} &= -2 \int (dQ) e^{iQy} \, \mathrm{Im} \left\{ \int_0^\infty \frac{dq}{2\pi} \int_{-\infty}^\infty \frac{d\omega}{2\pi} \, e^{iqx - i\omega t} M_{\vec{q}} \left[C_+^T(q,Q,\omega) + C_-^T(q,Q,\omega) \right] \right\} \\
&= \mathrm{Im} \left\{ \int_0^\infty \frac{dq}{2\pi} \int_{-\infty}^\infty (d\omega) \, e^{iqx - i\omega t} \right. \\
&\qquad \left. \left[\mathrm{Re} \left(\tilde{C}_+^T + \tilde{C}_-^T \right) + i \coth \left(\frac{\beta\omega}{2} \right) \mathrm{Im} \left(\tilde{C}_+^T + \tilde{C}_-^T \right) \right] \right\},
\end{aligned}
\tag{8.68}
$$

where in the last line we make use of the symmetry of the integrand with respect to the perpendicular momentum Q: $C_{+/-}^T(q,Q,\omega) = C_{+/-}^T(q,-Q,\omega)$ and define the functions

$$
\tilde{C}_{+/-}^T = \pm \frac{1}{\omega_+ - \Omega_q + \Sigma_{qn}} \int_0^\infty \frac{dQ}{2\pi} \frac{2\cos(Qy)|M_{\vec{q}}|^2}{\omega_+ \mp \omega_{\vec{q}}}.
\tag{8.69}
$$

8.6.2   Discussion of the numerical results

Here, we discuss the case of electrons coupled to acoustical phonons, where beside the coupling strength g between plasmons and phonons the ratio of the sound velocity v_s and the Fermi velocity v_F is as a second free parameter of the theory. The numerical evaluation of Eq. (8.68) in Fig. 8.3, emphasizes the close analogy between a chiral Luttinger liquid and an ordinary Euler liquid. Namely, to some extent, the behaviour of the correlation function $C(\vec{x}, t)$ can be understood in a simple classical picture of a liquid which is distorted by the interaction with some particle, inserted at $(x = 0, t = 0)$. In the classical picture, the correlation between the phonon density and the particle density should depend crucially on the ratio v_s/v_F. For $v_s > v_F$, the particle creates a pulse in the phonon-density, which follows the position of the particle such that a wave front, essentially propagating with v_F, emerges. The phonon density is largely increased in the close vicinity to the particle, but with increasing distance to the "epicenter" the radiated wave fronts lose coherence such that far apart from the particle the traces of the distortion vanish. In contrast, for $v_s/v_F < 1$ a "Mach cone" with an angle $\tilde{\alpha}$ is created, i.e., a shock-front builds up which is experienced as a sonic boom. The angle $\tilde{\alpha}$ is thereby given by $\sin \tilde{\alpha} = \frac{v_s}{v_F}$ (for $v_s < v_F$). Indeed, $C(\vec{x}, t)$ shows a very similiar behaviour with respect to a change of v_s/v_F.
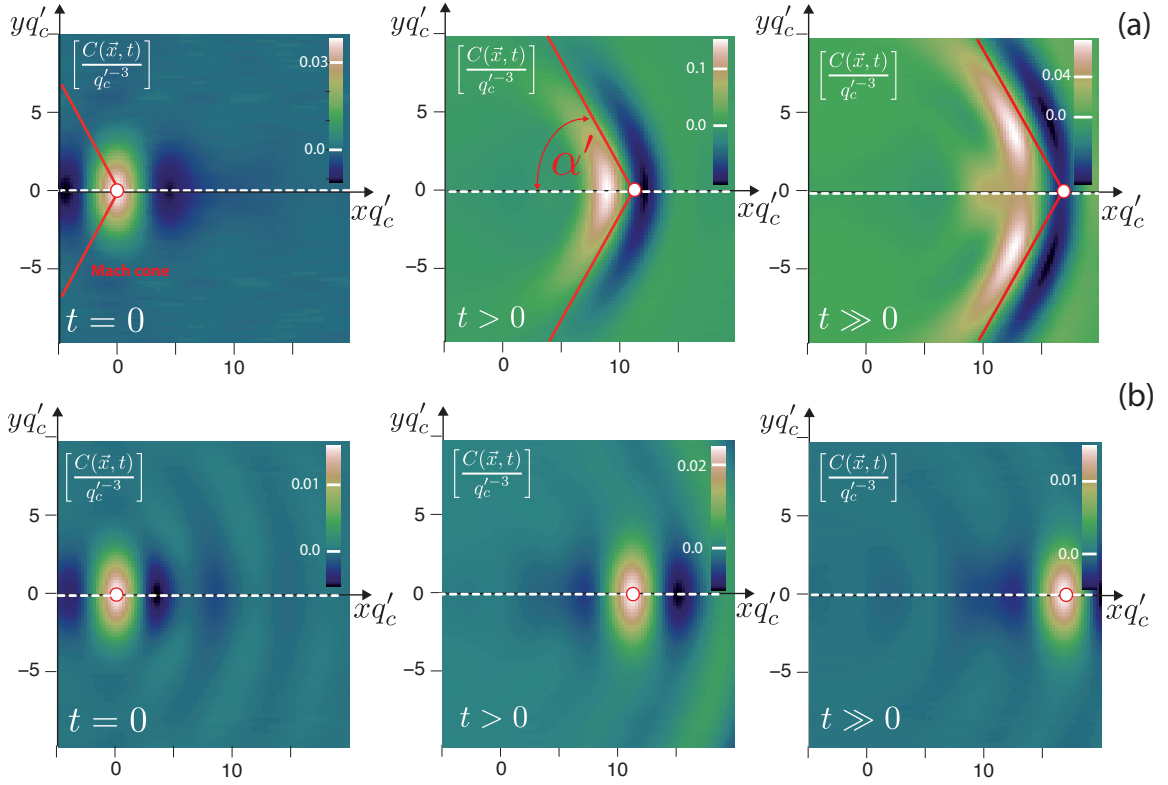
Figure 8.3: (a) Density-density correlation function $C(\vec{x}, t)$ for acoustical phonons with $v_s/v_F = 0.8$ as a function of $\vec{x} = (x, y)$ for different times (from left to the right): $tq'_c v_F = (0, 11.3, 17)$. The electron-phonon interaction potential is $\bar{U}_{\vec{q}} = 2\pi v_F g \exp(-(|\vec{q}|/q'_c)^2)$ with $g = 0.4$. Furthermore, the intrinsic electron-electron interaction is set to zero ($\alpha = 0$) and we consider the $T = 0$ case. The red lines show the Mach cone with opening angle $\tilde{\alpha} = \sin^{-1}(v_s/v_F)$, while the red dot represents the electron moving with v_F along the one-dimensional channel in x-direction. (b) Same configuration as in Fig.8.3a, but here $v_s/v_F = 2.0$.

Chapter 9

Summary and outlook

In the present work, we studied dephasing of chiral one-dimensional electron systems by electron-electron interaction as well as by coupling to an arbitrary harmonic oscillator bath. As a direct a measure for the electrons' coherence we considered the interference contrast of a ballistic electronic interferometer, as the Mach-Zehnder interferometer (Chapter 2). It was shown that for weakly tunnel-coupled interferometer arms the visibility and thus the coherence can be expressed only in terms of the single-particle Green's function $G^>(\epsilon, x)$. Therefore, in the following we referred to $G^>(\epsilon, x)$ as the coherence of a single electron. Consequently, the main part of this work was devoted to the analysis of the single-particle Green's function (Chapters 3, 4 and 5). We employed the full bosonization solution of $G^>(\epsilon, x)$ as a reference point and re-derived the single-particle Green's function in the high-energy limit within a physically transparent semiclassical method. While at first sight the physical mechanism of decoherence in strongly interacting one-dimensional electron systems was rather unclear, the semiclassical approach showed that the decoherence of high-energy electrons relies on a simple "pure dephasing" process, i.e., no complicated scattering processes are involved. As a main result we proofed that the coherence of high-energy electrons in one-dimensional chiral electron systems displays a universal power-law as a function of propagation distance: $|G^>(\epsilon \to \infty, x)| \sim 1/x$
.

In a next step, the semiclassical approach was extended by proposing an ansatz, meant to re-derive the Green's function $G^>(\epsilon, x)$ for arbitrary energies. Unfortunately, the semiclassical did not reproduce the bosonization result to the full extent. Nevertheless, the analysis showed how to derive the exact Green's function, at least mathematically, starting from non-interacting electrons moving with the bare Fermi velocity, thereby accumulating a random quantum phase due to the intrinsic fluctuations of the plasmonic bath. In passing, we considered the functional bosonization approach, which seems to be closely related to the semiclassical approach, however the latter might to be more transparent and technically simpler. A further investigation of the semiclassical approach seems to be rather

fruitful as it might provide a much more intuitive understanding for the decoherence in such systems. As a possible next step, for instance one could think of an extension of the semiclassical approach in order to describe the decoherence in the high-energy limit in arbitrary Luttinger liquids (instead of chiral Luttinger liquids).

Besides these very fundamental questions, the further investigation of the Mach-Zehnder interferometer seems to be of particular interest. As we mentioned in the beginning of this work, up to now only a fraction of the observed effects are well understood. To proceed further, an extension of the bosonization description of the interferometer to higher orders in tunneling seems to be necessary. We pointed out that in next non-trivial order in tunneling, the current is related to complicated convolutions of two-particle Green's functions. However, in Chapter 7 it became clear that in principle the numerical evaluation of the two-particle Green's functions is possible. Furthermore, the closer analysis of four-point functions should provide a deeper understanding of the non-equilibrium properties of Luttinger liquids. As an alternative, one could treat the interactions perturbatively, for instance in the framework of the presented Keldysh perturbation theory, in turn allowing for an arbitrary tunnel coupling of the interferometer arms. For stronger tunnel-coupled interferometer arms, these can not be conisdered to be inequilibrium any longer. However, as Keldysh perturbation theory remains applicable even in non-equilibrium, this could be an interesting approach.

In Chapter 8, we concluded this work coupling the one-dimensional electrons to an external bath. With help of the bosonization technique an exact solution for the electronic Green's function was derived. The main result of this chapter was that expanding the exact solution of $G^>(\epsilon, x)$ to lowest order in coupling between bath and electrons, an energy dependent dephasing rate was derived. This dephasing rate turned out to reflect the influence of the Fermi edge, i.e., Pauli blocking effects. Whereas this result was derived earlier in [31, 32, 36, 11], here it was obtained starting from the exact solution for the Green's function. This result might be only the starting point for the further investigation of the question how the influence of the Fermi edge (e.g., Pauli blocking etc.) on the electrons' coherence is contained within the bosonization solution.

Appendix A

Mach-Zehnder interferometer

A.1 Current operator

The current operator $\hat{I} \equiv q_e \frac{d}{dt} \hat{N}_1$ can be calculated in terms of the single particle fields $\hat{\psi}_j(x)$, only using the canonical anti-commutation relations in Eq. (2.2) and the Heisenberg equation $\frac{d}{dt} \hat{N}_1 = -i[\hat{N}_1, \hat{H}^T]$:

$$
\begin{aligned}
\hat{I} &= -iq_e \int dx \left[\hat{\psi}_1^\dagger(x)\hat{\psi}_1(x), t_A \hat{\psi}_1^\dagger(0)\hat{\psi}_2(0) + t_B \hat{\psi}_1^\dagger(x_1)\hat{\psi}_2(x_2) + \text{h.c.} \right] \\
&\equiv \hat{I}_1 + \hat{I}_2 + \text{h.c.},
\end{aligned}
\tag{A.1}
$$

with

$$
\begin{aligned}
\hat{I}_1 &\equiv -iq_e \int dx \, [\hat{\psi}_1^\dagger(x)\hat{\psi}_1(x), t_A \hat{\psi}_1^\dagger(0)\hat{\psi}_2(0)] \\
\hat{I}_2 &\equiv -iq_e \int dx \, [\hat{\psi}_1^\dagger(x)\hat{\psi}_1(x), t_B \hat{\psi}_1^\dagger(x_1)\hat{\psi}_2(x_2)].
\end{aligned}
$$

In the following, we evaluate the two emerging contributions $\hat{I}_1$ and $\hat{I}_2$ separately.

A.1.1 $\hat{I}_1$

The first part of the current operator $\hat{I}_1$ yields

$$
\begin{aligned}
\hat{I}_1 &= -iq_e t_A \int dx \, \left[\hat{\psi}_1^\dagger(x)\hat{\psi}_1(x)\hat{\psi}_1^\dagger(0)\hat{\psi}_2(0) \right. \\
&\quad \left. - \hat{\psi}_1^\dagger(0)\hat{\psi}_2(0)\hat{\psi}_1^\dagger(x)\hat{\psi}_1(x) \right] \\
&= -iq_e t_A \int dx \, \left[\hat{\psi}_1^\dagger(x)\hat{\psi}_1(x)\hat{\psi}_1^\dagger(0)\hat{\psi}_2(0) \right. \\
&\quad \left. + \hat{\psi}_1^\dagger(x)(\delta(x) - \hat{\psi}_1(x)\hat{\psi}_1^\dagger(0))\hat{\psi}_2(0) \right] \\
&= -iq_e t_A \hat{\psi}_1^\dagger(0)\hat{\psi}_2(0).
\end{aligned}
\tag{A.2}
$$

A.1.2 $\hat{I}_2$

The second part is given by

$$
\begin{aligned}
\hat{I}_2 &= -iq_e t_B \int dx \, \left[\hat{\psi}_1^\dagger(x)\hat{\psi}_1(x)\hat{\psi}_1^\dagger(x_1)\hat{\psi}_2(x_2) \right. \\
&\quad \left. + \hat{\psi}_1^\dagger(x)\hat{\psi}_1^\dagger(x_1)\hat{\psi}_1(x)\hat{\psi}_2(x_2) \right] \\
&= -iq_e t_B \int dx \, \left[\hat{\psi}_1^\dagger(x)\hat{\psi}_1(x)\hat{\psi}_1^\dagger(x_1)\hat{\psi}_2(x_2) \right. \\
&\quad \left. + \hat{\psi}_1^\dagger(x)(\delta(x - x_1) - \hat{\psi}_1(x)\hat{\psi}_1^\dagger(x_1))\hat{\psi}_2(x_2) \right] \\
&= -iq_e t_B \hat{\psi}_1^\dagger(x_1)\hat{\psi}_2(x_2).
\end{aligned}
\tag{A.3}
$$

Summing up the two contributions and adding the hermitian conjugated operator, the calculation yields

$$
\hat{I} = -iq_e t_A \hat{\psi}_1^\dagger(0)\hat{\psi}_2(0) - iq_e t_B \hat{\psi}_1^\dagger(x_1)\hat{\psi}_2(x_2) + \text{h.c.}
\tag{A.4}
$$

A.2 Calculation of the interferometer current

The calculation of the interferometer current in linear response to the tunnel operator starts from the Kubo formula

$$
I = i \int_{-\infty}^{0} dt' \, \left\langle \left[\hat{H}_{H_1}^T(t'), \hat{I}(0) \right] \right\rangle.
\tag{A.5}
$$

During the following calculations we set (see Eq. (A.4))

$$\hat{I} = \underbrace{-iq_e t_A \hat{\psi}_1^\dagger(0)\hat{\psi}_2(0) - iq_e t_B \hat{\psi}_1^\dagger(x_1)\hat{\psi}_2(x_2)}_{B^\dagger} + \underbrace{\text{h.c.}}_{B} \quad .$$

The tunnel operator $\hat{H}_{H_1}^T$ was defined in Eq. (2.3) as

$$\hat{H}_{H_1}^T = \underbrace{t_A \hat{\psi}_1^\dagger(0)\hat{\psi}_2(0) + t_B \hat{\psi}_1^\dagger(x_1)\hat{\psi}_2(x_2)}_{A} + \underbrace{\text{h.c.}}_{A^\dagger} \quad .$$

Using these abbreviations, the mean current can be written as

$$
\begin{aligned}
I &= i\int_{-\infty}^0 dt' \, \left\langle \left[A(t') + A^\dagger(t'), B + B^\dagger \right] \right\rangle \\
&= i\int_{-\infty}^0 dt' \, \langle [A(t'), B] \rangle + \text{h.c.} \quad .
\end{aligned}
\tag{A.6}
$$

In a next step we express the integrand in terms of the single particle Green's functions $G^>(x,t)$. The integrand consists of four contributions

$$
\begin{aligned}
\langle [A(t), B] \rangle &= iq_e|t_A|^2 \left\langle \left[\hat{\psi}_1^\dagger(0,t)\hat{\psi}_2(0,t), \hat{\psi}_2^\dagger(0,0)\hat{\psi}_1(0,0) \right] \right\rangle \\
&+ iq_e|t_B|^2 \left\langle \left[\hat{\psi}_1^\dagger(x_1,t)\hat{\psi}_2(x_2,t), \hat{\psi}_2^\dagger(x_2,0)\hat{\psi}_1(x_1,0) \right] \right\rangle \\
&+ iq_e t_A t_B^* \left\langle \left[\hat{\psi}_1^\dagger(0,t)\hat{\psi}_2(0,t), \hat{\psi}_2^\dagger(x_2,0)\hat{\psi}_1(x_1,0) \right] \right\rangle \\
&+ iq_e t_A^* t_B \left\langle \left[\hat{\psi}_1^\dagger(x_1,t)\hat{\psi}_2(x_2,t), \hat{\psi}_2^\dagger(0,0)\hat{\psi}_1(0,0) \right] \right\rangle .
\end{aligned}
\tag{A.7}
$$

With the definitions for the single-particle Green's functions Eq. (2.10) one gets

$$
\begin{aligned}
\langle [A(t), B] \rangle &= iq_e|t_A|^2 (G_1^<(0,-t)G_2^>(0,t) - G_1^>(0,-t)G_2^<(0,t)) \\
&+ iq_e|t_B|^2 (G_1^<(0,-t))G_2^>(0,t) - G_1^>(0,-t)G_2^<(0,t)) \\
&+ iq_e t_A t_B^* (G_1^<(x_1,-t)G_2^>(-x_2,t) - G^>(x_1,-t)G^<(-x_2,t)) \\
&+ iq_e t_A^* t_B (G_1^<(-x_1,-t)G_2^>(x_2,t) - G^>(-x_1,-t)G^<(x_2,t)).
\end{aligned}
\tag{A.8}
$$

The average current I therefore yields

$$
\begin{aligned}
I &= -q_e \int_{-\infty}^0 dt' \, \Big\{ \big[(|t_A|^2 + |t_B|^2)(G_1^<(0,-t)G_2^>(0,t) - G_1^>(0,-t)G_2^<(0,t)) \\
&\quad + t_A t_B^* (G_1^<(x_1,-t)G_2^>(-x_2,t) - G^>(x_1,-t)G^<(-x_2,t)) \\
&\quad + t_A^* t_B (G_1^<(-x_1,-t)G_2^>(x_2,t) - G^>(-x_1,-t)G^<(x_2,t)) \big] + \text{c.c.} \Big\} .
\end{aligned}
\tag{A.9}
$$

Now, we employ the identity $G^{>/<}(x,t) = -\left[G^{>/<}(-x,-t)\right]^*$ to extend the integral to $\int_{-\infty}^{\infty}$. It follows

$$
\begin{aligned}
I &= -q_e \int_{-\infty}^{\infty} dt \, \big((|t_A|^2 + |t_B|^2)(G_1^<(0,-t)G_2^>(0,t) - G_1^>(0,-t)G_2^<(0,t)) \\
&\quad + \left[t_A t_B^* (G_1^<(x_1,-t)G_2^>(-x_2,t) - G^>(x_1,-t)G^<(-x_2,t)) + \text{c.c} \right] \big) .
\end{aligned}
\tag{A.10}
$$

As an intermediate result, the current expressed in terms of the Green's functions in time domain yields (where we follow the notations of Chapter 2)

$$
\begin{aligned}
I_0 &= q_e [|t_A|^2 + |t_B|^2] \int_{-\infty}^{\infty} dt \, (G_1^>(0,-t)G_2^<(0,t) - G_1^<(0,-t)G_2^>(0,t)) \\
I_{\text{coh}} &= q_e |t_A t_B^*| \\
&\quad e^{i\phi} \int_{-\infty}^{\infty} dt \, (G^>(x_1,-t)G^<(-x_2,t) - G_1^<(x_1,-t)G_2^>(-x_2,t)) + \text{c.c.}
\end{aligned}
\tag{A.11}
$$

Introducing the Fourier transformed Green's functions $G^{>/<}(\epsilon,x)$ one changes to frequency domain:

$$
\begin{aligned}
I_0 &= q_e [|t_A|^2 + |t_B|^2] \int \frac{d\omega}{2\pi} \, (G_1^>(\omega,0)G_2^<(\omega,0) - G_1^<(\omega,0)G_2^>(\omega,0)) \\
I_{\text{coh}} &= q_e |t_A t_B^*| \\
&\quad e^{i\phi} \int \frac{d\omega}{2\pi} \, (G_1^>(\omega,x_1)G_2^<(\omega,-x_2) - G_1^<(\omega,x_1)G_2^>(\omega,-x_2)) + \text{c.c.} .
\end{aligned}
\tag{A.12}
$$

With help of the fluctuation-dissipation theorem the classical part of the current I_0 can be re-expressed in terms of the tunnel density of states. This leads directly to Eq. (2.19).

A.3   Visibility

Finally, here we derive the expression for the visibility v_I in Eqs. (2.25) and (2.26). The visibility is defined as the ratio between the maximal coherent current and the classical current: $v_I \equiv I_{\text{coh}}(\Phi)|_{\text{max}}/I_0$. With Eq. (A.12) it follows

$$
\begin{aligned}
v_I &= \frac{2|t_A t_B^*|}{|t_A|^2 + |t_B|^2} \times \\
&\quad \frac{\left| \int \frac{d\omega}{2\pi} \, (G_1^>(\omega,x_1)G_2^<(\omega,-x_2) - G_1^<(\omega,x_1)G_2^>(\omega,-x_2)) \right|}{\int \frac{d\omega}{2\pi} \, (G_1^>(\omega,0)G_2^<(\omega,0) - G_1^<(\omega,0)G_2^>(\omega,0))} .
\end{aligned}
$$

Employing the identity $G_\alpha^{>/<}(\omega,x) = e^{i\mu_\alpha x} G_{\mu=0}^{>/<}(x,\omega - \mu_\alpha)$ we can rewrite everything in terms of the Green's function $G^>(\omega,x)$. With help of the fluctuation-dissipation theorem in Eq. (2.13), the

expression can be simplified further (with $q_e V = \mu_1 - \mu_2$ and $V > 0$)

$$
\begin{aligned}
v_I &= \frac{2|t_A t_B^*|}{|t_A|^2 + |t_B|^2} \times \\
&\frac{\left| \int d\omega \, G^>(\omega, x_1) G^<(\omega - |q_e|V, -x_2) - G^<(\omega, x_1) G^>(\omega - |q_e|V, -x_2) \right|}{4\pi^2 \int d\omega \, [\nu(\omega)\nu(\omega - |q_e|V)][f(\omega - |q_e|V) - f(\omega)]}.
\end{aligned}
\tag{A.13}
$$

Appendix B

Keldysh perturbation theory

B.1 Propagator functions

B.1.1 Keldysh propagator for non-interacting electrons

In equilibrium, the non-interacting Keldysh propagator $G_0^K(x,t) = -i\langle[\hat{\psi}(x,t),\hat{\psi}^\dagger(0,0)]\rangle$ function for a linearized electron spectrum, yields:

$$
\begin{aligned}
G_0^K(x,t) &= -i\frac{1}{L}\sum_{kk'} e^{ikx-iv_F kt}\langle[\hat{c}_k,\hat{c}_{k'}^\dagger]\rangle \\
&= i\frac{1}{L}\sum_k e^{ikx-iv_F kt}\,(2f_k-1) \\
&= -i\int\frac{dk}{2\pi}\,e^{ikx-iv_F kt}\,\tanh(\frac{\beta v_F k}{2}).
\end{aligned}
\tag{B.1}
$$

In frequency and momentum space we get

$$
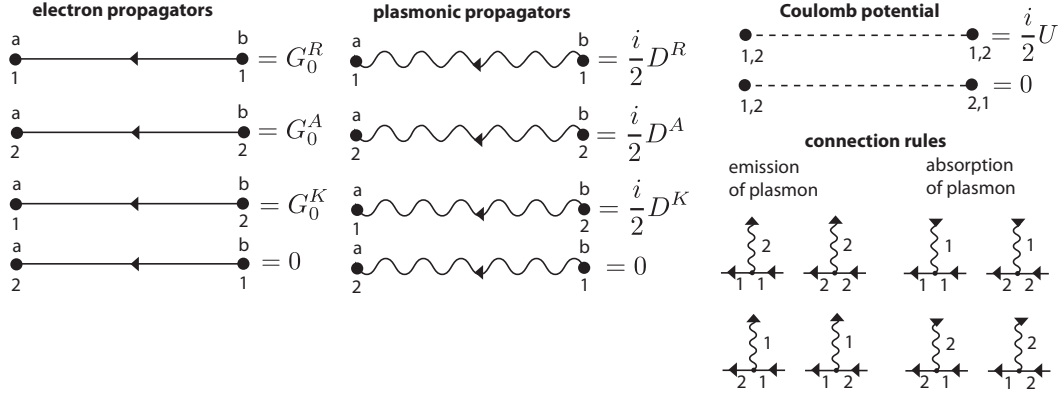G^K(k,\omega) = -2\pi i\,\tanh(\frac{\beta\omega}{2})\delta(\omega-v_F k).
\tag{B.2}
$$

Figure B.1: Construction rules for the diagrammatic perturbation theory in Keldysh time.

B.1.2   Plasmon propagator functions

For deriving the plasmon propagator functions $D^{R/A}(x,t) = \mp i\Theta(\pm t)\langle[\hat{V}(x,t),\hat{V}(0,0)]\rangle$ we start from the definition of $\hat{V}(x) = \int dx'\, U(x-x')\hat{\rho}(x')$, where as usual $\hat{\rho}(x) = L^{-1}\sum_k e^{ikx}\hat{\rho}_k$:

$$
\begin{aligned}
D^{R/A}(x,t) &= \mp i\Theta(\pm t)L^{-2}\sum_k |U_k|^2 e^{ikx}\,\langle[\hat{\rho}_k(t),\hat{\rho}_{-k}(0)]\rangle \\
&= \mp i\Theta(\pm t)L^{-2}\sum_{k,q}|U_k|^2 e^{ikx-iv_F kt}(f_q - f_{q+k}).
\end{aligned}
\tag{B.3}
$$

In frequency and momentum space this yields

$$
\begin{aligned}
D^{R/A}(q,\omega) &= \frac{1}{2\pi}\frac{|U_q|^2}{\omega - v_F q \pm i0^+}\int dk\,(f_k - f_{k+q}) \\
&= \frac{q}{2\pi}\frac{|U_q|^2}{\omega - v_F q \pm i0^+}.
\end{aligned}
\tag{B.4}
$$

As expected the retarded Green's function and therefore the linear response of the plasmonic bath turns out to be temperature independent. This is a general feature of harmonic oscillator baths.

B.2   Diagrammatic calculations

Working on the Keldysh contour complicates the diagrammatic calculation due to the matrix structure of the Green's functions. Especially, after performing the usual rotation in Keldysh space one can

not construct the diagrams intuitively. Therefore, in Fig. B.1 we sum up the construction rules for the diagrammatic perturbation theory as it is presented in [19]. The only subtility arises calculating equal-time diagrams. As in the standard perturbation theory in imaginary time, here one has to introduce a special rule. In this case on has to substitute the usual Keldysh propagator G_0^K by the slightly different propagator $\tilde{G}_0^K(k,\omega) \equiv 4\pi i f(\omega)\delta(\omega - v_F k)$.

In the following calculations we set $\int (dk) \equiv \int \frac{dk}{2\pi}$ and $\int (d\omega) \equiv \int \frac{d\omega}{2\pi}$.

B.2.1   First order diagrams

In first order one has to calculate the usual Hartree-Fock contribution to the retarded self-energy $\Sigma^R(k,\omega)$.

Hartree diagram   The Hartree diagram only leads to a constant energy shift due to the coupling of the electron to the total charge in the channel. The Hartree diagram contains a closed fermion loop, therefore an additional minus sign shows up. Applying the construction rules showed in Fig. B.1, there is only a single diagram contributing to the self-energy

$$
\begin{aligned}
\Sigma_{\mathrm{H}}(\epsilon, k) &= -\frac{i}{2}U(q = 0)\int (dq)\int (d\omega)\, \tilde{G}_0^K(q,\omega) \\
&= U(q = 0)\int (dq)\, f(q) \\
&= U(q = 0)\bar{\rho},
\end{aligned}
\tag{B.5}
$$

where $\bar{\rho}$ denotes the mean electron density and calculating the closed fermion loop we used $\tilde{G}_0^K$ instead of the Keldysh propagator.

Fock diagram   The Fock diagram described the energy renormalization of the electron as a result of a virtual process (cf. Fig. 6.1). This virtual process happens at one single time, i.e., it is an equal-time process. Therefore, in the single contribution to the retarded self-energy G_0^K is substituted by $\tilde{G}_0^K$:

$$
\begin{aligned}
\Sigma_{\mathrm{F}}^R(\epsilon, k) &= \frac{i}{2}\int (dq)\int (d\omega)\, U(q)\tilde{G}_0^K(\epsilon - \omega, k - q) \\
&= -\int (dq)\, U(q) f(k - q).
\end{aligned}
\tag{B.6}
$$

B.2.2   Second order diagrams

There are two second order processes contributing to the retarded self-energy (cf. Fig. 6.1): the excitation of plasmons and a vertex correction. We start with the evaluation of the plasmonic diagrams,

followed by the rather lengthy calculation of the vertex correction.

Excitation of plasmons Applying the rules depicted in Fig. B.1 it turns out that only two diagrams contribute to the self-energy Σ_P^R:

$$
\begin{aligned}
\Sigma_P^R(\epsilon, k) & = \frac{i}{2} \int (dq) \int (d\omega) \left[G_0^R(\epsilon - \omega, k - q) \cdot D_0^K(\omega, q) + G_0^K(\epsilon - \omega, k - q) \cdot D_0^R(\omega, q) \right] \\
& = \frac{1}{2} \int (dq) \int (d\omega) U_q^2 q \left[\frac{\coth(\beta\omega/2)}{(\epsilon - \omega) - v_F(k - q) + i0^+} \delta(\omega - v_F q) + \right. \\
& \qquad \left. \frac{\tanh(\beta(\epsilon - \omega)/2)}{\omega - v_F q + i0^+} \delta((\epsilon - \omega) - v_F(k - q)) \right] \\
& = \frac{G_0^R(\epsilon, k)}{8\pi^2} \cdot \int_{-\infty}^{\infty} dq \quad U_q^2 q \cdot \left[\coth(\beta\hbar v_F q/2) + \tanh(\beta\hbar v_F(k - q)/2) \right]. \quad (\text{B.7})
\end{aligned}
$$

Vertex correction The vertex correction to the retarded self-energy has the structure (compare to the review [19]):

$$
\Sigma_V(\epsilon, k) = \left(\frac{i}{2} \right)^2 \frac{1}{(2\pi)^4} \int dk_1 \int dk_2 \int d\omega_1 \int d\omega_2 \, U_{q_1} U_{q_2} \times [
$$

$$
G_0^R(\epsilon - \omega_2, k - k_2) G_0^K(\epsilon - \omega_1 - \omega_2, k - k_1 - k_2) G_0^K(\epsilon - \omega_1, k - k_1)
$$

$$
+ G_0^R(\epsilon - \omega_2, k - k_2) G_0^A(\epsilon - \omega_1 - \omega_2, k - k_1 - k_2) G_0^R(\epsilon - \omega_1, k - k_1)
$$

$$
+ G_0^K(\epsilon - \omega_2, k - k_2) G_0^K(\epsilon - \omega_1 - \omega_2, k - k_1 - k_2) G_0^R(\epsilon - \omega_1, k - k_1)
$$

$$
+ G_0^K(\epsilon - \omega_2, k - k_2) G_0^A(\epsilon - \omega_1 - \omega_2, k - k_1 - k_2) G_0^K(\epsilon - \omega_1, k - k_1)]. \quad (\text{B.8})
$$

The calculation of the four integrals is a straight forward task. In the following, we derive every integral separately labelling the diagrams by the involved Green's functions, e.g., we refer to the first term of Σ_V in Eq. (B.8) as Σ_{RKK}.

Diagram [RKK]

$$
\begin{aligned}
\Sigma_{RKK} &= \frac{1}{16\pi^2} \int dk_1 \int dk_2 \int d\omega_1 \int d\omega_2 \, U_{k_1} U_{k_2} \cdot \frac{1}{(\epsilon - \omega_2) - v_F(k - k_2) + i0^+} \\
&\quad \tanh(\beta(\epsilon - \omega_1 - \omega_2)/2) \cdot \tanh(\beta(\epsilon - \omega_1)/2) \\
&\quad \delta((\epsilon - \omega_1 - \omega_2) - v_F(k - k_1 - k_2))\delta((\epsilon - \omega_1) - v_F(k - k_1)) \\
&= \frac{1}{16\pi^2} \int dk_1 \int dk_2 \, U_{k_1} U_{k_2} \cdot \frac{1}{\epsilon - v_F k + i0^+} \\
&\quad \tanh[\beta v_F(k - k_1 - k_2)/2] \tanh[\beta v_F(k - k_1)/2] \\
&= \frac{G_0^R(\epsilon, k)}{16\pi^2} \int dk_1 \int dk_2 \, U_{k_1} U_{k_2} \times \\
&\quad \tanh[\frac{\beta v_F(k - k_1 - k_2)}{2}] \tanh[\frac{\beta v_F(k - k_1)}{2}].
\end{aligned} \tag{B.9}
$$

Diagram [KAK]

$$
\begin{aligned}
\Sigma_{KAK} &= \frac{1}{4 \cdot (2\pi)^2} \int dk_1 \int dk_2 \int d\omega_1 \int d\omega_2 \, U_{k_1} U_{k_2} \times \\
&\quad \frac{1}{(\epsilon - \omega_1 - \omega_2) - v_F(k - k_1 - k_2) - i0^+} \times \\
&\quad \tanh[\beta(\epsilon - \omega_2)/2]\delta((\epsilon - \omega_2) - v_F(k - k_2)) \times \\
&\quad \tanh[\beta(\epsilon - \omega_1)/2]\delta((\epsilon - \omega_1) - v_F(k - k_1)) \\
&= -\frac{1}{16\pi^2} \int dk_1 \int dk_2 \int d\omega_2 \, U_{k_1} U_{k_2} \delta((\epsilon - \omega_2) - v_F(k - k_2)) \\
&\quad \left[\frac{\tanh[\beta(\epsilon - \omega_2)/2] \tanh[\beta v_F(k - k_2)/2]}{\omega_2 - v_F k_2 + i0^+} \right] \\
&= -\frac{G_0^R(\epsilon, k)}{16\pi^2} \int dk_1 \int dk_2 \, U_{k_1} U_{k_2} \times \\
&\quad \tanh[\beta v_F(k - k_2)/2] \tanh[\beta v_F(k - k_1)/2]
\end{aligned} \tag{B.10}
$$

Diagram [KKR]

$$
\begin{aligned}
\Sigma_{KKR} &= \frac{1}{4 \cdot (2\pi)^2} \int dk_1 \int dk_2 \int d\omega_1 \int d\omega_2 \, U_{k_1} U_{k_2} \times \\
&\quad \tanh[\beta(\epsilon - \omega_2)/2]\delta((\epsilon - \omega_2) - v_F(k - k_2)) \\
&\quad [\delta((\epsilon - \omega_1 - \omega_2) - v_F(k - k_1 - k_2))] \left[\frac{\tanh[\beta(\epsilon - \omega_1 - \omega_2)/2]}{(\epsilon - \omega_1) - v_F(k - k_1) + i0^+} \right] \\
&= \frac{G_0^R(\epsilon, k)}{16\pi^2} \int dk_1 \int dk_2 \, U_{k_1} U_{k_2} \times \\
&\quad \tanh[\beta v_F(k - k_2)/2] \tanh[\beta v_F(k - k_1 - k_2)/2].
\end{aligned}
\tag{B.12}
$$

Diagram [RAR]

$$
\begin{aligned}
\Sigma_{RAR} &= \frac{i^2}{4 \cdot (2\pi)^4} \int dk_1 \int dk_2 \int d\omega_1 \int d\omega_2 \frac{U_{k_1} U_{k_2}}{(\epsilon - \omega_1) - v_F(k - k_1) + i0^+} \\
&\quad \frac{1}{(\epsilon - \omega_2) - v_F(k - k_2) + i0^+} \cdot \frac{1}{(\epsilon - \omega_2) - v_F(k - k_2) + i0^+} \\
&= \frac{2\pi i}{4 \cdot (2\pi)^4} \int dk_1 \int dk_2 \int d\omega_2 \frac{U_{k_1} U_{k_2}}{\omega_2 - \epsilon + v_F(k - k_2) - i0^+} \cdot \frac{1}{\omega_2 - v_F k_2 + i0^+} \\
&= -\frac{G_0^R(\epsilon, k)}{16\pi^2} \int dk_1 \int dk_2 \, U_{k_1} U_{k_2}.
\end{aligned}
\tag{B.12}
$$

Summing up the four contributions the vertex correction yields

$$
\Sigma_V^R(\epsilon, k) = \left[\frac{G_0^R(\epsilon, k)}{16\pi^2} \right] \int_{-\infty}^{\infty} dq_1 \int_{-\infty}^{\infty} dq_2 U_{q_1} U_{q_2}
$$

$$
\times \left[\tanh(\frac{\beta v_F(k - q_1 - q_2)}{2})) \cdot \left[\tanh(\frac{\beta v_F((k - q_1))}{2}) + \tanh(\frac{\beta v_F((k - q_2))}{2})) \right] - \right.
$$

$$
\left. - \tanh(\frac{\beta v_F((k - q_2))}{2}) \, \tanh(\frac{\beta v_F((k - q_1))}{2}) - 1 \right].
$$

Appendix C

Semiclassical approach and functional bosonization

C.1   Calculation of the exponent

Here, we present the explicit calculation of the exponent emerging in Chapter 5. The calculations are straight forward, however one has to take the limit $\gamma \to 0$ in the very end leading to a large number of terms. Therefore, the calculation is a bit cumbersome.

Calculation of F_1

$$
\begin{aligned}
F_1 + \delta F_1 &= \frac{1}{4} \int (d\omega) \left\langle \left[\hat{V}, \hat{V} \right] \right\rangle_\omega^{(0)} \int dt_1 \int dt_2 \, e^{-i\omega(t_1 - t_2)} \mathrm{sgn}(t_1 - t_2) \left(\lambda_2 \lambda_2 - \lambda_1 \lambda_1 \right) \\
&= \frac{i}{2} \int (d\omega) \left\langle \left[\hat{V}, \hat{V} \right] \right\rangle_\omega^{(0)} \mathrm{Im} \left\{ \int dt_1 e^{-i\omega t_1} \left(\int_{-\infty}^{t_0} dt_2 e^{i\omega t_2 + \gamma(t_2 - t_0)} \right. \right. \\
&\qquad \left. \left. \int_{t_0}^{0} dt_2 \, e^{i\omega t_2} + \int_0^{t_1} dt_2 e^{i\omega t_2} \right) \right\} \\
&= -\frac{i}{2} t \int (d\omega) \frac{\left\langle \left[\hat{V}, \hat{V} \right] \right\rangle_\omega^{(0)}}{\omega} \\
&\quad + \frac{i\pi}{2} \int (d\omega) \, \delta(\omega) \frac{\left\langle \left[\hat{V}, \hat{V} \right] \right\rangle_\omega^{(0)}}{\omega} \mathrm{Re} \left(e^{i\omega(t_0 - t)} - e^{i\omega t_0} \right).
\end{aligned}
\tag{C.1}
$$

Calculation of F_2

$$
\begin{aligned}
F_2 + \delta F_2 &= \frac{1}{4}\int (d\omega)\left\langle\left\{\hat{V},\hat{V}\right\}\right\rangle_\omega^{(0)}\left(\left|\int dt_1\lambda_1(t_1)e^{-i\omega t_1}\right|^2 + \left|\int dt_2\lambda_2(t_1)e^{-i\omega t_2}\right|^2\right)\\
&= \frac{1}{4}\int (d\omega)\left\langle\left\{\hat{V},\hat{V}\right\}\right\rangle_\omega^{(0)}\left(\left|\int_{-\infty}^{t_0} e^{-i\omega t_1+\gamma(t_1-t_0)} + \int_{t_0}^{0} e^{-i\omega t_1}\right|^2 +\right.\\
&\qquad \left.\left|\int_{-\infty}^{t_0} e^{-i\omega t_1+\gamma(t_1-t_0)} + \int_{t_0}^{t} e^{-i\omega t_1}\right|^2\right)\\
&= \frac{1}{4}\int (d\omega)\left\langle\left\{\hat{V},\hat{V}\right\}\right\rangle_\omega^{(0)}\left(\frac{1}{\omega^2} + \frac{1}{\omega^2}\left[2 - e^{-i\omega(t-t_0)} - e^{i\omega(t-t_0)}\right]\right.\\
&\qquad \left.\frac{e^{-i\omega(t_0-t)}-1}{(-i\omega+\gamma)i\omega} + \frac{e^{-i\omega(t-t_0)}-1}{(i\omega+\gamma)(-i\omega)} + (t=0)\right)\\
&= \frac{1}{2}\int (d\omega)\frac{\left\langle\left\{\hat{V},\hat{V}\right\}\right\rangle_\omega^{(0)}}{\omega^2} + \frac{1}{4}(t-2t_0)\left\langle\left\{\hat{V},\hat{V}\right\}\right\rangle_{\omega\to 0}^{(0)}.
\end{aligned}
\tag{C.2}
$$

Calculation of F_3

$$
\begin{aligned}
F_3 + \delta F_3 &= -\int (d\omega)\left\langle\hat{V}\hat{V}\right\rangle_\omega^{(1)}\int dt_1\int dt_2\, e^{-i\omega(t_2-t_1)}\lambda_2(t_2)\lambda_1(t_1)\\
&= -\int (d\omega)\left\langle\hat{V}\hat{V}\right\rangle_\omega^{(1)}\left(\int_{-\infty}^{t_0} dt_2 e^{-i\omega t_2+\gamma(t_2-t_0)} + \int_{t_0}^{t} dt_2\, e^{-i\omega t_2}\right)\\
&\qquad \times\left(\int_{-\infty}^{t_0} dt_1 e^{i\omega t_1+\gamma(t_1-t_0)} + \int_{t_0}^{0} dt_1\, e^{i\omega t_1}\right)\\
&= -\int (d\omega)\left\langle\hat{V}\hat{V}\right\rangle_\omega^{(1)}\left(\frac{e^{-i\omega t_0}}{-i\omega+\gamma} + \frac{e^{-i\omega t}-e^{-i\omega t_0}}{-i\omega}\right)\\
&\qquad \times\left(\frac{e^{i\omega t_0}}{i\omega+\gamma} + \frac{1-e^{i\omega t_0}}{i\omega}\right)\\
&= -\int (d\omega)\left\langle\hat{V}\hat{V}\right\rangle_\omega^{(1)}\left(\frac{1}{\omega^2}e^{-i\omega t}\right.\\
&\qquad \left.+ \frac{i\pi}{\omega}\delta(\omega)(e^{-i\omega(t-t_0)}-1) - \frac{i\pi}{\omega}\delta(\omega)(e^{-i\omega t_0}-1)\right)\\
&= -\int \frac{(d\omega)}{\omega^2}\left\langle\hat{V}\hat{V}\right\rangle_\omega^{(1)} e^{-i\omega t} - \frac{1}{2}(t-2t_0)\cdot\left\langle\hat{V}\hat{V}\right\rangle_{\omega\to 0}^{(1)}
\end{aligned}
\tag{C.3}
$$

C.1.1 Calculation of $\left\langle \hat{\Phi}\hat{\Phi} \right\rangle_{q\omega}$

Starting from the definition of the bosonic field $\hat{\Phi}(x,t) = -i\sum_{q>0} \sqrt{\frac{2\pi}{Lq}}\left(\hat{b}_q e^{iqx} - \text{h.c.}\right)$ the correlation function $\left\langle \hat{\Phi}\hat{\Phi} \right\rangle_{q\omega}$ yields

$$
\begin{aligned}
\left\langle \hat{\Phi}\hat{\Phi} \right\rangle_{q\omega} &= \int dt \int dx\, e^{i\omega t - ikx}\left\{\sum_{k>0} \frac{2\pi}{L|k|}\left(\left\langle \hat{b}_k(t)\hat{b}_k^\dagger \right\rangle e^{ikx} + \left\langle \hat{b}_k^\dagger(t)\hat{b}_k \right\rangle e^{-ikx}\right)\right\} \\
&= \frac{2\pi}{|q|}\left(\Theta_q \left\langle \hat{b}_q(t)\hat{b}_q^\dagger \right\rangle_\omega + \Theta_{-q}\left\langle \hat{b}_{-q}^\dagger(t)\hat{b}_{-q} \right\rangle_\omega\right) \\
&= \frac{4\pi^2}{|q|}\left(\Theta_q(1 + \bar{n}(\omega_q))\delta(\omega - \omega_q) + \Theta_{-q}\bar{n}(\omega_{|q|})\delta(\omega + \omega_{|q|})\right).
\end{aligned}
\tag{C.4}
$$

Bibliography

[1] B. Abel and F. Marquardt, *Decoherence by quantum telegraph noise*, arXiv:0805.0962 (2008).

[2] A Altland and B Simons, *Condensed matter field theory*, Cambridge University Press, 2006.

[3] D.A. Bagrets, I.V. Gornyi, A.D. Mirlin, and D.G. Polyakov, *Relaxation processes in a disordered luttinger liquid*, arXiv:0804.4887 (2008).

[4] H. Bruus and K. Flensberg, *Many-body quantum theory in condensed matter physics*, Oxford University Press, 2005.

[5] A. H. Castro-Neto, C. de C. Chamon, and C. Nayak, *Open Luttinger liquids*, Phys. Rev. Lett. **79** (1997), 4629.

[6] J. T. Chalker, Yuval Gefen, and M. Y. Veillette, *Decoherence and interactions in an electronic mach-zehnder interferometer*, Physical Review B (Condensed Matter and Materials Physics) **76** (2007), no. 8, 085320.

[7] A. D. Mirlin D. B. Gutman, Yuval Gefen, *Zero bias anomaly out of equilibrium*, arxiv (cond-mat) (2007).

[8] I.E. Dzyaloshinskii and K.B. Larkin, Sov. Phys JETP **38** (1976).

[9] S Engelsberg and B. B. Varga, *One-dimensional electron-phonon model*, Physical Review **136** (1964), no. 6A.

[10] Victoria Fernandez and Kang Li, *Bosonic description of a tomonaga-luttinger model with impurities*, Physics Letters B **452** (1999), no. 1-2, 98–102.

[11] F.Marquardt, J.v.Delft, and V.Ambegaokar, *Decoherence in weak localization 1: Pauli principle in influence functional*, Phys. Rev. B **76** (2007).

[12] H.C. Fogedby, *Correlation functions for the tomonaga model*, J. Phys. C: Solid State Phys. **9** (1976), 3757–3773.

[13] H. Förster, S. Pilgram, and M. Büttiker, *Decoherence and full counting statistics in a Mach-Zehnder interferometer*, Phys. Rev. B **72** (2005), 075301.

[14] Thierry Giamarchi, *Quantum physics in one dimension*, Oxford University Press, 2006.

[15] I. V. Gornyi, A. D. Mirlin, and D. G. Polyakov, *Dephasing and weak localization in disordered luttinger liquid*, Physical Review Letters **95** (2005), no. 4, 046404.

[16] Alex Grishin, Igor V. Yurkevich, and Igor V. Lerner, *Functional integral bosonization for an impurity in a luttinger liquid*, Phys. Rev. B **69** (2004), no. 16, 165108.

[17] O. Heinonen and Sebastian Eggert, *Electron-phonon interactions on a single-branch quantum hall edge*, Physical Review Letters **77** (1996), no. 2.

[18] F Marquardt I Neder, *Coherence oscillations in dephasing by non-gaussian shot noise*, New J. Phys. **9** (2007), no. 5.

[19] H. Smith J. Rammer, *Quantum field-theoretical methods in transport theory of metals*, Reviews of Modern Physics **58** (1986), no. 2, 323–359.

[20] Y Ji, Y Chung, D Sprinzak, M Heiblum, D Mahalu, and H Shtrikman, *An electronic Mach-Zehnder interferometer*, Nature **422** (2003), 415.

[21] Jv Delft H Schoeller, *Bosonization for beginners - Fermionization for experts*, Ann. Phys. **7** (1998).

[22] Peter Kopietz, *Bosonization of coupled electron-phonon systems*, Zeitschrift für Physik B Condensed Matter **100** (1996), no. 4, 561–565.

[23] D.K.K Lee and Y. Chen, *Functional bosonisation of the tomonaga-luttinger model*, Journal of Physics A: Mathematical and General **21** (1988), no. 22, 4155–4171.

[24] K. LeHur, *Dephasing of mesoscopic interferences from electron fractionalization*, Physical Review Letters **95** (2005), no. 7, 076801.

[25] ———, *Electron lifetime in luttinger liquids*, Physical Review B (Condensed Matter and Materials Physics) **74** (2006), no. 16, 165104.

[26] Ivan P. Levkivskyi and Eugene V. Sukhorukov, *Dephasing in the electronic mach-zehnder interferometer at filling factor nu = 2*, Physical Review B (Condensed Matter and Materials Physics) **78** (2008), no. 4, 045322–13.

[27] L. V. Litvin, A. Helzel, H.-P. Tranitz, W. Wegscheider, and C. Strunk, *Edge-channel interference controlled by landau level filling*, Physical Review B (Condensed Matter and Materials Physics) **78** (2008), no. 7, 075303.

[28] L. V. Litvin, H.-P. Tranitz, W. Wegscheider, and C. Strunk, *Decoherence and single electron charging in an electronic mach-zehnder interferometer*, Physical Review B (Condensed Matter and Materials Physics) **75** (2007), no. 3, 033315.

[29] J. M. Luttinger, *An exactly soluble model of a many-fermion system*, Journal of Mathematical Physics **4** (1963), no. 9, 1154–1162.

[30] G. D. Mahan, *Many-particle physics*, Kluwer Academic/Plenum Publishers, New York, 2000.

[31] F. Marquardt, *Fermionic Mach-Zehnder Interferometer subject to a quantum bath*, Europhysics Letter **72** (2005), no. 788.

[32] _____, *Decoherence of fermions subject to a quantum bath*, To be published in "Advances in Solid State Physics" (Springer), Vol. 46, ed. R. Haug [cond-mat/0604626] (2006).

[33] F. Marquardt and C. Bruder, *Effects of dephasing on shot noise in an electronic Mach-Zehnder interferometer*, Phys. Rev. B **70** (2004), 125305.

[34] F. Marquardt and C. Bruder, *Influence of dephasing on shot noise in an electronic Mach-Zehnder interferometer*, Phys. Rev. Lett. **92** (2004), 056805.

[35] F. Marquardt and D. S. Golubev, *A many-fermion generalization of the caldeira-leggett model*, Phys. Rev. A **72** (2005).

[36] Florian Marquardt, *Equations of motion approach to decoherence and current noise in ballistic interferometers coupled to a quantum bath*, Physical Review B (Condensed Matter and Materials Physics) **74** (2006), no. 12, 125319.

[37] Florian Marquardt and D. S. Golubev, *Relaxation and dephasing in a many-fermion generalization of the caldeira-leggett model*, Physical Review Letters **93** (2004), no. 13.

[38] V. Meden, K. Schönhammer, and O. Gunnarson, *Electron-phonon interaction in one dimension: Exact spectral properties*, Phys. Rev. B **50** (1994), no. 15.

[39] I. Neder, M. Heiblum, Y. Levinson, D. Mahalu, and V. Umansky, *Unexpected behavior in a two-path electron interferometer*, Physical Review Letters **96** (2006), no. 1, 016804.

[40] Izhar Neder, Florian Marquardt, Moty Heiblum, Diana Mahalu, and Vladimir Umansky, *Controlled dephasing of electrons by non-gaussian shot noise*, Nat Phys **3** (2007), no. 8, 534–537.

[41] C. Neuenhahn and F. Marquardt, *Universal dephasing in a chiral 1d interacting fermion system*, arxiv:0806.1211 (2008).

[42] Preden Roulleau, F. Portier, D. C. Glattli, P. Roche, A. Cavanna, G. Faini, U. Gennser, and D. Mailly, *Finite bias visibility of the electronic mach-zehnder interferometer*, Physical Review B (Condensed Matter and Materials Physics) **76** (2007), no. 16, 161309.

[43] K. Schönhammer and V. Meden, *Nonuniversal spectral properties of the luttinger model*, Phys. Rev. B **47** (1993), no. 24, 16205–16215.

[44] G. Seelig and M. Büttiker, *Charge-fluctuation-induced dephasing in a gated mesoscopic interferometer*, Phys. Rev. B **64** (2001), 245313.

[45] Eugene V. Sukhorukov and Vadim V. Cheianov, *Resonant dephasing in the electronic mach-zehnder interferometer*, Physical Review Letters **99** (2007), no. 15, 156801–4.

[46] S. Tomonaga, *Remarks on Bloch's Method of Sound Waves applied to Many-Fermion Problems*, Progress of Theoretical Physics **5** (1950), 544–569.

[47] J. Voit and H. J. Schulz, *Electron-phonon interaction and phonon dynamics in one-dimensional conductors*, Phys. Rev. B **37** (1988), no. 17, 10068–10085.

[48] U. Weiss, *Quantum dissipative systems*, World Scientific, Singapore, 2000.

Selbstständigkeitserklärung

Hiermit erkläre ich, dass ich die vorliegende Arbeit selbstständig angefertigt und nur die angegebenen Quellen und Hilfsmittel verwendet habe.

München, den 31. Oktober 2008

Clemens Neuenhahn